

The University of Nottingham

UNITED KINGDOM · CHINA · MALAYSIA

Machining of Metal Directed Energy Deposited Components

Olusola Oyelola
9-13-2019

Preface

This thesis is submitted towards the degree of Doctor of Philosophy at the University of Nottingham. The research work was carried out under the supervision of Professor A. T Clare in the Department of Mechanical, Materials and Manufacturing Engineering and at the Advanced Manufacturing Research Centre (AMRC), Sheffield.

I hereby certify the work presented in this thesis is original and suitable references are made to any work from the literature used in this work.

The list of publications resulting from the work carried out in this thesis is listed in the following. For clarity, research work is classified according to their medium of dissemination.

Journal Publications:

- O. Oyelola, P. Crawforth, R. M'Saoubi, A. Clare; **On the Machining of Directed energy deposited Ti6Al4V**, Additive Manufacturing, Volume 19, January 2018, pages 39-50. https://doi.org/10.1016/j.addma.2017.11.005
- O. Oyelola, P. Crawforth, R. M'Saoubi, A. Clare; **Machining of functionally graded Ti6Al4V/ WC produced by directed energy deposition,** Additive Manufacturing 24 (2018) 20–29. https://doi.org/10.1016/j.addma.2018.09.007
- O. Oyelola, A. Jackson-Crisp, P. Crawforth, D. M Pieris, R.J Smith, R. M'Saoubi, A.T Clare; **Machining of Directed Energy Deposited Ti6Al4V Using Adaptive Control**, Journal of Manufacturing Processes, Volume 54, June 2020, pages 240-250. https://doi.org/10.1016/j.jmapro.2020.03.004

Conference Papers (not included in this thesis)
Published

- O. Oyelola, P. Crawforth, R. M'Saoubi, A.T Clare; **Machining of Additively Manufactured Parts: Implications for Surface Integrity,** Procedia CIRP, Volume 45, 2016, Pages 119 -122. https://doi.org/10.1016/j.procir.2016.02.066.(Appendix E)

- G. Maculotti, N. Senin, O. Oyelola, M. Galetto, A. T Clare, R. Leach**; Multi-sensor data fusion for the characterisation of laser cladded cermet coatings, Euspen's 19th International Conference & Exhibition, Bilbao, ES, June 2019. (**Appendix E**)**

Acknowledgements

I would like to thank Professor Adam Clare, my supervisor who through patience and guidance, coupled with long hours of input has made this PhD possible. Adam has been a confidant and a reservoir of advice through the period. Also, I would like to thank Dr. Pete Crawforth for his invaluable technical contributions and his encouragement to always look beyond the ordinary throughout the work.

I am particularly grateful to Stuart Branston who helped with the laser deposition trials. The contributions of Alex Jackson-Crisp during this study has been immense and I would forever be grateful to him for his assistance in the accomplishment of this work. Alex has been more than a friend during this period. Special thanks to John Prentice who helped in the early stages of the control system.

I would like to thank my wife and my two lovely daughters for all their encouragement, love and patience during the trying times. They are the reason this work has come this far. I would forever love and cherish them for the support they afforded me.

I would like to also thank my parents and siblings for all types of support I received from them through the study. If only I could find a way to repay.

This work would never see the light of day without the most important of all- I would like to thank the creator of heaven and earth for life and for the grace that has been deposited in me to do exploits.

Abstract

The current manufacturing focus on the reduction of design to part time coupled with the need for more sustainable and economically viable delivery of intricate parts has led to a corresponding interest in the development of metal additive manufacturing processes. This interest has led to parts from these processes being deployed commercially for various applications from aerospace to biomedical functions.

However, current limitations of metal additive manufacturing methods requires the post processing of components produced in this way for eventual use in demanding engineering applications. The tolerances, surface/bulk integrity and homogeneity in builds consistent with typical production specifications cannot, in most cases, be achieved within a single process. Hence, researchers have begun to address this need through research targeted at improving upon these shortcomings.

This study investigates the post-processing of components produced using directed energy deposition. Components produced using these techniques often require post-processing to achieve dimensional tolerances and match end user surface requirements. Heat treatments, grinding, machining amongst other steps are often used in the achievement of surface improvement. Since additively manufactured components differ from wrought materials in terms of microstructure and by extension, mechanical properties, it follows the

machinability of these components also differ to those of wrought materials. This has been proven to be the case.

This present work focuses on the influence of build parameters on the resulting machinability of the components, the use of heat treatments for improving machinability and most importantly, the development of machining strategies for post processing components produced from these technologies. Heat treatments are found to cause a differentiation in measured cutting forces causing a percentage drop when comparing between the as built directed energy deposition component and a beta heat treated component by up to 40 % and 16 % at the same cutting speed for an alpha heat treated component .

In the development of machining strategies, an adaptive machining system for the machining of these components has been developed on an open architecture machine tool. This accommodates for the machining of anisotropic (changing) microstructures which are commonplace in metal AM components. The development of this system is also influenced by the need for seamless machining of functionally graded components which are produced using AM systems.

The use of adaptive machining of deposited components is shown in this study to lead to an improvement in surface finish in milling and drilling operations. Improvement in surface roughness in milling experiments show a reduction of up to 70% in surface roughness and 55% in subsurface deformation depth when comparing machined surfaces. Drilling trials show lower variation in values – up to 2 % in surface finish. However, an important finding - the effects of variation

in cutting forces as machining progressed through the varying microstructure is reported here – variations of up to 15 % (up to 100N) are recorded with increased number of holes drilled and tool use increased – this is correlated to the microstructural variation and grain refinement due to the reheating process during addition of subsequent layers.

Thus, towards obtaining these results, the study encompasses the deposition of materials, characterising before post-processing, post-process machining the components and characterisation after post-processing. Also, the influence of machining strategies on residual stress, surface and subsurface finish condition are all investigated.

List of Figures

Figure 2-1: ASTM classification of Metal AM processing principles [1] 11

Figure 2-2: (a) Powder bed fusion set up (b) Directed Energy deposited system [9] 12

Figure 2-3: Microstructures of Ti6Al4V (a) Wrought (b) Laser deposited [12] 14

Figure 2-4: Deterioration in surface roughness due to stair stepping effect 17

Figure 2-5: Machining (turning operations) for surface improvement and removal of the staircase effect and obvious undulations[35] 20

Figure 2-6: Island scanning strategy on surface of Ti6Al4V build [54] 23

Figure 2-7: Laser clad sample showing pores and crack propagation. Image taken from unpublished work by the author. 24

Figure 2-8: (a) Schematic showing rolling process[71]; (b) profiled and slotted roller design used for WAAM deposits [69] 30

Figure 2-9: Schematic of the laser polishing process showing a deposition and a subsequent polishing process 42

Figure 2-10: Schematic of hybrid additive and-machining process 45

Figure 2-11: Machine tool configurations adopted for integration of DED and CNC machining [124] 48

Figure 2-12: Shape adaptive grinding principle [141] 50

Figure 2-13: Machining induced deformation with different grain sized inserts after machining for 10 s (a) 1.0 µm (b) 0.68 µm. Deformation is more pronounced in (b) [159] 58

Figure 2-14: Adaptive control configuration for a machine tool [172, 177] 63

Figure 2-15: Methodology to develop monitoring system for machining processes [180] 65

Figure 3-1: Graphical abstract of the experimental methods showing dependencies an outcomes 76

Figure 3-2: Material delivery set up for multiple feedstock material delivery (a) Coaxial material delivery (b) Side feeding delivery..... 79

Figure 3-3: CAD image of built components (a) Rectangular block (b) Cylindrical component..... 81

Figure 3-4: (a) Alignment for feedstock delivery in multi component deposition (b) Entire set-up for the deposition of functionally graded components 82

Figure 3-5: (a) Fixture for clamping cylinder (b) Cylinder clamped with fixture 87

Figure 3-6: Direction of forces measured by the dynamometer 88

Figure 3-7: Schematic of process for outer diameter turning trials 89

Figure 3-8: Schematic of milling set up for roughing and finish machining passes. Square substrate dimensions, - 180 mm x 180 mm, thickness 12 mm. Regions machined to diameter of 70.5 ± 1 mm. 91

Figure 3-9: Schematic of cutting force measurement system 95

Figure 3-10: Schematic of process flow showing generic steps for material investigation 96

Figure 3-11: Definitions for surface roughness parameters (a) Ra (b) Rz [190] 98

Figure 4-1: Samples of cylinders deposited for turning trials using DED 107

Figure 4-2: Schematic of cylinder after machining and sectioned with WEDM... 112

Figure 4-3: Optical Microscope images of (a) 'as built' DED and (b) Alpha Anneal DED showing clear layer banding as a result of stacked layers. (c) Beta Anneal DED (d) Highlighted regions in a (e). Highlighted regions in b (f) Highlighted regions in c. All Samples etched with Krolls' reagent 113

Figure 4-4: SEM image showing alpha case formation in beta HT component. Average beta lath thickness in alpha case region = 8.29 µm, average beta lath thickness in deposit interior = 5.51 µm. Image is taken in SE mode 115

Figure 4-5: Microstructures from interior regions of the builds: (a) DED as built (b) DED post beta heat treatment (c) DED post alpha heat treatment (d) Wrought beta heat treatment. Images taken in SE mode 116

Figure 4-6: Cutting force data along the x (Radial), y (Feed) and z(tangential) planes. The acquired data monitors a complete cutting cycle with the corresponding cutting regions highlighted; start, contact, steady state and finish 118

Figure 4-7: Initial machining pass to remove the undulating layer by a machining pass. Tool runout leads to periodic decrease in cutting forces. Radial depth of cut was 0.25 mm in plot shown. Plots filtered with low pass FFT at 10 Hz. 119

Figure 4-8: Increase in average cutting force with increasing in vertical distance from 'outer skin' 121

Figure 4-9: Cutting Forces in the normal direction (fx) from initial machining (pass 1) to achievement of steady state (pass 6). Plots filtered with low pass FFT at 10 Hz. Increase in forces with subsequent passes. Y axis truncated at 250 N. Arrows indicate region in component structure with structural defect from the build process..... 122

Figure 4-10: (a) Variation of machining speed with cutting force (b) Subsurface deformation decreasing with cutting speed in DED components and increasing in the wrought beta sample 125

Figure 4-11: Variation in subsurface deformation with increasing speed (a) DED at 50m/min (b) DED at 100m/min (c) DED at 150m/min (d) beta DED at 50m/min (e) beta DED at 100m/min (f) beta DED at 150m/min (g) alpha DED at 50m/min (h) alpha DED at 100m/min (i) alpha DED at 150m/min (j) wrought beta at 50m/min (k) wrought beta at 100m/min (l) wrought beta at 150m/min. Broken lines included to show visible deformation depth from machined layer. Images taken in BSE mode. 127

Figure 4-12: (a) Effect of variable feed rate on cutting force (b) Deformation depth reducing with increase in feed rate ('as-built' component). Cutting forces shown are average values in the three directions 128

Figure 4-13: Increase in beta deformation in the as built component with increase in feed rate. Images taken in SE mode 129

Figure 4-14: (a) Schematic showing depth of cut variations (b) Cutting force increasing with increase in depth of cut (c) Increase in subsurface deformation with increase in depth of cut. Cutting forces shown are average values in the three directions 131

Figure 4-15: Increase in beta deformation with increasing depth of cut. Images taken in SE mode 132

Figure 4-16: Plot showing comparison of Surface Roughness values for the array of heat treatments used as a function of cutting speeds used in machining. Speeds include 50m/min, 100m/min and 150 m/min. Feed rate = 0.1 mm/rev and depth of cut = 0.25 mm..... 133

Figure 4-17: Increasing depth of cut showing increase in surface roughness in the as built component 134

Figure 4-18: Hardness was evaluated for all microstructural conditions at the machined surface with 300 gf (b) cutting force reduces with reduction in hardness post heat treatment for DED components..... 135

Figure 4-19: PVD coated insert with machining faces highlighted 137

Figure 4-20: Tool wear mechanism on flank face of inserts, showing abrasion and adhesion with different materials when machining at intermediate cutting speed (100m/min), (a) As built (b) Alpha DED (c) Beta DED (d) Billet Beta. Images taken in SE mode 138

Figure 4-21: Figure showing EDS scan results of inserts in Figure 4-20..... 139

Figure 4-22: Effects of process parameters on residual stress in 'as built' components (a) Cutting speed (b) feed rate (c) depth of cut..... 141

Figure 4-23: Optical micrograph of the various regions showing the gradation in microstructure between the wrought, Dilution zone and the DED layers (a) As built (b) Alpha HT (c) Beta HT. Samples etched with Kroll's reagent. 144

Figure 4-24: Surface Roughness of various regions post machining with standard errors included. AB2, Alpha 2 and Beta 2 samples are machined with higher cutting speeds..... 146

Figure 4-25: - Microstructures of the regions showing the DED region, HAZ region, and wrought. Comparison in subsurface deformation depth (after Milling) between AM region and wrought region with varying machining parameters. Images taken in BSE mode 148

Figure 4-26: Deformation depths in the various regions at low and high machining speeds. Errors bars showing deviation along the sample length included 150

Figure 4-27: Hardness relationships at low machining speeds for all regions considered. Error bars indicate deviation from average values along sampled regions 151

Figure 4-28: Residual stress for DED and wrought component regions. Error bars included to show variation in sampled values. 152

Figure 5-1: Functionally graded cylinder, region marked 'a' is Ti only, 'b' is Ti + WC Cylinder dimensions: Wall thickness in 'a' = 4.3±0.25 mm, wall thickness of 'b' = 4.92± 0.32 mm, cylinder height = 25mm, surface condition of both regions pre machining also shown 163

Figure 5-2: SEM image showing boundary between layers in the MMC region showing increased WC diffused content due to re-melting. EDS of highlighted region is taken and is discussed subsequently. Image is taken in BSE mode..... 169

Figure 5-3: Highlighted regions are selected for EDS analysis. Remelted region between clad layers is labelled Region 1 and Region 2 is the region within the clad interior. Image is taken in SE mode 170

Figure 5-4: Set up for machining trials with the component showing the MMC and single material region. After two passes, undulations in single material region were removed and this led to achievement of steady state cutting faster than the WC region due to difficulty of chip formation in MMC region..... 172

Figure 5-5: Schematic showing (a) Particle fragmentation and (b) reinforcement particle pull out mechanisms in MMC machining [215] 173

Figure 5-6: Highlighted region showing particle fragmentation of a WC particle in turning of the MMC region. 174

Figure 5-7: Subsurface deformation in Ti alloy region with different inserts (a) PCD (b) CBN. Visible beta deformation depth is a maximum of 11.8µm in the PCD machined component and 6.3 µm in the CBN machined component 175

Figure 5-8(a-f): Cutting force plots with subsequent passes when machining from outermost layer with PCD insert. Cutting progressed from MMC region to single material in all cases. Cutting force magnitude is indicative of material removal rate. Values filtered with low pass FFT at 10 Hz to reveal machining forces trend. Increase in tool wear also contributed to high rise in forces in single material region. Forces shown are in the radial direction 177

Figure 5-9: Variation in cutting force during machining with various inserts at steady state conditions (a) PCD (b) CBN across the Ti6Al4V region (ii) and the Ti6Al4V/ WC region (i). Values filtered with low pass FFT at 10 Hz to reveal machining forces trend..... 179

Figure 5-10: Average cutting forces in x, y and z directions with varying inserts in MMC and single material region at steady state with a new cutting tool. Error bars show variation in sampled values from the average values. 180

Figure 5-11: Surface condition post machining (a) optical image of surface showing both regions and boundary (b) MMC region (c) Ti alloy region. Images (b) and (c) rotated 90°..... 181

Figure 5-12: Component surface topography from MMC region post machining (a) Typical sample profile showing both material regions (b)CBN machined sample (c) PCD machined sample. Surface maps analysed using Mountain Maps software 182

Figure 5-13: Average surface roughness (Ra and Rz) of all regions post machining, MMC region machined with the PCD tool had highest surface roughness 183

Figure 5-14: Schematic showing particle position in reference to tool cutting edge and cutting edge limits (a) Particle along tool path (b) Particle above tool path (c) Particle below tool path [217]. Size of tool in relation to particle not to scale.... 185

Figure 5-15: Progressive improvement in tool wear condition with increased removal of outermost layer in CBN inserts. (a) Rake face of tool after first machining pass (b) Rake face of tool after second machining pass (c) Flank face after first pass (d) Flank face after second pass 187

Figure 5-16: Inserts after machining for similar duration of 30 secs (a) Rake face of PCD (b) Rake face of CBN (c) Rake face of coated carbide insert (d) Flank face of PCD insert (e) flank face of CBN insert (f) flank face of coated carbide insert..... 188

Figure 6-1: Linux CNC structure [222]..... 196

Figure 6-2: Tormach GUI with override slider controls for Feed rate, Spindle speed and MaxVel highlighted. 198

Figure 6-3: Flow chart showing steps involved in controller interfacing development..... 199

Figure 6-4: CAD model and actual set up of cutting force measurement rig developed. 203

Figure 6-5: VI for manual control of feed rate and spindle speed, also visualisation and recording of cutting forces. 205

Figure 6-6: Graphs showing variable feeds and speeds and the response threshold in cutting forces (a) Feed (b) Spindle speed. Forces shown are in the Z direction. 208

Figure 6-7: Schematic showing entire system components..... 209

Figure 6-8: LabVIEW VI showing front panel and block diagram for adaptive control of the CNC. VI was developed using the scan engine interface 210

Figure 6-9: Plot showing feed and cutting force response in a milling pass on mild steel with a Sine wave signal generator input as feed rate. Low pass filter at 30 Hz was used in filtering data. 212

Figure 6-10: Measured and estimated model output. Estimated model matches the measured up to 73.34 %. Signal to noise ratio accounts for loss in fidelity... 213

Figure 6-11: Plot showing feed and cutting force response in a drilling pass on mild steel with a Sine wave signal generator input as feed rate. 214

Figure 6-12: Measured and estimated model output for the drilling model. Model estimates 84.05 % fit to measured data..... 215

Figure 6-13: Procedure used in PID implementation 217

Figure 6-14: (a) Cutting force, set -point force during milling, controller input in adjusting feed rate to match set point values. Set point adjusted once during milling pass (b) Set point values adjusted multiple times during milling pass with controller effort to adjust feed to desired force value..... 218

Figure 6-15: Mild steel component used for milling and drilling trials 219

Figure 6-16: Cutting force and feed input plots for drilling mild steel component (a) without control system (d) with control system and set-point force was 700N 220

Figure 6-17: Steps in the machining of DED Ti6Al4V to determine the system transfer functions in milling and drilling trials..... 223

Figure 6-18: Plot of Cutting Force, Feed rate and Time from the (a) milling (b) Drilling experiments for determination of transfer function models. 224

Figure 6-19: Cutting force plot for drilling component with wrought and DED region (a) without control (b) Force constrained to 700N. Forces shown are in the drilling direction (z). 226

Figure 6-20: Plots from Milling trials for DED Ti6Al4V with (a) Milling without adaptive control (b) Milling with Adaptive control, set point = 65 N. 228

*Figure 7-1: Optical profilometer scan showing surface condition of the DED component before machining. As built surface roughness values: Ra = 5.27 µm, Rz = 8.35 µm. Difference in height in regions highlighted with top left (0) being the start point of deposition and milling. Values shown are relative to the start point. Component shown is a 30 mm * 30 mm section. 231*

Figure 7-2: Angular Distortion and variation in component build height and effects during face milling 233

Figure 7-3: SRAS scanned image (a) variation in component macrostructure and differences in component grain size (i) DED region (ii) Substrate heat affected / fusion zone (iii) Substrate region (b) Magnified view of highlighted region in 'a' showing regions of grain coarsening as a result of epitaxial columnar grain growth during cooling and also layer 'banding' due to remelting. 234

Figure 7-4: Cutting force in milling outermost layer with the control system. Signals filtered with 25 Hz low pass filter (b) Scan taken with the Alicona of the component with difference in height between points 'a' and 'b' which causes a variation in depth of cut. 236

Figure 7-5: (a) Cutting force plot from milling of the bulk region of DED Ti6Al4V with adaptive control (b) Result from surface profilometer scan showing surface condition of regions machined with AC (i and ii) and without the AC system (iii & iv). A 30 mm x 30 mm section from the build was used in the experiment shown. The grooving which is evident in passes iii and iv is consistent with a higher level of chatter. 237

Figure 7-6: Surface roughness in regions machined with and without adaptive control (a) Component divided into regions with tool progression (b) Ra in the identified regions for both machining strategies (c) Rz in the regions for both machining strategies 239

Figure 7-7: Subsurface deformation in machined regions (a) With adaptive control (b) Without adaptive control 240

Figure 7-8: (a) Component schematic showing regions of residual stress measurements. 'A' region was machined with AC system 'B' is region machined without the AC system. Measured stress values for the regions also shown 241

Figure 7-9: Schematic of process from as built surface condition to drilling of component (a) as built surface (b) Milled surface with up to 1.2 mm of material removed (c) Drilling process 243

Figure 7-10: Cutting force plots at intervals with and without adaptive control system. (a) 1st pass without AC (b) 1st pass with AC (c) 10th pass without AC (d) 10th pass with AC (e) 15th pass ewithout AC (f) 15th pass without AC (g) 20th pass without AC (h) 20th pass with AC 245

Figure 7-11: 'Cutting force - Distance drilled' graphs showing variation in cutting force along layer boundaries. Components machined without control system in plots shown..... 248

Figure 7-12: Optical Microscope images of (a) Cross section of drilled build showing DED, HAZ and wrought regions relating changes in cutting forces shown in Figure 11 to microstructural variations, Regions b, c, d and e relate to : (b) Clad mid region (c) Remelted regions (d) Substrate - Deposit interface/ HAZ (e) Unaffected substrate region. Sample etched with Kroll's reagent 250

Figure 7-13: Microstructure of deposited Ti6Al4V (a) Deposit showing variation in layers due to addition of new layers along entire build (b) Magnified view of region bounded by remelted regions highlighted by broken lines in 'a' (c) Higher magnification view of layer boundary showing variation in microstructure between the layer bands and the deposit regions...... 252

Figure 7-14: Surface roughness of drilled holes with and without AC system (a) Substrate Ra (b) DED region Ra (c) Substrate Rz (d) DED region Rz 254

Figure 7-15: Drilling plots showing passes for 10 holes in a 10 mm Ti6Al4V component. (a) without AC (b) machining with AC and adjusting set point force after 50 secs from 1400 N to 1000 N *256*

Figure 0-1 : force measurements showing variation with spindle speed adjustment. Increase in spindle speed leads to higher cutting force *294*

List of Tables

Table 3-1: Laser deposition parameters. Traverse speed indicated is rotational speed 80

Table 3-2: Parameters for deposition of functionally graded materials 83

Table 3-3: Heat treatment schedule used for DED and wrought Ti6Al4V 84

Table 3-4: Roughing and finishing parameters used in machining components ... 92

Table 3-5: Components and the corresponding finishing regime. Finish 1 is low speed and finish 2 is high speed and high feed rate 92

Table 3-6: Etchant for Titanium alloy 99

Table 3-7: Residual stress parameters 102

Table 4-1: Directed Energy deposition parameters used in fabricating cylinders 106

Table 4-2: Typical cylinder dimensions 107

Table 4-3: Inserts used in the turning DED components and their functions..... 108

Table 4-4: Parameters used in turning of Ti6Al4V 110

Table 5-1: Inserts used, functions, specifications and grades PCD refers to Polycrystalline diamond and PCBN is Polycrystalline Boron Nitride 166

Table 5-2: Parameters used in the machining of the functionally graded cylinders 167

Table 5-3: Elemental composition (wt. %) of phases in the regions (i) and (ii) in Figure 5-3. Tungsten content is higher in the re-melted layers 170

Table 6-1: Effects of PID controllers on a closed loop system [225] 210

Table 6-2: Machining parameters for milling and drilling Mild steel in obtaining a system model 211

Table 6-3: Cutting parameters and cutting tools used in milling and drilling trials 221

Table 7-1: Parameters used for Milling DED Ti6Al4V components 235

Table 7-2: Parameters used for Drilling DED Ti6Al4V components 244

Table 7-3: Statistical values of Surface Roughness (Ra and Rz) for substrate and DED regions machined with and without AC system. All values are in µm 253

Table 7-4: Comparison between surface roughness between both processes 254

Abbreviations

AC	**A**daptive **C**ontrol
AM	**A**dditive **M**anufacturing
CBN	**C**ubic **B**oron **N**itride
CNC	**C**omputer **N**umerically **C**ontrolled
DED	**D**irect **E**nergy **D**eposition
EDS	**E**nergy **D**ispersive **X**-ray **S**pectroscopy
FFT	**F**ast **F**ourier **T**ransform
GUI	**G**raphical **U**ser **I**nterface
HAL	**H**ardware **A**bstraction **L**ayer
HAZ	**H**eat **A**ffected **Z**one
MMC	**M**etal **M**atrix **C**omposite
Nd:YAG	**N**eodymium **Y**ttrium **A**luminium **G**arnet
OD	**O**uter **D**iameter
PCD	**P**oly **C**rystalline **D**iamond
PVD	**P**hysical **V**apour **D**eposition
SAW	**S**urface **A**coustic **W**ave
SEM	**S**canning **E**lectron **M**icroscopy
SRAS	**S**patially **R**esolved **A**coustic **S**pectroscopy
VI	**V**irtual **I**nstrument
WEDM	**W**ire **E**lectrical **D**ischarge **M**achining

Contents

Preface i

Acknowledgements ii

Abstract iii

List of Figures vi

List of Tables xvii

Abbreviations xix

1.0 Introduction 1

1.1 Themes explored in this thesis 3

1.2 Thesis Outline 5

2.0 Literature Review 8

2.1 Additive Manufacturing 8

2.2 Metal Additive Manufacturing 10

2.3 Surface integrity of metal AM parts 16

2.4 Post processing of Metal AM Components 25

2.4.1 Non-Conventional post processing of AM components 26

2.5 Post Process Machining 48

2.5.1 Machining induced microstructural damage 56

2.5.2 Adaptive control in machining 60

2.6 Summary of the literature and knowledge gaps 67

2.6.1 Research opportunities from literature 69

2.6.2 Research Hypothesis..... 72

2.6.3 Research Objectives..... 73

3.0 Experimental Methods..... 75

3.1 Materials..... 76

3.2 DED System..... 77

3.2.1 Directed Energy Deposition of Ti6Al4V 79

3.2.2 Deposition of functionally graded components..... 81

3.2.3 Heat treatment..... 83

3.3 Machining Trials..... 85

3.3.1 Turning Trials 87

3.3.2 Milling and Drilling Trials 90

3.4 Material Characterisation..... 95

3.4.1 Feedstock Material 96

3.4.2 Surface Roughness..... 97

3.4.3 Material Preparation 98

3.4.4 Microstructural Analysis..... 99

3.4.5 Microhardness Analysis..... 100

3.4.6 Residual stress Analysis 101

3.5 Control System Architecture 102

3.5.1 National Instruments CompactRIO..... 103

3.5.2 Microcontroller..... 103

3.5.3 Sensors 104

4.0 Machinability of Directed Energy Deposited Ti6Al4V 105

4.1 Directed Energy Deposition of Ti6Al4V 106

4.2 Turning Trials 108

4.2.1 Tooling selection 108

4.2.2 Machining Strategy 109

4.2.3 Material Characterisation 111

4.2.4 Results 112

4.3 Milling of DED and Wrought Components 141

4.4 Discussion 153

4.5 Conclusions 156

5.0 Machining of functionally graded Ti6Al4V/ WC produced via DED 160

5.1 Background 161

5.1.1 Metal Matrix Composites 161

5.2 Directed Energy deposition of Ti6Al4V/ WC 163

5.3 Turning Trials 165

5.3.1 Microstructure 167

5.3.2 Machining 171

5.3.3 Cutting Forces 175

5.3.4 Surface finish 180

5.3.5 Tool wear 186

5.4 Discussion 189

5.5 Conclusions 191

6.0 Adaptive Machining System Development 193

6.1 Machine Controller 194

6.2 Controller Interfacing 196

6.2.1 Microcontroller 199

6.2.2 Creation of the HAL component 200

6.2.3 Interfacing the system with LabView 202

6.2.4 Cutting Force Measurement 203

6.3 Development of the Control System 206

6.3.1 Adaptive Control System 208

6.3.2 Transfer Function Models 210

6.4 Results and Discussions- Machining trials with Adaptive control . 216

6.4.1 Machining DED Manufactured Components 221

6.4.2 Drilling of DED Ti6Al4V 225

6.4.3 Milling of DED Ti6Al4V 227

6.5 Conclusions 229

7.0 Adaptive Machining of DED produced Ti6Al4V 230

7.1 Milling 231

7.1.1 Subsurface Deformation 239

7.1.2 Residual Stress 241

7.2 Drilling 242

7.2.1 Microstructure Analysis 248

7.2.2 Surface Roughness 252

7.3 Adaptive Machining of Ti6Al4V/WC components 255

7.4 Discussion 257

7.5 Conclusions 260

8.0 Conclusions and further work 262

8.1 Machinability of DED produced *Ti6Al4V* Components 263

8.2 Machining of Functionally Graded Ti6Al4V/ WC 265

8.3 Adaptive Machining of DED produced Ti6Al4V 267

8.4 Future Work 268

References 272

Appendices 283

1.0 Introduction

The drive towards the use of additive manufacturing technologies in the manufacture of production quality parts has led to rapid growth in the industry and an interest in the capabilities of the systems. More commonly known as 3D printing, additive manufacturing is fundamentally a method of manufacturing parts from powder, wire or sheet feedstocks from 3-dimensional model data, using a layer by layer process. Fusion of layers is achieved via melting or solid state joining of the constituents. A number of techniques have been developed for producing parts based on this methodology. Mostly, the differences are in the delivery of feedstock material to the melt pool created, the energy source used or the build volume capability of the process. Directed energy deposition processes involve the use of a wire or powder feedstock delivered into a melt pool and the formation of the required components' shape by the relative motion of the energy beam and the substrate. These processes lend themselves to the repair of components, addition of layers of material to a new component, or for the selective addition of specific materials or material combinations on a part. Electron beam melting and selective laser melting are powder bed fusion (PBF) processes. These processes are capable of producing complex shapes and intricate structures with internal features as the parts are built in a powder bed using a layer by layer strategy.

The appeal of additive manufacturing technology has been the capacity of these techniques to produce parts which cannot necessarily be achieved with subtractive and forming techniques, the reduction in design to part production time and most importantly the material utilization efficiency which is increasingly becoming more important in the drive for sustainability. However, despite the appeal of the technology, a shortfall in part geometrical resolution remains and the development of new machines has not necessarily addressed the problem. Post processing of these components is most often required towards the attainment of the desired form or surface finish. Additively manufactured technologies are only capable of producing near net shape components due to the layer build strategy and the mismatch between the CAD model and the material deposition system. Also, in processes involving powders, since material is fused to form the required shape, there is a need to remove loose material towards realizing surface finish for aesthetic and functional requirements.

Recently, with more adopters of these technologies looking to deploy components from these processes in critical applications, the question of surface finish and post processing of these components has become more pertinent and relevant to the future of these technologies. Economic indices indicate the post processing market for components produced using these methods is rapidly growing and accounts for a large share of the overall global outlay in the use of these technologies. This is further evidenced by the entry of machine tool makers who combine the basic additive manufacturing

system with secondary post processing technologies towards providing so called hybrid machines.

Larger parts with more obvious differentiation in their macrostructures and microstructures are obtainable from directed energy deposition systems and also the importance of these systems to the high value adopters due to increased material deposition efficiency has influenced the decision to investigate the post processing of components produced using this technology.

1.1 Themes explored in this thesis

This study investigates the post processing of components produced using directed energy deposition. Components produced using these techniques often require post processing to achieve dimensional tolerances and match end user surface requirements. Heat treatments; grinding; machining amongst other steps are often used in the achievement of surface improvements. Since additively manufactured components differ from wrought materials in terms of microstructure and by extension, mechanical properties, it follows the machinability of these components also differ to those of wrought materials. This has been proven to be the case, as shown in this work. There is a need for the understanding of material response to tooling designed for wrought materials and to provide information about machinability of these components in relation to standard wrought materials.

This present work focuses on the influence of build parameters on the resulting machinability of the components, the use of heat treatments for improving machinability and most importantly, the development of machining strategies for machining components produced from these technologies. In the development of machining strategies, an adaptive machining system for the machining of these components has been developed on an open architecture machine tool. This accommodates for the machining of anisotropic microstructures which are commonplace in metal AM components. The development of this system is also influenced by the need for seamless machining of functionally graded components which are produced using AM systems. Thus, the study entails the deposition of materials, characterising in the as built state, post processing these components and characterisation after post processing.

Thus, in the achievement of these goals, the approach has been summarized in the following stages which correspond to chapters within this thesis:

- Literature review of post processing techniques for metal additively manufactured components
- Investigation of machining processes and tooling
- Preliminary machining of additively manufactured components
- Sensor selection for the monitoring of process conditions
- Open architecture identification and control system development
- Adaptive control system development
- Implementation and testing of control system

- Surface integrity analysis from case study.

The processes listed have however been iterative and run concurrently. An outline of the rest of the thesis is narrated as follows;

1.2 Thesis Outline

- Chapter 2.0 – Literature review - details additive manufacturing technology with a focus on metal additive manufacturing, the reasons for post processing components from these technologies, the post processing techniques commonly used, machining of metal additively manufactured components, importance of maintaining surface integrity during machining and a review of adaptive machining systems. The chapter concludes with the research opportunities and hypothesis based on the review.
- Chapter 3.0- Experimental Methods details the experimental methods and procedures used in achieving the stated goals. A description of the equipment used in experimental work is given here. Due to the varied nature of the experimental work carried out, a more detailed description is provided in subsequent chapters relating to the use of various equipment. Assumptions used in the work and the necessary deductions used in later chapters are also defined here.
- Chapter 4.0 - Machinability of directed energy deposited Ti6Al4V. This chapter provides a demonstration of relevant heat treatments in promoting microstructure uniformity, machining processes for the material and the

surface integrity and subsurface deformation observed in machining using conventional tooling. The chapter also investigates the influence of machining process parameters on resulting component condition and the relationships with cutting forces.

- Chapter 5.0- 'Machining of functionally graded Ti6Al4V/ WC produced via DED' details investigations on the machining of a directed energy deposited produced functionally graded material – Ti6Al4V/ WC. in keeping with the theme of industrial applications and investigation of extreme cases of machining these components using traditional methods with commercially available tooling. Discussions focus on surface integrity post machining, the prevailing cutting forces and the influence of matrix composition on tool wear and degradation.
- Chapter 6.0- Adaptive Machining system development discusses the development of an adaptive control system on an open architecture computer numerically controlled (CNC) machine tool. The development of a monitoring system and incorporating this as a part of the controller is detailed. Preliminary results from testing this system are presented.
- Chapter 7.0: This details the testing of the developed adaptive control system. The use of the system in milling and drilling trials for materials from a directed energy deposited process. Surface integrity, tool wear and cutting forces are presented here.
- Chapter 8.0 Conclusions and future work, gives an overview of the results obtained, the opportunities from this research work and gives a

recommendation for future studies that can be undertaken to further understand and facilitate machining of components produced using these means.

2.0 Literature Review

This chapter reviews the various post processing techniques used for metal additive components. The shortcomings due to the characteristic build strategy which leads to the need for post processing are discussed. The current state of the art in machining of metal additively manufactured components is discussed and the attendant issues affecting part quality highlighted. Adaptive control techniques in machining are discussed and proposed for machining anisotropic microstructures such as seen in these components. The chapter also highlights opportunities and hypothesis based on the deductions from the review and presents the research objectives of this work.

2.1 Additive Manufacturing

Additive Manufacturing (AM) is a process of joining materials to make parts from model data using a layer upon layer build strategy as opposed to the use of subtractive manufacturing and formative manufacturing [1]. The use of AM systems allows for components initially generated using a three-dimensional Computer Aided Design (CAD) system to be built directly. The parts of the component are broken down into successive layers and the additive manufacturing system proceeds to deposit these layers on the required

platform/ substrate. Most commercially available AM machines use this underlying principle for component manufacture and the main differences are in the method of layer formation and the interrelationship between layers regarding how they are bonded together. These factors affect the productivity of the equipment and the resulting component mechanical properties. Ultimately, it also influences the required effort and type of post processing required for the component [2].

Due to the wide range of capabilities, evolution, usage and popularity of AM systems, they have been referred to using various terms; Rapid Prototyping, Tooling and Manufacturing, Direct CAD Manufacturing, Material Deposit Manufacturing, Layered Manufacturing, Solid freeform Manufacturing, Material Addition Manufacturing, amongst others [3]. AM systems allow for design flexibility and freedom as the constraints inherent in subtractive methods are avoided. Thus, this leads to opportunities in manufacture of complex geometries that would otherwise be impossible or prohibitively difficult to achieve using previous manufacturing techniques. However, there are barriers to the general adoption of AM. These include the need to post process components, the high cost of AM systems and materials and the wide variation in quality of the components produced from different AM systems. Regardless of these barriers, the use of AM technologies for finished part production in various industries is becoming increasingly popular and has witnessed year on year growth with the entry of new machine builders and high value industrial adopters into AM. In the most recent annual report on

the state of the AM industry, Wohlers' estimates an annual growth of $ 1.2 billion in the overall AM industry with particular reference to the number of metal AM machines purchased globally increasing from the preceding year by 80% [4].

Currently, commercially available AM systems are capable of building components of three basic types of materials: polymers, ceramics and metals. AM techniques are also used in fabricating components from composite materials. Composites are a combination of any of the basic material classes; they could be metal-polymer composites, ceramic-polymer composites, or ceramic- metal composites. Due to the advantage of being able to retain the desirable properties of the combined materials, composites have increased in popularity over time and the composites of the three basic classes are also used in AM techniques.

2.2 Metal Additive Manufacturing

Metal additive manufacturing may be classified using various criteria – energy source, build volume, feedstock material amongst others. Frazier [5], in a review of the subject classified AM manufacturing systems into three broad categories based on material feedstock, viz. powder bed systems, powder feed systems and wire feed systems. The current ASTM classification for metal AM systems for a single step processing operation lists the various metal AM systems as being differentiated by the feedstock material delivery and distribution to the melt pool which underlines the basic AM principle and

the process category [1]. *Figure 2-1* shows the ASTM classification of the current state of metal AM for a single step processing operation.

A common characteristic using any of the methods is the thermal history the material undergoes in forming the required geometries. Although cooling rates may be vastly different, these thermal treatment lead to variations in the metal AM parts produced, which differentiates the resulting microstructure and properties of the products from wrought materials.

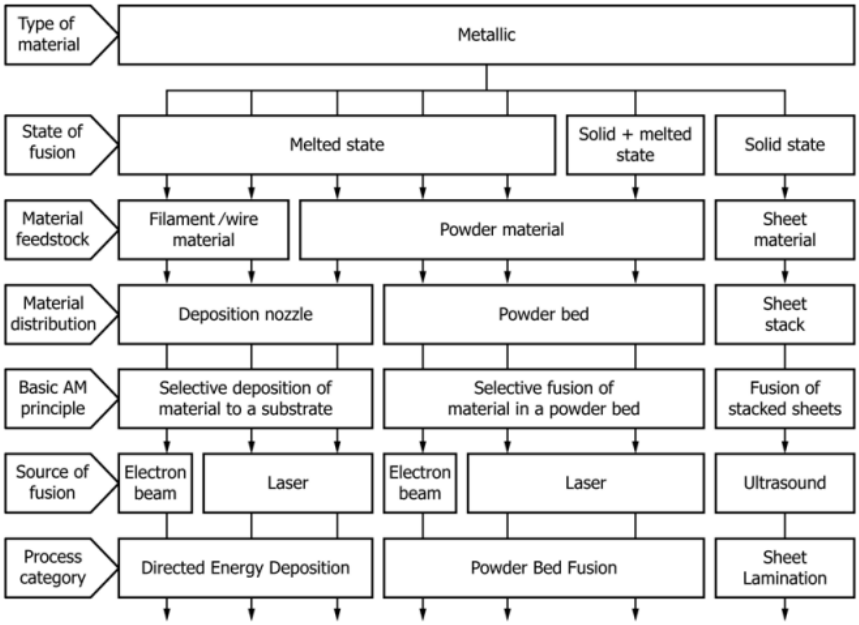


Figure 2-1: ASTM classification of Metal AM processing principles [1]

In metal AM, the material is fed into the energy beams' (electron beam, laser beam, or plasma in arc welding) path and the interaction between the beam and the material causes the material to melt and solidify forming a section of the build. Thin layers of the shape required are built in a 'layer by layer' sequence as the previously deposited layer solidifies. By overlapping individual deposits, a large area can be covered, thus forming the required

geometry. The desired 3-dimensional shape is thus generated from successive deposits of 2-dimensional layers. With control of the heat input into the melt pool, the melting of the substrate is controlled to maintain the integrity of the material added to the surface. However, there is a need to maintain the metallurgical bond at the substrate – deposit interface whilst avoiding the formation of undesirable properties in the component. In directed energy deposition (DED), this can be achieved by understanding the relationship between the deposition parameters. Variables that affect laser deposition capabilities include; energy density, beam spot size, traverse speed, material delivery rate, layer thickness, substrate microstructure, texture, material laser beam absorptivity and reflectivity amongst others [6]. Deposition processes usually undergo rapid solidification with cooling rates of up to 10^3 -10^7 K/s [7, 8], due to the energy input distributed over a thin cross section and the thermal gradient created between the substrate and the deposit. *Figure 2-2* is a schematic showing the operation modes of a powder bed system and a powder feed delivery system.

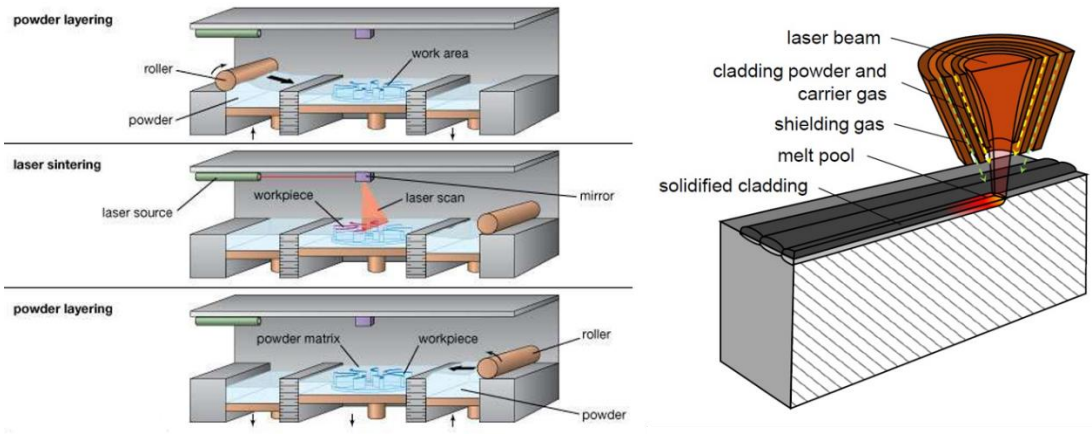


Figure 2-2: (a) Powder bed fusion set up (b) Directed Energy deposited system [9]

Microstructures of the deposited layer in AM are usually different from those produced using wrought and casting means due to the thermal processing they undergo. High input energy with rapid cooling of the resulting components causes this difference. The thermal cycles lead to finer microstructures with directional cooling in most materials often leading to increased yield and ultimate tensile strength when compared to cast and wrought components [10, 11]. An example of this is shown in *Figure 2-3* which shows differences in microstructures between a wrought component and a laser deposited component. Metal AM produced parts usually have anisotropic microstructures due to the various thermal histories and localised solidification rates that can occur within the same component during fabrication. In 'layer by layer' deposition, this characteristic is prevalent as there is a build-up of thermal energy as the build progresses. With the addition of subsequent layers to a build, new heat affected zones are formed which lead to further material variation in regions due to a variation in cooling rates. Thus, layer remelting leads to recurring solid and liquid- solid phase transformations which leads to non-uniformity in the microstructures obtained.

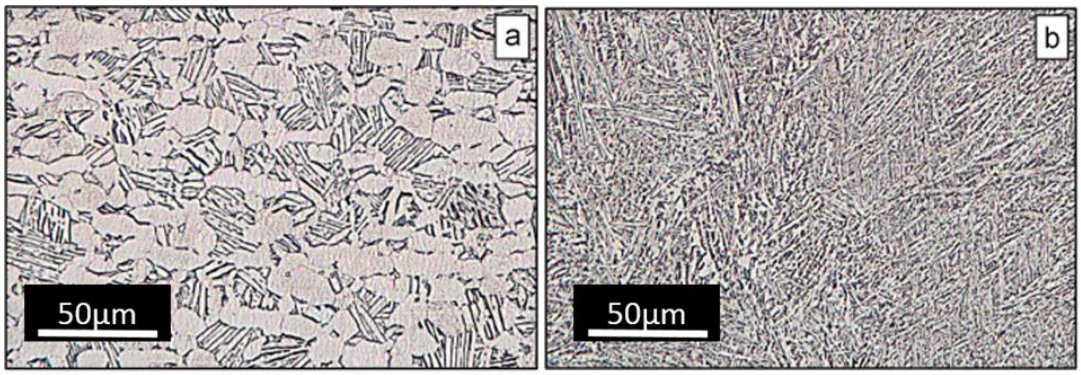


Figure 2-3: Microstructures of Ti6Al4V (a) Wrought (b) Laser deposited [12]

Metal AM processes have been demonstrated with several materials and geometries, particularly for high value applications. In DED systems, several material systems have been demonstrated and have found applications in high value applications such as aerospace and biomedical applications. Titanium and Nickel alloys have generated a lot of interest due to their apparent industrial applications and relevance. These materials can strengthen by deformation and retain their mechanical properties at elevated temperatures. *Ti6Al4V* has been a material of interest due to its desired properties of high strength and formability. Extensive studies on the resulting microstructure, defects, and mechanical properties have been reported [13-18]. This alloy has also been combined with other materials in a laser deposition process with a view to producing 'composite' materials with improved properties harnessing the desirable properties of the individual components [15, 19, 20].

An example of a demonstration application is in use of metal AM systems for the production of parts for dental applications [21]. In the study, the authors

fabricated dental components made of biocompatible metal alloys; Titanium alloy (*Ti6Al4V*) and Cobalt Chromium (Co-Cr-Mo) using a powder bed fusion process. The components were compared to cast and milled components in terms of their corrosion resistance, stiffness and hardness. The components produced were post processed by blasting with glass beads and also grinding with silicon carbide paper. The authors reported increased hardness with increasing energy density as porosity of the build component reduced. In the study, PBF was shown to provide an economical route for producing dental parts with properties comparable to other processes. Chemical tests also show the components maintained integrity when exposed to corrosion promoting effects.

Metal AM technologies provide a solution for utilising material combinations that would usually be difficult to achieve due to the constituent material properties. As these technologies become more widely deployed, there is expected to be an increase in the requested capabilities of the processes. The production of specialized feedstock, new material combinations, functionally graded materials and crucially, the tailoring of individual microstructures and resulting properties to meet specific requirements are expected to increase.

2.3 Surface integrity of metal AM parts

Surface finish requirements for certain applications may be critical as it affects component performance such as wear resistance, fatigue strength and also for component assembly or system performance [22]. It is thus expedient to attain surfaces which can readily go into service with minimal processing. Aesthetic requirements of some components also affect the deployment of such parts for various functions. Requirements for high value applications are even more stringent and dictate high precision parts devoid of surface and subsurface defects. This, and the standardization of quality in these parts has been one of the hindrances to the general acceptance of AM produced components in critical applications.

Anomalies in components produced using AM processes have a deleterious effect on the mechanical properties and can ultimately limit the acceptance and viability of those parts and the adaptation of the underlying process' use in critical applications [23]. According to Vilar [24], defects in components built by directed energy deposition processes can be classified as being due to:

(1) Process constraints – this relates to defects arising from limitations and processing conditions in the deposition process e.g. excessive remelting, deposition instabilities

(2) Material defects- presence of inclusions, partially melted particles

(3) Residual stress related defects

In metal AM, for similar feedstock materials, a consensus is that irrespective of the metal AM process used in the fabrication of components, they are prone to similar defects. One of such shortcomings prevalent in parts built using metal AM technologies is the 'staircase effect'. This occurs as a result of the difference in the amount of material used in actual layer build-up compared to the volume specified by the computer aided design (CAD) model [25]. The anomaly affects dimensional accuracy as well as surface finish for different build directions. *Figure 2-4* shows an illustration of this anomaly.

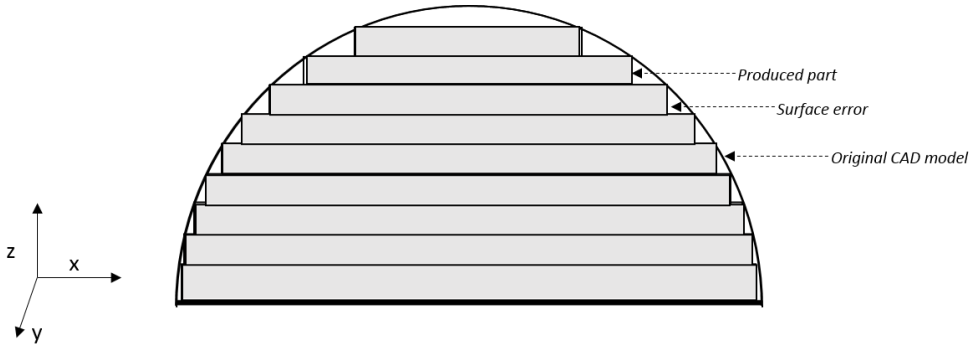


Figure 2-4: Deterioration in surface roughness due to stair stepping effect

However, decreasing the layer thickness will decrease the staircase effect and also improve surface roughness – this however leads to longer process times [26]. Also, control of the layer thickness by adaptive slicing, feedback control and uniform slicing of the CAD model layers have been demonstrated as methods used in reducing the staircase effect and improving part quality [27-29]. Stair stepping is the major contributor to surface roughness at low sloped

angles to horizontal. At higher angles (above 50°), there can be an increase in the amount of partially bonded particles, this compensates for the gaps between layers and accounts for the measured surface roughness [30]. At these angles, there is a discontinuity in the melt pool due to the 'balling' effect- which is due to the difference in thermal gradients within various parts of the molten material causing a difference in surface tension thereby causing material flow by Marangoni convection. 'Balling' causes the melt pool to breakup into small spherical sections scattering droplets of the material on the sides of the melt pool. It occurs as a result of the molten material not 'wetting' well enough to the surface [31]. This negatively impacts multilayer deposition as it leads to a decrease in part density and increases surface roughness [32]. In PBF, it has been reported that a combination of laser power and scanning speed are the primary factors that influence surface roughness. The use of a process window comprising both factors has thus been demonstrated in aiding parameter selection towards improving surface finish [31, 33]. Feature size in AM components is determined by the diameter of the energy beam and the size of the feedstock. Thus, for DED systems which have larger layer thickness, the build is limited to being near net shape as part geometry cannot be adequately defined.

The presence of inclusions, voids, cracks, delamination, porosity amongst other defects within the build affects the integrity and usability of an AM part. For a component, the permissible amount of defects is dependent on the criticality of the component during service. These defects in metal AM parts

affect the post processing of such parts. Post processing procedures can have a positive or adverse effect on a component. For instance, machining a component might lead to an increase in the severity of defects originally present. The presence of inclusions (due to unmelted feedstock) and pores can also be detrimental to the cutting tool edge during machining due to shock impact this can generate. Cracks and voids can also be worsened if present before post processing commences. Usually, machining processes can often lead to various geometrical and metallurgical defects and these defects and their distribution within the build influences the performance of the machined component [34]. On the other hand, aside from the obvious surface roughness improvements attainable, machining can also be used to induce beneficial compressive stresses in a component and remove surface anomalies. *Figure 2-5* shows an example of the use of machining in surface improvement of an otherwise oxidised part with obvious surface undulations due to deposition instabilities during multiple material deposition. The component in the figure was produced using DED and it demonstrates the use of multiple materials in achieving a functionally graded component. Instabilities in deposition during material addition leads to the surface finish observed and subsequent machining was required to match design specifications.



Figure 2-5: Machining (turning operations) for surface improvement and removal of the staircase effect and obvious undulations[35]

For most powder bed AM processes, support structures are required when building surfaces with overhangs greater than 30° [36]. The need for removal of these supports afterwards necessitates additional finishing steps to be carried out. Design considerations to reduce the need for such structures and to also facilitate their removal has been explored and proposed [37].

Residual stresses and deformation are induced in 'as built' metal AM components due to the thermal gradients achieved during melting and solidification of the components. Contraction of melted zones during solidification produces residual tensile stresses which can lead to brittleness and cracking [38]. Dislocations in the solidified material, thermal expansion coefficients of the materials, their elastic-plastic behaviour, the predominant phase transformations and thermal shrinkage are all thought to influence the formation of residual stress [39, 40]. Plati et al. [41] investigated the evolution of residual stresses due to thermal gradient and mechanical deflection during laser deposition of a metal matrix composite (MMC). A finite element model was developed, and the results were reported to be comparable to

experimental results. Changes in the curvature of the component which conformed to the predictions of the model was reported. In the study however, only a single pass of the laser beam which deposited a thin layer of the MMC was done. Similarly, in [42], Ding et al. developed a finite element model for estimating deflection and residual stresses in a large component deposited using wire and arc additive layer manufacture (WAALM). In developing the model, the authors used steady state temperature distributions with an Eulerian reference frame attached to the energy source. Comparable results with the more widely used transient thermo-mechanical model and experimental data was achieved using the model.

The surface integrity of a metal AM part can be further impacted during post processing leading to further undesirable attributes. For instance, during machining operations, the residual stress state of a component is disrupted due to the plastic deformations prevalent [43]. Alterations to the surface during machining processes affects the stress-corrosion properties of a number of materials [44]. A number of authors have postulated on the evolution of residual stresses during machining processes, as reviewed by the authors in [45, 46] .

During cutting operations, residual stress has been reported to be influenced by the grain deformation of the surface layer, which is due to the mechanical action of the tool. Also, a relationship has been shown to exist between the tool temperature and the in depth profile of residual stress [47]. Another study postulates the region ahead of the cutting edge undergoes compressive

deformation whilst the region behind the tool experiences tensile deformation. Resultant stress state of the component would thus be dependent on the resultant of the various stress effects on the component [48].

Fatigue life, corrosion and wear resistance are all dependent on the final residual stress state of the material. They can either be compromised or enhanced, depending on the residual stresses present in the part. In limiting the effects of residual stresses in AM components during the build process, it has been reported that pre-heating substrates and manipulation of the heat source as well as adapting the scanning pattern is beneficial [49, 50]. High pressure rolling has also been demonstrated to induce beneficial compressive stress in larger DED components [51]. In an attempt to reduce the residual stresses in a PBF built part, the authors in [52] used an 'island' scanning strategy. In using this method, the build volume is divided into small squares. Within each square, the laser spot is rastered in a single direction which is perpendicular to the direction of the squares adjacent to it. The strategy thus gives a checkerboard pattern. The aim was to reduce the temperature gradients by distributing the process heat. In a more recent study [53], directional adaption of the scanning strategies was demonstrated with the aim of reducing residual stresses and increasing bulk density of PBF parts.

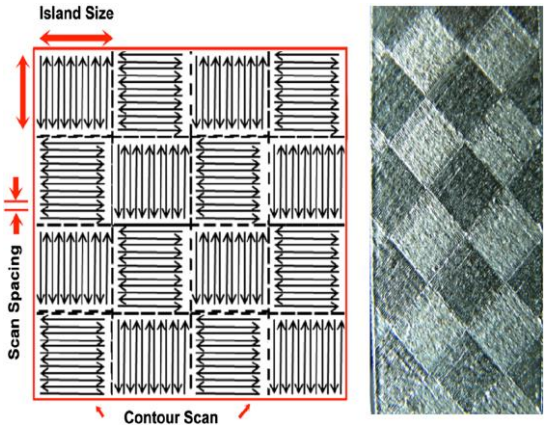


Figure 2-6: Island scanning strategy on surface of Ti6Al4V build [54]

Porosity has been shown to have a deleterious effect on the mechanical properties of AM components if not properly controlled [55-57]. Pores are usually generated as a result of a number of mechanisms which can include; gas entrapment, gas condensation and shrinkage porosity [51]. Irregular or clustered pores promote crack propagation due to the high stress concentration. In DED components, pores can also be a result of mismatch in deposition parameters during multilayer and large area deposition. Two types have been reported in DED components – interlayer and /intralayer porosity. Interlayer porosity occurs due to insufficient energy input during deposition leading to unmelted regions. Intralayer is a result of using inert shielding gas during deposition leading to gas entrapment [58]. The type and distribution of pores formed in AM components is closely related to scan speeds and scan strategy used in fabricating the component and can also be a result of pores already present in the feedstock powder [59]. *Figure 2-7* shows laser deposited samples with a high distribution of pores between subsequent

layers of the deposit. Crack propagation through a deposit region to the substrate surface is also shown.

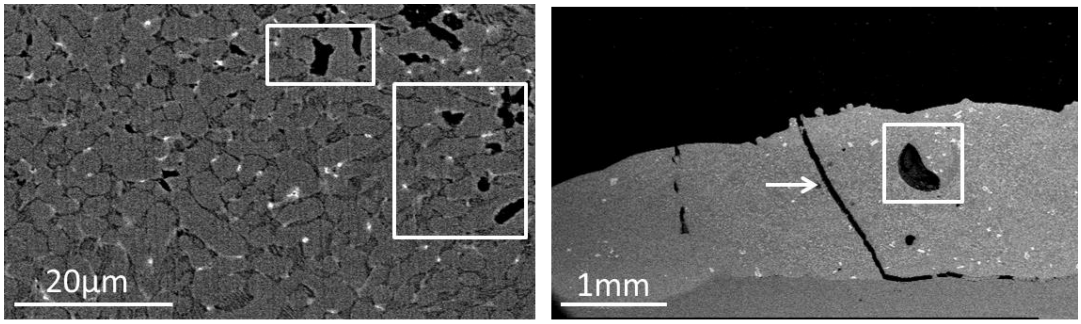


Figure 2-7: Laser clad sample showing pores and crack propagation. Image taken from unpublished work by the author.

It is thus necessary to ensure that the number of defects should be reduced to a minimum through the selection and use of the appropriate process parameters in both the AM process stage and the post processing of resulting components. Parameter selection and post process effects on the resulting deposits have been widely studied for different materials using various AM technologies. To reduce the influence of defects, minimise their occurrence and provide a viable means of post processing AM components, hybrid workstations and in situ monitoring systems have been proposed and developed.

2.4 Post processing of Metal AM Components

Due to the layer by layer build strategy and as a result of the requirements for part quality, several post processing techniques are used for component surface quality improvement. The post processing method adopted is dependent on the criticality of the surface finish required and the metal AM technique used. For example, in PBF processes, support material removal is a necessary step towards attaining part quality requirements. In addition, for such processes and other AM systems involving the use of powders, removal of loosely adhered powder components is also required as a starting step. Design processes have also evolved towards integrating build support structures as a functional part of the component itself. A number of investigators have reported on various post processing techniques used in meeting production quality requirements of AM produced components. Here, for differentiation and to ensure clarity, techniques other than machining used in improving part quality post deposition are classified as non-conventional techniques. These methods are discussed subsequently.

2.4.1 Non-Conventional post processing of AM components

Non-conventional methods of post processing are particularly useful in post processing of components with complex geometries and internal structures. These techniques are commonly used as a first stage post processing step either with other techniques or as a standalone process where subsurface condition is critical and would be more beneficial compared to machining processes or in cases where machining is not entirely practical as a result of component shape.

2.4.1.1 Electrochemical Machining

The use of Electrochemical machining in improving surface quality of a component built using Electron Beam PBF was demonstrated in [60]. Krolls' reagent was used in the study for etching Electron Beam PBF fabricated component made from *Ti6Al4V*. In the study, comparisons between the etched component, a machined part and an 'as-built' part were carried out. The authors reported improvements in the ultimate tensile strength and the yield strength for the post processed components, thus showing the surface condition has a profound effect on the mechanical properties of the samples. Machining gave the smoothest surface finish in the study. Chemical polishing has been demonstrated for removing particles of partially melted powder in a component built using Laser beam PBF [61]. The authors used the method

in post processing ''scaffolds'' made from Ti6Al7Nb and used in tissue engineering for treating cavities in bones. The authors reported favourable material removal rates and repeatability of the process by controlling the chemical bath concentration, the immersion time and also using a magnetic stirrer for agitation of the set up. In [62], the authors demonstrated the use of electrochemical polishing in the post processing of Inconel 718 components produced using PBF. In the study, the authors reported improvement in surface roughness with increasing polishing duration. Conversely, the components' hardness and the Young's modulus found to be higher in the 'as built' component when compared to the polished specimens. The variation in properties was attributed to a reduction in surface residual stress and the dissolution of the strengthening phase after the polishing process.

Anodization has been demonstrated to be a viable means for post processing porous parts manufactured using Laser Engineered Net Shaping (LENS) – A DED process. Das et al [63] reported that anodization of titanium implants fabricated using this process improved the biocompatibility of the implants due to the surface becoming hydrophilic after processing, thus allowing liquid to penetrate deeper into the structure and subsequently promoting wettability. In [64], Vaithilingam et al demonstrated coating of a self-assembled monolayer (SAM) to a PBF part. SAM's are useful in tailoring surface properties to promote biocompatibility of a surface. In the study, they were used for surface modification of Ti6Al4V components. The PBF components were coated with the SAM in the as built condition and with the

surface mechanically polished. The authors reported both cases gave similar wettability results and the higher surface roughness of the as built part did not influence the stability of the SAM.

In [65], Yang et al commented on the suitability of using chemical machining and electroplating for surface improvement in AM parts. The authors discussed that chemical methods can only reduce satellite structures and not completely eliminate them. Therefore, the fatigue performance would be considerably lower when compared to machined components. Similarly, electro- polishing of Ti6Al4V components produced with Electron Beam PBF has also been investigated [66, 67]. Significant improvements in surface roughness and fatigue life with increase in electro-polishing time was reported with a loss in shape accuracy of the part due to non-uniformity in agitation. Studies on the electrochemical machining of metal AM parts in literature have mostly focused on the post processing of parts for medical purposes.

2.4.1.2 Compressive stress induction

High pressure rolling reduces distortion and induces compressive stresses by applying a large compressive force in the normal direction to an objects' surface which causes plastic expansion in the longitudinal direction. Rolling is suited for metal AM applications with comparatively large build volumes such as the Wire and Arc Manufacturing (WAAM) process. In a study to investigate the effects of rolling in situ and after deposition is completed, the authors

found that post deposition rolling impacted the material residual stress distribution, whilst in situ rolling had no effect on the residual stress distribution. This was attributed to the time it takes the material to cool and yielding which still occurs during cooling. Compressive stress applied to the build during the cooling period is less effective as the thermal contraction has a larger effect on the structure of the component at elevated temperatures. Consequently, it was concluded that mechanical post processing techniques at high temperatures are not suited to relieving residual stresses as the structure is still prone to metallurgical changes due to the effects of cooling [68]. Within the scope of the study, the effects of dynamic loads and constant load on the residual stress distribution in a weld was also evaluated. In [69], Colegrove et al. demonstrated the viability of using rolling as a post processing step in a WAAM process. Two rollers with different profiles- ''profiled'' and ''slotted'' were used in the study with rolling done at varying intervals. The slotted roller was reported to provide better reduction in distortion to the deposited profile. The slotted roller provided additional side restraints which resulted in a larger strain in the longitudinal direction [70]. A schematic of the rolling process is shown in *Figure 2-8.*

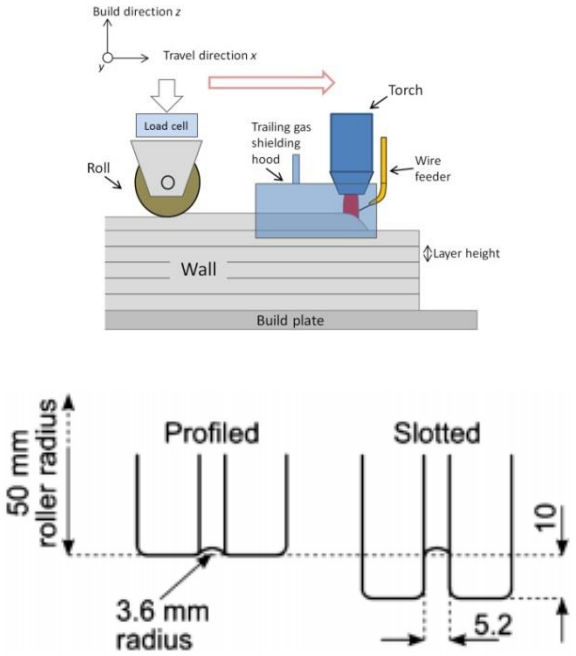


Figure 2-8: (a) Schematic showing rolling process[71]; (b) profiled and slotted roller design used for WAAM deposits [69]

Shot peening processes have been used to influence surface compressive stresses towards the improvement of properties. The use of shot peening to relieve tensile stresses at the surface of a metal AM part was investigated in [72]. Parts built using laser sintering were stress relieved before being shot peened. Improvements to the surface roughness and decrease in porosity were reported. In a comparison between shot peening processes and Ultrasonic Impact Treatment (UIT) for inducing compressive stresses in welds, shot peening was reported to produce a compressive layer comparable in magnitude to the UIT process but only up to a depth of 0.8mm in the weld [73]. This was half the depth of the compressive layer due to the UIT process. Residual stress was measured using X-ray diffraction and neutron diffraction methods. The effect of shot peening on improving mechanical properties of

PBF fabricated stainless steel components was investigated by the authors in [74] . The authors reported shot peening led to grain refinement at the surface and induced a martensitic phase transformation. In [75], the authors demonstrated shot peening of a PBF produced AlSi10Mg component. They reported the near surface regions had undergone strain hardening and this was reported to limit the growth of micro-cracks.

2.4.1.3 Heat Treatment

Heat treatments are often used for optimising mechanical properties, ductility and improving machinability. Due to the dynamic thermal gradient characteristic, layered manufacturing processes are often plagued with residual stresses and anisotropic microstructures. The residual stresses are a result of the contractions due to the deposition of subsequent layers of material [76]. In metal AM, post heat treatment processing forms an integral part of most processes in the quest to produce fully dense parts whilst preventing crack propagation and enabling microstructural control. The ASTM recommends heat treatments as a requirement for powder bed AM processes towards ensuring homogenisation of the components post build and also matching quality specifications [77]. In [78], Shiomi et al. proposed a model for the reduction of residual stresses in a chrome molybdenum steel component built using PBF. It was estimated that by using heat treatment for stress relieving, the tensile stress could be reduced by up to 70% of the as built value. The model assumed conditions for a sample placed in a furnace for an

hour at 600°C to 700°C. A comparison was also carried out with other processing methods with the purpose of reducing the tensile stress. The authors computed the effect of laser re-melting on residual stress and also the influence of pre-heating the base plate, which subsequently increases the temperature within the powder bed. Both methods also showed a substantial reduction in residual stress. Heat treatment of medical grade Ti6Al7Nb components manufactured with PBF and used as implants has also been reported. In [79], Sercombe et al. attempted to alter the microstructure of as-built components to produce a microstructure which is thought to promote fatigue resistance. In the study, the authors used a number of heat treatment and cooling strategies towards achieving the desired objective. They concluded the optimum treatment in terms of α colony size, was that done with a temperature above the β transus and with moderate cooling rate.

Brandl et al. [80] showed the effects of pre-heating and post heat treatment on the fatigue resistance of as built metal AM components of an aluminium alloy commonly used for castings. The effects of the build direction on fatigue resistance were also evaluated. It was reported that both pre and post heat treatments improved the fatigue resistance, and the effects are more evident when compared to the influence of build direction.

The effects of heat treatments on components fabricated using direct laser deposition has also been reported. Investigating with a *Ti4Al1.5Mn* alloy deposited using DED and subsequently heat treated, Tian et al. [81] reported an initial increase in impact toughness which decreases with increase in

annealing temperature. In the study, the maximum impact toughness achieved was up to 51% higher than the as-deposited alloy. In a subsequent study [82], the authors discussed the effects of anneal parameters and cooling rates on the microstructural and tensile properties of the alloy, reporting an increase in tensile and yield strength with increasing anneal temperature with both air and water cooling strategies. In [83], the authors reported improved ductility in laser deposited *Ti6Al4V* for scaffolds after specimens were annealed at 950 ^{o}C to 1050 ^{o}C. The aim was to achieve conformity to ASTM limits for ductility in *Ti6Al4V* implants. The authors reported the optimum values for annealing the component was at 950 ^{o}C with furnace cooling. In [84], the authors compared yield strength and ultimate strength for a laser fabricated part to a conventionally manufactured part. A process window for the optimum laser fabrication of stainless steel (grade- *SS034*) was presented. It was concluded the yield strength in both scenarios was similar but there was a significant difference in the ultimate strength. The component formed was less ductile compared to wrought *SS304*. This difference was attributed to the rapid cooling post fabrication. During production of wrought *SS304*, it is annealed to limit residual stress formation.

Lu et al. [85] investigated the influence of annealing treatment on the microstructural evolution of laser deposited *Ti6Al4V* alloy. The authors reported on the effects of anneal temperature; time; cooling rate and post anneal aging treatment on microstructure and hardness. In the study, it was reported annealing with temperatures below the β transus temperature in

the α+ β phase leads to the formation of a bimodal microstructure which consist of plate primary α and transformed β. Relative volume fraction of the primary α to the transformed β increases with decrease in annealing temperature. It was also reported that there was a reduction of 5% in micro hardness after annealing. Increase in aging temperature however causes an initial increase in micro hardness. However, with increasing aging temperature, micro hardness decreases. Micro hardness of the aged alloy is however reported to be higher than the annealed and as-deposited samples. Similar results were reported in [86] where the authors attributed an initial increase in tensile strength and decrease in ductility of a heat treated sample to a microstructural evolution which involves the coarsening of the primary and secondary α laths with increasing solution time.

2.4.1.4 Hot Isostatic Pressing (HIP)

Hot isostatic pressing (HIPing) process has been extensively used for the removal of pores without adversely influencing the microstructure. The process is capable of removing both macro and micro-porosity [87]. In HIPing, the component is placed in an envelope capable of deforming in a plastic manner and is of a larger size filled with a consolidating powder. As densification occurs, the powder shrinks causing the application of isostatic pressure in all directions. The combination of temperature and pressure achieves a density at a lower temperature than would be required for a sintering process, limiting the effect of undesirable grain growth [87].

Ti6Al4V components built using PBF were post treated using HIPing to improve their material properties in [54]. The authors, combining heat treatment of the built samples with HIPing demonstrated the process effectively reduced the porosity, and subsequent heat treatment of the components did not lead to the reopening of the closed pores- they postulated this was due to the pores not being originally formed by trapped gases but by partial melting of surfaces which subsequently affects the spread of molten material, limiting penetration. The investigators also showed the components had comparable physical properties to thermo-mechanically processed and annealed material after post processing. Post treatment with HIP was shown to have a strong effect on fatigue behaviour in PBF samples. Similarly, Zhao et al in [88] compared properties of Ti6Al4V samples fabricated using two PBF processes (Laser PBF and Electron beam PBF). The authors commented on the effects of HIPing on the microstructural changes observed using both processes. It was reported the HIP treatment coarsens the 'α' lamellae in both cases with the Laser PBF samples having thicker, longer 'α' lamellae. There was thus a subsequent decrease in tensile strength and an increase in ductility in both cases, however, this was more pronounced in the Laser PBF component.

In comparing PBF as built components, heat treated components and HIPed components, the authors in [89] inferred the HIPed components showed improved performance under high cycle fatigue conditions. Santos et al [90], discussed HIPing as one of the additional post processing techniques aside

from machining which was demonstrated in improving the fatigue strength of a PBF built component. In a similar study, the authors in [52] used HIP in post processing a Ni based superalloy (CM247LC) produced from a metal AM process. It was reported the process was useful in closing internal cracks but surface cracks remained unaffected.

In [91, 92], HIP was used in the post processing of bronze-nickel parts fabricated using a laser PBF process- selective laser sintering (SLS) . Glass encapsulation was used due to the ability of shaping glass to conform to the part geometry, with the sample placed within and the vessel evacuated to prevent contamination. Various temperature and pressure values were used in densification trials to determine the optimum combination. Density was reported to increase with increasing temperature and pressure. It was reported that at low temperatures, chemical homogenization takes place as the bronze phase disappears leaving behind pores and there is an expanded solid solution of bronze in nickel. Parts processed at high temperatures and pressures also showed partial homogenization but exhibited nearly full density with the absence of pores. A SLS/HIP hybrid process was developed for the production of high value components used in defence aircrafts [93, 94]. In the study, the aim was to reduce the cost associated with the removal of the encapsulation skin required for the HIP process and ultimately reduce the process complexities. SLS was used to consolidate the powder layers and boundaries in situ. This is then post processed using containerless HIP to the required density. Components produced using this method reportedly

showed similar properties to those produced by glass encapsulation HIP and conventionally processed materials. They reported using this method eliminated the need for tooling and pre- processing steps. Also, container-powder interactions are also avoided [95]. More recent work on a hybrid PBF/ HIP system has been done by Qiu et al [96]. The authors predicted using finite element models the shape of tooling required for HIPing and incorporated this in the component design. They however reported good bonding between the PBF produced tool and the consolidated powder after HIPing. In [97], Kobryn and Semiatin successfully used HIPing in eliminating porosity in a component built using a DED process- LENS. Components built with the same process parameters and different post processing regimes where compared for viability of the post processing system used. Samples were either annealed or HIP'ed. It was reported the samples had similar Widmanstatten transformed beta microstructure - however the HIP'ed components showed a coarser alpha phase. The coarser structure being weaker affected the material properties resulting in the material showing less yield and ultimate strength in comparison to the annealed component. It however showed better ductility due to the absence of porosity.

Similar results showing a reduction in yield strength and ultimate strength when compared to heat treated components were obtained in a study to determine the effect of HIPing on the structural integrity, microstructure and mechanical properties of DLD'ed Ti6Al4V structures [98]. HIPing was reported to reduce the effects of distortion on clamped samples whilst also causing a

reduction in size and quantity of pores found in the samples post deposition. It was also reported to promote the transformation of martensite to lamellar α + β. The stability of Electron Beam PBF fabricated Ti6Al4V components for biomedical applications was characterized for stability after heat treatment and HIPing [99]. Microstructural coarsening which is a result of the growth of the lamellar structure was reported. Invariably, and as reported by other authors, this coarsening effect leads to decreased strength and a corresponding increase in ductility.

Blackwell [100], investigated the use of HIP in post processing a component built from Inconel 718 and fabricated via direct laser deposition on an Inconel 718 substrate. The author reported a difference in the grain growth and elongation post HIP treatment, pointing to a difference in reaction to HIP processes between AM parts and wrought components. This was also shown to impact the material properties as tensile tests post HIPing showed failure from the substrate region. Similar results were reported on the grain growth post HIPing in a study with the same material [101]. In the study, it was reported the process temperature has a larger influence on the process when compared to the operating pressure. Optimum temperature and pressure parameters for the HIPing process were also discussed.

2.4.1.5 Surface treatment with Energy beams

Surface modification of metals using heat treatments has been shown to improve material characteristics and properties. However, the use of high

energy beams (lasers/electron beam) ensures the improved control of the beam towards obtaining the required microstructures and properties within various parts of a build. It also has the advantage of ensuring only the target surface is treated. A surface layer exposed to a high energy beam undergoes rapid heating, melting and evaporation leading to modifications in the material and improvement of surface integrity. As the beam passes and the process is completed, rapid solidification at the melt zone occurs, which leads to the creation of improved physiochemical and strength properties [102]. These surface treatment techniques have also been used in increasing corrosion resistance without affecting the bulk mechanical and physical properties [103]. Electron beams have advantages over laser beams as they have been reported to possess better energy conversion efficiency, optimum absorption by the material surface which is independent of surface optical properties and faster scan speeds [102, 104]. A setback in using these processes is the formation of micro-cracks and heat affected zones in the regions exposed to the energy beam.

2.4.1.5.1 Laser polishing / Remelting of AM parts

Laser polishing is the melting and subsequent solidification of a micro layer of a component using a laser beam with the intent of improving the surface microstructural properties with surface tension causing material to flow from peaks to valleys [105]. For laser polishing to be successful, the energy of the heating source needs to be controlled to limit the extent and the subsequent effects of re-melting. Selective laser polishing has been used in design

processes to produce surfaces of varying quality and appearance. Selective Laser polishing allows for modification of localised regions within a component making it possible to attain varying surface properties within the component [106, 107]. A similar method was used in structuring metallic components by reallocating material when the material is molten [108]. When this process is utilized in improving a surface initially developed with a laser process, it is referred to as laser re-melting. To improve the density of parts produced using metal AM processes, this method is used with different build strategies [109]. In using this for post processing, there is usually no need to remove the part from the build platform and thus avoiding fixation errors [110].

In [111], the authors described a process of laser polishing a part originally built using PBF. In the study, the authors demonstrated the process using a CO_2 laser with a Gaussian profile installed within a 3-axis gantry set up. The authors successfully reduced the surface roughness of the sintered components and deduced from experimental work and design that the most important parameter in laser polishing is the laser energy density. It was also concluded that laser melting affected the surface hardness due to the formation of a homogenous surface without cracks or porosity. The authors in [112], demonstrated laser polishing of PBF produced components using a continuous wave fibre laser and concluded surface roughness achievable is dependent on the melt pool velocity, which is a function of the speed and the laser power.

Laser re-melting has also been shown to reduce interlayer porosity in PBF components. For this, after a layer is formed, it is scanned again with the laser beam before another layer of powder is added to form a new layer. This build strategy provides a means of modifying the properties of the internal structures in a build [113, 114]. In [115, 116], laser re-melting was used in improving the density and surface roughness of a stainless steel part built using PBF. It was reported to be beneficial in the elimination of pores within the build. The authors in a similar study [117] investigated the effects of laser surface remelting on a Ti6Al4V component. It was reported the use of laser remelting with optimised laser power and scan speed led to; improved surface roughness, an increase in micro hardness due to the formation of finer microstructures, and an improvement in the part density. The authors in [118] demonstrated the influence of laser polishing on the surface properties of additively manufactured Ti alloys. In the study, a change in microstructure occurred as the polished regions consisted of α' martensitic phase due to the thermal conditioning the region undergoes. As a result of this transformation, hardness was reported to increase with a corresponding improvement in wear resistance.

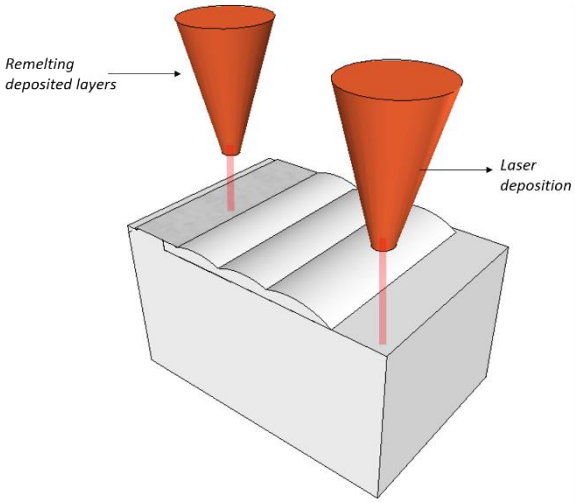


Figure 2-9: Schematic of the laser polishing process showing a deposition and a subsequent polishing process

In [119], the authors demonstrated a strategy for laser polishing which involved multiple passes of the laser beam on a DED component. The effects of the shielding gas on reducing oxidation during the laser polishing process was highlighted. The use of this technique was demonstrated on a thin part to replicate an industrial application of the process and a surface roughness improvement of up to 62% was reported. The effect of multiple laser passes on the microstructural properties of the component was however not discussed in the study.

Laser polishing of an Inconel alloy deposited using DED has been demonstrated [120]. The aim of the study was to find an alternative means for polishing the alloy due to the hardness and difficulty in polishing using conventional methods. The authors reported two mechanisms that occur during laser remelting - Surface shallow melting (SSM) and Surface over melting (SOM). They both affect the surface roughness and are due to the energy density. The polishing regime in effect is dependent on the thickness

of the melted layer. In SSM, the layer thickness of the melted zone is less than the peak to valley distance. Conversely, SOM occurs under the condition of high energy density which leads to the melted layer thickness being greater than the peak to valley distance. This leads to the formation of a material melt pool, which invariably leads to an increase in surface roughness [105]. However, a drawback of this approach is the effect of remelting on surface chemistry. Surface chemistry plays a crucial role in determining the surface properties of a material. The effect of remelting on the surface chemistry of a *Ti6Al4V* component produced with PBF was investigated by the authors in [121]. In the study, the authors found increased concentration of aluminium and vanadium at the surface of the component after laser remelting. Also, a surface oxide layer was reportedly formed due to the remelting process. This would have an adverse effect on any subsequent post process machining of the component as the formation of a surface alpha case in titanium causes an increase in surface hardness.

2.4.1.6 Hybrid Workstations

The growing popularity of AM in building production parts and the need for post processing such parts has led to the development of hybrid workstations which have capabilities to combine both additive and subtractive manufacturing (SM) technologies. These workstations allow for design flexibility and facilitate the use of AM technologies in producing high value components with complex geometries. The capability to add and subtract

material simultaneously from a workpiece opens up opportunities in the development of intricate structures with internal and external features and the repair of damaged parts. Aside from the cost saving implications, there is also a positive environmental impact as waste is reduced. Process capability and design is enhanced with the use of these workstations as they allow for feedstock materials to be converted into production parts in one set-up [122, 123]. Hybrid machines also advance possibilities of the use of multiple materials in producing functionally graded components. Through a simultaneous and controlled interaction between the processes, quality and repeatability is enhanced as parts can be inspected and re-worked to achieve conformity to specifications [124, 125]. These workstations have also been introduced to eliminate the need for removing a component and setting up on another machine for further processing, thus eliminating the need for the purchase of multiple machines and ensuring effective utilisation of workspaces and man hours. The use of hybrid systems has been reviewed and reported by various authors. However, due to the relative lack of published research work in the area of post processing, this closely related aspect has not provided much understanding on issues such as the machinability and the metallurgical effects of post processing metal AM components.

Hybrid workstations in manufacturing technology context have been extensively used to describe enclosures which have multiple capabilities due to a combination of various technologies [125]. It has been defined with respect to multiple machining processes incorporated within a system to

achieve higher material removal rates and optimize efficiency by leveraging on the advantages of the individual processes [126-128]. When used in the context of a machining station, the strategy is such that, one of the processes is actively involved in material removal whilst the other process promotes material removal by changing the processing conditions to enhance machining. An example is use of a laser assisted machining system. The term has also been used to describe a combination of two or more processes with different mechanisms of material removal [129, 130]. In additive manufacturing, it has been used to describe processes that involve deposition of various material combinations/ processes under varying thermal conditions [113, 131].

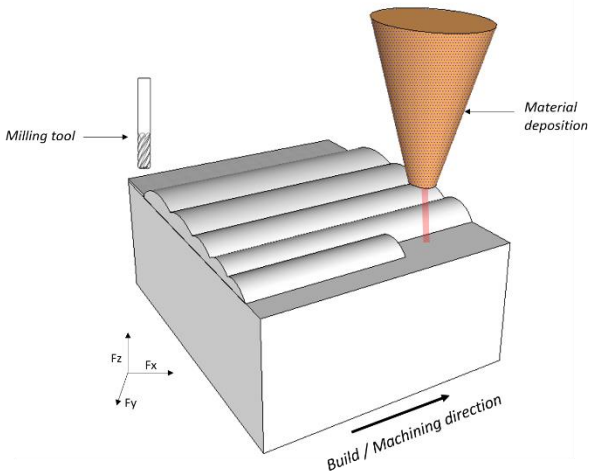


Figure 2-10: Schematic of hybrid additive and-machining process

Kerschbaumer and Ernst [132] developed a hybrid laser deposition and CNC machining system with which a finished (deposited and post processed)

component was produced from a CAD file. A laser deposition nozzle with coaxial powder feeding delivery was incorporated in a 5-axis CNC machine in the study. The set up permitted for multiple build planes and development of intricate geometries with reduced requirements for support structures, also avoiding molten material flow along an inclined build surface. Machining was possible along these planes due to increased tool accessibility and multiple axis access of the machine tool. The authors favoured the use of powder feedstock for deposition over wire as it allowed for the combination of multiple materials in one part - More than one powder-feeding unit was used for delivering powder at different feed rates. Cutting fluid was not used during machining due to the intermittent laser deposition process. Wei et al [133] demonstrated the use of a hybrid system comprising of a PBF system and a milling tool in the manufacture of a Maraging steel part, whilst comparing the resulting components to those fabricated using only the PBF process. The authors concluded microstructure in both cases differed and higher hardness was reported in the components fabricated with the hybrid arrangement.

In [134], Ren et al demonstrated a surface patching method for die repair which excluded the pre-machining of the damaged part and using an adaptive zigzag pattern for toolpath generation. In a study to demonstrate the efficacy of a hybrid manufacturing system in repair of components, a set-up which comprised a laser deposition system, an inspection system and CNC machining was used in the repair of a turbine blade [135]. In using the process

for blade tip repair, the blades used were from stock initially rejected for reconditioning. By combining all these processes, the repair was reported to be completed. Also, by incorporating automatic tool changers in the set up, it was possible to use coolant during the machining step as the laser optics were stowed away during the machining process.

In [136], the development of a hybrid machine with a laser metal deposition system incorporated in 5-axis CNC workstation comprising turning and milling capabilities with tool changers was discussed. A demonstration of the cost saving capabilities of using such system was discussed by the authors in the study. Using an example of a part used in the oil and gas energy industry and usually machined from a billet of Inconel 718, the authors substituted less sensitive areas of the component with stainless steel whilst depositing the Inconel coating to areas more susceptible to damage. The capability to selectively deposit material and machine difficult to reach areas made it possible for the structure to be fabricated. Significant cost savings were estimated by the authors in using this method with the equipment developed.

In a review on the development of hybrid systems incorporating AM with material removal systems, machine tool configurations which have been developed by various machine builders and the commercially available machines were discussed [124]. A schematic showing the different available machine tool arrangements and orientations in relation to the component being built is shown in *Figure* 2-11.

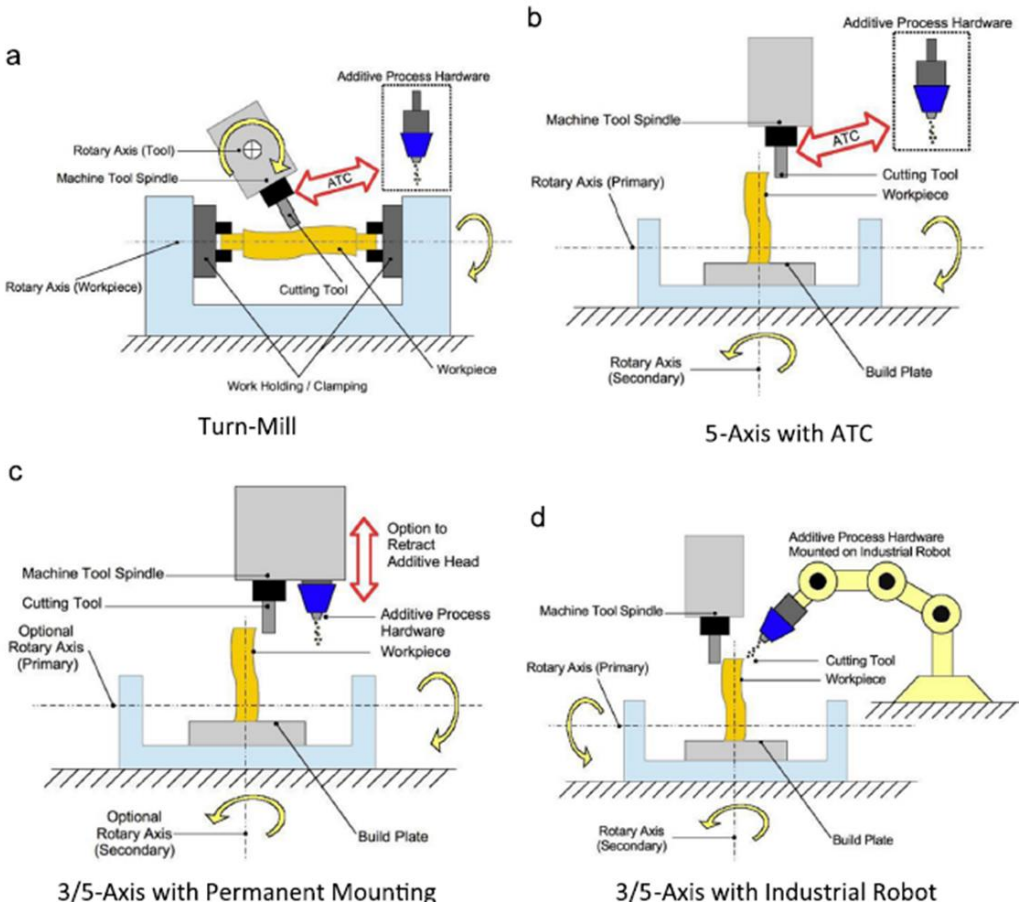


Figure 2-11: Machine tool configurations adopted for integration of DED and CNC machining [124]

2.5 Post Process Machining

Machining has been widely used in the post processing of AM parts. Due to the relative availability of machine tools on most workshop floors, it is the primary option for post processing metal AM components for achieving dimensional tolerances. Post processing operations in AM are not desirable as they lead to longer lead times and increased costs, thus reducing the need for post processing to the absolute minimum is essential and critical for the technologies to remain sustainable. The authors in [137, 138] discussed the

development of a hybrid process which combines a DMD process with a metal AM process. In the study, a cost model was developed for comparing the outlay of using the process to machining the component from billet. It was reported the use of the hybrid combination was more cost-effective when used in fabricating harder, difficult to machine materials.

In metal AM, dimensional accuracy and improvement of surface quality are the primary requirements for post processing. With the development of new technologies in metal AM, there exists a wide range of accuracy capabilities between processes. For faster build processes and larger build volumes, accuracy is often sacrificed [139].

In demonstrating the effects of various post processing methods on the surface integrity of AM parts, Löber et al. [140] compared the use of grinding to other post processing methods; electro-polishing, plasma polishing and sand blasting. For a single post processing step, grinding gave the lowest surface roughness value. However, a combination of various abrasion methods gave the best surface finish. Beaucamp et al. [141], developed a shape adaptive grinding method for the post processing of AM parts with convex or concave features. The method utilises polishing and grinding techniques within an elastic tool with rigid pellets for material removal and surface modification. A schematic of the operating principle is shown in *Figure 2-12*. To demonstrate the capabilities of the process, the tool was used in machining flat Ti6Al4V samples fabricated using PBF processes. The process achieved surface roughness improvements from 5µm to 3nm.

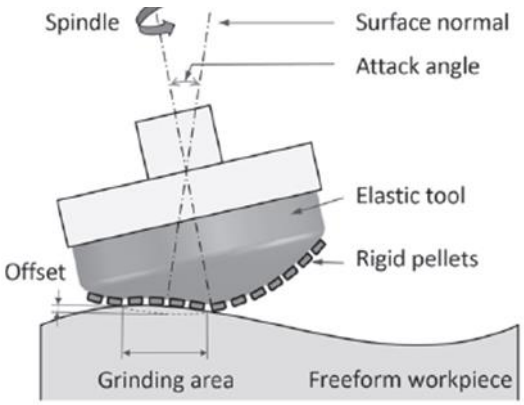


Figure 2-12: Shape adaptive grinding principle [141]

In another study [12], aluminium alloys, stainless steel and Ti6Al4V structures built using Laser Beam PBF was compared to the wrought, machined forms of the materials. The components were tested in as fabricated condition with minimal post processing. The authors reported the components had lower fatigue strength compared to the conventionally produced specimens. Laser beam PBF samples however showed elevated fatigue strength when post processed using HIPing. Low fatigue strength in the as fabricated samples was attributed to the presence of surface defects which initiate cracks which then propagate and cause failure. Post deposition treatment of the samples with mechanical polishing and electro- polishing was reported to show minimal improvement in the fatigue behaviour, this was correlated to the minimal effect the processes had on improving the surface roughness of the parts. The effects of machining in elevating fatigue strength was reported in [90]. In the study, the effect of processing parameters on properties of a PBF built sample was investigated. The authors further investigated the influence of various

post processing techniques on the fatigue strength of the component. The effects of; HIPing, annealing and machining on the components were all evaluated. HIP'ed samples had the highest number of cycles before failure and the machined samples showed improved fatigue strength compared to the as-built samples.

Similarly, in [142], a comparison of the various methods for post processing a pylon made from Aluminium alloy and fabricated using the Electron Beam Freeform Fabrication (EBFF) process was carried out. EBFF processes are carried out in a vacuum and use a metal wire placed in a melt pool to generate required geometries – thus making them by definition to be DED processes. The methods used in post processing include: high speed milling, wire electro discharge machining (EDM), glass bead blasting and electron beam glazing. The component subjected to high speed machining was reported to have the lowest root mean square surface finish and also the minimum long-range waviness of all the methods used. The results also show the machined samples had large compressive residual stresses in the build direction when compared to the other subtractive methods used.

Xiong et al. [143] demonstrated a strategy for manufacturing components by combining a plasma deposition process with a CNC milling set up in the same workstation, effectively making it a hybrid workstation. With this combination, they demonstrated milling after subsequent passes of each single bead and milling after the process is completed as a post processing step. They adopted a milling strategy which included both planar and contour

milling of the part. In the study, air cooling was used during machining and the authors also demonstrated the viability of the process in fabricating a hollow vase. Subsequent heat treatment was carried out on the component to reduce stress and avoid crack propagation. A similar study was carried out in [144], where the authors incorporated gas metal arc welding (GMAW) equipment within a three-axis CNC milling machine. In the study, the authors described the need and the process of isolating the CNC controller from the spatter generated during weld deposition and developed software for controlling both processes from a common interface. They showed the use of the hybrid machine took 37% less time than milling from billet and the cost was 22% less than the use of the milling process.

Studies to compare the machinability of wrought materials to additively manufactured components have also been undertaken. In [145], using a turning process, the authors, compared the machinability of PBF fabricated Ti6Al4V to its wrought counterpart. In the study, average cutting forces measured during the machining of the PBF component was measured to be greater than those in wrought components. This was attributed to the higher strength and hardness of the former. The rate of wear of the inserts used were also compared to determine the mechanisms of wear during both processes. In a similar study [146], the influence of post processing on surface integrity of PBF Ti6Al4V was also investigated. The authors in the study used a face milling process for the post processing operation. The fabricated metal AM samples were compared to hot rolled wrought material. It was reported the

work hardening of the machined layer of the AM sample was greater in proportion to the conventional material. Also, higher cutting forces were observed in the PBF components and was found to be greater by a margin of 22%. The authors attributed this variation to discontinuities in the microstructure of the PBF fabricated component. The authors in [147] used a slot milling process in comparing between DED Ti6Al4V and wrought forms of the material. They postulated the finer microstructure of the AM material led to better machining finish as they recorded comparatively lower values of surface roughness in the AM material. Bordin et al. [148], compared the machinability of wrought and Electron Beam PBF fabricated components using turning. Basing their investigations on the variation in mechanical behaviour of AM components compared to wrought alloys and an anticipated change in machinability. The authors reported higher surface roughness values post machining which was attributed to lower ductility in the Electron Beam PBF component influencing the chip formation mechanism. Also, the tool life was relatively shorter in the machining of the Electron Beam PBF component as the authors reported a time difference of up to 100 % (twice the time) in reaching a prescribed tool wear limit in the wrought component. The authors however reported on the formation of subsurface deformation in the cutting direction for both materials. The deformed layer was indicated to be 20 µm from the machined surface in both materials.

Brinksmeier et al. [149] investigated the surface integrity of metal AM - Maraging steel components post processed using milling and grinding

processes. The study was based on the premise that hardness and residual stress of a component are primary influencers of surface integrity. Residual stress measurements showed the surface integrity of the samples was improved post machining- with the measured stress values being predominantly compressive. They also surmised the post machining step did not cause significant variation in hardness. Montevecchi et al. in [150] investigated the cutting forces during machining of WAAM and LENS fabricated AISI H13 steel alloy. Prior to machining the components, hardness values were measured and reported to be higher in the AM components than in the wrought material. Using milling as the material removal process, it was observed that cutting forces in the machining of the AM components were higher than those for wrought materials. In [151], Rysava et al. demonstrated drilling of a Laser beam PBF fabricated component for medical applications. The component intended for use in dental applications was drilled and threaded towards achieving dimensional requirements. The authors reported on the optimum cutting speed (60 m/min) and feed per tooth (10 μm) for the drilling process.

Tool manufacturers often recommend tooling for various materials and material combinations. However, most tooling is developed to perform well for wrought materials and not necessarily designed to cope with microstructural variations and deviations from these wrought forms. This represents a problem in the machining of AM parts as the products from AM mostly have similar desirable characteristics with different microstructures

and hence different properties. In studies to determine the effects of cutting zone cooling strategies on the tool wear mechanism [152, 153], the authors compared tool wear using dry and cryogenic cooling methods in semi finishing turning operations. The authors analysed the tool wear craters formed in Laser Beam PBF, Electron Beam PBF, wrought and heat-treated Laser Beam PBF Ti6Al4V components. Laser Beam PBF components were reported to have the highest crater depth under dry conditions and cryogenic cooling was reported to reduce crater wear depth by up to 58%. With a focus on the effects of post machining on surface integrity of AM components used in biomedical applications, machining of Electron Beam PBF fabricated Ti6Al4V was attempted by Bruschi et al. [154]. Similar to other studies in this area, the authors compared the machinability of the AM component to wrought material. It was reported that in cryogenic machining of the AM components, there was a decrease in abrasion wear and the dominant wear mechanism was adhesion. In another study [155], the authors investigated the effects of tooling on surface integrity and microstructural properties of DMD Ti6Al4V. The authors reported that by using two different inserts of similar geometry, difference in surface integrity was observed. Variations in residual stresses, surface roughness and the chip morphology - which pointed to a different formation mechanism was reported.

A common underlying in investigations is that the machining of components fabricated via metal AM means provides a challenge when compared to the machining of wrought components of the same materials. However, due to

anisotropic microstructures, finer grain size and the ability to selectively deposit various materials in AM components, there is a potential drawback in the use of these tools in machining AM components economically. This thus indicates that for these processes, investigations on machining parameter selection would be necessary. In a study on the characteristics of the process during the machining of Ti6Al4V produced by Laser Beam PBF, the authors reported the formation of subsurface deformation beneath the machined surface in the cutting direction [156]. Subsurface deformation such as this is not desirable for critical applications as it often impairs the mechanical properties of the component. It is thus expedient to pursue a machining regime which readily adapts to changes in material microstructure and is robust enough to machine through layers of alternating material without disruption in surface finish and subsurface condition.

2.5.1 Machining induced microstructural damage

In the machining of components for use in critical applications, attention should be given to the avoidance of machining induced defects which can lead to the failure of the component when placed in service. Fatigue life of machined components is dependent on the surface and subsurface condition. Aside from the geometrical irregularities which need to be controlled on a surface, the surface integrity should also be defined and controlled. Surface integrity generalises as a term for the surface characteristics of a part which influences the part durability – these characteristics include surface

roughness, residual stress, microstructure and hardness [157]. In chip formation processes involving difficult to machine alloys, high cutting forces and heat are generated as a result of the high strength and fracture strain of such materials. The heat generated, coupled with the low thermal conductivity prevalent with these alloys leads to high localised temperatures at the cutting regions which in turn causes rapid tool wear, failure and ultimately degrades the surface integrity of the workpiece [46]. Surface integrity in machined components encompasses plastic deformation and residual stress effects. Residual stress has been reported to be related to the fatigue life of a component. In [158], the authors discussed compressive stresses were beneficial to fatigue life in a machined component. During a turning operation, they achieved surface compressive stresses by decreasing the feed rate and by using a chamfered tool with a small radius.

Materials used in AM are typically those which are difficult to machine from billet and as such gains from fabrication using AM would be appreciable. These materials, due to other related desirable properties would usually find functions in high value critical applications. Focusing on Ti6Al4V which has been referred to as the 'work horse' of the AM industry, these alloys, as with other titanium alloys have low thermal conductivity and high chemical reactivity. Thus, cutting tool and parameter selection in the machining of these alloys is critical in achieving optimum finish required without machining defects. In a study on the surface integrity achieved during the machining of Ti6Al4V alloys using various tooling and machining parameters [159], the

authors reported the formation of a 'white layer' and plastic deformation in the machining direction during '*abusive'* machining of the alloy (machining with high feed rates, large depths of cut and with a worn tool for extended periods). Using two straight grade cemented carbide inserts of different grain size, the authors concluded the finer grained variant gave a lower surface integrity as deformation was more pronounced with the insert.

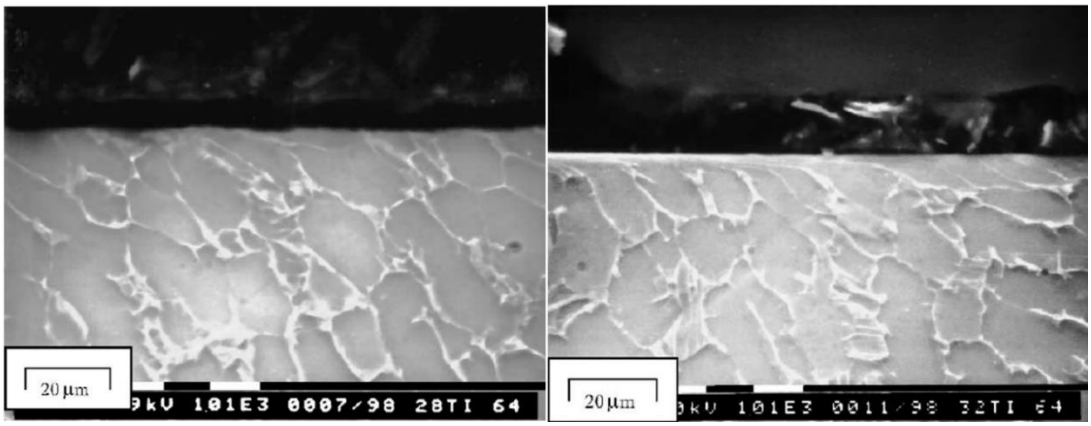


Figure 2-13: Machining induced deformation with different grain sized inserts after machining for 10 s (a) 1.0 µm (b) 0.68 µm. Deformation is more pronounced in (b) [159]

According to the Hall- Petch effect, hardness of a component increases with decreasing grain size, with hardness being one of the factors impacting machinability. Grain sizes obtainable from metal AM processes are generally smaller compared to those from wrought. It thus presents that machining of metal AM components would vary from those of the same materials processed via other conventional processes. The existence of an anisotropic microstructure and the relative difference between grain sizes would be important factors to also consider during the machining of these components. These discontinuities due to microstructural variation has been postulated to

be a reason for increased cutting forces during the machining of metal AM produced Ti6Al4V [146]. Wilms and Aghan [160] reported a variation in machining behaviour and higher machining forces when comparing between an anisotropic microstructure steel with ferrite – pearlite banding and a steel plate with homogeneous microstructure. In machining processes, variation in material composition, microstructure and geometry are expected to lead to changes in material machinability and as a consequence, the attainable overall surface finish of a component. Such variations in material machinability within a component can lead to vibrations and a variation in chip thickness which influence the cutting forces and invariably causes regenerative chatter during machining [161-163]. Machine tool chatter is undesirable as it deteriorates the machined surface quality, affects productivity and results in accelerated tool failure [164]. Spindle speed variation has been demonstrated as a method for reducing regenerative chatter in high speed machining operations [165, 166], and indeed some machine tool manufacturers have included this functionality on their machine tools. Yoneoka et al. [167] have also demonstrated the use of a combination of spindle speed and feed rate variation for the reduction of self-excited chatter vibrations during machining. Exploring the force-feed nonlinearity relationship, Landers et al. [168] demonstrated the effects of feed variation in suppressing chatter in turning and milling operations. Thus, by adopting this background, a strategy for countering the effects of the changing

microstructure on part quality during machining is the use of a strategy which adjusts to the prevailing cutting conditions.

2.5.2 Adaptive control in machining

A shortcoming of the modern machining system is that machining parameters are programmed off line and as a consequence, a number of these systems are inefficient during machining processes that differ from optimal conditions [169, 170]. Adaptive/process control systems in machining primarily function by self- adjusting the input parameters to adapt to changes in cutting conditions towards maintaining optimal machining conditions [171]. Automation in machining increases productivity and ultimately reduces production costs, improves surface finish, increases machining accuracy and repeatability and altogether increases the efficiency of the machining process. The aim of process control is to maximize material removal whilst minimizing tool wear and maintaining quality specifications in the machined part.

In numerical control machining, data input to the machine is translated and converted into the applicable machine tool movements. The movement of the operative unit is sensed and fed back to the machine control unit, which compares the movement to the input command and adjusts until the error signal is zero [172]. Machine tool controls are classified into three levels based on their scope of operations: The servomechanism control loop which regulates the position and velocity of the axes, the interpolar loop, co-ordinates multiple axes to maintain a specified tool path and orientation, and

the process control which controls the automatic adjustment of process parameters [173]. Process control is not usually included by majority of machine builders as a standard feature in their machines due to the complexity of adding sensory devices which provide feedback on the cutting process to the machine controller.

In machining with CNC systems, parameters are selected conservatively based on operator experience and advisory machining parameter ranges provided by toolmakers. Toolmakers determine these parameters based on wrought form of the materials. In the case of operator experience, failure of the tool is often overcompensated for with the selection of parameters often below the abilities of the tooling and the machine tool spindle capabilities. Adaptive control (AC) systems have been proposed and demonstrated as a means of overcoming physical constraints and promoting performance during machining. Constraints in machining can be machine tool dependent, tool or workpiece dependent. An AC system measures a performance index (PI) of the control system and from a comparison of this index with the set of given parameters, the adaptation mechanism modifies the parameters of the controller in order to maintain the performance of the control system close to the specified control values [174]. Also, variation from the expected measured cutting forces can be controlled / reduced by utilising sensors which provide feedback useful for effecting the necessary changes by the controller [175]. In the development and deployment of an AC system, the following are of importance towards the successful integration: process control strategies,

sensors and sensing techniques and open architecture software systems. The listed are expatiated further below.

2.5.2.1 Process control strategies

Process control strategies in machining systems are generally classified into three categories. In selecting any of these strategies, the basis for control and the extent to which the controller can be adapted are the main factors for consideration. The categories include;

- Adaptive control with optimization (ACO): In using this control strategy, a PI is used to optimise the process subject to process and system constraints. This strategy often involves maximizing material removal rate or improving surface quality.
- Adaptive control with constraints (ACC): Here, the process is controlled using real time measurements to maintain a process variable within a specified boundary with reference to process and system constraints. They are mostly aimed at improvement in productivity by increasing material removal rate. Hence, they are mostly used in rough cutting operation A performance index is not used in this case and that further differentiates this from an ACO strategy.
- Geometric adaptive control (GAC): This strategy is mostly used in finishing operations, and part quality is preserved by compensation for tool wear and deflection. Real time measurements are used to maintain

dimensional accuracy and consistency in surface finish by using this method [176, 177]

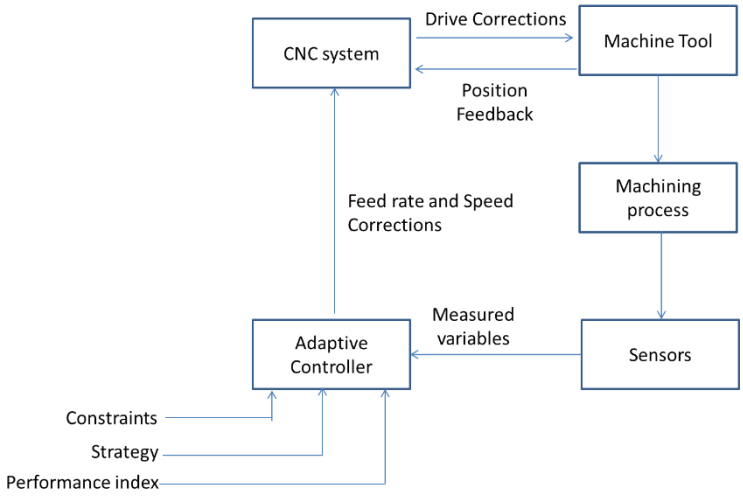


Figure 2-14: Adaptive control configuration for a machine tool [172, 177]

In practice, the difficulty of on-line measurement of tool wear and machine tool temperature limits the use of ACO strategies in functional systems. Of the strategies listed, ACC strategies are most easily incorporated into machine tools and its use has been reviewed by various authors. Process constraints that are controlled using ACC strategies include; force, power, and temperature amongst others. In [178], the authors inferred the use of AC alone cannot effectively control cutting forces and they implemented an off-line optimization in conjunction with the adaptive control system for reducing feed rate by using cutting force as a constraint. The authors reported machining time savings and higher maximum forces by using this method. In a similar study, the authors in [170] demonstrated the use of an AC system in the improvement of material removal rate by up to 27% in end milling

operations. In the study, the investigators used a fuzzy control strategy with simulations and optimised feed rate towards the optimisation of cutting forces. The use of AC for improving surface finish in high speed machining process was demonstrated in [179]. In addition to the development of the control system, the authors used a process capability chart in computing the upper and lower limits of the system and determine the process capability of the system.

The sensor and feedback mechanism are important components of machining control systems as they provide the basis for data collection and feedback. In developing an intelligent, robust machining system, the sensor and the signal processing peripherals are components that need to be considered [180, 181].

2.5.2.2 Sensors in Machining

Process monitoring involves the measurement and estimation of variables within a process. Sensors in a machining system are used for detecting and sending signals to either a CNC controller or a human interface for corrections and adjustments to be made to the system. Sensors have capabilities to convert a physical stimulus to a corresponding electrical signal for the purpose of measurement. Signal processing is also required to amplify and filter signals from a sensor. In selecting a sensor for an application, the reliability, the cost/performance ratio, repeatability, the size and intrusiveness, and most importantly, the suitability to the monitoring purpose are considered. Measuring techniques can be categorised as direct or indirect. Direct

measuring techniques measure the actual quantity of the variable. Examples of application areas includes laser measurement, visual monitoring and use of a dynamometer in measuring cutting force. Indirect methods involve deducing the values of interest from other measured values using empirical relationships. An example of this is the use of acoustic emission sensors in measuring cutting force. In increasing the reliability of feedback from a system, it may be useful to use several sensors in a complementary manner. This provides for better prediction of the machining conditions/ attributes. The sensors however have to be complementary for it to be considered as sensor fusion; otherwise, it is regarded to be a multisensor arrangement.

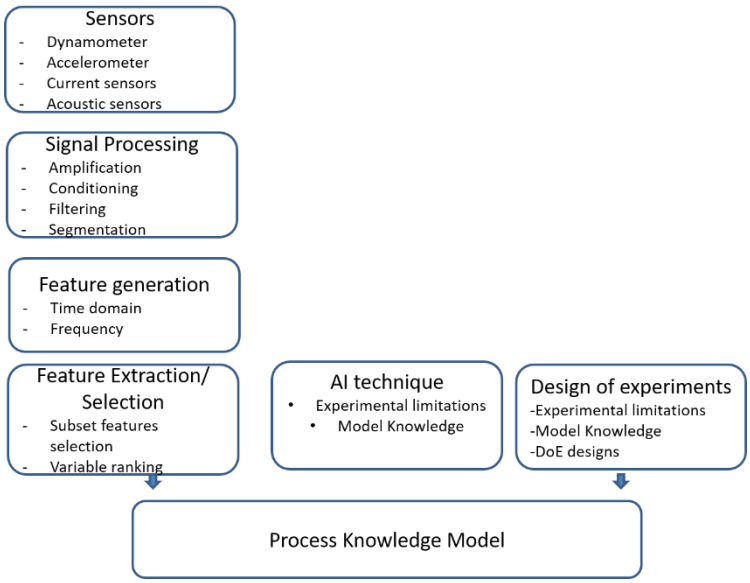


Figure 2-15: Methodology to develop monitoring system for machining processes [180]

Tool condition monitoring systems have been used for monitoring in machining workstations. The condition of the cutting tool influences physical process variables in the cutting region. Measurement of these physical variables gives a view of the state of the cutting tool. Since cutting forces

cannot be measured directly, the deformation a component undergoes when subjected to a force is measured and the forces acting on the component derived from the results. Dynamometers are designed based on this characteristic property. Cutting force has been widely used as a predictor for tool condition and wear detection. Measurement of cutting forces has been widely done using dynamometers. Dynamometers are required to measure the component forces and have been developed to have multiple channels with no cross talk between these channels.

2.5.2.3 Open architecture software systems

For any process monitoring and control system to be operative, it requires the machine tool hardware and software to be both flexible and adaptable. Flexibility would permit for the use of alternate programming languages, operating systems, control strategies and methods for processing sensor information [173]. In a preliminary study on the development of an open architecture system, Jaehyun et al. [182] surmised that an open system would require vendor neutrality and component integrability to be easily adaptable for purpose. Generally, most of the commercially available advanced CNC controllers and hardware have closed architecture schemes. This is due to system architecture design, configuration and implementation being proprietary for most machine builders. In [183], the authors proposed and implemented an open architecture system for isolating and controlling specific functions on a controller, this method has been attempted by a

number of investigators towards realising adaptive control. These systems typically have their control functions partitioned into components and documented to a point where third-party users can seamlessly integrate peripheral components towards building an operational machine with the required functions and modifications in the controller. The introduction of the enhanced machine controller (EMC) led to an upturn in the use of open architecture software in CNC systems [184]. The use of EMC systems eliminated the need for peripheral motion control computer boards but instead the control of axis and spindle motion using a range of developed ports running on Linux. The project has however evolved to an open source project with various iterations and is presently referred to as LinuxCNC.

2.6 Summary of the literature and knowledge gaps

Deductions from the review can be highlighted into the below points:

- Metal additive manufacturing processes are growing in use and more applications are being proposed for these processes. Growth in the market has been commensurate with increased interest in manufacture of finished components and entry of machine makers into the industry. Therefore, further research work is required to underpin this.
- The use of AM processes opens new opportunities to produce components with varying geometry and material combinations. The use of

these processes is expected to increase and there is presently a shift into design of parts having intricate structures and internal features with AM processes in mind.

- The need for post processing components produced using these technologies remain and would most likely be a recurring factor due to the underlying build strategy of the processes. The need for this is further underlined by the growth in the market for the post processing of these components. Also, workstations coming to market are aimed at combining both additive and subtractive manufacturing processes towards improving process planning and material development.
- Components from metal AM processes are prone to the presence of undesirable mechanical properties and defects such as pores and cracks if conditions and process parameters are not optimum. Mostly, these components are subject to heat treatment and HIPing processes post build to alleviate of these undesirable 'properties'. The use of these post processing methods further affects the microstructural properties and invariably any subsequent post processing to be done on the part.
- Despite the increased interest in developing AM processes to be more efficient and the plethora of studies on the processes, there is comparably limited amount of work so far on the effects of post processing on the resulting components. Recent work on this area has shown machinability of these components somewhat differ from machining characteristics of their wrought counterparts.

- An understanding of the machinability of components- particularly difficult to machine components which are used in DED processes would be useful for adopters of the technology and also to tool manufacturers towards development of tooling which would be useful in machining these components.
- Machining has been used widely for improvement of surface finish of metal AM parts. Mostly, machining processes are used in conjunction with other post processing steps towards achieving desirable mechanical properties and matching surface requirements.
- The use of heat treatments in homogenising microstructures leads to variation in mechanical properties. The effect of this on machining has not been widely reported in literature.

2.6.1 Research opportunities from literature

The machining of AM components particularly from DED processes have been investigated and reported by a number of authors. Given the difference in microstructure and hence properties of these components and a resulting difference in machinability when compared to wrought material. The influence of machining parameters on the mechanical properties has not been thoroughly investigated and a strategy for machining these components is presently not existent in the public domain.

In particular, Titanium alloys have been at the forefront of development of metal AM techniques. Investigations in the use of Ti6Al4V in metal AM

according to statistical data from Scopus ranks as the most researched alloy in recent years. Thus, a decision to adopt this as the material of choice was taken early on. The alpha-beta nature of the alloy leads to complexities due to the competing interactions when fabricated using layer manufacturing methods. Also, being an alloy adopted in high temperature applications, the thermal properties and processing route which can lead to variations from the wrought forms is important to adopters and investigators. Thus, Ti6Al4V is selected for use in this work due to these factors.

Heat treatment of Titanium alloys are usually for the reduction of stresses developed during the fabrication process, the improvement of ductility, machinability, structural stability and optimisation of mechanical properties [185]. As a result, various heat treatment techniques are used in achieving desired properties. For two-phase titanium alloys with a lamellar microstructure, the mechanical properties are primarily dependent on the α lamella thickness, the size of the α colonies and the β grain size [186]. Due to the rapid cooling rates achievable during DED processes, components built using these methods have a finer α lamellar structure compared to their wrought counterparts [187]. These finer microstructures incur inherently poor machinability in the resulting components. Therefore, control of the grain growth and increasing α lamellar width during heat treatment is significant and can provide advantages towards tailoring the mechanical properties to requirements. Heat treatment of wrought α/β Titanium alloys,

when leading to substantial changes in microstructure have been shown to influence machinability and thus impact tool life [188].

Tool makers manufacture tooling and advice machining parameters for the tools based on wrought materials. Thus, when machining AM components using these parameters, due to a relative difference in mechanical properties, a mismatch exists which can lead to a less than optimum cutting condition. Thus, the following opportunities can be derived from this study:

- An investigation of the cutting process to determine the causal effects of increased mechanical action on cutting tool reported by other authors during machining of AM parts
- Development of a strategy for the machining of DED components which minimises subsurface deformation whilst improving surface finish
- A comparison between machining wrought and DED components and investing the effects of machining on the heat affected zone and material component boundaries
- An investigation on the prevailing characteristics during the machining of multiple material combination in a functionally graded material produced using directed energy deposited means.
- Development of a machining system on an open architecture controller which can be easily adapted to match the machining requirements during cutting processes and annul the effects of microstructural variation on part quality.

2.6.2 Research Hypothesis

Deductions from a critical literature review of both the additive manufacturing and subtractive manufacturing methods used in post processing has led to the following hypothesis:

- Components produced using metal AM means often present with comparatively smaller grains compared to their wrought counterparts due to the rapid cooling they undergo. These components exhibit higher hardness and a deviation from other mechanical properties of their wrought counterparts. this would be expected to have an impact on machinability.
- In the machining of wrought materials, the material microstructure is mostly uniform along all directions, thus microstructure variation contributes less to machining variations. However, AM components are anisotropic as the material microstructure varies in different directions due to differential cooling rates. This thus means machining requirements would vary with these changes in microstructure – with changes in grain size and texture. A machining strategy which limits the effect of this on the tool while ensuring preservation of surface integrity would limit the influence of these variations and improve resultant surface finish.
- Post process machining of multiple material components with functional grading, produced using DED processes would benefit from adaptive machining as the tooling parameters and requirements of the various parts of these components would be adequately compensated for.

- Heat treatments would be beneficial in improving machinability as the use of these treatments in increasing grain size would ensure the metal AM components are easier to machine due to a depreciation of their mechanical properties- such as hardness.

2.6.3 Research Objectives

Towards meeting the highlighted research opportunities from literature, the objectives of this work were set out to address the identified gaps. The following objectives were thus set for this research work:

- To deposit materials using DED techniques and investigate the machinability of such components in relation to wrought materials. The effects of machining parameters on cutting forces and the subsequent effects on component microstructure in the immediate machining zone would be investigated.
- To systematically, through the use of heat treatments investigate and report on opportunities for improving machinability and overall process chain design
- To develop an adaptive machining system which would readily react to changes in microstructure and improve surface finish by adjusting the prevailing cutting force within a system through control of a machining parameter that most readily influences cutting force. Also, the system would serve to reduce process times of post processing AM parts and enhance productivity.

- To investigate the influence of the addition of carbide inclusions which are capable of increasing material hardness and toughness on the machining of DED components. Also, to investigate the effects of remelted microstructures consisting of these dissolve carbides on machining processes and tooling.

3.0 Experimental Methods

This chapter describes the materials, equipment and techniques used in the fabrication and post process machining of components in this study. Characterisation methods used for analysing the feedstock and the resulting components are also reviewed. As this research study spans additive and subtractive manufacturing technologies, equipment and processes used from both aspects are discussed accordingly. Techniques for measuring surface finish, microstructural analysis, hardness amongst other physical attributes and the assumptions in evaluating these parameters are discussed herein. Also, a preliminary discussion of the components required in the development of an adaptive control system is presented.

Figure 3-1 provides a graphical abstract of the process discussed in this thesis and gives an overview of how the various aspects selected are relevant towards attaining the research objectives listed in section 2.6.3. It also sets a framework for the subsequent chapters of this thesis in terms of how the results are presented and the anticipated outcomes.

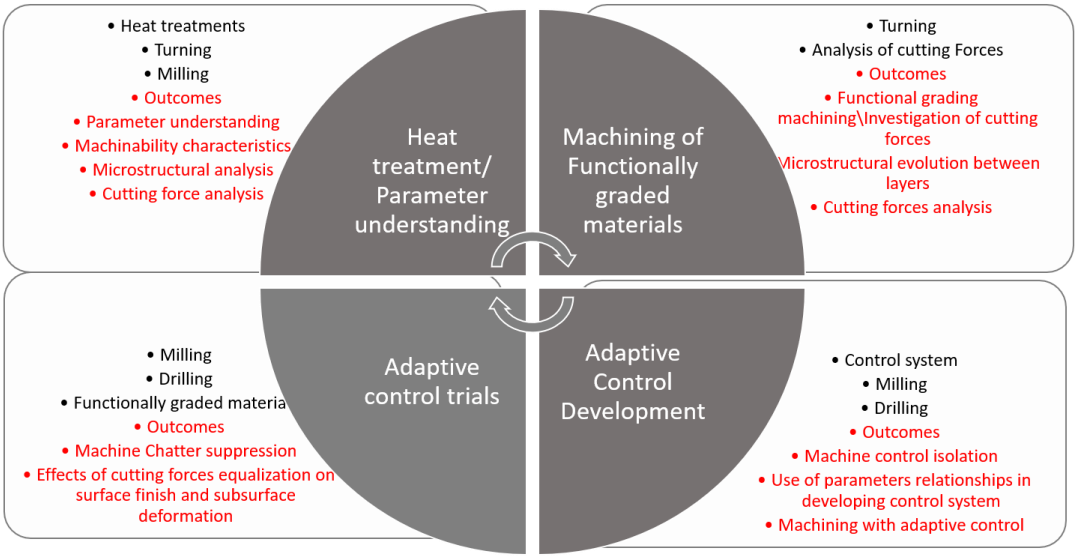


Figure 3-1: Graphical abstract of the experimental methods showing dependencies an outcomes

3.1 Materials

In the selection of materials for deposition experiments towards producing test components for machining, focus was on materials widely researched in metal AM due to their obvious industrial and economic importance. Also, since this study is centred on the machinability, it was expedient to select a material whose machinability characteristics are properly documented. *Ti6Al4V* is the most widely used titanium alloy in high value industries due to its corrosion resistance properties and the attainable strength to weight ratio. As a result of these desirable properties and applications, it has also become a material of significant interest in studies aimed at developing AM processes for finished part production. Hence, it is selected as the material of primary focus for this study. One of the advantages of using metal AM processes for

part manufacture is in the use of multiple materials towards the production of 'tailored' microstructures and by extension, functionally graded components. Towards this end, a material which has been demonstrated to readily produce a relevant metal matrix composite with the Ti alloy is selected for use. Thus, the materials used in this study are; 1.2 mm diameter *Ti6Al4V* wire supplied by VBC Group (Loughborough, UK) and Spherotene powder (WC/W_2C) supplied by Laser Cladding Technologies (Worksop, UK). An analysis of the particle size of the powder indicated the powder had a size range of 40 μm – 180 μm with a mean size of 118 μm. All substrates used for component production are Ti6Al4V plates. Plate thicknesses were 6 mm, 12 mm and 25 mm for the different trials. For all deposition trials, the substrates were grit blast in a Guyson Euroblast machine with an alumina-based powder to reduce laser reflection from the top surface and thereafter degreased. The substrates used for specific experiments are outlined in detail subsequently.

3.2 DED System

Deposition of components was carried out on a 2-kW rated Ytterium- doped continuous wave fibre laser (IPG Photonics). The laser system operates at a wavelength of 1070 nm and can be coupled with fibres of diameters; 200 μm, 400 μm and 600μm. For all deposition trials in this study, the 600 μm fibre is used and this delivers a laser beam with a Gaussian profile and a spot size of approximately 1 mm diameter when operated at focus. However, to obtain a wider spot size towards achieving a higher material deposition rate, the laser

is operated at a defocused distance of 20 mm. This in turn gives a laser spot size with a diameter of 3.1 mm. This spot size is selected as it gives a top hat profile and allows for the set up for the wire feed to be included in the standoff distance. Working at focus would hamper this and lead to smaller deposit beads which are undesirable here. The system has capabilities to be coupled with a coaxial deposition head or with side feeding for material delivery to the melt pool created. The setup is mounted on a 4-axis CNC and relative motion of the workpiece in relation to the laser beam is achieved by the motion in the x, y, z and rotational axis directions. The coaxial feeding system is not used as it has the limitation of - producing smaller sized deposits when used at focus.

As such, material delivery to the melt pool for both feedstock types in this study is via side-fed nozzles. For wire feedstock, the material is fed into the guide nozzles using a Redman WF200DC wire feeder with a control mechanism for regulating material delivery to the melt pool. For the powder material, delivery to the melt pool is via a Miller thermal (Model 1264) powder feeder. Powder feed delivery is also controlled with the feeder to allow for known quantities to be delivered to the melt pool – the feeder consists of a mechanism for regulating flow rate and allowing for the flow of the powder particles under pressure into the required delivery area. For every batch of powder, calibration of the feeder to deliver known quantities of material per unit time is carried out before experimental trials to ensure known quantities are delivered to the melt pool. Argon is used as the carrier gas and the powder

feeder chamber is pressurized with the gas at a flow rate of 10 l/min. For deposition experiments involving the use of both feedstock materials, an arrangement comprising of both material delivery systems is used. A schematic of the set up using both arrangements is shown in *Figure 3-2*.

For all processes, deposition is carried out in an enclosure to prevent oxidation of the resulting components and to preserve the integrity of the deposits. A transparent bag is used as an enclosure which is filled with Argon gas prior to and during the deposition trials.

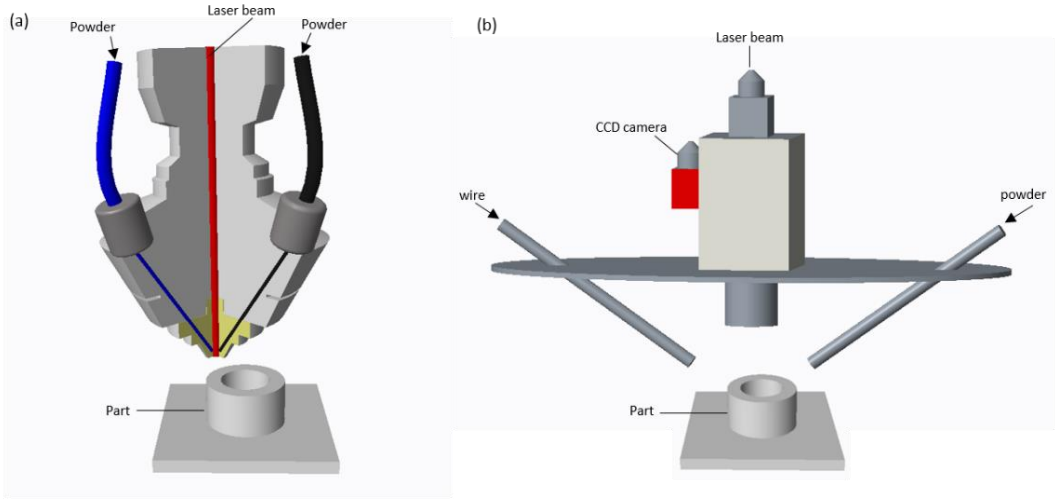


Figure 3-2: Material delivery set up for multiple feedstock material delivery (a) Coaxial material delivery (b) Side feeding delivery

3.2.1 Directed Energy Deposition of Ti6Al4V

The structures proposed for machining include a cylinder for turning trials and a rectangular block for milling and drilling experiments. CAD images of the material shapes are shown in *Figure 3-3*. Preliminary trials towards providing

a baseline for the defect free deposition of materials were carried out to determine the material characteristics and geometry for subsequent multi-layer deposition experiments. During this process, single track beads of the material were deposited on the substrate. The samples were thereafter sectioned, mounted, polished and viewed under an optical microscope to investigate for defects and process repeatability. This was aimed at deducing optimum parameters for producing pore free deposits and for determination of parameters required for multilayer deposits. Parameters required for multilayer deposits include the step up and overlap dimensions which are determined from the analysis of the single layer beads produced. It was deduced that the optimum overlap width to give satisfactory deposits was 60% of the previously deposited clad width. Deposit height for subsequent clads was at 80% height of the previous deposit produced. Parameter ranges used for the deposition of these structures are shown in *Table 3-1*.

Table 3-1: Laser deposition parameters. Traverse speed indicated is rotational speed

Parameters	***Data***
Laser power (kW)	1.2-1.6
Traverse speed- (deg/min)	323 (200 mm/min)
Wire feed rate (mm/s)	13.33
Step-up in Z (mm)	1.5
Step over in X (mm)	0.8

For all experiments involving Ti6Al4V feedstock material, Ti6Al4V was used as the substrate. This was to protect material integrity and for experimental repeatability. Also, machining experiments to demonstrate the machining conditions beyond the boundary and fusion regions between both material systems were proposed.

In the deposition of cylindrical components, a rotary table which revolves in relation to the laser beam is used. The movement of the rotary axis with the feedstock material being fed into the laser beam, in relation to an incremental change in height produces a helical path which produces the required shape.

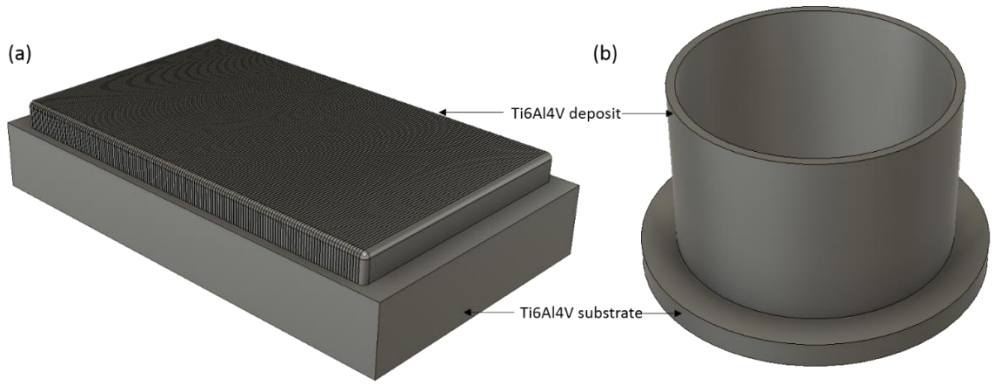


Figure 3-3: CAD image of built components (a) Rectangular block (b) Cylindrical component

3.2.2 Deposition of functionally graded components

Towards the production of functionally graded components, an understanding of the deposition characteristics of *Ti6Al4V* feedstock (wire) was essential before proceeding to deposit materials with the addition of WC

powder. The deposition of multiple materials is one of the key advantages of metal additive manufacturing processes and in this case, was critical in the manufacture of a MMC with varying composition of the composite material. To achieve this, both materials were side fed into the laser beam as per the experimental arrangement shown in *Figure 3-2*. *Figure 3-4* shows the alignment of the wire and powder delivery nozzles in relation to the laser beam path.

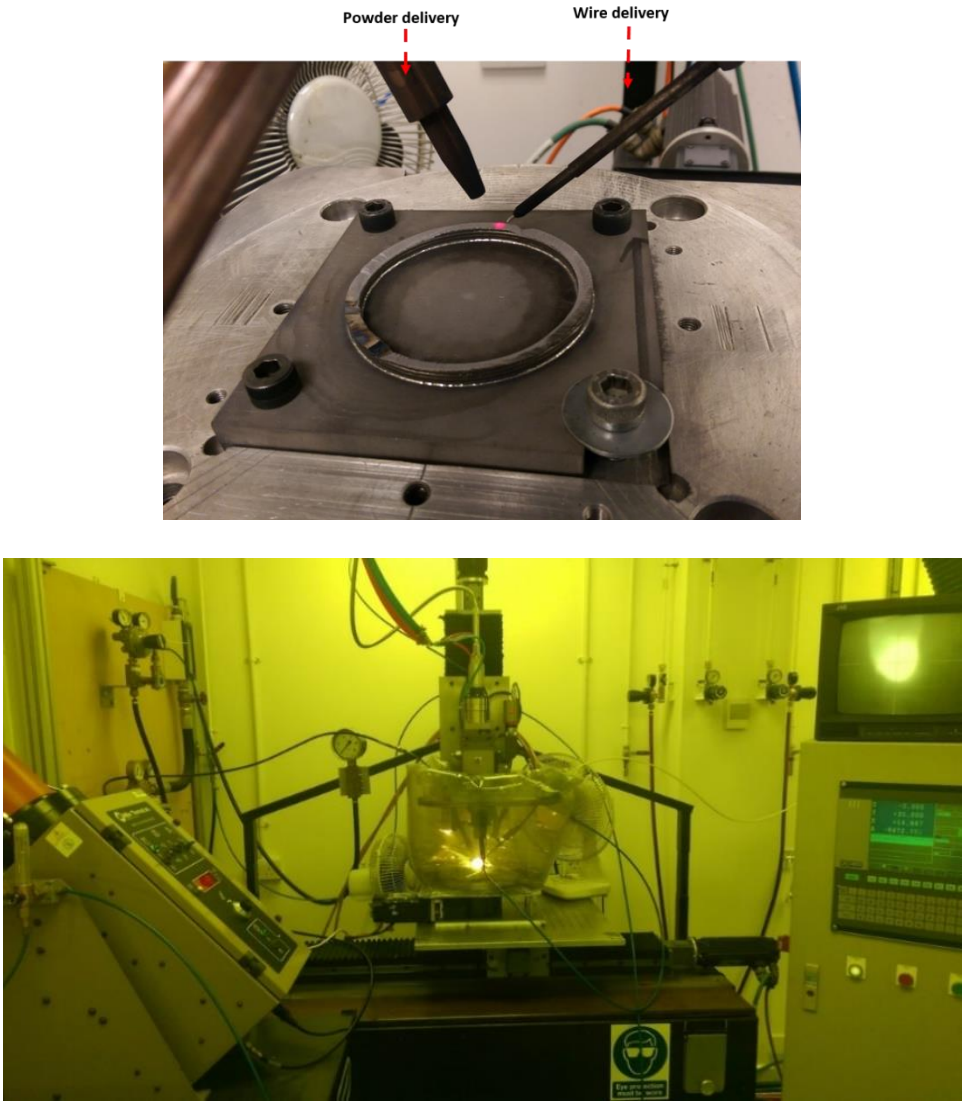


Figure 3-4: (a) Alignment for feedstock delivery in multi component deposition (b) Entire set-up for the deposition of functionally graded components

Parameters used in achieving crack and porosity free deposits are highlighted in *Table 3-2.* As detailed in the deposition of single material previously, initial single tracks were deposited to establish a baseline for parameters giving defect free deposits. Deposit width and height were obtained from these experiments and these were used in producing multilayer deposits. Grading of the cylindrical component produced is achieved by regulation of powder flow from the feeder.

Table 3-2: Parameters for deposition of functionally graded materials

Parameters	**Data**
Laser power (kW)	1.2 - 1.6
Traverse speed (mm/min)	250 – 300
Wire feed rate (mm/min)	750
Powder feed rate (g/min)	15

3.2.3 Heat treatment

Materials from metal AM processes are known to be anisotropic due to the rapid cooling and differential cooling rates in various directions within a component. Towards achieving a homogeneous microstructure, a number of heat treatments were carried out in this study. Heat treatments were carried out in accordance with the ASTM/ SAE thermal post processing specifications for Titanium alloys produced via additive manufacturing methods [77, 189].

The heat treatments used were the beta and alpha anneal treatments. Investigation of heat treatment of components was carried out in two phases. The initial step was to determine the effect of heat treatments on the smaller Ti6Al4V sections using a Lenton thermal tube furnace tube furnace with Argon gas flowing through the enclosure to prevent oxidation of the components. Components measuring 20 mm by 20 mm were used for this purpose- these were sectioned using waterjet machining from a larger deposited sample. Larger components (the deposited cylinders) used for the turning trials were heat treated in a vacuum furnace at Castings Technology International (AMRC), Sheffield. The heat treatment parameters used are detailed in *Table 3-3*. For both processes, in order to ensure uniformity of results and prevent oxidation, the furnace pressure was kept at 3 x 10^{-3} mBar and operating temperature of the furnace was kept within the tolerance temperatures (± 14° C) as specified by the SAE standard on the heat treatment of titanium alloys [189]. For the heat treatment experiments, two samples each were selected for the various procedures.

Table 3-3: Heat treatment schedule used for DED and wrought Ti6Al4V

Heat Treatment	
Alpha Anneal	Samples (2) held in a furnace at 850°C for 2 hours, followed by a furnace cool to room temperature
Beta Anneal	Samples (2) was held in a furnace at 1050°C for 10 minutes, furnace cooled and held for a

	further 2 hours at 850°C, followed by a furnace cool to room temperature
Beta Anneal (wrought)	Sample was held in a furnace at 1050°C for 1 hour, followed by air cool

To achieve a baseline for comparison with wrought components, a beta anneal was also undertaken for a wrought material to replicate the beta heat treatment microstructure of the DED component. These heat treatments were selected with a view to homogenising the components' microstructures. The term **'homogeneity'** is used in this study to refer to processes that promote the removal of the layer band structure which is a characteristic of additive layer manufacturing processes.

For all three heat treatments, charts showing the operating temperatures, pressures and the vacuum conditions of the furnace is shown in Appendix A. Cooling rate in both instances is 0.035 °C / s.

3.3 Machining Trials

Machining experiments carried out include: Turning, milling and drilling. Due to resource availability however, the turning experiments were limited to understanding the influence of constant tool interaction with the workpiece and was thus more beneficial towards establishing the influence of variation in machining parameters on machinability. The milling and drilling trials were

carried out on a dedicated machine tool which could be adapted for the development of the adaptive control system.

In all cases however, before machining operations could proceed, preconditioning of the deposited components was required. Due to the high heat input during deposition processes, distortion of the substrate was a common occurrence in deposition trials. To ensure uniformity and constant tool engagement during machining, the substrate was pre-conditioned by milling the substrate to give a uniform surface which was level relative to the workpiece holder surface. It should however be noted that due to the use of different machine tools with different spindle capabilities, work holding and tooling the parameters were not transferable for the experiments. However, the underlying process relationships in terms of how parameters affect the cutting process are the same.

For turning trials, 12 mm thick plates were used as substrate for the deposition of cylinders. To ensure concentricity of the cylinder to the cutting tool, the distance to the centre of the cylinder was consistent for all trials and a fixture for clamping the workpiece to the chuck was designed and fabricated. This reduced set up times and overall machining time. The fixture and the component clamped onto it are shown in *Figure 3-5*. For the milling and drilling experiments, preliminary milling of the substrate was necessary to reduce the effects of distortion and ensure the component can be held firmly in a vice.

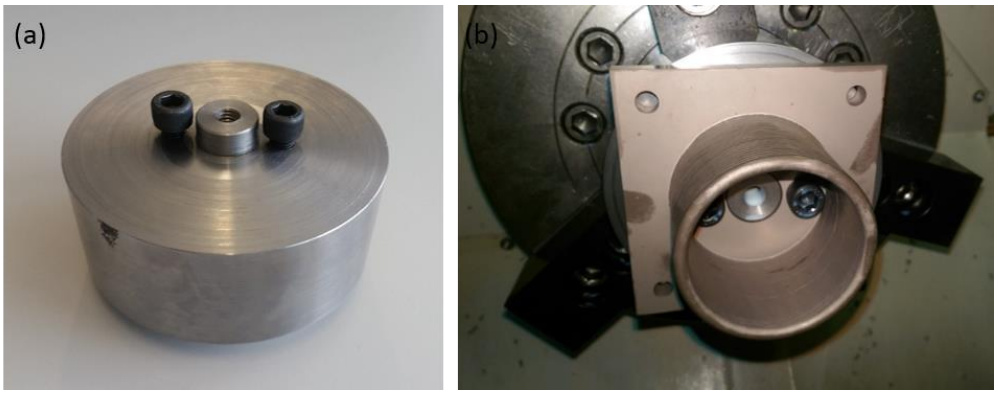


Figure 3-5: (a) Fixture for clamping cylinder (b) Cylinder clamped with fixture

3.3.1 Turning Trials

Outer diameter (OD) turning trials was carried out on a Cincinnati Hawk 300 lathe with spindle power of 55 hp, a 7.5 kW main motor, and maximum spindle speed of 7500 RPM with a 12-station turret. For all machining trials on the lathe, a water-based coolant, Hocut 795B at 5% concentration was used as coolant and was delivered to the cutting region. A Kistler 9121 dynamometer was used for measuring the feed, radial and tangential cutting forces during these trials. A schematic of the forces and the relevant directions is shown in *Figure 3-6*.

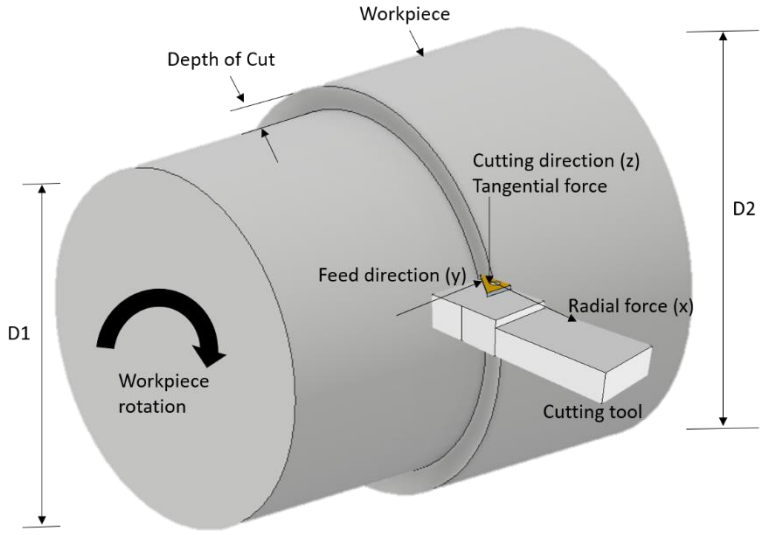


Figure 3-6: Direction of forces measured by the dynamometer

The dynamometer also served as a fixture for the tool holder. Output signals from the dynamometer were conditioned using a Kistler 5070, 8 channel amplifier, with the data observed, recorded and analysed using Kistler's proprietary software, Dynoware at an acquisition rate of 20 kHz. Data obtained was thereafter transferred to other data evaluation software for further analysis. A schematic of the set-up is shown in *Figure 3-7*.

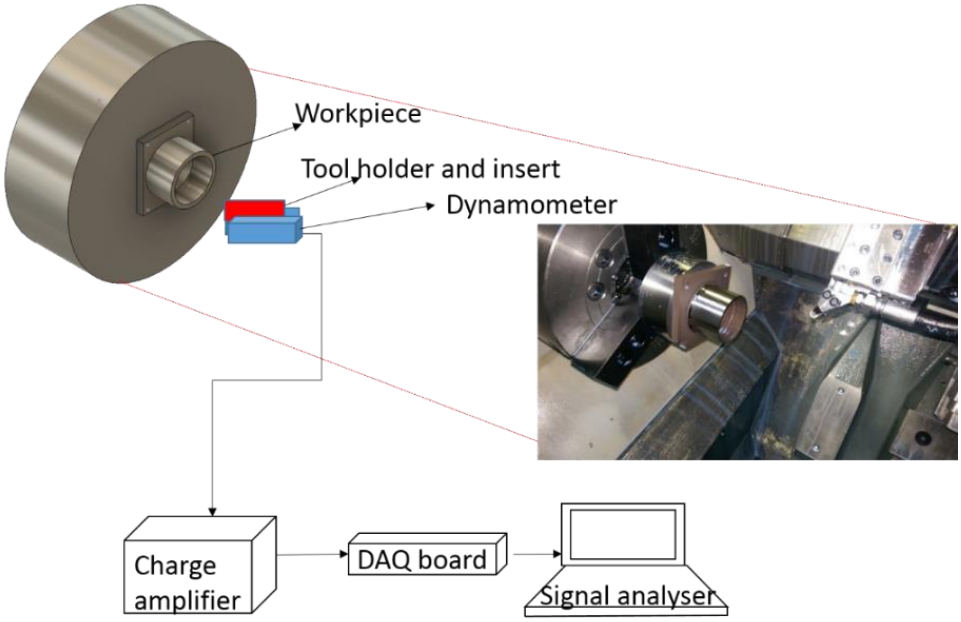


Figure 3-7: Schematic of process for outer diameter turning trials

Inserts and tool holders used in turning trials were provided by Seco tools. The tool grades and uses in this study are described further in subsequent chapters. Turning trials were carried out on single material Ti6Al4V and Ti6Al4V combined with WC. Methods relating to these are presented in the chapters relating to the trials. The aim of these set of experiments was to determine the relationships between process parameters and cutting forces. It was also to deduce the effects of heat treatment on machinability and how improving homogeneity in DED components can be a means of improving machinability.

3.3.2 Milling and Drilling Trials

Milling experiments were carried out on two machine tools, in one instance, the cylindrical components from the turning study were used for the milling trials. In this case, the trials were carried out on a Mori Seiki MSX-501 vertical machining centre. In the second instance, towards development of the adaptive control system, milling and drilling trials were done on a Tormach PCNC 1100 machine tool. The milling trials on the vertical machining centre (Mori Seiki) were aimed at getting results for the comparative evaluation of the effects of machining on the various regions in a built-up part – the deposited region, the dilution region and the substrate. In this case, the component was the material of focus- *Ti6Al4V*. For the latter milling and drilling experiments which were done on the Tormach, the aim was to develop parameters for the development of the adaptive control system. It should be noted this could not be done on the Mori Seiki machine. An alternate set of experiments was thus carried out as the achievable spindle speeds and feeds on the Tormach are considerably lower than those on the Mori Seiki machine. For clarity, these processes involved are differentiated and discussed here.

3.3.2.1 Milling of Cylindrical Components

In using samples from the turning trials, the base substrate was milled from a square to attain a circular base of similar diameter to the deposited cylinder. Thereafter, a finishing pass was carried out on both regions. A schematic of the machining set-up is shown in *Figure 3-8*.

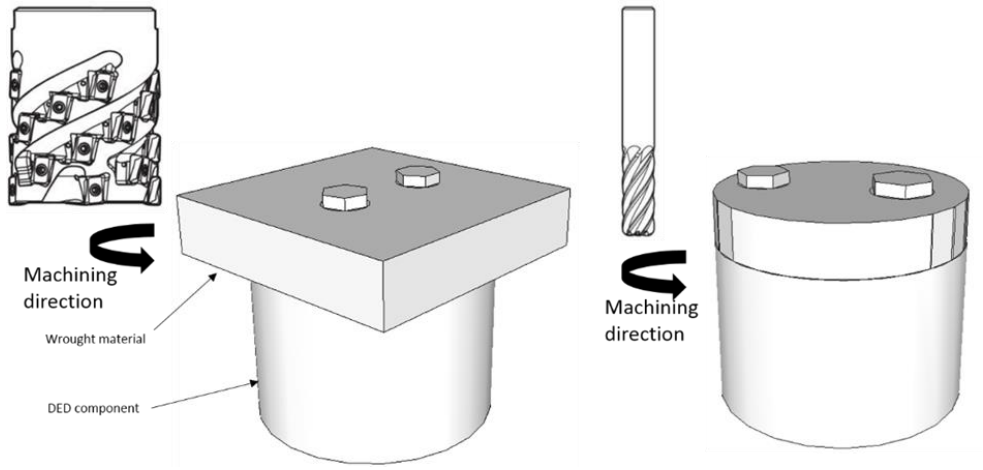


Figure 3-8: Schematic of milling set up for roughing and finish machining passes. Square substrate dimensions, - 180 mm x 180 mm, thickness 12 mm. Regions machined to diameter of 70.5 ± 1 mm.

Inserts and end mills supplied by Seco tools were used for the milling trials. An indexable milling cutter with square double-sided inserts was used for initial roughing passes. These roughing passes were for increased material removal rate during the machining of the substrate to attain a section equal to the desired diameter. Thereafter, solid carbide end mills with a 16 mm diameter were used for the finishing passes. Coolant used, Hocut 795B at 5% concentration was flood delivered (30 l/min) to the cutting region in all machining processes. The machining strategy adopted was to provide a baseline for the investigation of components' regions response to the machining parameters under similar conditions. The regions are divided into three based on their thermal histories - the **DED** region, the **dilution** zone- which is the interface between the DED region and the **wrought** substrate region. Parameters used for the initial machining and finish machining processes are shown in *Table 3-4*. For all finishing passes, a new tool is used

for machining. Cutting force measurements were not taken during these trials.

Table 3-4: Roughing and finishing parameters used in machining components

Operation	Insert / Cutter	Tool type	Tool diameter (mm)	No of flutes	Speed (m/min)	Feed rate (mm/ tooth)	Table feed (mm/ min)	Radial Depth of Cut (mm)	Axial depth of Cut (mm)
Roughing	R220.94-00050-046-12.4A/ LOEX120708TR-M12	Carbide	50	4	45	0.08	92	2.5	5
Finishing 1	JS720160D2R050.0Z6	Carbide	16	6	80	0.06	573	0.5	5
Finishing 2	JS720160D2R050.0Z6	Carbide	16	6	160	0.06	1146	0.5	5

As detailed in the table, two parameter sets were used in the finishing passes and the variation in parameters was for the investigation of the effect of changing machining conditions on the surface quality in the various regions. Finishing parameters were selected were selected with a view to keeping the feed per tooth constant whilst changing the spindle speed and feed rates. *Table 3-5* highlights the components used and the finishing machining passes they were subjected to. The naming convention adopted includes the heat treatment the material was subjected to and the finish machining parameters used on the sample. Typically, in the machining of wrought titanium alloys, low cutting speed with high feed rate values are preferred towards providing a combination of reduced tool wear and optimum surface integrity.

Table 3-5: Components and the corresponding finishing regime. Finish 1 is low speed and finish 2 is high speed and high feed rate

Sample	Machining regime
As built 1 (AB1)	Finish 1
As built 2 (AB2)	Finish 2
Alpha 1	Finish 1
Alpha 2	Finish 2
Beta 1	Finish 1
Beta 2	Finish 2

3.3.2.2 Milling for Adaptive control system development

The advantage of using the Tormach machine tool in the development of the control system was due to the open architecture design of its controller which lends to part of its operations to being modifiable. The development of the control system is discussed further in Chapter 6.0. The CNC is an open source machine tool with the spindle and drive run by a 3-phase induction motor which is powered by a single-phase variable frequency drive that operates on 230 V. The spindle power for the machine tool is 1.5 hp with a maximum spindle speed of 4500 RPM. The maximum attainable feed rate is 1650 mm/min. Several cutting tools were used in the study, a description of the tools and their functions is detailed in subsequent chapters as their use is discussed. Parameters used in machining were based on the recommendations from the tool manufacturer based on the wrought forms of the material. For all experiments carried out using the Tormach CNC, water-based coolant (V-cut SS) was used and this was delivered to the cutting region at 12 litres /min.

Similar to the turning trials, the cutting forces during machining in the milling and drilling trials were also measured and analysed. Kistler dynamometers, 9257B, and a 4-component stationary drilling dynamometer, 9272 were used in both the development of the control system for the Tormach and for the measurement of cutting forces during machining operations. The sampling

rate here was dependent on the cutting operation and the resulting cutting force signals are conditioned using a *Kistler* charge amplifier 5017 B together with a National Instruments *CompactRio* 9022 coupled with an analogue input module NI 9205. For the monitoring, conversion and recording of the acquired force signals into relevant cutting force data, a LabVIEW Virtual Instrument (VI) was developed and used. By using the appropriate scaling factor, output signals were converted to cutting force, monitored and recorded directly into spreadsheets. This formed the foundation for the development of the control system as one part of the required loop was the monitoring of cutting conditions during the machining process. The other vital part was the control of the CNC drives with feedback cutting force data. A schematic of the set-up is shown in *Figure 3-9*. The use of cutting forces in the control loop is based on the premise that the machinability of a material is assessed in terms of the cutting forces, chip formation characteristics, surface condition and tool life. Cutting forces being measureable during the process, was selected as a constraint as it gives an indication of the prevailing conditions of the cutting process, the variation in material cutting requirements, and an indication of the tool condition. The LabVIEW VI developed for in-process monitoring of cutting force is further discussed and shown in Section 6.2.4.

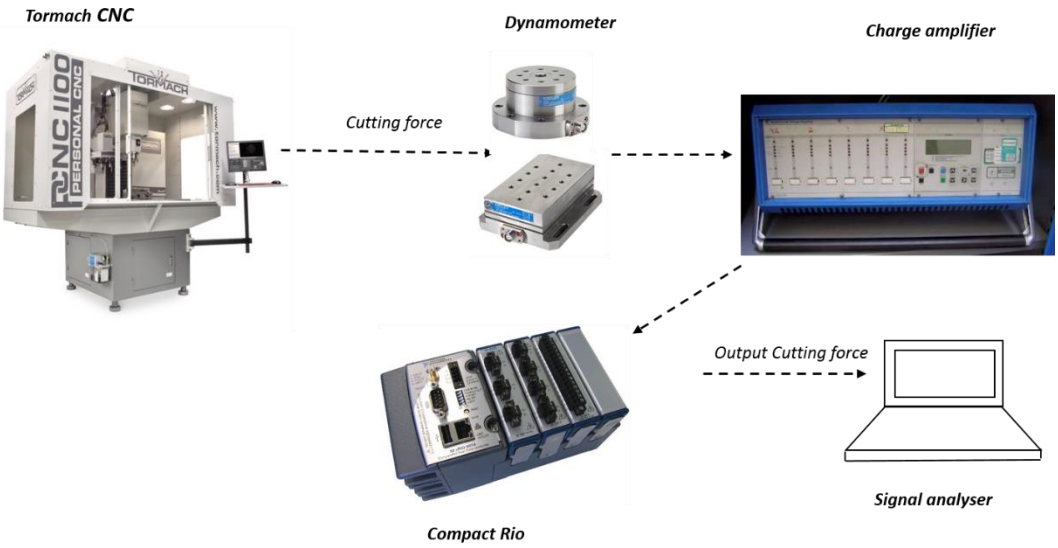


Figure 3-9: Schematic of cutting force measurement system

3.4 Material Characterisation

A number of processes were required in the characterisation of components deposited and machined in the study. The characterisation steps used depended on the machining operation carried out on the component, the feedstock material, component shape, post heat treatments amongst other processing steps. A schematic of the steps involved is shown in *Figure 3-10* and is discussed accordingly. For all quantitative data in this study aside from residual stress, error data (σ_x) is computed by obtaining the mean, the standard deviation (σ) and the square root of the sampling range (N). The relation used is as below:

$$\sigma_x = \frac{\sigma}{\sqrt{N}} \qquad (3\text{-}1)$$

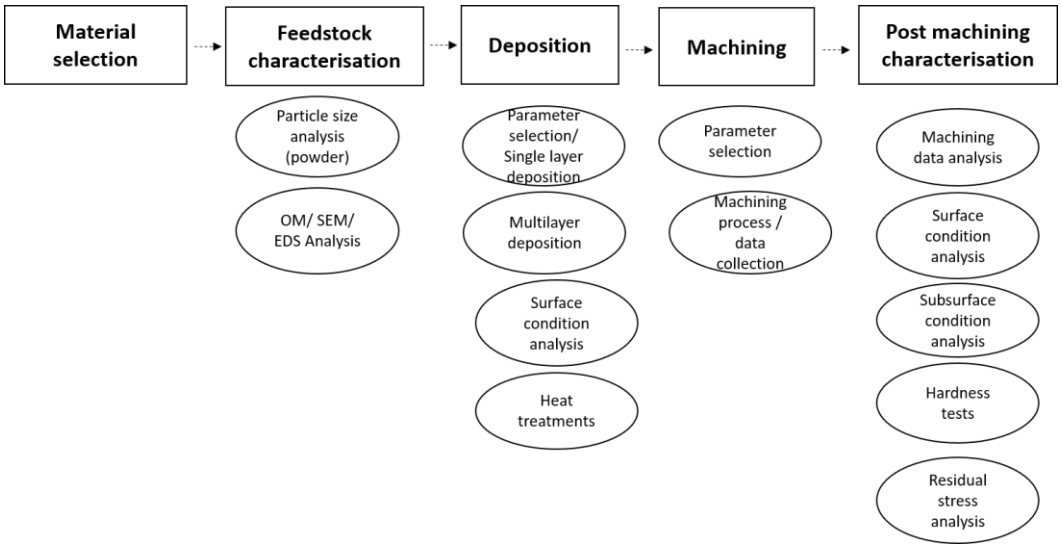


Figure 3-10: Schematic of process flow showing generic steps for material investigation

3.4.1 Feedstock Material

Characterisation of materials was required before deposition processes. Pre-deposition characterisation was mostly for powder feedstock materials. Characterisation of these components was important in determining the material characteristics including particle size fraction, favourable deposition conditions required and to predict flowability. Material characterisation for feedstock powders was done using optical microscopy (OM), scanning electron microscopy (SEM) and energy dispersive X-ray spectroscopy (EDS). Particle size analysis was done using a Malvern 3000 Mastersizer particle size analyser. The particle size analyser used functions based on the principle of laser diffraction in measuring particle size. Dry powder method was used in the analysis of the material.

3.4.2 Surface Roughness

Surface roughness of all components used was measured post machining. There was a need to investigate the influence of machining parameters on the resulting surface condition. Since the basis for post processing these components is primarily for the improvement of surface quality, measurement of surface roughness is relevant to quantify the gains from any machining strategy adopted. An Alicona G5 Infinite focus, a Talysurf Hobson Form Talysurf 50 and a Bruker white light interferometer were used at various stages of the study for the measurement of surface roughness. The Alicona and Bruker devices function based on non-contact profilometry and are capable of measuring form and surface finish. The Talysurf 50 used in this study operates based on contact profilometry and as such included a stylus for surface condition measurements. This was particularly useful in measuring the surface finish of drilled holes. In measuring the surface roughness in drilled holes, three measurements are taken and the mean of these was used as the roughness value. Also, the use of the surface profilometers in addition to OM was useful in the visualisation of wear of the tooling used. Results from the measurements from both instruments was further analysed using Mountains Map - an image analysis and surface metrology software. In analysing surface roughness values from measured maps, the arithmetical mean of deviation in roughness value from the mean line of roughness value (Ra) and the mean value of the greatest height of roughness profile from consecutive sampling lengths (Rz) are evaluated and used in comparative

analysis. These are as defined in *Figure 3-11*. These parameters are selected for computing roughness of surfaces in this study as they give a close approximation of the height variations in the surface.

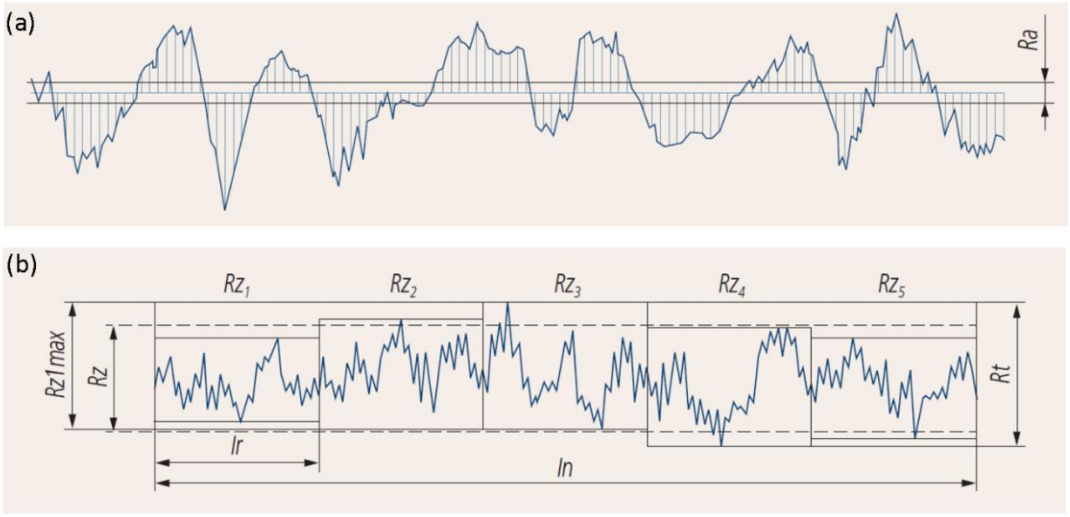


Figure 3-11: Definitions for surface roughness parameters (a) Ra (b) Rz [190]

3.4.3 Material Preparation

Preparation of samples for characterisation involved sectioning the components to smaller representative sizes which can be mounted in resin for further investigations. Components were sectioned using various methods, the most notable of which is wire electrical discharge machining (WEDM) to limit the distortions to the sectioned interface. Other techniques used in sectioning components include; waterjet machining and also an abrasive wheel cutter. Samples obtained were thereafter mounted in conductive resin for microstructural examination. Mounted samples were polished using

standard metallographic techniques for Titanium alloys. *Table 3-6* shows the etching criteria used for the components. Samples for OM were etched using Krolls' reagent to reveal grain structure.

Table 3-6: Etchant for Titanium alloy

Alloy	Etching used
Ti6Al4V	Krolls' Reagent - 2 mL HF, 4 mL HNO_3, 1000 mL H_2O *Samples swabbed for 10 - 15 seconds*

3.4.4 Microstructural Analysis

Microstructural analysis of the as-deposited microstructure, heat treated components, and post machining sub-surface condition was undertaken. OM, SEM were used in the completion of these. Also, EDS was used in the characterisation of interface layers in the deposition of functionally graded components. SEM imaging was carried out on a Quanta FEI 600 SEM (operating at an accelerating voltage of 15 - 20 kV, working distance of 10 mm, spot size of 4.5- 5.0) and a Philips XL30 FEI SEM. A Hitachi TM3030 desktop SEM was also used for imaging tools and inserts used for machining. Subsurface deformation analysis was carried out on the components after machining. This was to determine the effects of the machining process on the components integrity and to provide a basis for comparison of machinability. In carrying out the analysis, a combination of visual inspection by measuring the observed deformation depth and the use of an opensource software 'ImageJ' (with the threshold tool) for determining the depth with the 'swept' microstructure – which represents the deformed region.

In revealing the variations in material microstructure and orientation, a laser ultrasonic technique, Spatially Resolved Acoustic Spectroscopy (SRAS) has been used. SRAS measures the Surface Acoustic Wave (SAW) velocity, which varies across the sample as the underlying crystallographic orientation of the material changes. This produces contrast maps which show the grain structure or texture of the material. In this study, SRAS was used as an alternative to EBSD due to the relatively larger sampling region that can be mapped and the relative ease of material preparation. The SAW's were generated using a pulsed generation laser (Q-switched Nd:YAG with a wavelength of 1064 nm, a repetition rate of 2 KHz, pulse energy of 7.5 µJ at the sample), a mask was also used to define the acoustic wavelength of 24 µm. A second laser (continuous wave with a wavelength of 532 nm, 60 mW at the sample) in conjunction with a Knife Edge Detector (KED) was used to detect the frequency of the SAW. The use of SRAS was limited to the study on the effects of adaptive machining as it presented a resource which supported the microstructural variations in the component.

3.4.5 Microhardness Analysis

Hardness data was measured using a Buehler microhardness tester with a Vickers profile attached. Towards ensuring consistency and repeatability in all trials, the load used for similar materials is kept constant. A load of 300 gf with an indentation of 15 s was used for all Ti alloy trials. In measurement of hardness of materials with hardening phases (WC particles), the regions

adjacent the particles and the particles themselves are avoided to prevent anomalous readings due to variations in hardness prevalent due to these particles. Microhardness of regions close to the machined surfaces were also taken to determine the effect of subsurface deformation on the changes in hardness at these regions. In the measurement of hardness, the indents are spaced at intervals of no less than three times the Vickers indenter width to satisfy the requirements of the associated ASTM standard [191]. The spacing used in all hardness experiments was 0.75 mm. For hardness measurements, a minimum of ten measurements were taken and the mean derived.

3.4.6 Residual stress Analysis

Residual stress can be described as the stress state of a material without the influence of an external load. It can also be defined as the stress which remains in a body which is stationary and at equilibrium with its immediate surroundings. X-ray diffraction technique is a non-destructive method for measuring residual stress which uses the distance between the crystallographic planes as a strain gauge, and the deformations on the material which would have led to changes in the lattice spacing from the stress-free condition is read as the magnitude of the residual stress of the material. Relating this to the Poisson's ratio effect, a tensile load applied on a body leads to the lattice spacing increasing in planes perpendicular to the stress direction and a consequent decrease in planes parallel to the stress direction.

In this study, residual stress was measured in the normal direction to the machined surface using a Proto iXRD instrument with X-ray diffraction from a Cu Kα source and a Nickel filter. Residual stress measurements were taken with operating parameters of 20 kV and 4 mA. Analysis of resulting stress values was realized using the proprietary XRDWIN 2.0 software. The equipment uses X-ray diffraction for the measurement of residual stress. *Table 3-7* shows the residual stress measurement parameters.

Table 3-7: Residual stress parameters

Parameter	Value
Tube	Cu_K alpha
Filter	Ni
Wavelength	1.541838
Voltage (kV)	20
Current (mA)	4
Beta angles	30° to -30°

In all trials involving residual stress measurements, the samples used were flat and the readings were taken in central regions avoiding regions with curvature. The results obtained from the analysis is further evaluated with the XRDWIN software and this outputs the error data with the results which were adopted in computing the final residual stress values.

3.5 Control System Architecture

In the development of an adaptive control system on the Tormach CNC, a number of components were required, these are discussed briefly here and in more detail in Chapter 6.0. A closed loop control system was proposed which

would be capable of responding to changes in material microstructure and adapt machining conditions to suit the prevailing conditions. In doing this, LabVIEW was used in combining signals from all the resources required for the controller to function. Components of the system are discussed here.

3.5.1 National Instruments CompactRIO

A CompactRio consists of a processor running a real-time operating system, a reconfigurable FPGA and interchangeable I/O modules. The device provides a platform for peripheral components such as sensors and controllers connected to it to be monitored and controlled from a single interface. Modules used with the controller in this study include; NI 9205 analog input module and the NI 9263 which is an analog output module. The processor has the capabilities to provide real time measurement and response to changing conditions and can give acquisition rates up to 1 kHz.

3.5.2 Microcontroller

A single board Arduino microcontroller is used for the control of the CNC. The microcontroller provides a low-cost alternative for the control of input signals. Arduino boards are equipped with sets of digital and analog input/ output pins which may be interfaced to other expansion boards or circuits. The boards also have serial communication interfaces which include the Universal Serial Bus (USB) which provides for seamless means for loading developed codes from a personal computer. The USB connection was used in interfacing with

the Tormach CNC. An existing Arduino code was developed and modified to suit the purposes intended in this study without causing undue lag to the system during machining trials.

3.5.3 Sensors

Sensors used in the development of the control system include an accelerometer and the Kistler dynamometer discussed previously. Dynamometers were used in this study for the measurement of cutting forces. These dynamometers consist of piezoelectric sensors and are of the stationary type. In turning operations, the dynamometer is placed directly on the turret and the tool is placed on the dynamometer. For milling and drilling operations, dynamometers used were fastened to the machine bed and the work holding apparatus attached to the set up.

Cutting forces obtained from the dynamometers are averaged in all cases and these are clearly indicated in the plots. Mean values of the cutting force are computed over a period where full tool engagement occurs. In the computation of standard errors, the method adopted is as defined in equation 3-1.

4.0 Machinability of Directed Energy Deposited Ti6Al4V

This chapter details the investigation on the machinability of Ti6Al4V components produced using Directed Energy Deposition. The machinability of the components in relation to the machining process parameters – depth of cut, feed rate and spindle speed are investigated. The effects of traditional machining approaches on the resultant surface integrity of Ti6Al4V produced by DED is investigated. Also, the effects of alpha and beta anneal heat treatments applied post DED build in homogenising component microstructure and mechanical properties towards improving the machinability of the material is explored. The effects of these thermal treatments on mechanical properties such as hardness and surface stress condition are discussed. Surface finish, post machining in the various components are compared and a deduction is made on the effects of prior microstructure to the attainable machinability of the component. This chapter also provides a background for understanding the associated peculiarities in machining DED deposited components with process parameter variation. Components are subjected to turning and milling trials and the associated methodologies peculiar to both machining processes are discussed.

4.1 Directed Energy Deposition of Ti6Al4V

The deposition of components for machining was carried out using the 2 kW IPG fibre laser system described in Secti on 3.2. The start point for deposition trials for these components was the deposition of single bead deposits. This was to determine the optimum parameters for deposition and to determine the clad morphology which serves as a guide for multilayer deposition. Thereafter, parameters were adapted for the deposition of multilayer deposits. However, it was observed during deposition of multilayer builds that it was expedient to adjust the laser power, as the build progressed due to the elevated temperature of the build. This was also to ensure the stability of the set up in producing metallurgically sound deposits. The parameters used towards achieving a stable deposit for both deposition processes (cylindrical builds) are as follows:

Table 4-1: Directed Energy deposition parameters used in fabricating cylinders

Parameters	Value
Laser power (kW)	1.4 – 1.6
Traverse speed (deg/min)	323
Wire feed rate (mm/min)	800
Step up in Z (mm)	1.5
Beam diameter (mm)	3.1
Ti6Al4V wire diameter (mm)	1.2
Substrate thickness (mm)	12

For these processes, the procedures outlined in Section 3.2.1 were used. *Figure 4-1* shows the as-deposited components. The remainder of this chapter

discusses the machining trials carried out on the cylinders i.e. turning and milling trials.



Figure 4-1: Samples of cylinders deposited for turning trials using DED

For the turning trials, an array of cylinders was produced using the techniques and parameters listed. The DED process was repeatable with the components built to dimensions with minimal variations (± 0.5mm of target thickness). A total of eight (8) cylinders were deposited for the machining trials. Typical dimensions for the cylinder are shown in *Table 4-2*. From the cylinders produced, a total of four (4) samples were selected at random for heat treatment.

Table 4-2: Typical cylinder dimensions

	Cylinder dimensions (mm)
Internal diameter	62
Outer diameter	72
Height	50
Thickness	5

4.2 Turning Trials

4.2.1 Tooling selection

Two commercial cemented carbide cutting inserts and the corresponding tool holders were supplied by Seco Tools for the turning trials. Details of the inserts used here and their functions is detailed in *Table 4-3*. In order to overcome the undulating surface texture of the as built component and protect component integrity, round carbide inserts with a large cutting edge were selected for machining. The cutting-edge shape makes the insert less prone to shock impact due to variation in the workpiece surface geometry and the consequent anticipated workpiece run out during machining. Compared to triangular and rhombic shaped inserts, these round inserts have a robust cutting edge and are suitable for use in applications requiring large machining depths of cut. The inserts are also useful in the machining of heat resistant alloys as they do not possess corner weak points which are more susceptible to damage when making larger depths of cuts. In using these inserts, multiple cutting edges along the diameter can be used on the same insert for new machining trials, thus making it a preferred solution.

Table 4-3: Inserts used in the turning DED components and their functions.

Insert ID	Grade	Use	Tool holder	Coolant delivery

RCMT10T3M0-F2, HX	HX, Uncoated	Preliminary surface preparation	SRSCL-20-10JET	High pressure through tool (50 bar)
RCMT10T3M0-F2, TS2000	TS 2000, coated	Surface preparation /Finish machining	SRSCL-20-10JET	High pressure through tool (50 bar)

4.2.2 Machining Strategy

Following appropriate preconditioning of the substrate to minimise workpiece run out during machining, the as-built, alpha annealed and beta annealed cylinders were subjected to outer diameter (OD) turning operations on the Cincinnati Hawk 300 lathe. Throughout the investigation, coolant used was Hocut 795B at 5% concentration and was delivered through tool at a pressure of 50 bar to avoid excessive increase in temperature of the tool.

For comparison, wrought Ti6Al4V subjected to a beta anneal was also machined with the same parameters used for the DED components. For every parameter variation, a new insert was used to ensure repeatability of the experimental process and create a basis for comparable results.

Two strategies were used in machining, in the first instance, a ‘clean up’ machining process for removal of the outermost layer was required for all components before machining the bulk region. This was to limit the effect of workpiece run out and provide a reference point for subsequent machining trials on the workpiece. As detailed in *Table 4-3*, the uncoated carbide tool

was used for surface preparation in all trials relating to investigating the effects of varying cutting speed and feed rate. However, for depth of cut and the effect of the outermost layer experiments, the preliminary 'clean up' machining activity was not carried out. The objective of this was to replicate a near net machining process in order to determine the minimum amount of material required to be removed to produce a component with a desirable surface finish, with a limited number of machining passes. Also, the machining of this layer in comparison to machining the bulk region was of interest as the reasonable strategy in an industrial application would be to remove this layer with the least number of machining passes whilst still producing a desirable surface finish. It has been suggested that the outermost layer in metal AM produced components are mostly tensile in the as built condition [192]. A variation in machinability between these layers would provide some insight into this occurrence. Parameters used in machining the components during the various machining operations are shown in *Table 4-4*. Parameter selection is based on the tool manufacturers' recommendations – which is based on machining wrought components.

Table 4-4: Parameters used in turning of Ti6Al4V

Operation	Insert	Speed (m/mir	Feed (mm/rev)	Depth of Cut (mm)
Clean up	Uncoated Carbide	100	0.1	0.25
Depth of Cut	Carbide PVD	100	0.1	)5, 0.1, 0.15, 0.20
Cutting Speed	Carbide PVD	50, 100, 150	0.1	0.25

Feed rate	Carbide PVD	100	0.05, 0.10, 0.15, 0.2, 0.25	0.25

A Kistler 9121 dynamometer was used for measuring the radial, feed and tangential forces during these turning experiments. For these experiments, acquisition software from Kistler, Dynoware, was used in recording the resulting cutting forces and for preliminary offline data processing.

4.2.3 Material Characterisation

After machining, the resulting components were sectioned using WEDM as shown in *Figure 4-2*. From the resulting samples, the cross sectioned face, parallel to the cutting direction was mounted in conductive resin and prepared for analysis using the procedures discussed in Section 3.4.3. SEM imaging was carried out on a Quanta FEI 600 SEM operating at 20 kV with the same operating conditions for imaging all samples. Analysis of the inserts used in the study was done using a Hitachi TM3030 desktop SEM. Microhardness and residual stress analysis for the resulting samples were carried out using the processes and equipment described in Section 3.4.

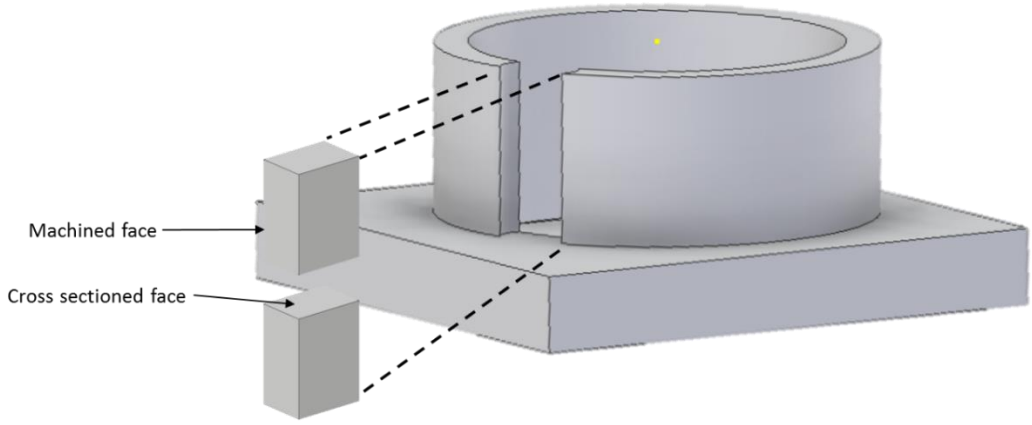


Figure 4-2: Schematic of cylinder after machining and sectioned with WEDM

4.2.4 Results

4.2.4.1 Microstructural Evolution

Analysis of the DED components post heat treatment shows a marked variation in microstructures across heat treatments. In the as-built condition, the structure is typical of DED Ti6Al4V components reported previously [13, 187]. The macrostructure shows large columnar grains due to the directional grain growth with bands which correspond to the interface between each deposited layer. Microstructure between bands comprises of a Widmanstatten microstructure with α laths of approximately 1.5 µm width in retained β, with the α laths continuous at the β boundaries [16]. The 'banding' regions due to layer re-melting can be readily observed in *Figure 4-3*(a). These re-melted regions show comparably finer lamellar structure in the 'as built' component and comprises larger colonies of acicular α. During the deposition process, the temperature of previously deposited layers are prone to exceeding the beta transus temperature (~ 1000°C) with the addition of

subsequent layers. This leads to the formation of new heat affected zones and subsequent coarsening of α laths. The finer α laths observed are due to the rapid cooling of the deposited layer.

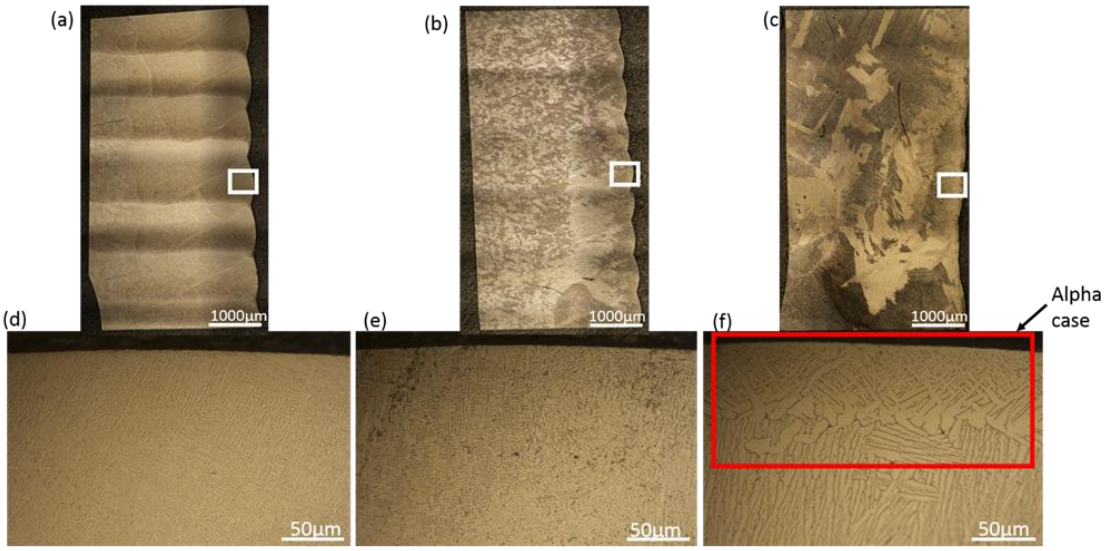


*Figure 4-3: Optical Microscope images of (a) 'as built' DED and (b) Alpha Anneal DED showing clear **'layer banding'** as a result of stacked layers. (c) Beta Anneal DED (d) Highlighted regions in a (e). Highlighted regions in b (f) Highlighted regions in c. All Samples etched with Krolls' reagent*

In the heat-treated samples, the remelted layers become indiscernible as grain growth migrates across the remelted regions improving layer band removal. The alpha annealed component, *Figure 4-3*(b) shows slight coarsening of the alpha laths (increase in width to 2.5 µm) with the remelted layers remaining apparent. The beta heat treated component, *Figure 4-3*(c) undergoes a transformation in microstructure with no evidence of the pre-heat treatment bands in the microstructure, and no distinguishable difference between the re-melted layers and the bulk regions. In the beta heat treated components, with the heat treatment temperatures above beta transus, the columnar β grains transform to lamellar α+ β with coarse α laths and fewer

colonies. Higher magnification images of the highlighted regions in *Figure 4-3* (a), (b) and (c) are shown in *Figure 4-3*(d), (e) and (f) respectively. The periphery of the beta DED component, highlighted in *Figure 4-3* (c), shows a 100 µm thick band of larger grains pre-machining, which is a surface alpha case. This is despite the heat treatment process being undertaken in a high vacuum environment. At temperatures above 600 °C, titanium alloys oxidise in oxygen containing environments resulting in the formation of TiO_2 and an alpha case. The alpha case has been reported by other investigators to be a continuous hard brittle layer which degrades mechanical properties. Evidently, there is a need for the avoidance and removal of this phase from heat treated Titanium alloy components. An SEM image of the observed alpha case is shown in *Figure 4-4.* However, it should be noted that this layer was not observed in the alpha annealed component despite the anneal temperatures reaching beyond the referenced temperature for alpha case formation. Thus, the formation of this layer is attributed to the higher maximum temperature and prolonged exposure period which aids the reaction with oxygen. The presence of this variation in grain size and morphology at this region is expected to further influence dissimilarity in machining behaviour between the outermost and interior regions in the beta component.

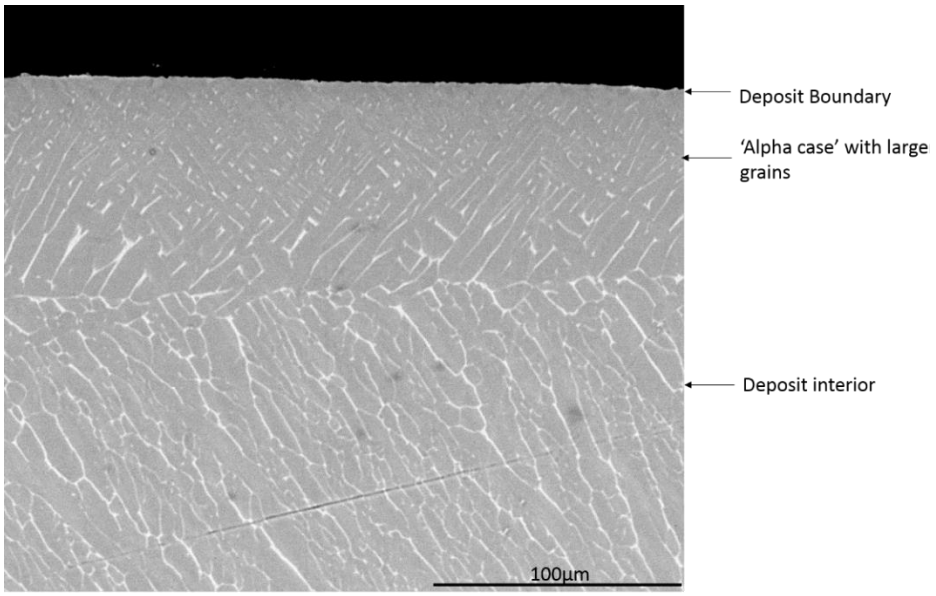


Figure 4-4: SEM image showing alpha case formation in beta HT component. Mean beta lath thickness in alpha case region = 8.29 µm, mean beta lath thickness in deposit interior = 5.51 µm. Image is taken in SE mode

SEM images of the microstructures obtained for the array of heat treatments used are shown in *Figure 4-5*. The images show the lamellar microstructure is retained in the alpha DED sample (*Figure 4-5* (b)). This morphology is however not observed in the beta DED component (*Figure 4-5*(c)). The wrought beta microstructure is comparable to the beta DED sample with both microstructures showing larger alpha laths and elongated beta, with the elongation in alpha laths being more pronounced in the beta heat treated DED component.

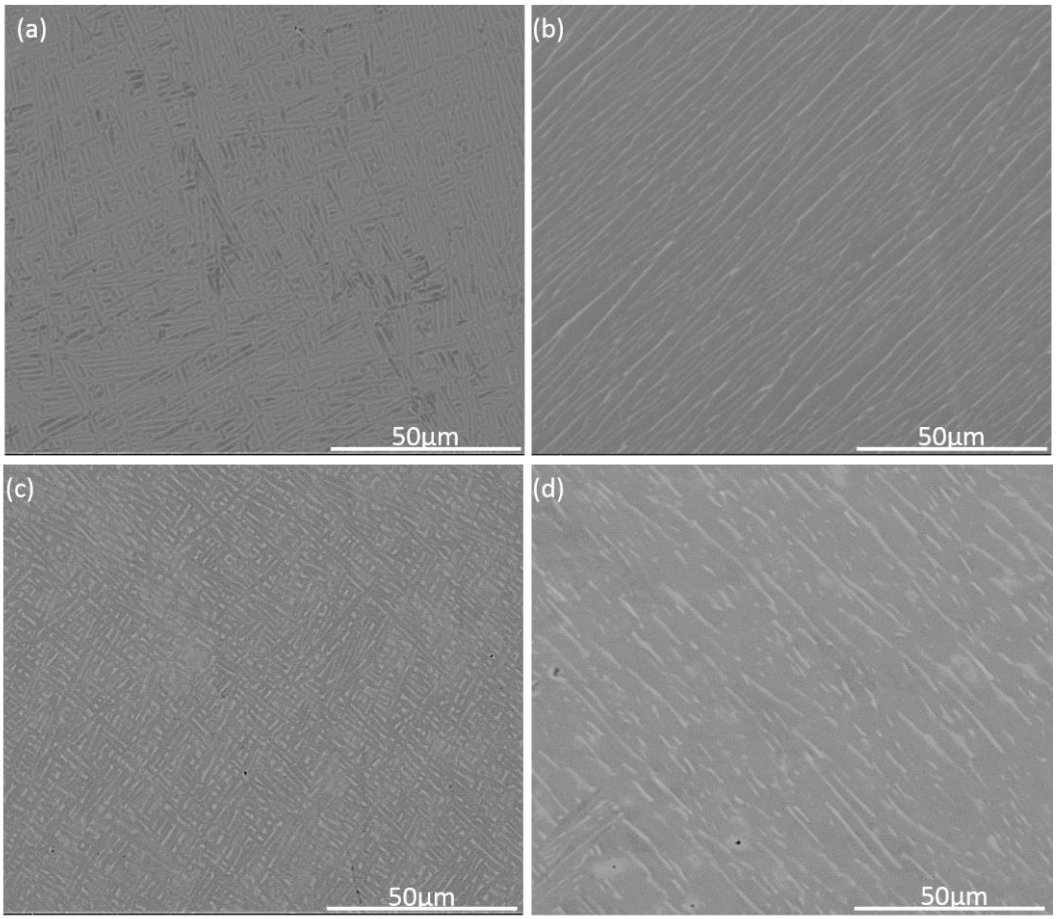


Figure 4-5: Microstructures from interior regions of the builds: (a) DED as built (b) DED post beta heat treatment (c) DED post alpha heat treatment (d) Wrought beta heat treatment. Images taken in SE mode

4.2.4.2 Cutting forces

Analysis of cutting force plots was conducted with a view to understanding the difference in chip formation mechanism in both regions and the effects on cutting forces. The cutting forces in the radial (fx), feed (fy) and tangential (fz) were acquired at 20 kHz. A typical force feedback signal data plot during a turning trial in this study is shown in *Figure 4-6*. From the figure, the

interaction of the cutting edge with the workpiece leads to a variation in cutting force response which can be identified as:

- **Start;** No interaction between tool and workpiece. Data acquisition begins earlier than the cutting process to ensure the entire process is adequately recorded. The process also records offset in the setup which can be termed as noise due to the system dynamics - such as; machine vibration, the start of the coolant delivery. The offset value is noted, and the corresponding data adjusted with the value during offline analysis.
- **Contact;** in the preliminary stages of contact, the z force data is observed to rise much faster than the x and y force data. This is due to the difference in the size of the cutting area in front of the tool between the regions. With increased contact of the tool and workpiece, the force in the radial direction (fx) becomes prominent indicating the progression from sliding contact to full engagement of the tool and subsequent cutting.
- **Steady state;** after tool contact and with full tool engagement, the forces increase to a magnitude which gives a description of the cutting process after about 2- 5 revolutions of the workpiece. The forces here are susceptible to variation due to the changes to the cutting-edge geometry due to wear or the formation of a built-up edge or variation in microstructural properties of the material. This is the region of interest in this study as it gives an indication of the influence of microstructural variation and the effect of the undulating profile of AM surfaces on tooling. Mean of the measured values in this region are computed and are taken to be representative of the process. Error values

are also computed using the values obtained in this region using the standard error computation equation described in section 3.4 .

- **Finish;** at the completion of cutting, the tool retracts, and the force returns to zero.

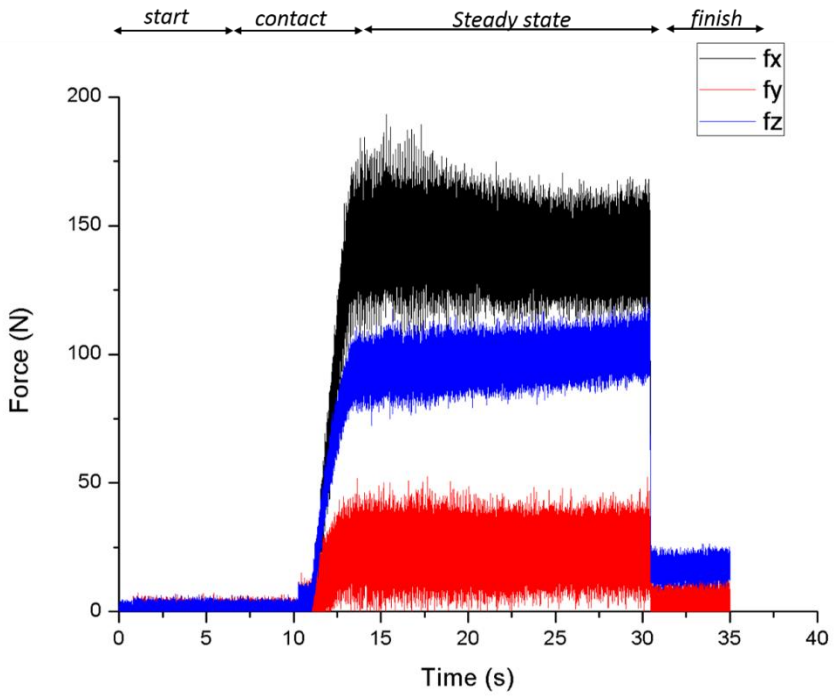


Figure 4-6: Cutting force data along the x (Radial), y (Feed) and z(tangential) planes. The acquired data monitors a complete cutting cycle with the corresponding cutting regions highlighted; start, contact, steady state and finish

Figure 4-7 shows the variation due to undulating surface profile on the cutting forces during the machining of a single material region. These undulations in the surface cause workpiece run out which leads to the tool undergoing cyclic loading and unloading at short intervals. Plots such as these are representative of machining AM components with undulating surfaces at shallow depths of cut.

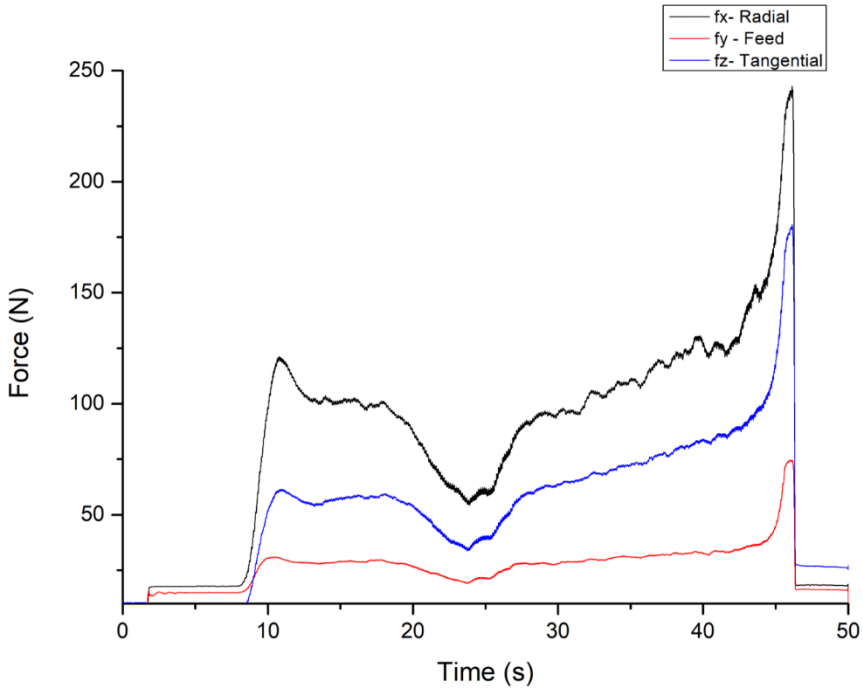


Figure 4-7: Initial machining pass to remove the undulating layer by a machining pass. Tool runout leads to periodic decrease in cutting forces. Radial depth of cut for all passes was 0.25 mm in plots shown. Plots filtered with low pass FFT at 10 Hz.

4.2.4.3 Post DED Machining – 'Clean up' procedures

For initial 'clean up' passes, a radial depth of cut of 0.25 mm was used in machining. For most of the components, one machining pass at this depth of cut was sufficient for the removal of the outermost layer. The use of components with this 'as built' layer for most applications is undesirable as these rough surfaces can act as crack nucleation sites due to the surface morphology. For the purpose of investigating the properties of the outermost layer in comparison to the subsurface, successive equal machining passes with a depth of cut of 0.25 mm were used with cutting forces measured for each machining pass. During the preliminary machining process, due to the surface

texture, workpiece run-out was prevalent. Workpiece run out is an area of interest in machining AM components as it leads to premature tool failure and as such, tooling should be capable of withstanding variable loads during the machining of these surfaces. Also, for industrial applications, this would be the most important layer during machining as it might be necessary for this to be the only layer to be removed to achieve the required shape and surface finish. In the initial machining of AM components, due to the characteristic wavy surface, larger depths of cut can be taken to mitigate the effects of run out towards achieving a steady state cut.

The measured mean steady state forces during the removal of the outermost layer was found to be lower than the forces during machining of the subsurface. At a depth of 1.5 mm (after 6 passes) from the original surface and with increased stability of the cutting process, the difference in mean cutting force is observed to have increased by over 100% (a 110 N increase) of the value from the surface in the radial direction. Machining depth and corresponding cutting force values are shown in *Figure 4-8*. Cutting force values are measured and plotted in the radial (fx), feed (fy) and tangential (fz) directions.

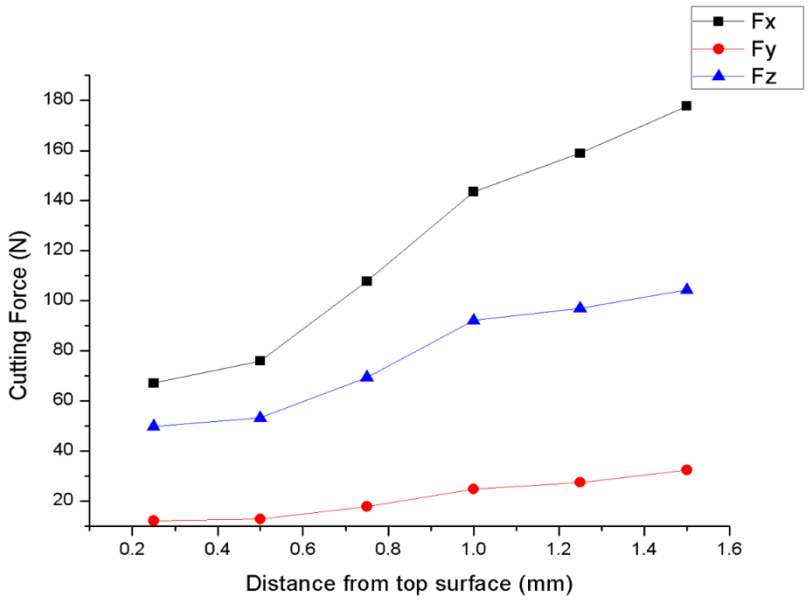


Figure 4-8: Increase in mean cutting force with increase in vertical distance from 'outermost skin'. Subsequent passes into the material yield the cutting forces shown.

Whilst workpiece run out is a factor in the reduction of the measured mean cutting forces, during solidification, the difference in cooling rates in various regions of the component results in variable microstructure and the anisotropic mechanical properties of the components which in turn results in variable machinability. Plots relating to the progression of cutting forces during machining passes to achieving steady state and acceptable finish are shown in *Figure 4-9*. From the plots, undulations and deposition instabilities during the build process which affect the components' geometry leads to workpiece runout and also a reduction in cutting force observed in all the plots done with the presence of surface undulations (passes 1-5) between the 25 - 30 seconds marks. In the machining process at steady state (pass 6), comparatively higher mean forces are obtained which relates to the tool becoming fully engaged with the component geometry not initially machined

in the initial passes. Issues such as this can be avoided without the need for multiple passes by ensuring geometrical accuracy of the component is adequately accounted for, or by taking a larger depth of cut during preliminary machining which would entail accounting for material removal as a result of post process machining in the deposition strategy.

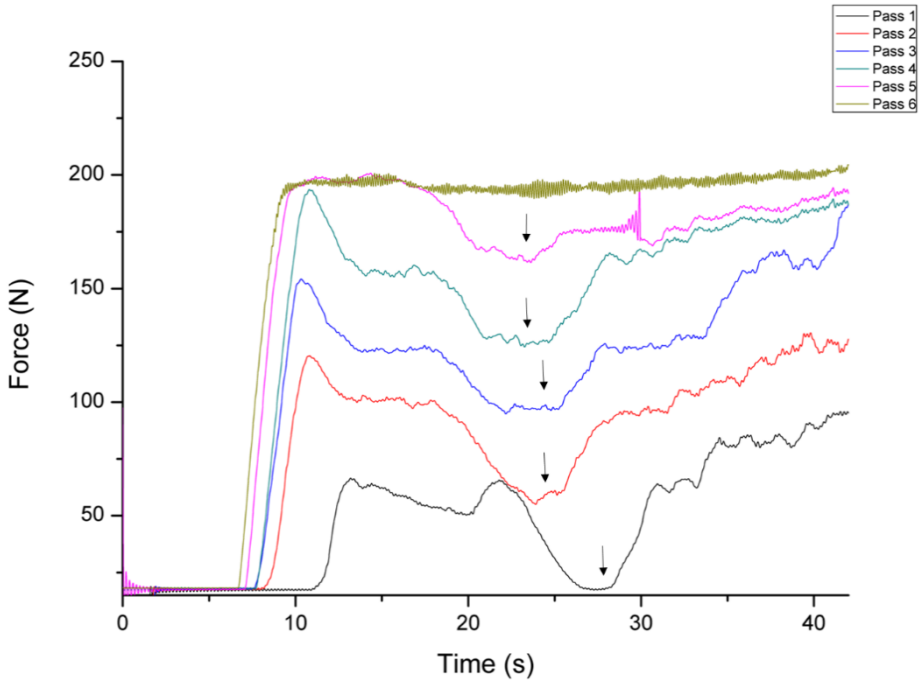


Figure 4-9: Cutting Forces in the normal direction (fx) from initial machining (pass 1) to achievement of steady state (pass 6). Plots filtered with low pass FFT at 10 Hz. Increase in forces with subsequent passes. Y axis truncated at 250 N. Arrows indicate region in component structure with structural defect from the build process

4.2.4.4 Machining - Cutting speed and Feed rate

Machining trials were carried out to investigate the effect of cutting speed, feed rate and depth of cut on the surface integrity of the components. Cutting speeds selected are representative of typical parameters used in turning wrought Ti6Al4V components [193, 194]. Also, towards investigating the

influence of these parameters on the resulting material properties, the parameters were varied outside the typical range used in machining wrought alloys. The relationship between machining speed and measured cutting force is shown in *Figure 4-10*. For all material systems, aside from the alpha heat-treated component, it was observed there was an initial increase in the cutting forces, which then decreases with increasing cutting speed. Veiga et al. in their review on the subject discussed this occurrence as being typical during the machining of titanium alloys, attributing the effect to the relationship between strain rate sensitivity and thermal softening. With variation in cutting speeds at intermediate values (below 50 m/min), the temperature sensitivity dominates over the strain rate sensitivity [195]. The alpha heat treated DED component however shows a rise in cutting forces with increasing speed, indicating the work hardening behaviour dominates in this material.

With increase in cutting speed, work hardening effects in some materials leads to an increase in cutting forces while other materials undergo adiabatic shear which reduces the cutting forces due to thermal softening [196]. Titanium alloys noted as having low thermal conductivity would be expected to show the latter as the temperature at the cutting region remains elevated. Here, lower mean cutting forces are observed with an increase in machining speed due to the temperature at the cutting zone remaining elevated during machining.

At the cutting speed attempted (50 m/min), cutting forces are up to 60 % (100N) higher in the 'as built' sample compared to the beta heat treated component. At higher cutting speeds (150 m/min), the difference in cutting force reduces to 31 % (50 N) of the 'as built' value. Variation in the alpha heat-treated sample also follows a similar trend, with the difference in cutting force at low cutting speed (50 m/min) being up to 45 % (80 N) and 5 % (10N) at the highest cutting speed (150 m/min) investigated. In comparison to the wrought heat-treated sample, the 'as built' sample required higher cutting forces for machining at lower speeds. However, the heat-treated DED components showed a reduction in machining forces compared to the heat-treated wrought material. This is believed to be due to the variations in components particle size (based on microstructural analysis as shown in Figure 4-5) and a reduction in ductility after heat treating. *Figure 4-10*(a) shows the cutting force – machining speed relationship for all the components. Forces shown in the plots are in the machining direction.

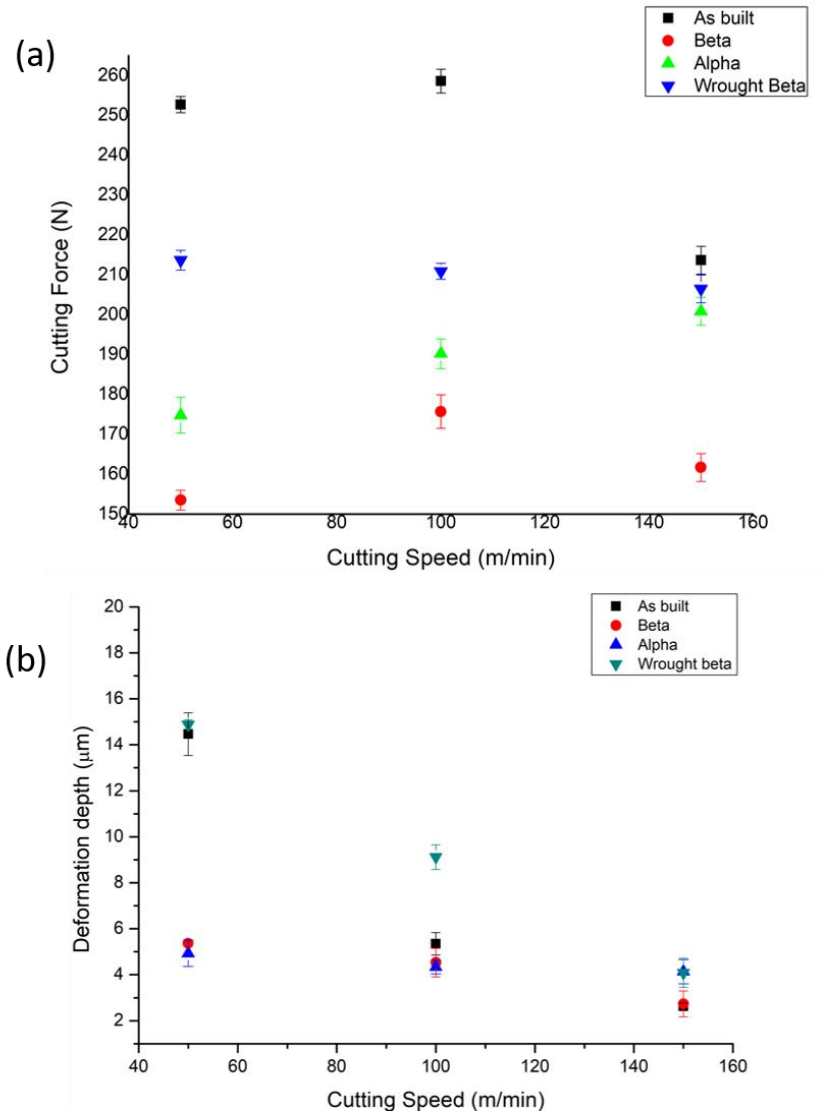


Figure 4-10: (a) Relationship between machining speed and cutting force across the heat treatments- At high speeds, the cutting forces tend to a similar value(b) Subsurface deformation decreasing with cutting speed in DED components and increasing in the wrought beta sample.

*Figure 4-10 (b) s*hows the deformation depth – cutting speed relationship for the components. Subsurface beta deformation at the machined region for the DED components reduces with increasing cutting speed. The peak deformation is observed in the 'as built' sample at low cutting speed (50 m/min), with maximum beta distortion depth of 14.4 ± 1.2 µm from the machined surface. Comparatively, the heat treated DED samples show a

reduction in surface deformation depth (approximately 5 µm for both components from the surface) at the same cutting speed. The wrought beta sample also showed a decrease in subsurface deformation with increase in cutting speed. The heat treatments used are thus useful in reducing subsurface beta distortion in DED *Ti6Al4V* components. Microstructures detailing the extent of subsurface deformation with increasing cutting speed are shown in *Figure 4-11*. The decrease in subsurface deformation in the DED components agrees with conventional subsurface deformation analysis which show similar response with increasing machining speeds [197].

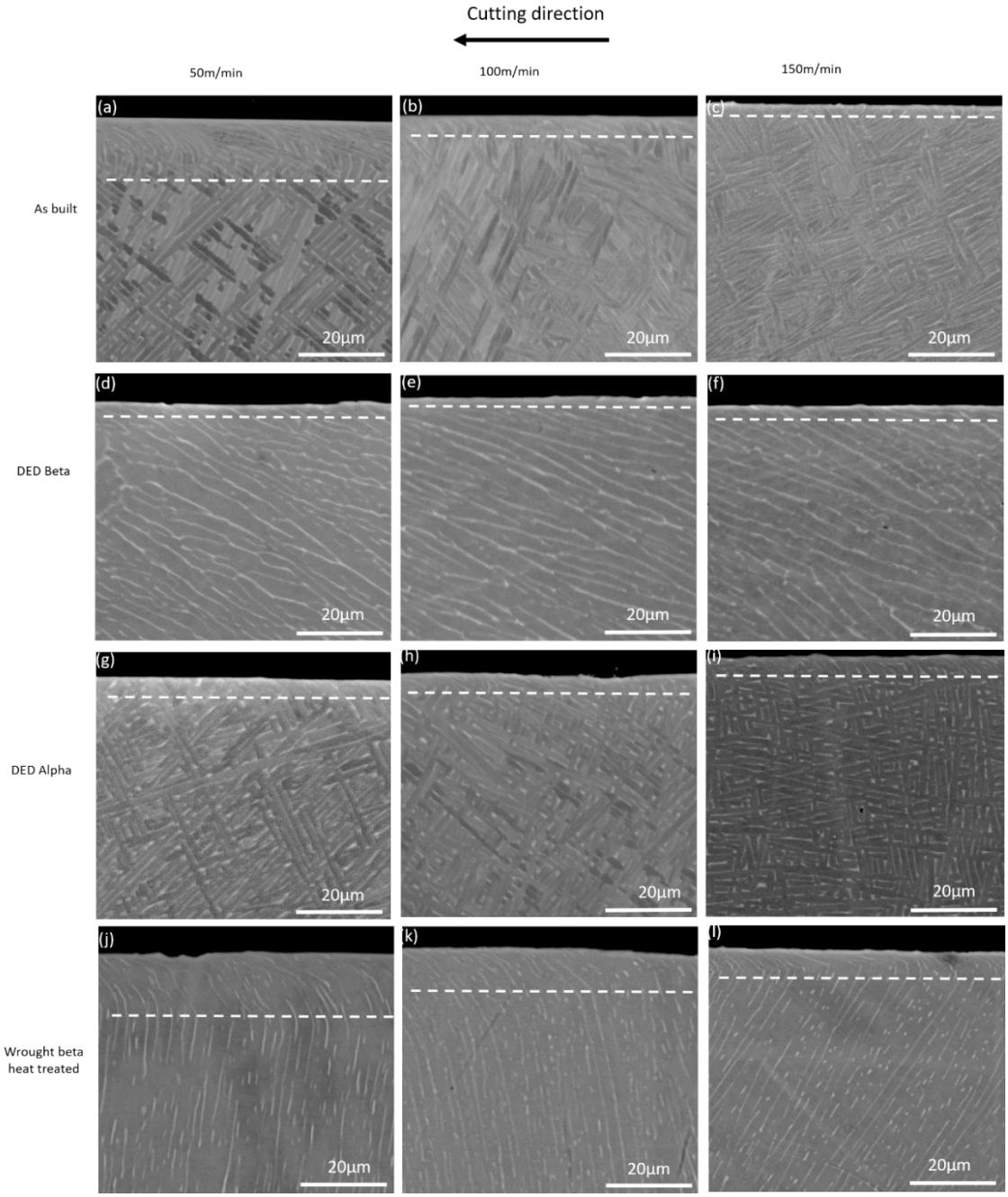


Figure 4-11: Difference in subsurface deformation depth with increasing speed (a) DED at 50m/min (b) DED at 100m/min (c) DED at 150m/min (d) beta DED at 50m/min (e) beta DED at 100m/min (f) beta DED at 150m/min (g) alpha DED at 50m/min (h) alpha DED at 100m/min (i) alpha DED at 150m/min (j) wrought beta at 50m/min (k) wrought beta at 100m/min (l) wrought beta at 150m/min. Broken lines included to show visible deformation depth from machined layer. Images taken in BSE mode.

Analysis of the influence of feed rate and depth of cut on the cutting force was undertaken for the 'as built' component only. The relationship between feed

rate and cutting force resulted in a near linear relationship, which for the 'as built' component showed an increase in cutting force with increasing feed rate. *Figure 4-12* (a) is a plot of the cutting force - feed rate relationship in the radial (fx), feed (fy) and tangential (fz), directions.

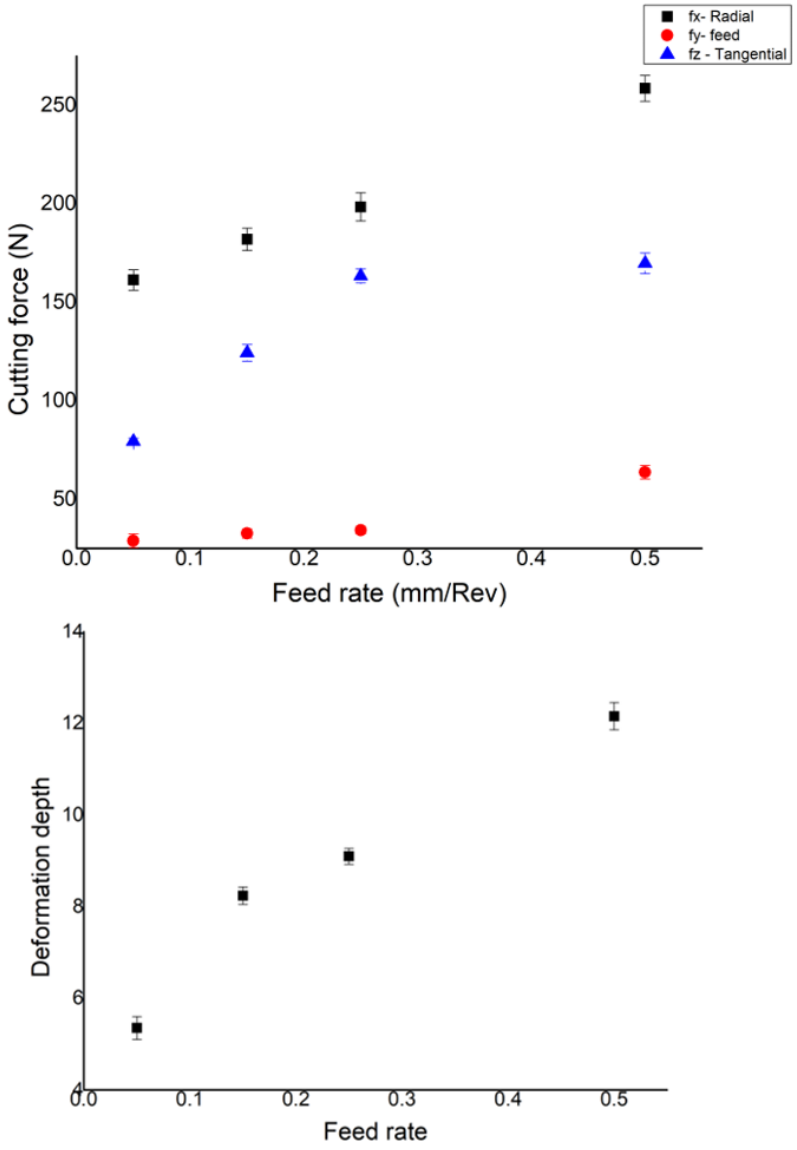


Figure 4-12: (a) Effect of variable feed rate on cutting force. Cutting forces shown are mean values in the three directions (b) Deformation depth increases with increase in feed rate ('as-built' component).

An increase in feed rate led to an increase in cutting forces and a subsequent increase in the subsurface deformation depth within the range of machining parameters trialled. *Figure 4-12*(b) is a plot of the feed rate- deformation depth relationship. Micrographs showing the increase in subsurface deformation as machining proceeds with increasing feed rate is shown in *Figure 4-13*.

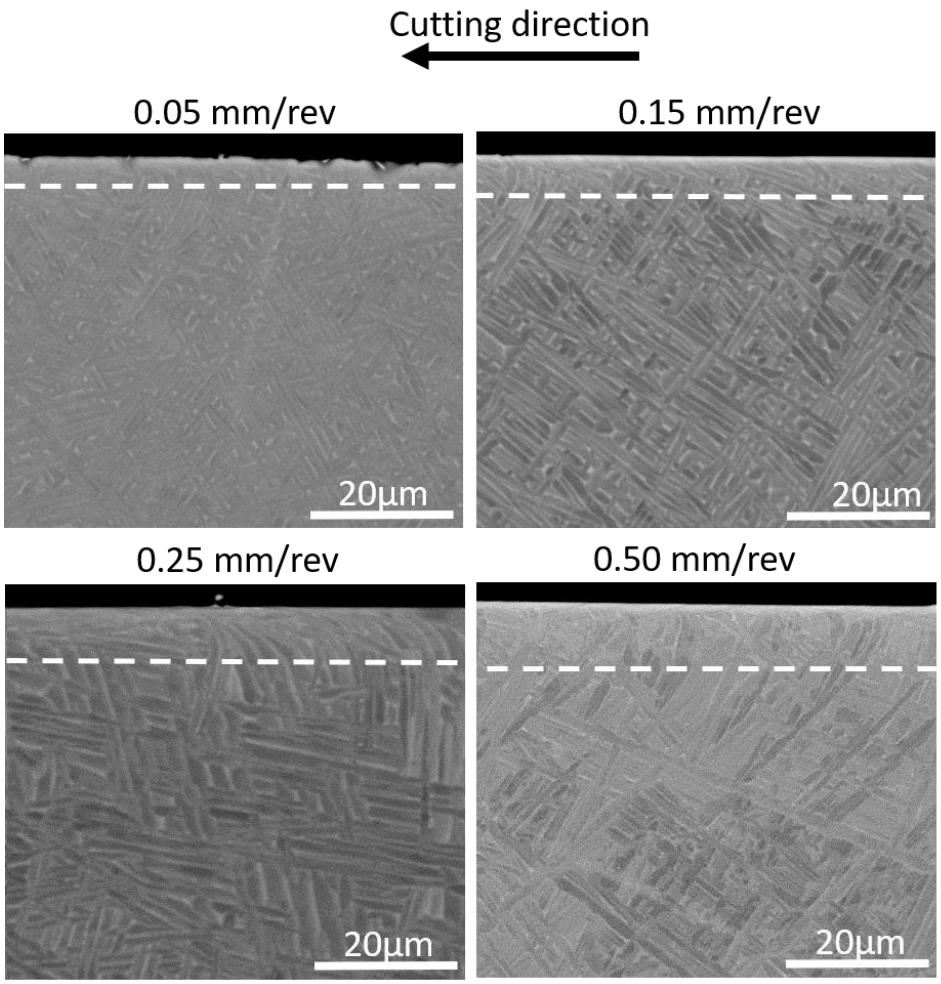


Figure 4-13: Increase in beta deformation in the as built component with increase in feed rate. Images taken in SE mode

4.2.4.5 Depth of cut

Results from the depth of cut trials together with the schematic of a section of the cylinder showing the corresponding depths of cut used in machining is presented in *Figure 4-14*. As expected, cutting force increases with increase in depth of cut due to increased chip load on the insert. It is assumed that with increased chip loads, temperature is reduced at the cutting region due to increased heat transfer with increased chip formation, this reduces the effects of thermal softening. However, the effect of shear strain on material substructure is directly proportional to the depth of cut [198]. Thus, for larger values of depth of cut, there is expected to be an increase in the subsurface deformation. Analysis of the maximum subsurface deformation due to increased depth of cut shows the subsurface deformation increases. The deformation- depth of cut relationship is also shown in *Figure 4-14*(c). At smaller depth of cut, the distortions observed are around the machining zone. However, a larger cutting depth activates dislocation nucleation and motion deeper into the subsurface interior due to a higher cutting force exerted on the workpiece and the subsequent higher deviatoric stress in the interior of the material [199]. *Figure 4-15* shows the micrographs highlighting the beta deformation.

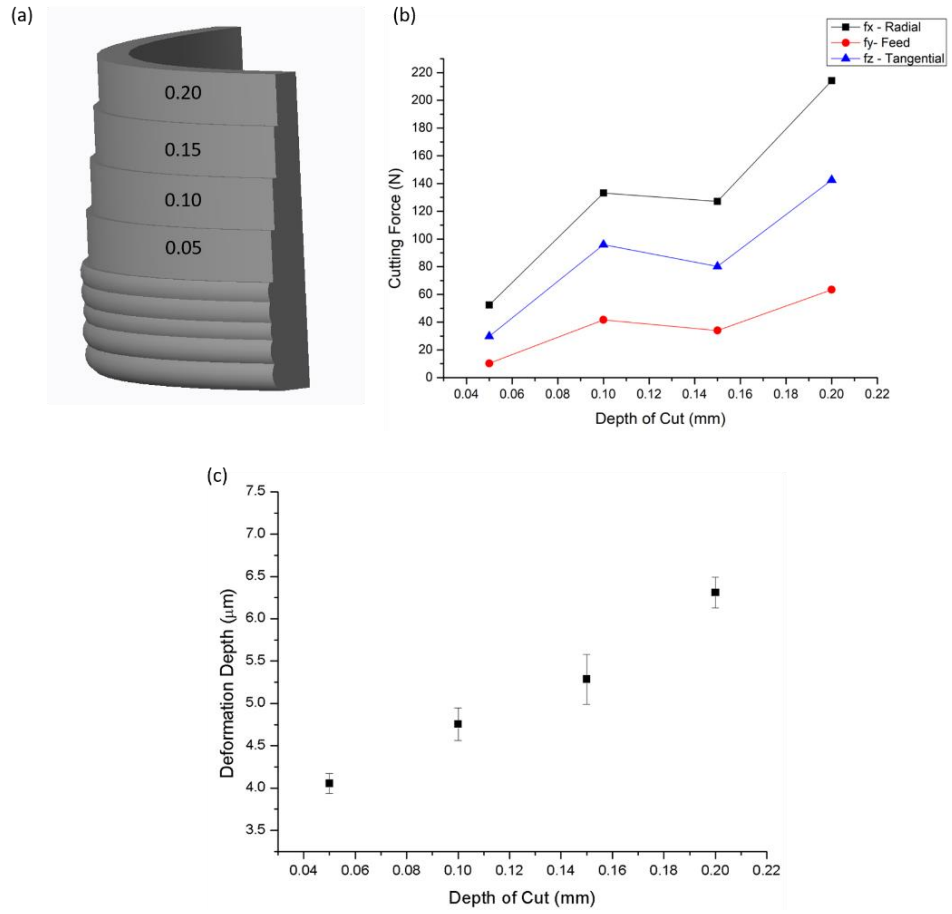


Figure 4-14: (a) Schematic showing experimented depth of cut variations (b) Cutting force increasing with increase in depth of cut (c) Increase in subsurface deformation with increase in depth of cut. Cutting forces shown are mean values in the three directions

The depth of cut analysis detailed by *Figure 4-14(a)* was used to determine the minimum amount of material to be removed in reaching a uniform steady-state cutting condition with zero workpiece run out and complete removal of the outermost layer on the cylinders' surface. Based on an analysis of the obtained surface scans of the samples, the minimum depth of cut at which the outer surface was removed was at 0.20 mm from the top surface. An investigation of this is useful for component designers in determining the additional material required to accommodate for post process machining

during the deposition process. However, due to the dynamic nature of DED processes, equipment and materials, it is believed this depth of cut is applicable to the deposition dynamics used in this study – feedstock gauge, laser processing parameters, build strategy and process stability during deposition.

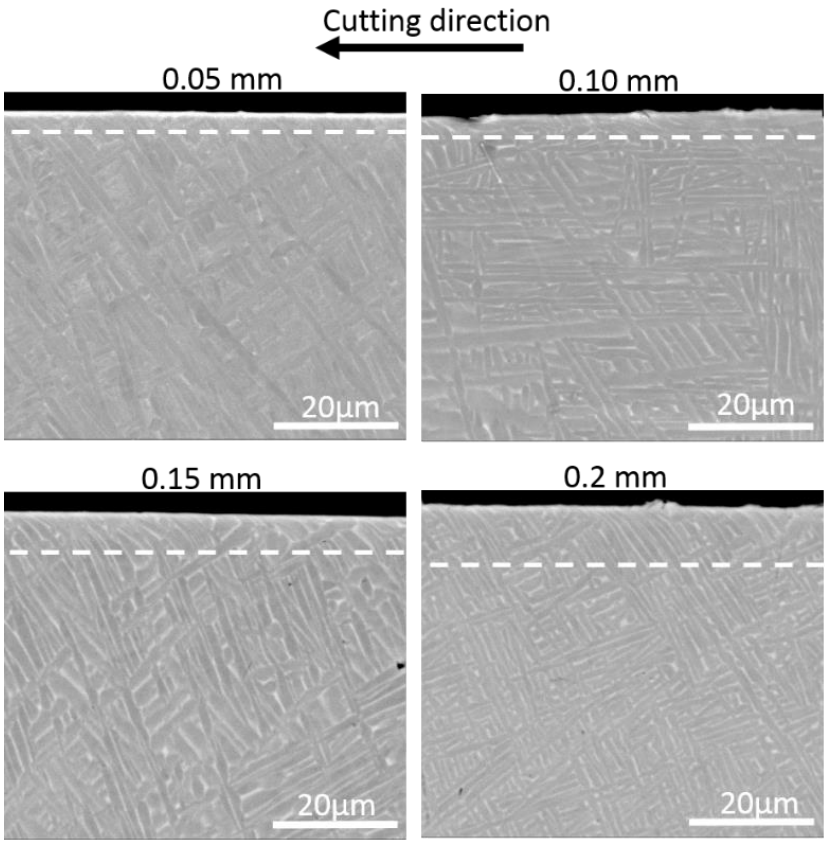


Figure 4-15: Increase in beta deformation with increasing depth of cut. Images taken in SE mode

4.2.4.6 Surface Roughness

Mean surface roughness (Ra) in the 'as built' condition without post processing was 5 µm, without accounting for surface waviness. Post machining mean surface roughness values are shown in *Figure 4-16*. From the

data and the resulting plot, it was observed that for similar parameters and cut durations, variations are observed in surface roughness of the materials. Higher surface roughness values were obtained in the 'as built' samples which could be an indication of higher tool wear, inconsistency in tool-work engagement and reduced machinability. In the 'as built' component and the wrought beta component, there is a progressive improvement in surface roughness with increasing cutting speed.

Surface roughness of the alpha DED sample showed similar parameters at 50 m/min and 100 m/min cutting speeds, this however reduces significantly at speeds of 150 m/min. Roughness in the beta DED sample showed limited response to changes in cutting speed.

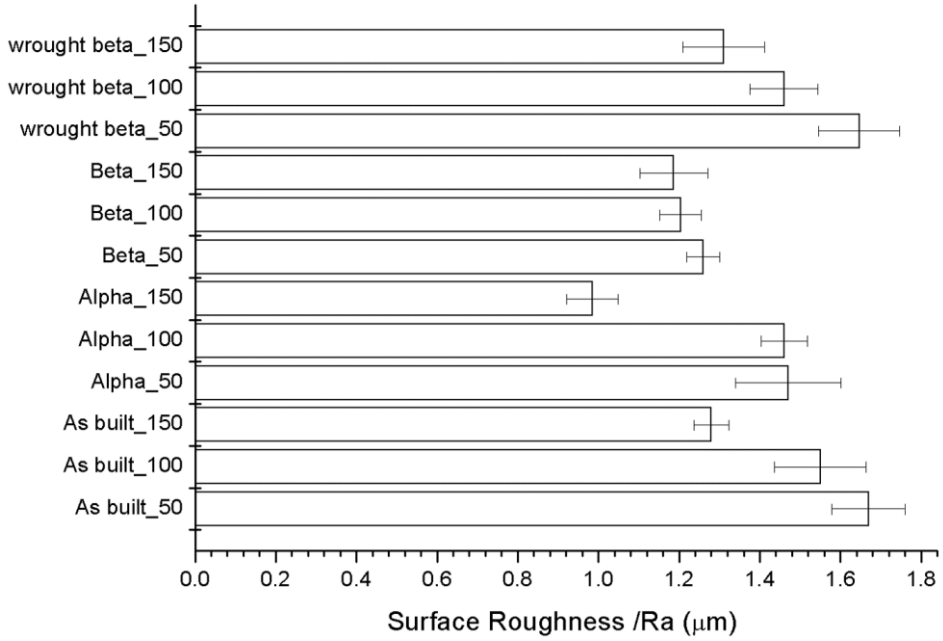


Figure 4-16: Plot showing comparison of Surface Roughness values for the array of heat treatments used as a function of cutting speeds used in machining. Speeds include 50m/min, 100m/min and 150 m/min. Feed rate = 0.1 mm/rev and depth of cut = 0.25 mm.

Surface roughness analysis of the 'as built' component with respect to variation in depth of cut is shown in *Figure 4-17*. With increase in depth of cut, the surface roughness of the material increases. This may be due to increased material removal rate and the corresponding increase in machining effort and cutting forces required to remove material.

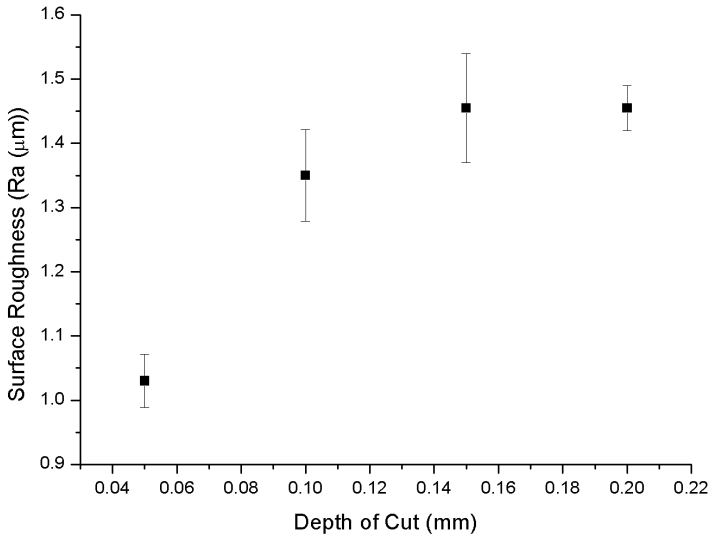


Figure 4-17: Increasing depth of cut showing an increase in surface roughness in the as-built component

4.2.4.7 Near Surface hardness

Indents for the hardness measurements of the cross sectioned samples were taken at the machined regions of the samples. The obtained values showed slight variation to those in the bulk region of the components. For all components tested (Samples from the cutting speed experiments were evaluated here), an initial drop in hardness is seen at the machining affected region with an increase in hardness with subsequent indents away from this

region. This may be due to the effects of subsurface beta deformation influencing the microstructure around these regions.

A plot of mean hardness values is shown in *Figure 4-18*. The 'as built' and the alpha DED samples had comparable hardness values which were greater than the beta DED component. A 10% decrease in hardness is observed after heat treatment from 'as built' condition for the beta heat treated sample. Larger grain size of the alpha laths post heat treatment influences this decrease as there is a reduction in mechanical strength. Relating this to the measured cutting forces, *Figure 4-18*(b) is a plot of the hardness and mean cutting forces. From the plots, the wrought beta sample show a similar mean hardness to the beta DED component. For components processed via DED, hardness is found to show a correlation to the cutting forces, as the 'as built' component machined with the highest forces and the beta heat treated DED component machined with the lowest forces.

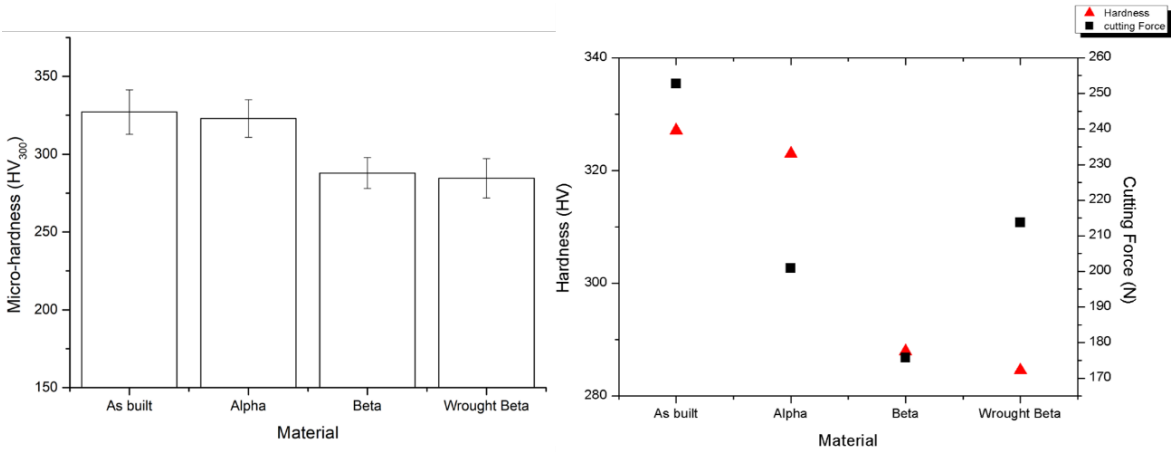


Figure 4-18: Hardness was evaluated for all microstructural conditions at the machined surface with 300 gf (b) Cutting force reduces with reduction in hardness post heat treatment for DED components. Cutting force shown is a mean value.

The hardness of the wrought beta component shows minimal effect on the machinability as the material has a similar starting hardness value to the beta annealed component but requires higher machining forces, this can be attributed to the effects of work hardening at the machined surface. The beta DED component is thus believed to possess a depreciation in ductility and fatigue strength after heat treatment, hence the reduction in cutting forces observed.

4.2.4.8 Tool wear

The inserts used in the study were analysed using an SEM to investigate the prevailing wear mechanisms. Inserts used in machining of titanium alloys have been reported to be mostly affected by coating delamination, abrasion and adhesion [200, 201]. Tool failure was not reached under any of the machining conditions used in this study, both in preliminary machining to remove the outermost layer and the machining of the interior regions. In the machining of Ti6Al4V at low cutting speeds, the formation of a built-up TiC layer on the tool rake face was observed. This reduces tool wear as it prevents sliding at the tool-chip boundary and impedes the reaction of the tool coating with the workpiece [193]. Carbon readily diffuses from the tool to the workpiece, reacting with titanium to form this layer. At higher cutting speeds, this layer is removed more frequently, and tool tends to deteriorate faster. A representation showing the rake face of an insert used during cutting speed variation trials with the areas used in machining is shown in *Figure 4-19*.

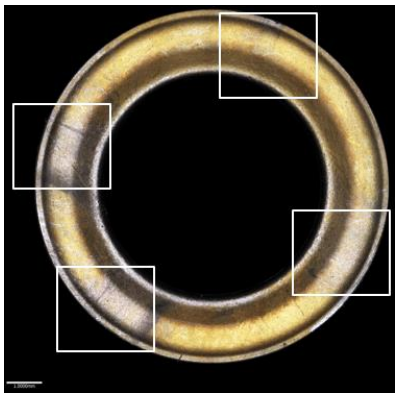


Figure 4-19: PVD coated insert with machining faces highlighted

Delamination of the coating due to abrasion of coating on the cutting tool is evident in the inserts used in machining the 'as built' and alpha heat treated components, *Figure 4-20*(a) and (b). In *Figure 4-20*(c) and (d), which corresponds to the inserts used for machining the beta DED and wrought heat treated components, a TiC layer is observed at the cutting edge after machining and the insert coating is less affected by the effects of delamination. The presence of the adhered TiC layer indicates the formation of a built up edge at the cutting region during machining. The presence of which can aid material removal if stable and if unstable can lead to premature tool failure.

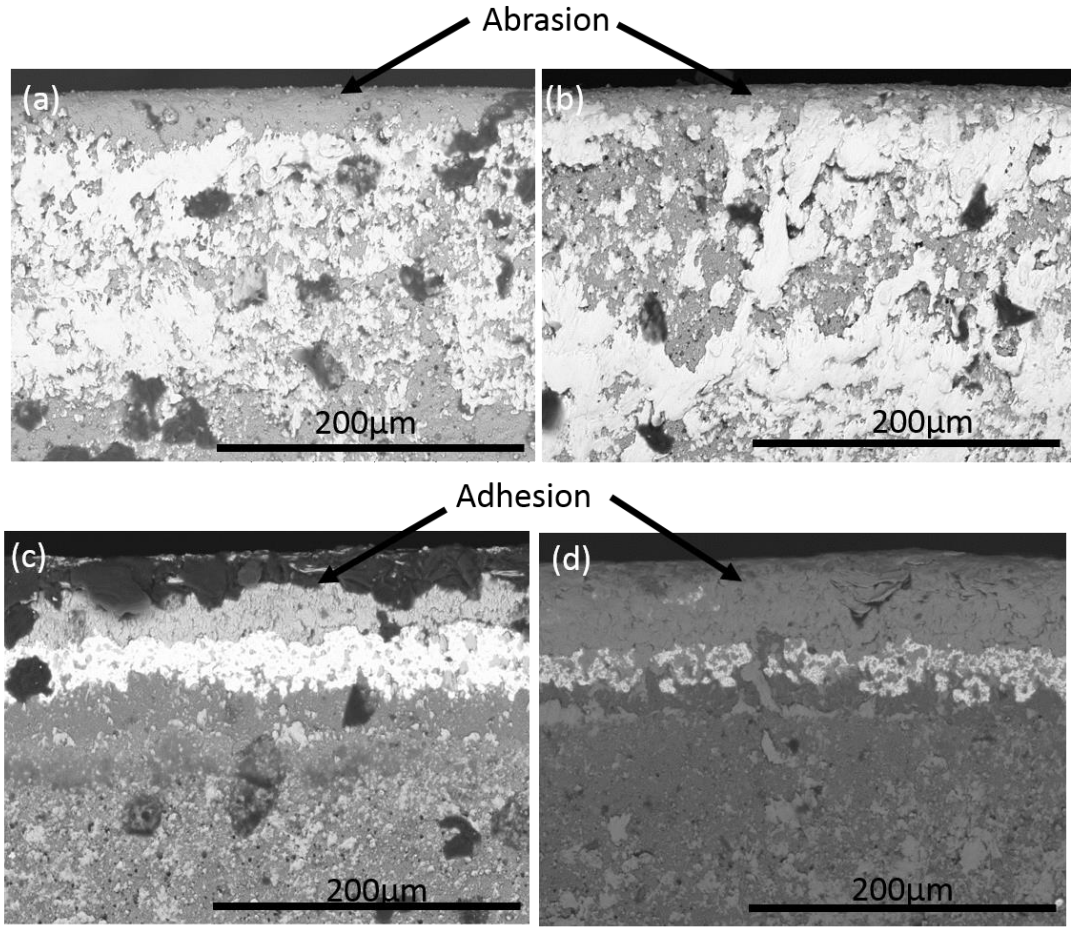


Figure 4-20: Tool wear mechanism on flank face of inserts, showing abrasion and adhesion with different materials when machining at intermediate cutting speed (100m/min), (a) As built (b) Alpha DED (c) Beta DED (d) Billet Beta. Images taken in SE mode

Correlating the formation of this built up edge to the observed surface roughness values in both beta heat treated components, the adhered built up edge has a comparatively greater effect during the machining of the beta DED component than the wrought beta component. It is postulated that due to the reduction in ductility as a result of the heat treatments in the DED component, preferential formation of a stable built up edge leads to lower cutting forces whilst also leading to improved surface and subsurface finish values observed

in the component. An EDS analysis showing the prevalence of Ti and C in the adhered regions in *Figure 4-20* is shown in *Figure 4-21* below.

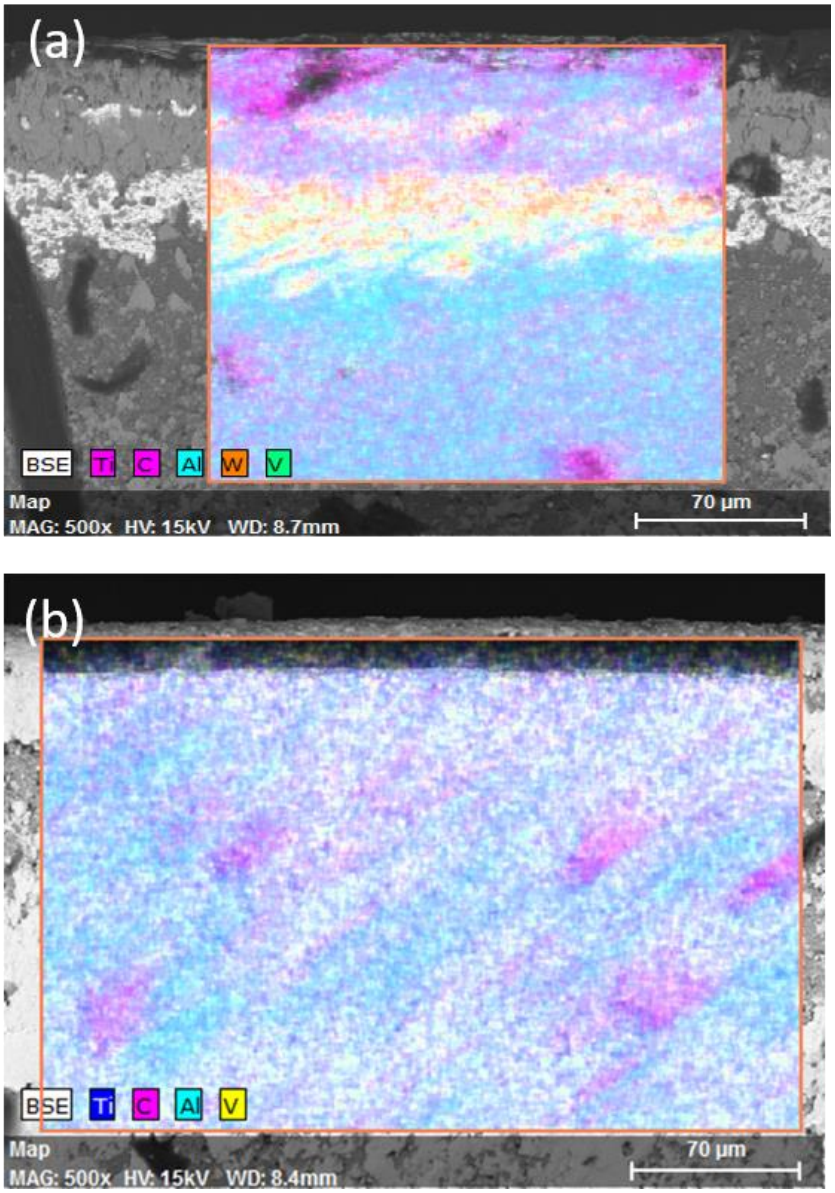


Figure 4-21: Figure showing EDS scan results of inserts in Figure 4-20.

4.2.4.9 Residual Stress

Residual stress measurements in the 'as built' samples before machining indicated the stress at the surface is tensile, which conforms to reported observations by Fergani et al [192]. Residual stress in AM components is formed due to temperature gradients generated during the building process which leads to differential cooling during solidification. In this scenario, tensile stresses are generated in the exterior and compressive stresses in the interior [202]. The corresponding expansion and contraction of these layers makes the formation and final stress state of an AM component challenging to predict. Tensile residual stress has been reported to occur at the top and periphery of layers in AM components with compressive stress in the deposit interior [203, 204].

Post machined components however showed compressive stresses along the machined surface. The influence of depth of cut, cutting speed and feed rate on the resultant residual stress is shown in *Figure 4-22*.

In machining operations, resultant residual stress is dependent on the material properties and the machining parameters. Capello [205], found in a study to determine the influence of machining parameters on residual stresses, that feed rate was the primary machining parameter in controlling surface residual stress. However, in this study, both the depth of cut and feed rate in the machining of DED components can be seen to have an influence on the residual stress state of the component. Changes in feed rate show a correlation with the increasing compressive residual stress as residual stress

increases significantly with change in feed rate. The depth of cut becomes less prominent in determining the residual stress state as machining progresses beyond removing the outer layer of the component. From the plot in *Figure 4-22*(c), the stresses evolve from being tensile to compressive with increase in depth of cut. Aside from the effects of machining, the interior region is also under compressive stress, as observed after machining [206].

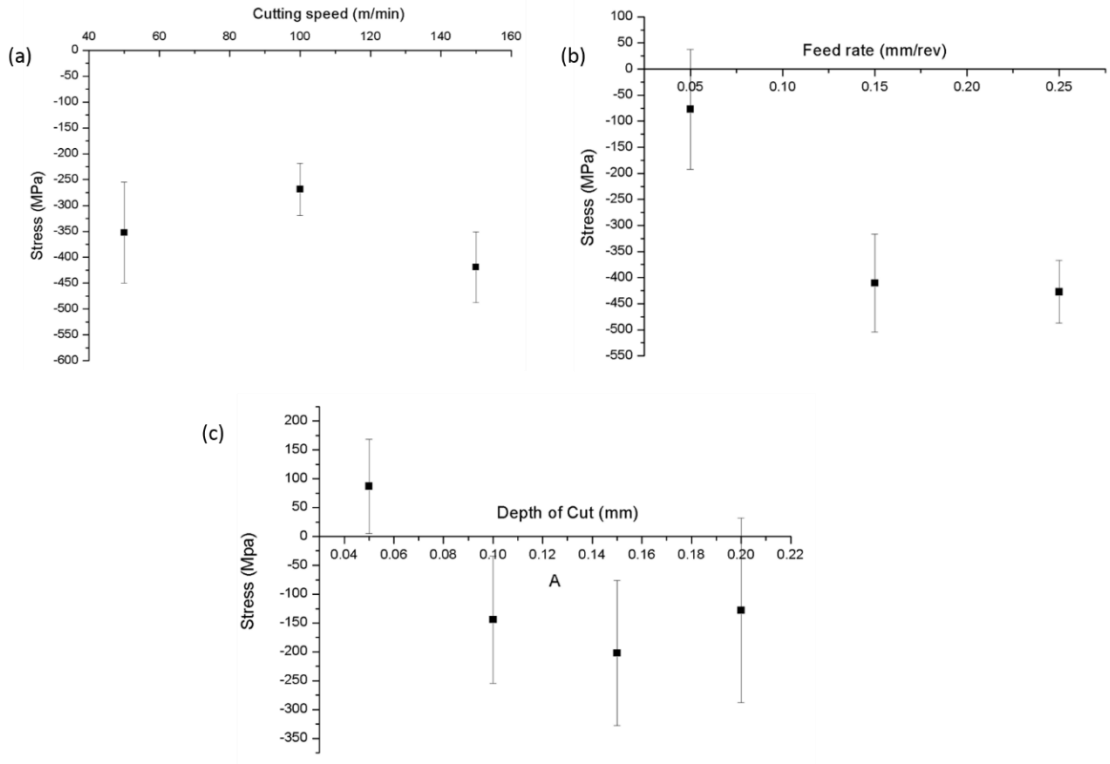


Figure 4-22: Effects of process parameters on residual stress in 'as built' components (a) Cutting speed (b) feed rate (c) depth of cut

4.3 Milling of DED and Wrought Components

Milling trials were carried out on the DED produced components. For these milling experiments, the samples from the turning study were used. The aim

of the investigation was for a comparison in machinability of DED produced Ti6Al4V and the wrought substrate under the same machining conditions. Hence, the study highlights the relative differences in surface and subsurface condition as a result of machining these components. Also, the influence of heat treatment on the material surface condition in both instances of machining the wrought and DED components is presented. This section also explores the changes in post machining surface conditions of the heat affected zones between the deposited material region and the wrought substrate with a view to determining the integrity of this region towards the avoidance of defect formation as a result of the processing route the material undergoes. The procedures and parameters used are as described in Section 3.3.2.1

4.3.1.1 Dilution/ Heat Affected Zone

An analysis of the materials' dilution zone between the substrate and DED produced region is critical to determining the integrity of the components after processing. The relevance of this region stems from the likelihood of the formation of a hard-brittle region which can be a source of failure in the component. During deposition, as a result of the localised input of the energy beam used and the high temperature gradient generated within a short interval, this region acts as a '*heat sink*' with the resulting thermal cycles leading to a change in microstructure. Relevant information on the machining

of this region is required to determine the effects of post processing techniques and in this case, machining on these regions. In the as built components, these regions have an average width of 675 ± 40 µm between the material boundaries into the substrate. Homogenisation of the microstructures of the entire component occurs with heat treatment conditions rising above the β transus temperatures. However, the region remains discernible with the alpha heat treatment. *Figure 4-23* shows the microstructural variations from the substrate through the heat affected region in all the material systems.

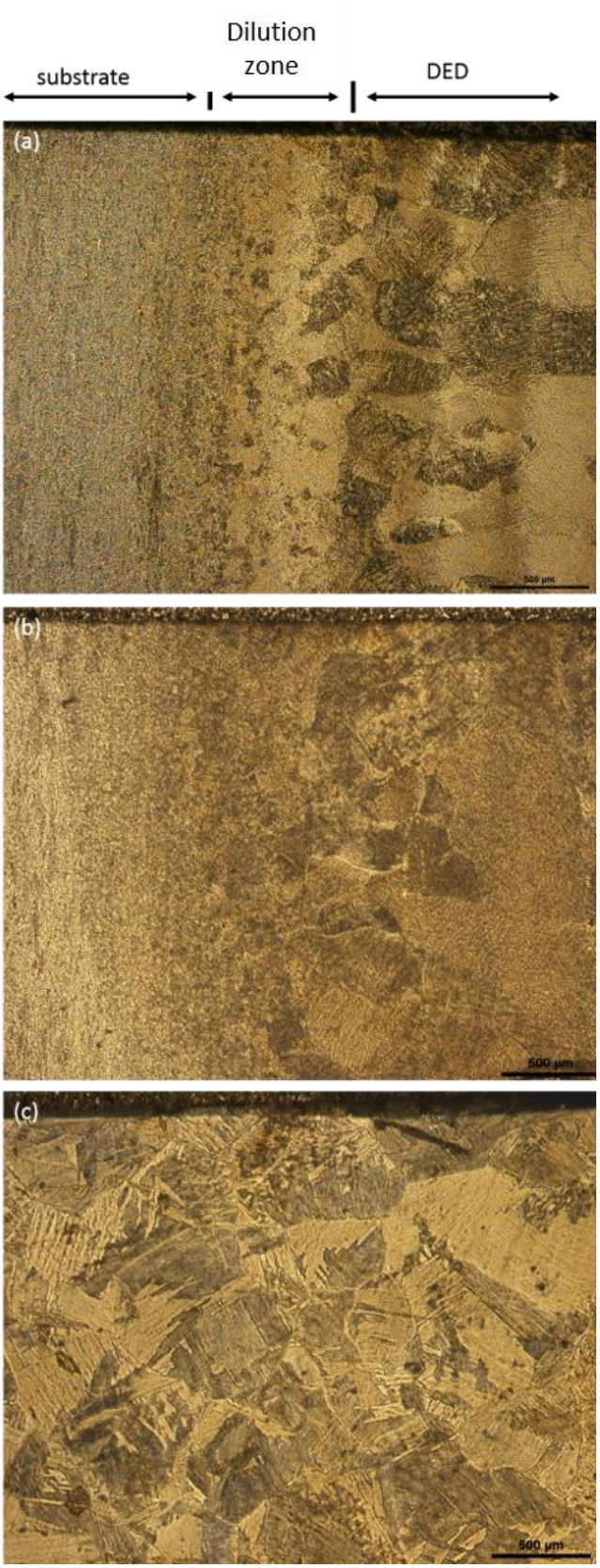


Figure 4-23: Optical micrograph of the various regions showing the gradation in microstructure between the wrought, Dilution zone and the DED layers (a) As built (b) Alpha HT (c) Beta HT. Samples etched with Kroll's reagent.

4.3.1.2 Surface Roughness

Due to the variations in microstructure, surface roughness (*Ra*) values for the regions highlighted in *Figure 4-23* were found to vary with machining conditions. From *Figure 4-24*, the surface finish is improved in the substrate regions for all machining conditions with the DED regions having larger roughness values under the same machining conditions in all cases. Here, the difference in response to machining between regions after heat treatment suggests the material properties remain subject to the previous processing routes.

In the DED regions considered, improvements in surface roughness are observed with an increase in spindle speed. The wrought material region also shows similar progression aside from the wrought beta region machined with higher spindle speed which shows an increase in roughness. Also, comparing between material types machined with low spindle speed (80 m/min), the DED regions in the various material conditions gave similar values (approximately 0.69 µm). However, the widest variation was observed in the alpha 1 sample heat affected zone and the wrought region pointing to a difference in response to machining parameters between these regions. The maximum variation between the substrate and DED machined region was observed in the Beta 1 component which had a 32 % increase in roughness in

the DED region. This however reduces to 8 % when machined with the high spindle speed conditions.

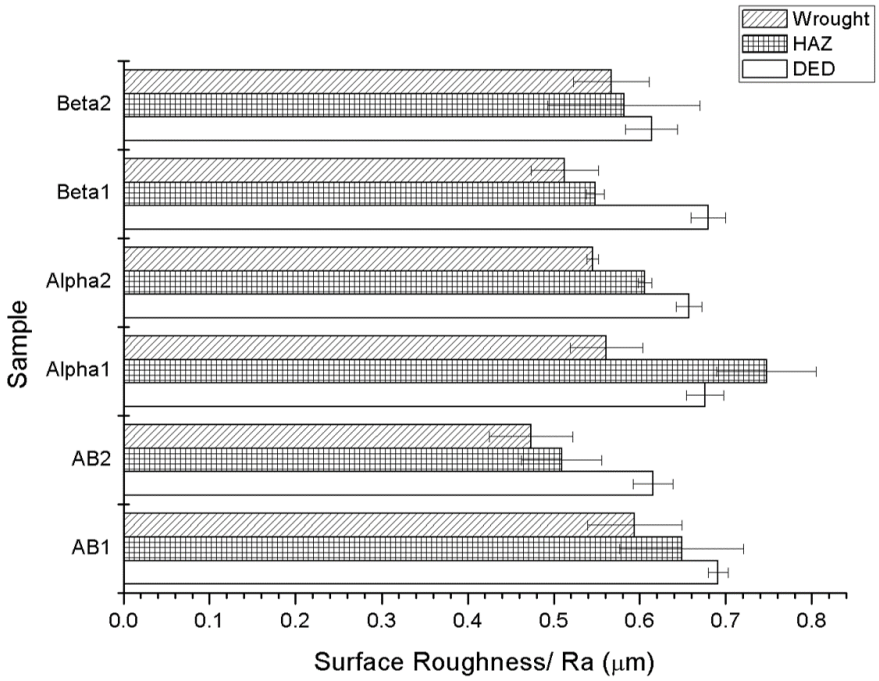


Figure 4-24: Surface Roughness of various regions post machining with standard errors included. AB2, Alpha 2 and Beta 2 samples are machined with higher cutting speeds.

4.3.1.3 Subsurface Deformation

Towards understanding the influence of the machining parameters on the components surface integrity, the subsurface condition after machining was analysed. Micrographs showing the variation in deformation depths across the DED and wrought material regions are shown in *Figure 4-25*. Considering the components machined with low spindle speeds, as observed in *Figure 4-25* and the plots in *Figure 4-26*, the DED region in all cases shows an increase in deformation depth compared to the wrought as built component material regions.

In the components machined with higher spindle speed, the 'as built' component shows limited deformation with depths of less than 5 µm in both the DED and wrought regions. Deformation depth is also found to increase in all component regions with heat treatment under similar machining conditions. The beta DED region shows the peak observed deformation with the observed depth reaching up to a minimum of 18 µm. At lower spindle speeds, an increase of up to 25 % (2 µm) and 200 % (12 µm) was observed in the alpha and beta regions machined compared to the as built regions respectively.

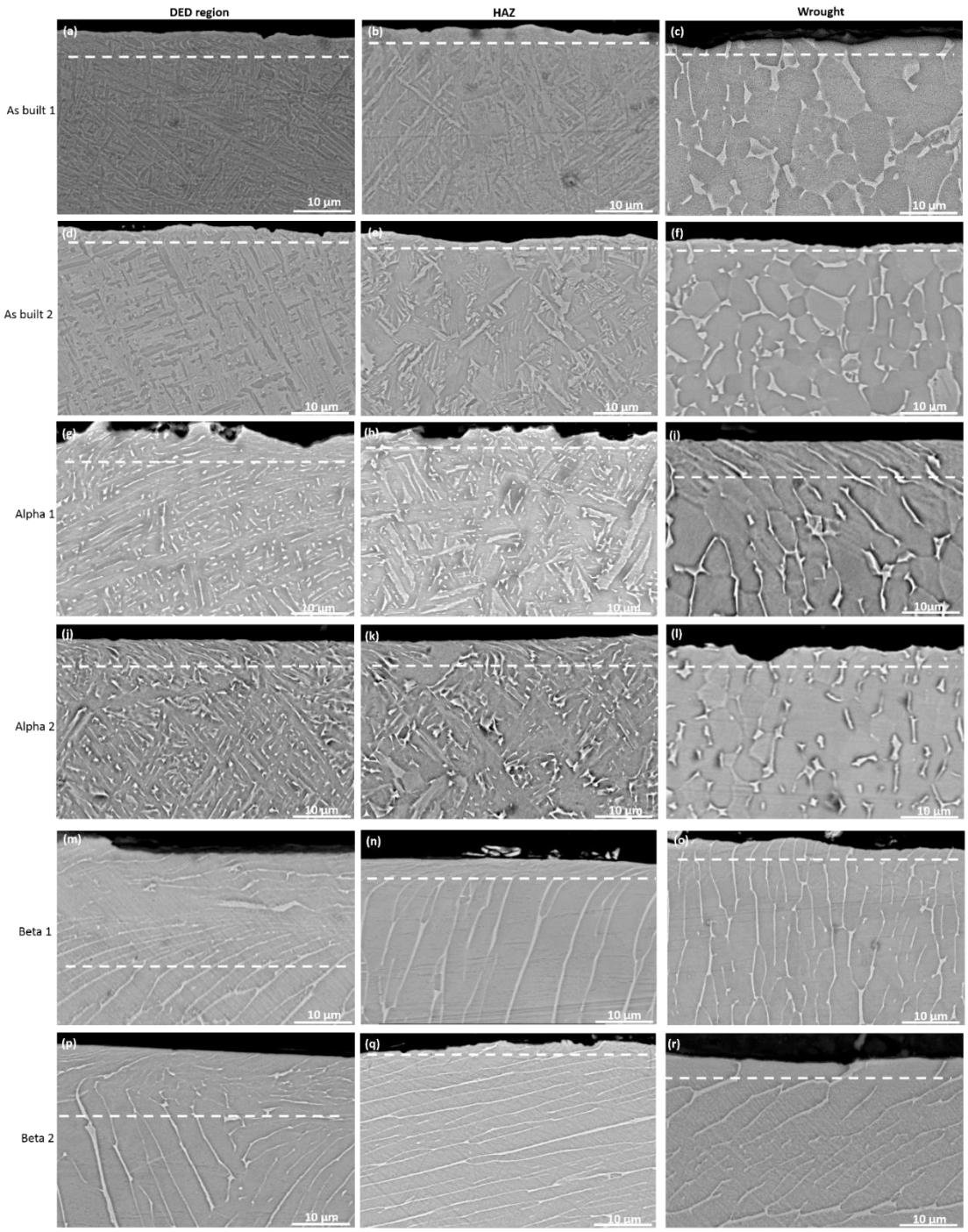


Figure 4-25: - Microstructures of the regions showing the DED region, HAZ region, and wrought. Comparison in subsurface deformation depth (after Milling) between AM region and wrought region with varying machining parameters. Images taken in BSE mode

An increase in cutting speed would be expected to lead to a decrease in the subsurface damage depth. This holds for the all the components as there is a

reduction in deformation damage with increasing speed. Heat treating of α + β alloys in the beta transus range with low cooling rates leads to the formation of the aformentioned lamellar microstructure, which consists of colonies of parallel α phase lamellae within large β phase grains. The thickness of the α lamellae and the diameter of the colonies determine the mechanical properties of the titanium two phase alloys [207]. Lower yield stress and tensile strength are characteristic of α + β alloys cooled from β transus temperatures at low cooling rates (cooling rates for the beta component = 0.035 °C / sec). At this cooling rate, the phase lamellae and colony size increases, acting as the singular strengthening element of the microstructure with the thin layers of the β phase not providing sufficient strength to prevent deformation. The effects of these mechanisms in the microstructure leads to the higher deformation depths observed in the beta heat treated DED components.

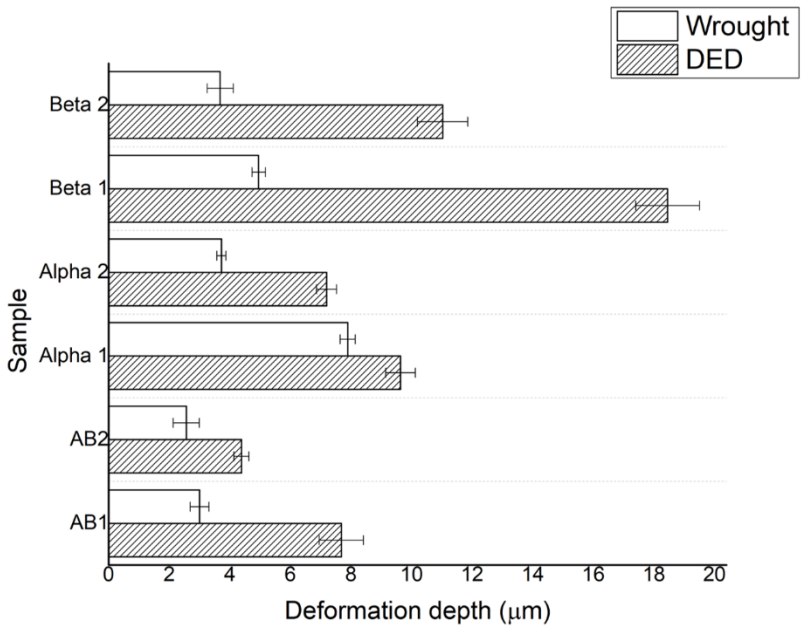


Figure 4-26: Deformation depths in the various regions at low and high machining speeds. Errors bars showing deviation along the sample length included

4.3.1.4 Hardness

As observed in the turning trials, hardness of the component is adversely affected by thermal treatments. In this case, an analysis of the hardness at the bulk regions and the near surface regions of the components was undertaken. In machining Ti alloys, the regions close to the machined layer have been reported to either possess increased hardness or machining induced softening. The HAZ is observed to have elevated values of hardness - compared to the substrate material in all cases. *Figure 4-27* shows the obtained hardness values in the regions analysed. In most of the material systems, the hardness at the machined region is observed to be lower than the hardness within the bulk of the material. An exception to this observation is in the beta DED region which has higher hardness in the machined region compared to the deposit interior. It is however worthy to point out that given

the deformed regions from the surface close to the edge of the samples, a source of error in the hardness measurements can be due to the edge effect in hardness measurements which can lead to exaggerated values.

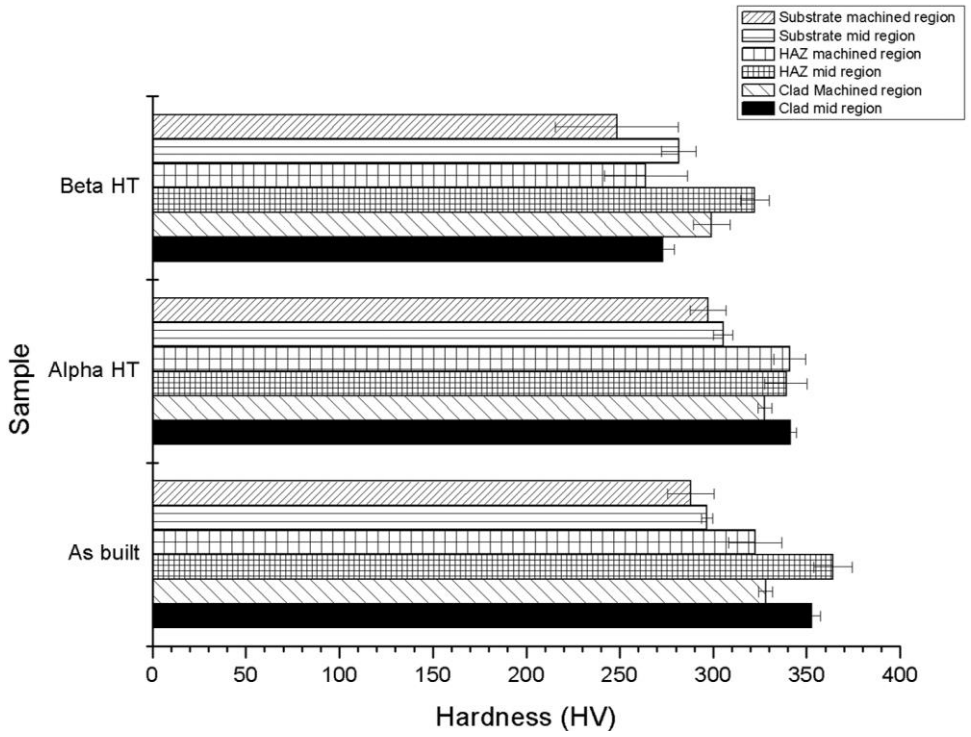


Figure 4-27: Hardness relationships at low machining speeds for all regions considered. Error bars indicate deviation from mean values along sampled regions

4.3.1.5 Residual Stress

Analysis of residual stress measurements indicate the residual stresses evolve with different response to changes in machining conditions. Both material regions present as having surface compressive residual stress post machining. Within the parameter sets investigated, a reduction in compressive stress can be seen with an increase in cutting speed, which is typical for titanium alloys [46]. The DED beta microstructures are observed to be most responsive to parameter changes during machining and this leads to the excessive plastic

deformation as a result of the deterioration in mechanical properties post heat treatment. Comparatively, the wrought region subjected to similar treatments shows less variation in residual stress magnitude. It is thought that the dominant cause of observed variation in residual stress values in the beta regions is due to the plastic deformation observed at the machined surface and alternative methods for quantifying residual stress would be beneficial in determining the residual stress condition in this aspect. Also, in the milling of these components, the DED produced regions due to their anisotropic property and the stress condition from the as built state, show increased response to the mechanical action of the cutting tool edge.

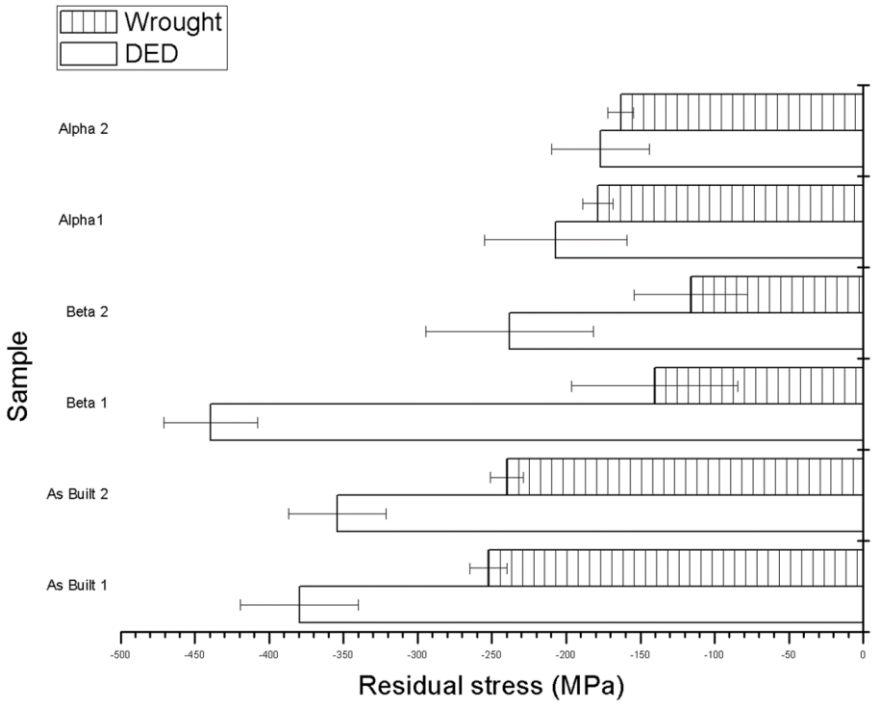


Figure 4-28: Residual stress for DED and wrought component regions. Error bars included to show variation in sampled values.

4.4 Discussion

Microstructural evolution of the 'as built' samples after the heat treatment processes led to appreciable changes in the machinability of the components. Maximum temperatures reached during the heat treatment of α + β alloys together with the cooling rate influences the mechanical properties attainable in these alloys. These findings agree with results obtained in a study on the post heat treatment of components produced using PBF, where the thermal treatments were reported to lead to a reduction in yield stress and ultimate tensile strength, with the material losing the ability to strengthen by deformation [208]. As the temperatures during heat treatment progress towards and beyond the beta transus, there is an increase in the size of the alpha laths which influences the hardness and mechanical properties of the components. This accounts for the lower measured bulk hardness and cutting forces during the machining of the heat-treated components.

During the machining of the outermost layer of the 'as built' component, it is observed that the mean cutting forces increase with machining passes into the material with successive equal values of depth of cut. Following the Hall - Petch relationship [209], a possible cause for this is that the finer grain size and grain orientation at these regions influence the mechanical properties by limiting dislocation and thus requiring increased machining forces for material removal. In the comparative machining of 'as built', heat treated and the wrought beta material, the relatively finer grain size, which leads to higher slip

resistance and the ability of the 'as built' microstructure to strengthen by deformation are reasons for increased machining forces. Hardness of the components influences machinability and the hardness is also a function of the grain size and microstructure.

Increase in subsurface deformation depth is due to the increased imparted strain on the workpiece during machining. The strain rate sensitivity of the material also influences the amount of sub grain deformation. Here, in the turning trials, the subsurface deformation depth is seen to decrease with increasing machining speed for the DED components which is similar with observations for wrought components. During turning of a near alpha titanium alloy at a low cutting speed (50 m/min), Crawforth et al [210] reported on the formation of a blunt built up edge in front of the tool. They reported this built up edge led to surface damage each time it fragments and is pulled beneath the leading edge. Lower surface roughness and increased subsurface deformation at these speeds supports this observation. Increase in subsurface deformation is however observed with increase in depth of cut and feed rate.

In the milling trials however, heat treatments are seen to play a crucial role in the subsurface deformation depths observed. Within the parameters selected, the deformation depth is found to reduce with increased cutting speed and reduced interaction time between the tool and the components' surface.

Residual stress state during machining has been postulated to be due to the combined influence of thermal and mechanical deformation, with thermal effects causing tensile stress and mechanical effects causing compressive stresses [47]. At lower cutting speeds, temperature has been reported to be the dominant factor in stress determination whilst mechanical effects are more prevalent at higher cutting speeds [211]. In this study, the interior regions of the component pre-machining is in compression, machining at low speeds (50 m/min and 100 m/min) leads to generation of tensile stresses which leads to the reduction in compressive stress observed at 100 m/min (*Figure 4-22*a)). However, machining at higher speeds (150 m/min) promotes compressive stresses in turning.

Improvements to surface roughness were observed with increases in cutting speed for all the components during machining. Surface roughness values of the 'as built' condition machined at low speeds was highest for the DED materials in all the trials indicating the material hardness had an effect on the resulting surface condition post-machining. Also, the beta heat treated components showed limited variation in surface roughness with changes in cutting speed. This is believed to be due to the lower hardness and the comparatively lower forces during the machining of these components. However, for the 'as built' and alpha components, improvement in the surface roughness is presumed to be due to adiabatic shearing during machining at higher speeds which enhances material deformation and removal. For the 'as built' component, increasing depth of cut was detrimental to surface quality.

Gallab et al. [34] have reported improvements in surface roughness when machining with inserts with a smaller nose radius. The use of an insert with a smaller nose radius might thus be beneficial in machining these materials towards obtaining improved surface finish. However, in this study the surface roughness values obtained post machining are within the acceptable range for most engineering applications. Thus, the strategy used in fabricating and machining the components here is representative of industrial use cases.

Discontinuities in the microstructure of AM components [146] and the characteristic boundary zones leads to increased cutting forces. These discontinuities ultimately lead to higher mean cutting forces. This phenomenon is mostly observed in the 'as built' component. Finer grains in these regions lead to higher hardness and a consequent increase in cutting force. Changes in feed rate and depth of cut led to predictable changes in the cutting forces as the materials did not deviate from expected machining convention for Ti6Al4V.

4.5 Conclusions

In this chapter, the influence of heat treatment, and machining conditions on the machinability of DED components has been investigated. Based on the results, conclusions from the results are as follows:

For the material being investigated, in the as built state, DED components have been shown to require higher machining forces compared to wrought heat-treated material due to the comparatively smaller grain sizes attainable

from DED components as a result of the rapid cooling during manufacture. Heat treatment of these components reduces the hardness of the material and consequently reduces machining forces. Beta heat treatment was found to reduce cutting forces during machining by up to 60 % (100N) at low cutting and 31 % (50 N) at the highest cutting speed trialled and the alpha heat treated sample varied from 45 % to 5 % (80 N to 10 N) of the as built component values at the same speeds.

- The outer layer in the as built condition showed reduced machining forces provided the effects of workpiece run out are removed. Also, in this study, the minimum amount of material that can be removed to achieve a desired surface finish has been investigated and reported. For the components used in these trials, a depth of cut of 0.2 mm was sufficient to remove the outermost layer.
- Surface roughness is largely influenced by the tool-workpiece interaction and for AM materials, the effects are more pronounced component's mechanical properties – such as hardness, varying from wrought. Subsurface deformation is also dependent on machining parameters and conditions. For instance, here, cutting speed has been shown to influence deformation depth as an increase in speed leads to a reduction in deformation depth. In machining AM components, parameter selection is thus critical in order to maintain surface integrity. The relationships between machining parameters and cutting forces has been investigated and reported in this chapter. Results from this would

be important in the development of the control system discussed in further chapters.

- Turning and milling processes have a positive effect on the residual stress state of DED produced component as they have been shown to induce beneficial compressive stresses in the components. This is important to ensuring prolonged fatigue life as these components would usually possess surface tensile stresses in the as built state. Further study on the control of residual stress and the resulting machinability would be beneficial to the understanding of the formation and control process and would replicate an industrial application.
- Heat treatments have been shown in this study to be relevant in the improvement of machinability of DED components. Removing the layer band artefacts in the microstructure is presumed to promote stability during machining which in turn leads to a reduction in the calculated mean cutting force. Larger grain size post heat treatment led to reduced hardness which in turn led to an improvement in machinability, surface roughness and a substantial reduction in subsurface deformation. The heat treatments would also be beneficial in tailoring components manufactured using this means to specific microstructures and properties.
- A marked difference is observed in both surface and subsurface integrity of DED and wrought components when machined under similar conditions. This translates to a difficulty in ensuring complete material integrity when machining components that have an AM part and a wrought part. Heat

treatments towards removing the 'layer bands' in the microstructures has also been shown to not completely solve the problem as the material properties are seemingly dependent on their processing histories. For such combinations, an adaptive system might be a reasonable solution for machining between the material boundaries.

5.0 Machining of functionally graded Ti6Al4V/ WC produced via DED

This chapter details the post process machining of functionally graded components produced using a directed energy deposition process. Components are fabricated using a DED process with selective material delivery of Ti6Al4V/ WC feedstocks to produce two material regions – a metal matrix composite region and a single alloy region within the components. Subsequently, the machining of these produced components using commercially available tooling is explored. The cutting forces in machining these regions together with an analysis of the surface and subsurface conditions of both material regions post machining is presented. Microstructural analysis of the regions is also reviewed and reported. Tool wear mechanisms are investigated and reported with the influence of the material variation on tool life analysed. The influence of post process machining on surface integrity is studied. Cutting forces due to microstructural changes in the MMC regions are analysed and used in assessing machinability of the various regions and the shortcomings of machining these characteristically wear resistant components with

commercially available tooling. A strategy for machining such components is also proposed.

5.1 Background

5.1.1 Metal Matrix Composites

MMC's offer high strength to weight ratio, elevated stiffness and improved damage resistance over a range of operating conditions making them a viable option to replace conventional materials in a number of engineering applications. The use of an energy beam in melting feedstock material opens up new opportunities for the use of various material combinations in producing desired geometries. This has led to renewed interest in materials that were hitherto difficult to combine within a component and also the production of functionally graded components. Functionally graded components have thus far been produced using a variety of processing methods including vapour deposition methods, powder metallurgy and solid free form processes [212]. However, the use of directed energy deposition (DED) techniques in material processing opens up new opportunities for the fabrication of intricate structures and, importantly for functionally graded materials, the controlled use of various material combinations. Selective addition of high value materials of desirable mechanical properties during fabrication to areas prone to damage can confer desired properties to specific regions and consequently reduce the total cost of producing the component.

Functionally graded components are mostly deployed in areas where material combinations offer advantages in properties which are superior to those obtainable from the use of a monolithic material.

To investigate the complexities involved in machining these, components consisting of a Ti6Al4V region and a Ti6Al4V/ WC region, demonstrating functional grading are produced for machining trials. As a consequence of the desirable characteristics of MMC's such as high hardness and improved wear resistance, machining of these components is often tasking, leading to excessive tool wear and component damage such as particle fracture, material pull out and debonding at the particle- matrix interface. However, for DED processes involving MMCs, the amount of reinforcement particles melting within the matrix is an area of interest and opportunity as the control of this is fundamental towards tailoring the microstructure to requirements. Although most reinforcement materials have relatively elevated melting points- (SiC- 2730 °C, WC - 2870 °C, TiC- 3150 °C) compared to the matrix materials, typically, deposition processes are mostly carried out using energy beams with high intensities, which often leads to full or partial melting of the constituents. Though process parameters can be largely regulated to moderate melting of constituents during manufacture, this characteristic further differentiates components produced using these processes from other processes used in the manufacture of MMC's in terms of attainable microstructures and by extension, mechanical properties.

5.2 Directed Energy deposition of Ti6Al4V/ WC

The parameters, strategy and a description of all equipment used in producing the components processed in this chapter is discussed in Section 3.2.2. During the building process, the deposition strategy involved building a Ti6Al4V cylinder from the substrate up to a height of 10 mm before the addition of the tungsten carbide powder to the melt pool. This was to demonstrate the selective addition of materials at different regions along the build of the cylinder, producing a functionally graded part. Using this strategy, cylinders were built up to a height of 25 mm. *Figure 5-1* shows a schematic of the cylinder. Region 'a' represents the area with Ti6Al4V only and 'b' is the MMC region. Typical surface condition before machining for the two regions is also shown.

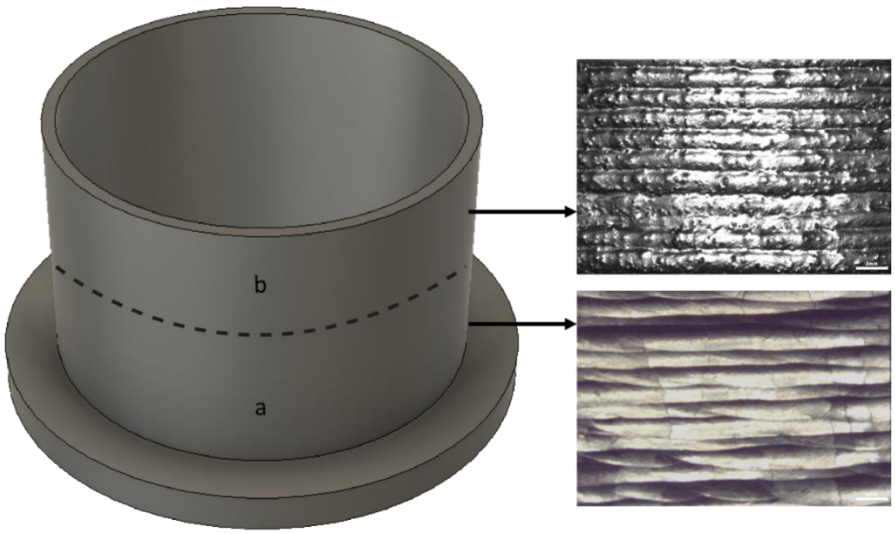


Figure 5-1: Functionally graded cylinder, region marked 'a' is Ti only, 'b' is Ti + WC Cylinder dimensions: Wall thickness in 'a' = 4.3±0.25 mm, wall thickness of 'b' = 4.92±

0.32 mm, cylinder height = 25mm, surface condition of both regions pre machining also shown

The components resulting from the deposition process are susceptible to cracking due to the difference in coefficient of thermal expansion of the constituent materials and the stresses generated during the embedding of the WC particles in the solidifying matrix. The difference in thermal expansion coefficient (*min values /K (Ti6Al4V =8.7 x 10^{-6} , WC = 4.5 x 10^{-6})*) between the constituents of the melt pool leads to a considerable change in volume and also the evolution of residual stresses which invariably causes cracking during rapid cooling and solidification.

Whenever surface cracks were observed during the build process, these propagate to form larger cracks during cooling, post deposition. The formation of a network of smaller cracks via the eutectic phases consequently leads to a larger crack being formed across layers. In order to reduce the appearance of cracks, laser power and traverse speed of the system were adjusted during the deposition process to ensure the input energy was optimised and prevailing conditions were kept within a threshold required for producing defect free components. As a result of the addition of material to the existing melt pool, clad morphology is affected and there was a need to adapt deposition parameters to accommodate for the variation in melt pool quality. Cylinder thickness and deposition height are found to increase by approximately 0.6 ± 0.1 mm and 0.5 ± 0.2 mm respectively. To ensure clad height was kept constant, there was an alteration to the step-up height in the

build direction to ensure deposit uniformity along the build. The step-up height was thus adjusted to maintain a desired ratio of depositing a new layer at 80 % height of the previous layer along the build.

Characteristically, the single material region showed better surface finish compared to the MMC region which had a surface finish synonymous with components produced via powder deposition techniques- presence of adhered powder particles with a high surface roughness.

5.3 Turning Trials

Outer diameter turning of the produced cylinders was carried out on a Cincinnati Hawk 200 lathe using the procedures described in Section 3.3.1. The Inserts and tool holders used in turning trials were supplied by Seco tools. The inserts were selected based on their suitability for machining titanium alloys and their effectiveness in machining MMCs.

In the machining of metal matrix composites, CBN and PCD tools are the preferred tooling. This is due to their inherent high hardness and low chemical affinity which afford for improved performance of these tools in the machining of so called 'difficult to machine' components. Tool wear during the machining of MMC's is primarily dependent on the interaction between the reinforcing material and the cutting edge. Abrasion due to a number of underlying wear mechanisms is the reason for expedited tool wear. These mechanisms include: micro-cracking, micro-ploughing and micro-fatigue [213]. Also, as machining progresses, the cutting edge encounters changing

matrix and reinforcement regions which have different machining properties [214]. This can also be detrimental to the integrity of the tool cutting edge. For all machining trials, a new cutting edge was used at the start of each machining operation. The inserts, their usage relating to the workpiece surface condition, and the coolant delivery methods are outlined in *Table 5-1*.

Table 5-1: Inserts used, functions, specifications and grades PCD refers to Polycrystalline diamond and PCBN is Polycrystalline Boron Nitride

	Grade	**Use**	**Tool holder**	**Coolant delivery (**Hocut 795B)
RCMT10T3M0-F2,	TS2000, PVD coated	Surface preparation /Finish machining	SRSCL-20-10JET	High pressure through tool
CCMW120408F-L1	PCD 20	Surface preparation /Finish machining	SCLCL 2020K12	Flood delivery at 13 l/min
CCGW120408S-02020-L1-B	PCBN 200	Surface preparation /Finish machining	SCLCL 2020K12	Flood delivery at 13 l/min

Similar to the monolithic material machining strategy in Chapter 4.0, the machining strategy was for the initial removal of the outer layer and subsequent machining of the interior regions towards obtaining an acceptable finish. For any AM process to be economically viable, machining of the resulting components towards improving surface finish needs to be minimised towards limiting the influence on the components' subsurface integrity and ensuring surface and geometrical requirements are attained.

However, to prevent damage to the components and to improve tool life during the machining, shallow depths of cut were successively taken during this 'clean-up' process. The 'clean-up' process was effectively for the removal of the characteristic 'wavy' surface layer due to the layer build strategy. Cutting forces during the machining trials were also recorded using the Kistler cutting force dynamometer and amplifier set up described in Section 3.3.1. Preconditioning of the deposited components' substrate was required before the machining trials could proceed. This was to ensure concentricity of the cylinder towards limiting workpiece run out when taking the final machining passes. Machining parameters used are shown in *Table 5-2*. Conservative machining parameters which would limit tool wear and prevent the formation of subsurface deformation were selected in the machining trials. This was as a result of preliminary machining trials with parameters suggested for machining Ti alloys which resulted in increased tool attrition with minimal material removal in the MMC region.

Table 5-2: Parameters used in the machining of the functionally graded cylinders

Parameter	**Machining data**
Cutting speed (m/min)	80
Radial depth of cut (mm)	0.025- 0.05
Feed rate (mm/rev)	0.1

5.3.1 Microstructure

In the MMC region, distribution of the WC particles varies along the deposited structure. The stirring action within the melt pool during solidification causes

the unmelted and partially melted WC particles to be relocated to the clad periphery. This leads to the clad periphery having a higher concentration of WC particles with the clad centre having comparatively less undissolved WC. The high composition of undissolved WC at these edges is expected to influence machining forces and the tool is expected to abrade at a faster rate due to the presence of these hard particles at the tool – workpiece interface region.

Interface between layers, hereafter referred to as remelted regions, are formed due to the melting of previously deposited layers for the addition of subsequent layers. These regions in AM components are regions of grain growth between layers. In the deposition of monolithic materials, these regions are characterised by the appearance of layer bands and coarse grains in the macrostructure [13, 155]. The remelted regions were found to contain a higher proportion of β-Ti and smaller sized TiC particles. This is due to the remelting of previously deposited WC particulates at the clad periphery during addition of a subsequent layer, which increases the WC concentration within the matrix. Increased dissolution of WC leads to a higher concentration of TiC and W within the β-Ti matrix. *Figure 5-2* shows the boundary region with the aforementioned variation in microstructure due to increased WC melting in the matrix.

The variation in microstructure due to the increased dissolution of WC in the matrix leads to an expected difference in hardness between the deposit regions. From *Figure 5-2*, the region labelled (i) is the middle of the clad which

is less affected by the effects of remelting whilst (ii) is the overlap region. Hardness test results of the matrix in regions (i) indicate mean value is 530 ± 20 HV whilst mean hardness within the - region (ii) is 875 ± 95 HV. Hardness values of up to 345 ± 10 HV was observed in the Ti alloy region.

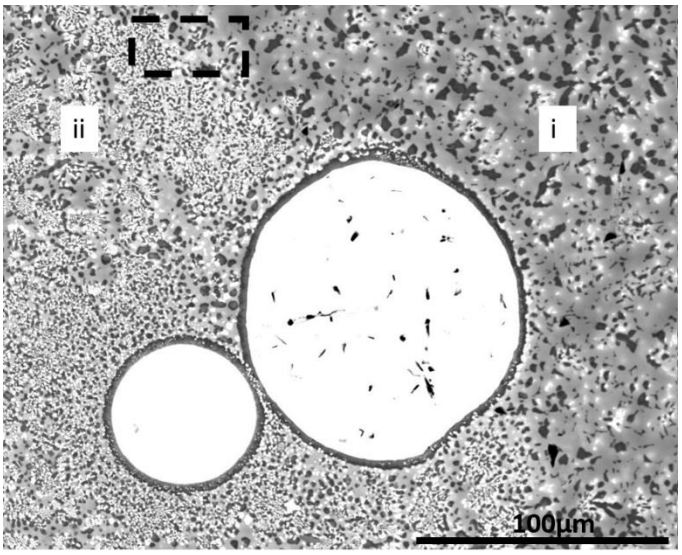


Figure 5-2: SEM image showing boundary between layers in the MMC region showing increased WC diffused content due to re-melting. EDS of highlighted region is taken and is discussed subsequently. Image is taken in BSE mode

EDS was used in the analysis of the regions to determine the constituent elements in the remelted regions, also to compare material composition and deduce expected metallurgical variation between these regions. The highlighted region in *Figure 5-3* corresponds to the region of EDS analysis shown in *Figure 5-2.*

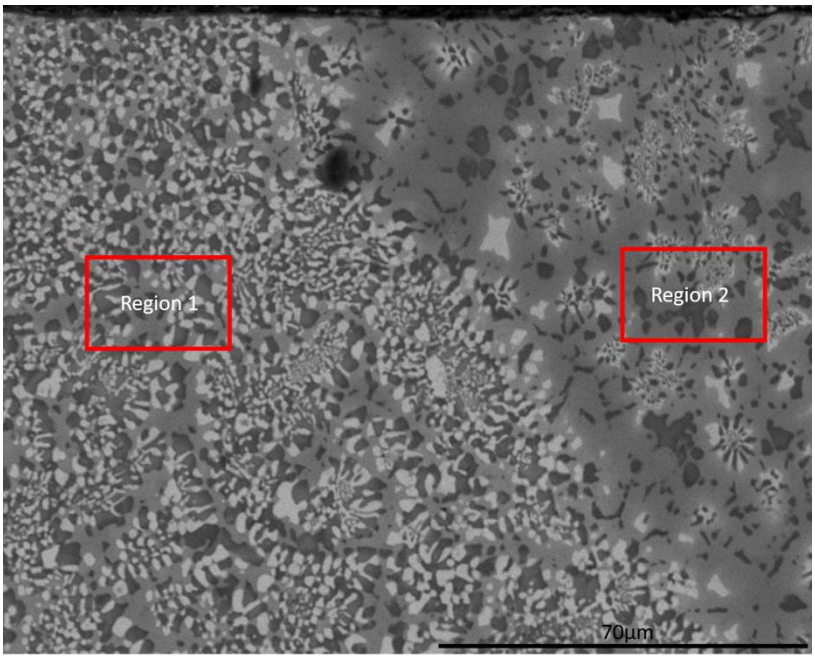


Figure 5-3: Highlighted regions are selected for EDS analysis. Remelted region between clad layers is labelled Region 1 and Region 2 is the region within the clad interior. Image is taken in SE mode

Results from EDS analysis indicate there is an increase of up to 15 % (weight composition) of dissolved WC in the remelted regions. It is expected the increase in tungsten particulates and the corresponding increase in hardness in the remelted regions would cause a variation in tooling response during machining. The presence of such a layer has not been widely reported by authors investigating conventional methods of manufacturing or machining MMCs. The influence of this variation in hardness on the component machining and tooling is discussed subsequently.

Table 5-3: Elemental composition (wt. %) of phases in the regions (i) and (ii) in Figure 5-3. Tungsten content is higher in the re-melted layers

	Ti	Al	V	W	C
Region (i)	44.79	3.09	1.51	41.21	9.4
Region (ii)	31.87	1.28	1.29	54.64	10.92

5.3.2 Machining

The coated carbide inserts used in the preliminary turning trials showed accelerated wear during machining. The rapid wear of the inserts is due to the hard particulates acting as small cutting edges and grinding the cutting tool edge during machining, leading to abrasion of the cutting edge. This is postulated to be due to the comparatively larger undissolved carbide particles at the MMC outermost surface in relation to the thickness of the insert coating. The use of the insert was thus discontinued, and subsequent machining trials were carried out with the PCD and CBN inserts. Workpiece run out, coupled with intermittent interaction of the cutting edge with the hard WC particles in the MMC region during the initial machining process led to variation in cutting forces and accelerated tool wear. For all trials, machining proceeded from the MMC region to the titanium alloy region as highlighted in *Figure 5-4*. In the machining of these components, lower feed rate and spindle speeds were used in order to reduce tool wear. Also, the use of these conservative parameters was based on the premise that components to be machined would be produced as near net shape and the amount of material to be removed in achieving net dimensions would be limited and as such for these types of materials where machinability is poor, a single finishing pass might be more desirable in removal of the outermost layer. As shown in *Figure 5-4*, during machining, the Ti alloy region reached steady state cutting condition earlier than the MMC region. This is due to the comparative ease of chip formation in the single material region. As a result of this, the MMC

region required more machining passes to ensure the removal of the outermost layer.

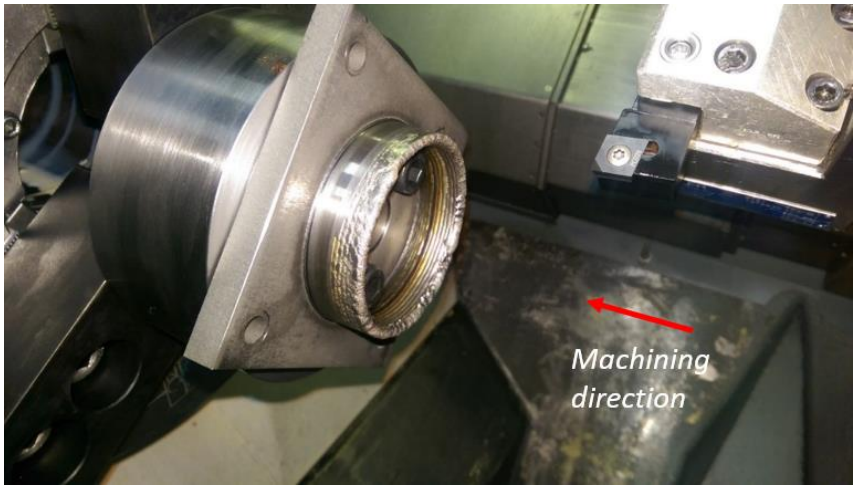


Figure 5-4: Set up for machining trials with the component showing the MMC and single material region. After two passes, undulations in single material region were removed and this led to achievement of steady state cutting faster than the WC region due to difficulty of chip formation in MMC region

In machining MMC's, the interaction between the tool cutting edge and particles of the reinforcement material in the cutting region leads to material pull out or particle cut through, thus inhibiting attainable surface finish. *Figure 5-5* shows schematics of both material removal mechanisms.

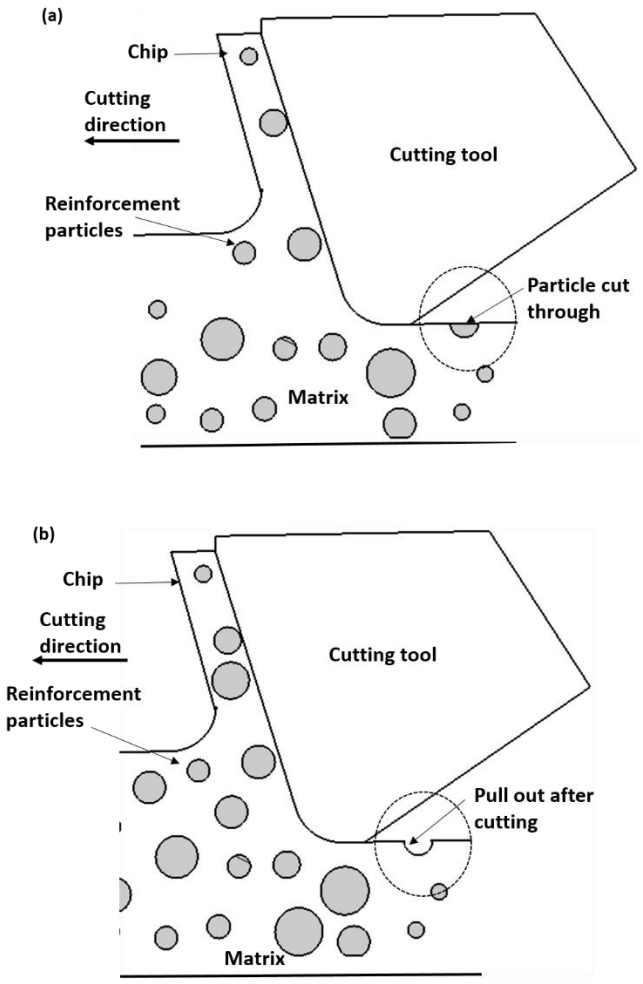


Figure 5-5: Schematic showing (a) Particle fragmentation and (b) reinforcement particle pull out mechanisms in MMC machining [215]

Comparatively, the particle fracture mechanism gives an improved surface finish as the pull out mechanism leads to the formation of cracks and pits at the machined surface [216]. Particulate reinforcement pull out during the machining of these MMCs' impacts surface integrity negatively due to the formation of grooves and cavities at the machined surface which can ultimately lead to chipping of the insert cutting edge. The formation of these cavities also leads to widening of surface cracks if originally present. As is the case in the machining of particulate MMC's, it is expected that material pull

out would lead to the formation of an unstable built-up edge as the loose material adheres to the tool cutting edge, causing a poor surface finish. From *Figure 5-6*, the particle fragmentation mechanism in the machining of MMC's can be seen to have occurred as the WC particles at the machined surface have been subject to brittle fracture by the action of the cutting tool. This mechanism is observed at the machined regions with both cutting tools. However, further subsurface damage to the microstructure was not observed in the MMC regions with both inserts.

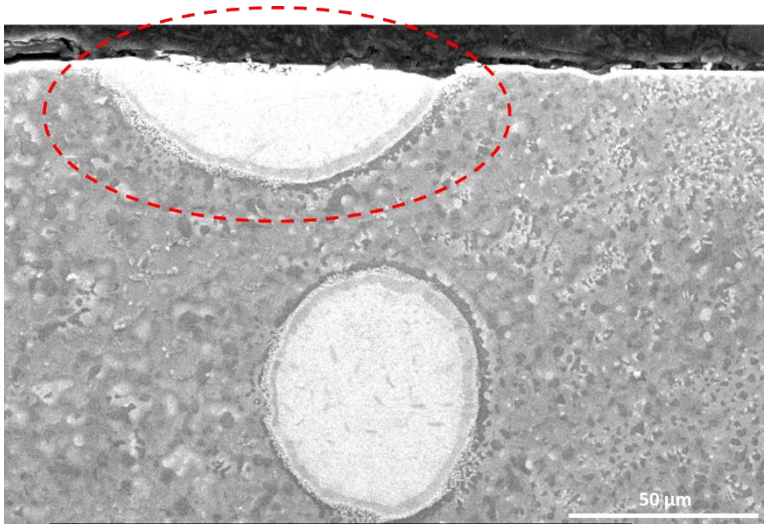


Figure 5-6: Highlighted region showing particle fragmentation of a WC particle in turning of the MMC region.

In the Ti6Al4V region, subsurface deformation was observed as shown in *Figure 5-7*. Deformation depth with the PCD inserts was found to be larger and was measured to be a maximum of 11.8 µm from the machined surface. In the Ti alloy region machined with the CBN inserts, deformation depth was found to be a maximum of 6.3 µm from the machined surface. Variations in deformed depth of the monolithic region is presumed to be a consequence of the change in cutting tool geometry which in this case would be dependent

on the wear rate of the tool. Hardness in the regions of beta deformed microstructure in the cutting direction (325 ± 5 HV), was found to be lower compared to the bulk material region. The size of the region in relation to the size of the indenter and also the edge effects due to the resin are thought to influence the hardness values measured. Microstructures typical of DED Ti6Al4V are observed as shown in *Figure 5-7*. At the Ti alloy- MMC boundary region, in both cases, a metallurgical bond is formed with no observed cracks and failure initiation points propagating from these areas.

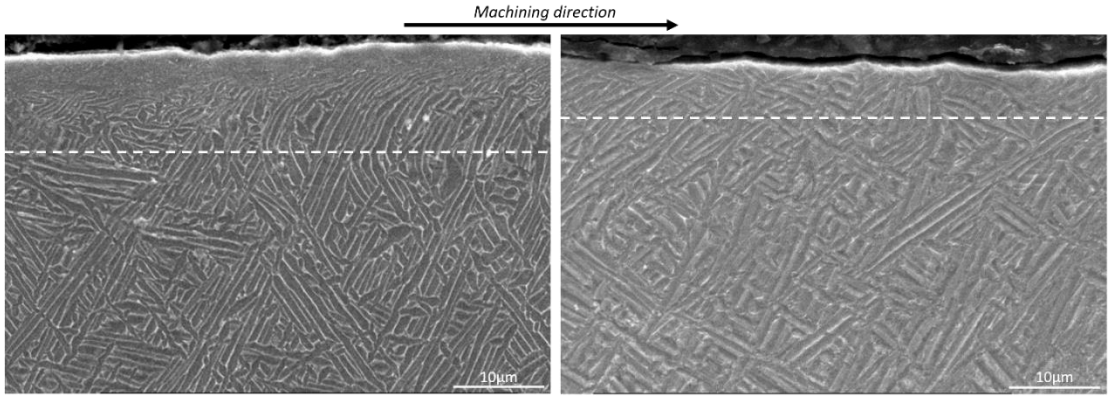


Figure 5-7: Subsurface deformation in Ti alloy region with different inserts (a) PCD (b) CBN. Visible beta deformation depth is a maximum of 11.8µm in the PCD machined component and 6.3 µm in the CBN machined component

5.3.3 Cutting Forces

Steady state cutting forces measured during the machining of both regions with the inserts had varying characteristics due to the difference in machinability of both regions and the difference in tooling. During the preliminary machining of the components, cutting force was less stable with periodic variations in the WC enriched region when compared to the *Ti6Al4V*

region. Evolution of cutting forces with increasing number of passes is shown in *Figure 5-8*. In the preliminary passes, after the first machining pass, *Figure 5-8* (a), higher machining forces are observed in the single material region with subsequent passes. The forces in this region are found to increase with each pass. Machining in the plots shown proceeded from the Ti6Al4V/ WC region to the Ti alloy region in all instances. Tool wear was found to increase and this leads to the degradation of the tool before the cutting edge reaches the single material region, hence leading to the higher cutting forces observed. For the machining passes labelled (e) and (f), the tool was not swapped for a new tool. Thus, the higher cutting forces observed are due to the high attrition of the tool. Tool failure was observed in the pass (f) which explains the increase in cutting force. Incompatibility in machining parameters between these regions coupled with the tendency for work hardening in the single material region particularly at elevated temperatures may cause the observed increase in cutting forces. An explanation of the tool wear mechanisms promoting the increased forces is discussed subsequently.

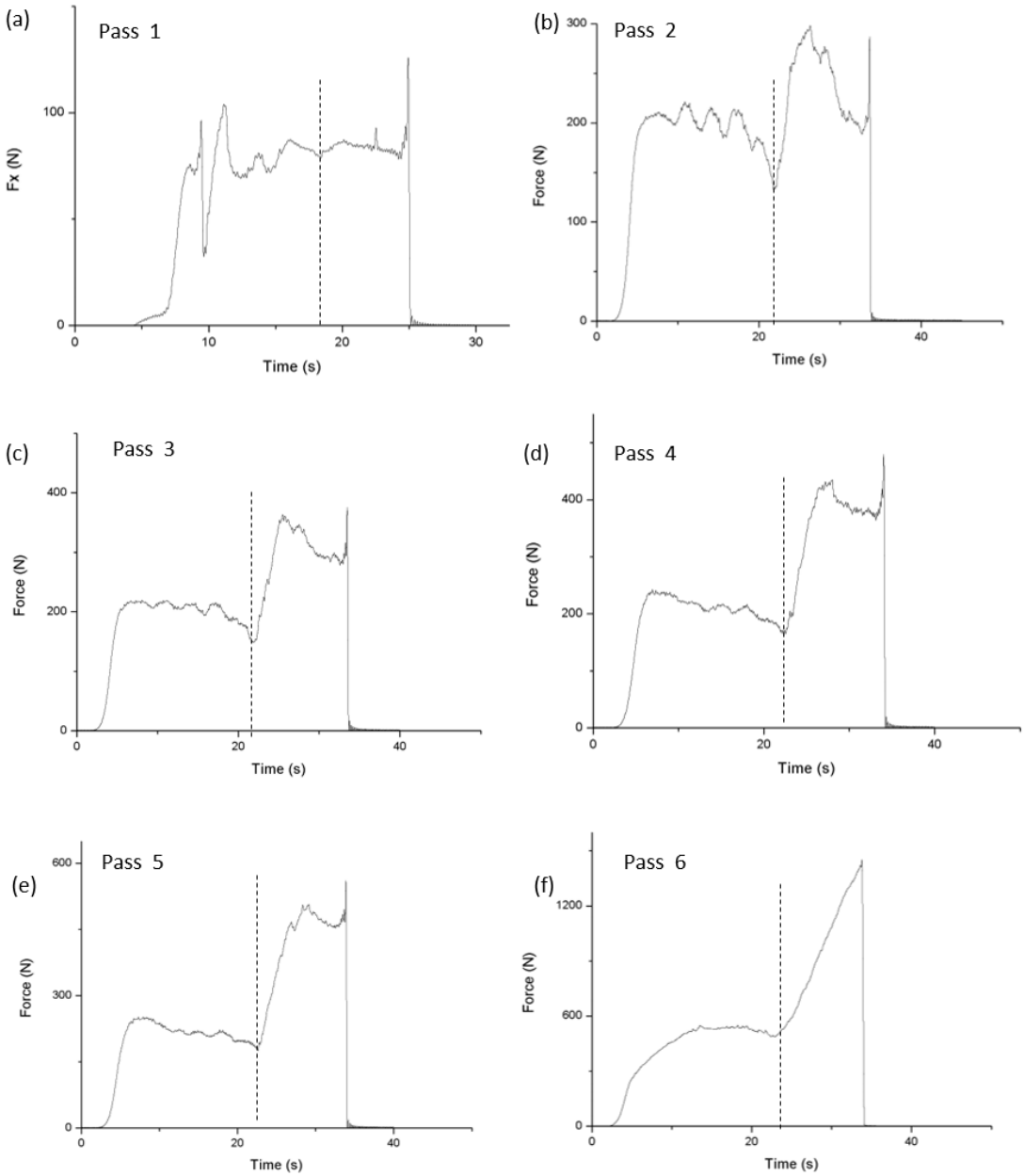


Figure 5-8(a-f): Cutting force plots with subsequent passes when machining from outermost layer with PCD insert. Cutting progressed from MMC region to single material in all cases. Cutting force magnitude is indicative of material removal rate. Values filtered with low pass FFT at 10 Hz to reveal machining forces trend. Increase in tool wear also contributed to high rise in forces in single material region. Forces shown are in the radial direction

Steady state cutting force plots in the normal direction to the cutting surface during a machining pass of the components with the inserts are shown in *Figure 5-9*. Region (i) in both plots corresponds to the areas with WC and (ii)

corresponds to the areas with only Ti6Al4V. Periodicity in cutting force measurements is observed with both inserts during machining the Ti + WC region. The periodicity is a result of variation in hardness due to the non-uniform composition of dissolved WC within the layers. The appearance of these periodic increase in cutting force also correlate to the layer height and number of layers making up the structure. Areas with higher dissolved WC content - re-melted regions between layers, vary in hardness by up to 40 % (345 ± 60 HV) compared to the interior regions and this leads to the periodic variation in cutting forces observed during machining. From *Figure 5-9* (b), the cutting force variations are also seen to progressively increase as machining progresses within the MMC region. A new insert was used at the start of the trials represented by the plots and the rapid rate of wear causes an increase in cutting force variation.

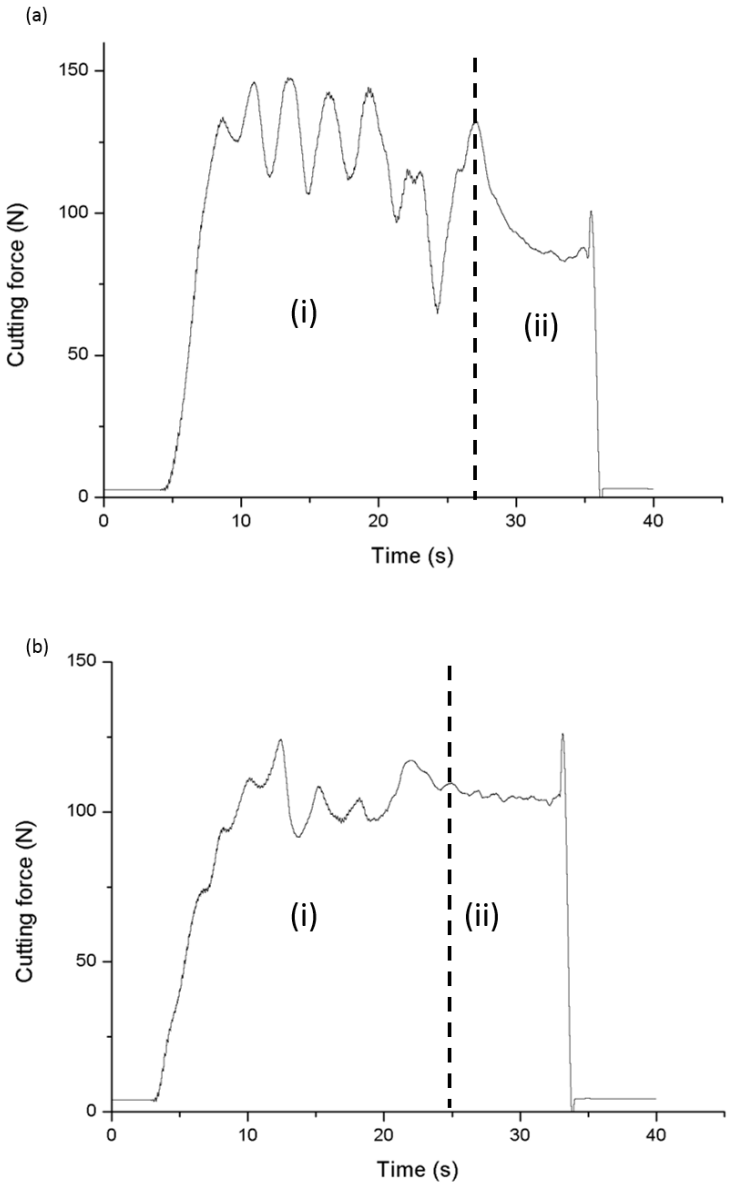


Figure 5-9: Variation in cutting force during machining with various inserts at steady state conditions (a) PCD (b) CBN across the Ti6Al4V region (ii) and the Ti6Al4V/ WC region (i). Values filtered with low pass FFT at 10 Hz to reveal machining forces trend

Mean cutting forces during machining trials for both regions with the inserts is shown in *Figure 5-10*. In both processes, the mean cutting force value is similar except when machining the MMC region with the PCD insert. Higher cutting forces with increased periodicity in the data was observed with this cutting tool. The decrease in cutting force in *Figure 5-9* (a) is associated with

the formation of a built up edge which temporarily reduces cutting force during the machining pass but breaks off at the onset of the subsequent machining pass causing cutting forces to increase back to its normal level.

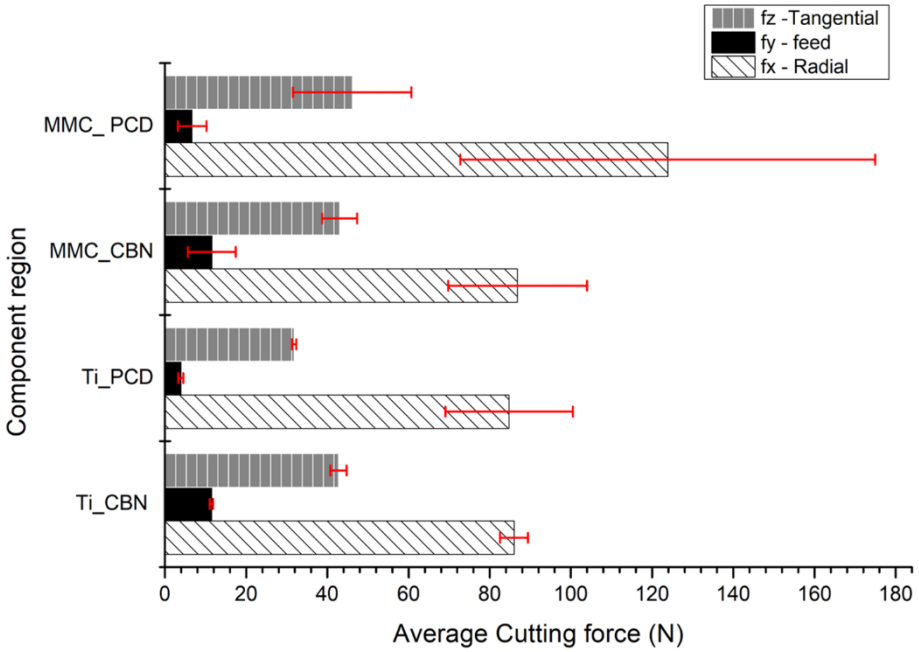


Figure 5-10: Mean cutting forces in x, y and z directions with varying inserts in MMC and single material region at steady state with a new cutting tool. Error bars show variation in sampled values from the mean values.

5.3.4 Surface finish

Grain pull out was observed in the MMC region with the use of the CBN and PCD inserts. Characteristic surface finish in the MMC and monolithic material region is shown in in *Figure 5-11*. In *Figure 5-11*(a) and (b), the voids formed due to material pull out can be observed in the MMC region. Analysis of surface roughness measurements confirms surface finish is improved in the Ti alloy region (*Figure 5-11*(c)).

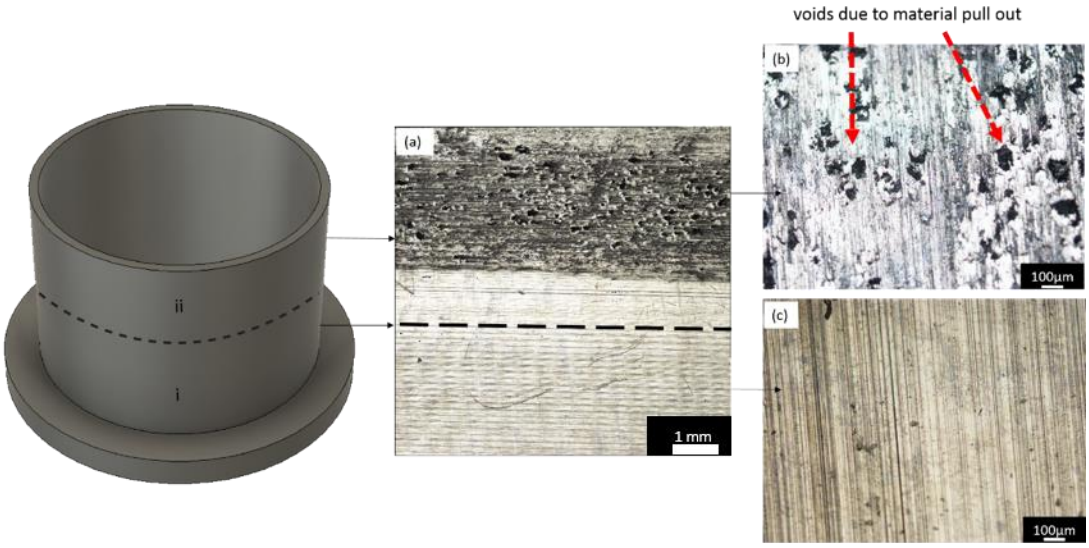


Figure 5-11: Surface condition post machining (a) optical image of surface showing both regions and boundary (b) MMC region (c) Ti alloy region. Images (b) and (c) rotated 90°

Surface profile maps generated from the machined surfaces of the MMC regions with both inserts are shown in *Figure 5-12*. An analysis of the component topographic features reveals the effects of variation in tooling on the obtained surfaces. Comparatively, the CBN machined surface presents an improved surface finish with the evidence of grain pull out and surface 'undulations' visible in both surfaces. The undulations observed are regions of fractured and debonded WC particles at the surface after the removal of a layer of material and are not removed as chip during the machining pass due to tool wear. These undulations are more pronounced in the surface map of the PCD machined component obscuring the characteristic feed marks and causing the irregular surface morphology observed in *Figure 5-12*(c).

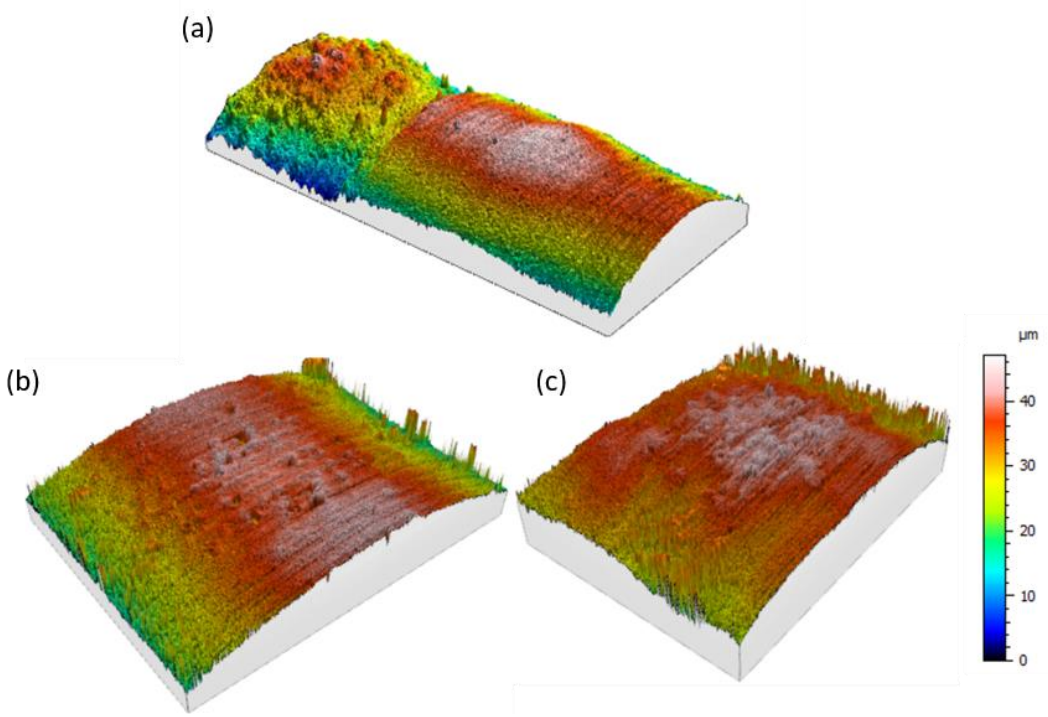


Figure 5-12: Component surface topography from MMC region post machining (a) Typical sample profile showing both material regions (b)CBN machined sample (c) PCD machined sample. Surface maps analysed using Mountain Maps software

Figure 5-13 is a plot of the Mean surface roughness values (Ra & Rz) measured at the central regions of the components. The MMC region machined with the PCD insert is observed to have the highest surface roughness values, corroborating observations from the texture observations in *Figure 5-12*. Also, this region was found to contain a higher number of cavities per unit area due to pull out compared to the CBN machined region. The relative improvement in surface finish observed with the CBN inserts is related to the lower cutting forces which may be due to the cutting tool maintaining its hardness at elevated machining temperatures and a reduction in the inserts' tendency to react with the carbides in the workpiece at these elevated temperatures. Machining the Ti6Al4V matrix regions with both inserts however shows

improved surface roughness. The effects of grain pull out and built-up edge formation on the single material region is however minimal, although machining marks on the surface around the boundary of both components up to 2 mm into the single matrix region are less obvious when compared to the marks observed when the tool is fully engaged in the single material region alone. In both component regions, measured Ra and Rz values show similar variation in relation to tooling and machined region.

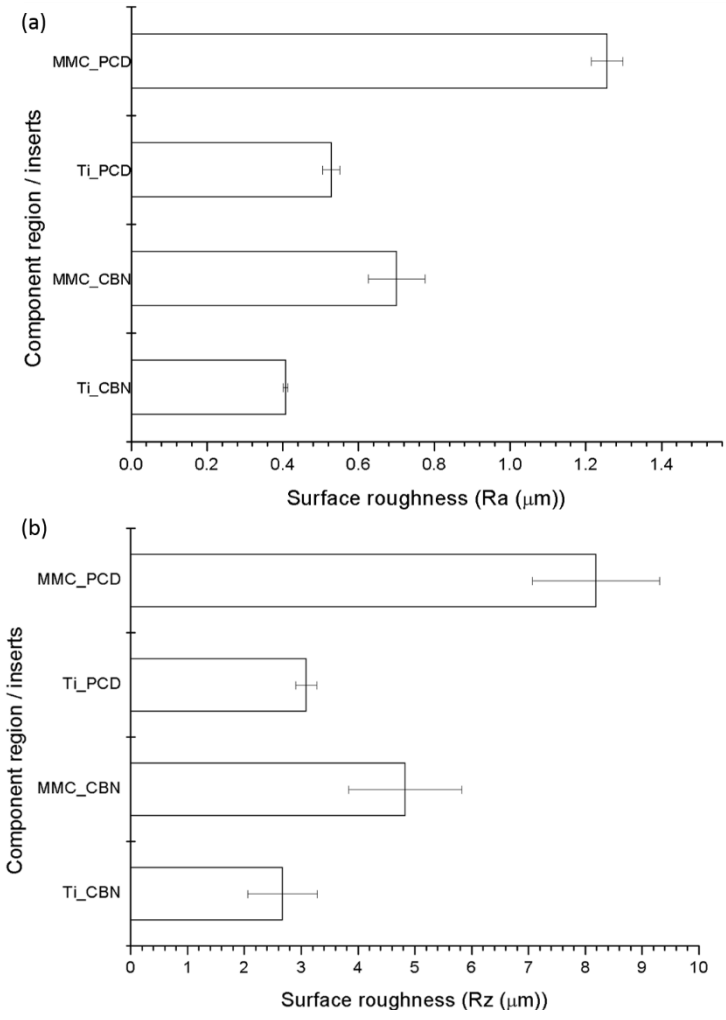


Figure 5-13: Mean surface roughness (Ra and Rz) of all regions post machining, MMC region machined with the PCD tool had highest surface roughness

Particle pull out and fragmentation are dependent on the strength of the bonds between the particles and the surrounding matrix and the location of the material in relation to the cutting tool edge. A difference between MMC's produced using this means and alternate methods is the dispersion homogeneity of the particles due to the Marangoni convection. The Gaussian beam profile used in these experiments leads to the formation of a temperature gradient between the centre of the beam and the edges, thus inducing surface tension gradients and capillary forces for liquid flow. The distribution of the particles is thus dependent on the advancing liquid flow. In this scenario, this leads to the particles being pushed to the centre of the laser beam path and a subsequent pile up in this region. This in effect leads to a high composition of WC components at the periphery, retarding machinability due to cutting edge – particle interactions.

Figure 5-14 shows the different particle locations in relation to the tool cutting edge. From the diagram, three scenarios can be deduced: particles along the cutting path, particles above the cutting path and particles below the cutting paths.

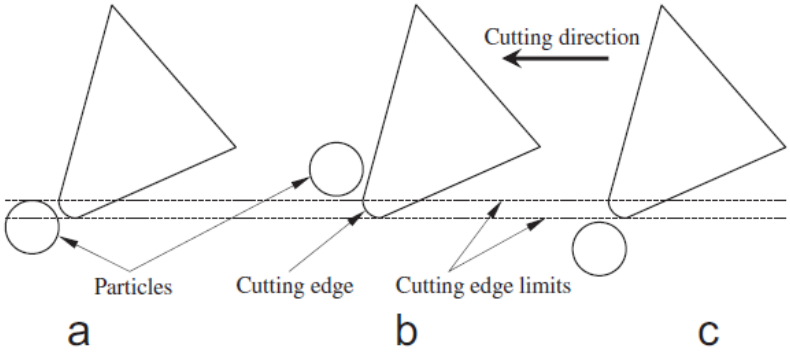


Figure 5-14: Schematic showing particle position in reference to tool cutting edge and cutting edge limits (a) Particle along tool path (b) Particle above tool path (c) Particle below tool path [217]. Size of tool in relation to particle not to scale.

For the particles along the tool path, the position of the particles in the lower or upper cutting limits dictates the particle behaviour during and after tool interaction. For a particle in the lower part of the cutting edge, as the tool approaches, the matrix between the tool and the particle is in compression and as cutting progresses, the tool interacts with the particle and the particle is either debonded or fragmented. With particles in the upper part of the cutting edge, as the tool approaches, the strain in the matrix is lower and the particle is displaced upwards by the action of the tool and hence slides along the rake face of the tool. The sliding action over the rake face and the repeated interactions with the tool edge and flank face deteriorates the tool as it leads to pull out of tool material particles from the cutting edge and flank face, thus causing self-abrasion of the cutting tool. Particles above the tool path would usually become detached as a result of the interface of the reinforcement particles cracking in front of the tool along the secondary shear zone. The reinforcement particles thus accumulate and align along the shear plane and slide along the rake face which leads to scratches on the rake face.

For particles below the cutting-edge limit, as the tool approaches, the matrix between the particle and the tool is under compressive stress radial to the cutting edge. These mechanisms lead to inhomogeneous deformation and flow of the matrix leading to the undulations observed in *Figure 5-12*.

5.3.5 Tool wear

The heterogeneous microstructure and the presence of hard reinforcements in the components leads to increased tool wear during machining. However, with subsequent passes to remove the outermost layer and as workpiece run out reduced, tool life also improved. This is related to a reduction in material pull out at the surface in the MMC region and the subsequent reduction in shock impact the tool undergoes as the machining process reaches steady state. Also, the generation of high temperatures during the machining process was evidenced by a 'glow' in the cutting region albeit with the high coolant delivery pressure. This also contributes to tool wear.

Abrasion has been reported to be the main mechanism of tool wear during the machining of MMCs' [218]. Two body and three body abrasion mechanisms as a result of material pull out and interactions at the cutting region impact on both tool and workpiece integrity. In this study, abrasion of the rake and flank face of the tool was prevalent at all stages of machining, including during the finishing passes. *Figure 5-15* shows the tool wear after two preliminary machining passes for removal of the outermost layer with the CBN inserts. In both instances, a new tool was used at the start of machining.

Flank wear, crater wear on the rake face and chipping of the cutting edge are all observed in the inserts pointing to various formation mechanisms occurring during the turning process.

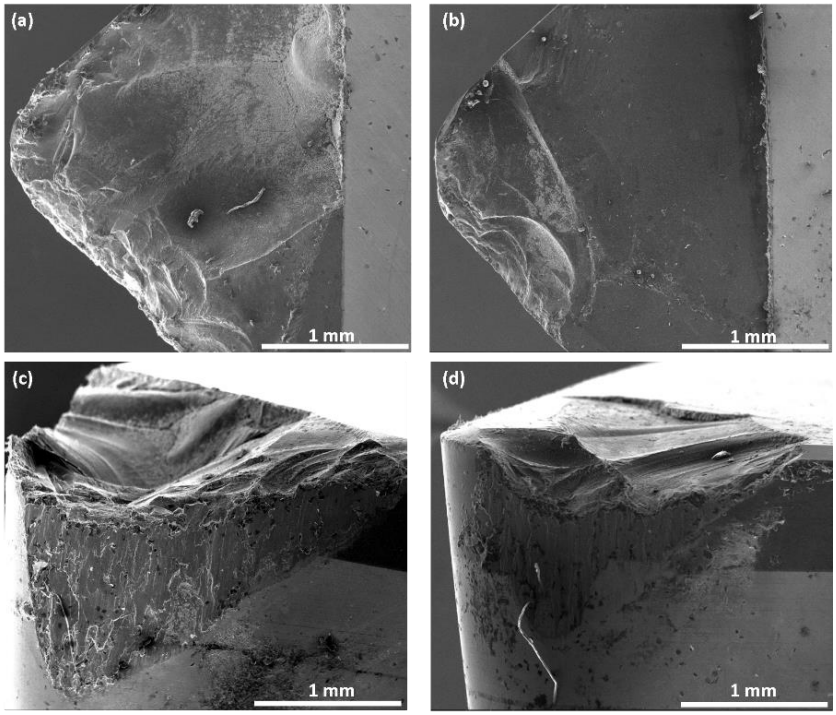


Figure 5-15: Progressive improvement in tool wear condition with increased removal of outermost layer in CBN inserts. (a) Rake face of tool after first machining pass (b) Rake face of tool after second machining pass (c) Flank face after first pass (d) Flank face after second pass

Tool condition for the three inserts after a machining duration of 30 seconds at the preliminary stage of machining and during the last machining pass is shown in *Figure 5-16*. The figure shows the damage to the flank and rake face of all the inserts. Chipping of the cutting edge as a result of the high hardness of the workpiece is also observed in all instances.

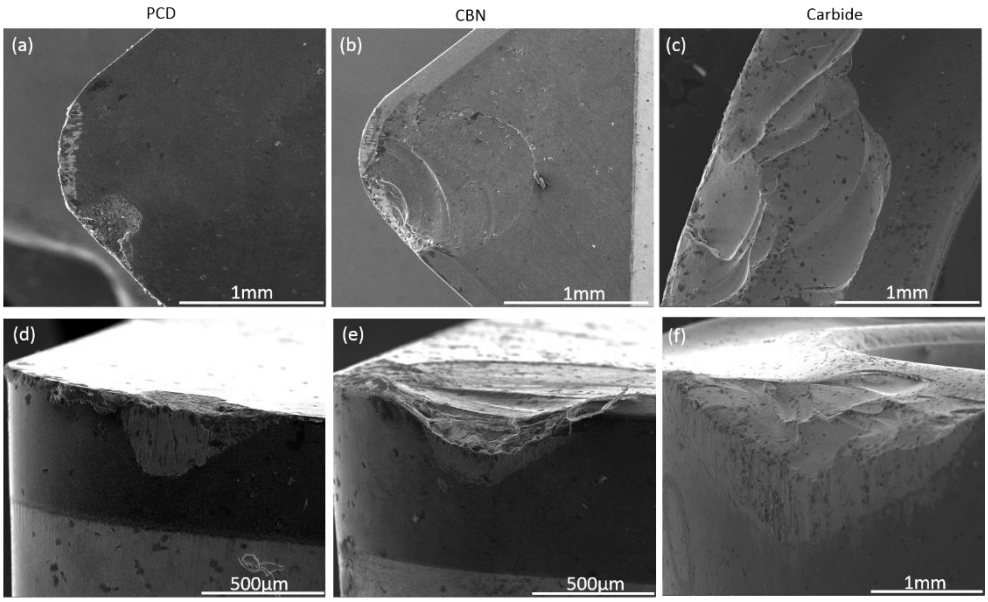


Figure 5-16: Inserts after machining for similar duration of 30 secs (a) Rake face of PCD (b) Rake face of CBN (c) Rake face of coated carbide insert (d) Flank face of PCD insert (e) flank face of CBN insert (f) flank face of coated carbide insert

During the preliminary machining process, high rates of wear which were considered less than an economically viable average tool life of the insert cutting edge was observed with all the tooling. Comparing tool deterioration after a machining pass of 30 seconds, the PCD inserts performed better at the different machining stages – from outer layer removal to the finishing passes, compared to the CBN tools. In the CBN inserts, wear of the tool was more pronounced as the tool cutting edge was significantly abraded.

In the PCD insert, preferential abrasion of the surrounding matrix material in the tool leads to particles from the tooling detaching and forming part of a three-body abrasive system which grinds the tool flank face. In the three body abrasion processes, the pulled material remains between the tool and the workpiece surface and causes abrasion to cutting surfaces.

Increased cutting temperatures also impacts tool wear negatively. Although the temperatures during machining were not measured in this study, the effect of increase in temperature due to the nature of the workpiece material during machining is detrimental to the tool life as this is an acknowledged cause of thermal flaking of the cutting edge and it also promotes the formation of an unstable built up edge.

5.4 Discussion

In the machining of MMCs produced using conventional means, tool wear has been reported to be influenced primarily by the reinforcement hardness [219]. However, during the DED process, despite the high melting temperature of tungsten carbide, partial melting of the reinforcement particles was observed. This leads to the formation of TiC and W rich precipitates within the matrix material, which invariably leads to higher hardness and accelerated tool wear, causing the matrix to have a greater influence on the machining process and hence tool condition. From the review of literature sources, the effects of reinforcement melting on machining has not been widely reviewed by other authors for MMC's as the methods used in producing MMCs are usually aimed at avoiding melting of the reinforcement material. Wilson et al. [220], commented that partial melting of the reinforcement during the laser deposition process led to the formation of intermetallic phases which reduce the strength of the deposited material. Here, the re-melted regions due to the increased melting of the reinforcement

has a larger effect on the insert compared to the central regions as a result of the comparative higher hardness in these regions and the alternating effect on cutting force during machining. The layer build strategy requires that a previous layer of deposited material be partially re-melted during the addition of a new layer. Marangoni convection causes an increase in WC particles at the clad periphery, coupled with the addition of new material to the melt pool leads to an increase in WC composition around this region. This leads to a pronounced variation in microstructure and material anisotropy.

However, localised increase in matrix hardness due to the partial melting of the reinforcement particles leads to the periodicities in cutting forces observed during machining, causing the matrix to have a greater influence on the machining process and hence tool condition. The formation of TIC and W rich precipitates within the matrix material accounts for this increase in hardness.

Whilst a study on the effect of reinforcement size and percentage quantity on machinability of the components has not been out carried here, the effects can be seen to be relevant in the initial machining with the coated carbide insert where the selective abrasion leads to increased tool wear. The larger particle sizes and their resulting strength limits the effectiveness of the insert. In the machining of the components with the use of commercially available tools (PCD and CBN), acceptable surface finish was attained albeit with a high tool wear rate. Subsurface deformation depth in the single matrix region is found to vary with the tooling in the Ti6Al4V region and not observed in the

MMC region with both inserts due to the avoidance of aggressive parameters in machining. However, grain pull out remains a limiting factor towards achieving defect free surfaces. The MMC region shows a considerable amount of pull-out with both PCD and CBN inserts and this consequently led to poor surface finish in these regions. Cavities due to grain pull out are however seen to manifest mostly in the PCD machined MMC region. This is possibly due to the PCD material having a higher hardness and ability to retain this at elevated temperatures. Comparatively higher mean cutting forces, surface roughness and higher subsurface deformation are also observed in machining the MMC region with this insert.

5.5 Conclusions

In this chapter, functionally graded components were successfully machined commercially available tooling. Wear of the cutting tools was however high in all cases. Based on experimental observations, the following conclusions can be drawn:

- The laser beam partially melts the WC reinforcement and consequently increases the matrix hardness which indicates MMC's produced by DED processes would be potentially difficult to machine compared to other process routes due to the potential high hardness of the matrix. Thus, if a post processing step is required, it would be expedient to limit the amount of dissolved hard facing material by adjusting laser process parameters or material combination volumes.

- Material pull out was prevalent in the machining of the MMC region, with characteristic machining marks on the single matrix region. Surface roughness values of the single matrix region are however within an acceptable range. Whilst pull out during machining MMC's is a widely reported occurrence, it is believed this would lead to sites of crack initiation and fatigue of the component when in service.
- Variation in hardness during the machining of the MMC region led to higher cutting forces and accelerated tool wear. It is believed that a machining regime which adapts to changes in machining conditions due to material properties would be beneficial in machining such components. Such a system would regulate cutting forces independent of tool condition and minimise variation in surface roughness difference.
- Tool wear was observed to be particularly high, despite the relatively conservative parameters used in machining. Further study on the machinability of these components with varying parameters will be necessary to determine the optimum conditions for machining with these inserts. Tool wear mechanisms have been shown to be dependent on reinforcement particle position relative to the tool cutting edge and surface finish is dependent on the interaction between the cutting edge and the reinforcements
- Boundary regions between layers have been shown to possess higher hardness by up to 40 % (345 ± 60 HV) which led to difficulty in the machining of these parts and caused a high rate of tool insert wear.

6.0 Adaptive Machining System Development

This chapter discusses the processes undertaken in the development of an adaptive control system on an open architecture CNC machine tool. The primary purpose for developing the control system is for the machining of metal additively manufactured components. It is postulated the use of a strategy which aligns machining parameters to the prevailing cutting conditions would be beneficial towards producing parts with improved surface quality whilst providing a more beneficial means of machining metal AM parts by limiting tool wear and component damage during post process machining operations.

To achieve adaptive control on a machine tool requires an understanding of the controller's system architecture and a means for communicating required inputs and reading outputs on the controllers' Graphical User Interface (*GUI)*. A description of the machine tool control architecture, the required sensors and the processes used in isolating and controlling the machining parameters during machining operations are discussed in this chapter. Also, preliminary machining trials towards understanding the relationship between machining input parameters and cutting conditions are presented. The developed control system overview is presented and the assumptions in the

development of the system are also discussed. Initial machining trials which include the drilling and milling of wrought materials and DED Ti6Al4V using the developed adaptive control system is presented.

6.1 Machine Controller

Tormach CNC workstations are affordable machine tools with an open architecture controller which allows the user access to the machine controller for adjusting and adding peripherals to meet their requirements. Open architecture in this context refers to a controller wherein the control functions of the various aspects of the machine have been partitioned into components by the machine manufacturer and documented in a manner which allows end users the flexibility of being able to integrate peripherals from other sources to suit their functionalities and maintain working machining centres [184]. The Tormach 1100 CNC incorporates a machine controller which runs on a Linux operating system. Linux CNC is an open source machine controller which was developed for driving machine tools and other computer numerically controlled machines. The Linux CNC variant that controls the functions of the Tormach workstation used in this study is 'Pathpilot', a control software developed specifically for Tormach CNC machines. As with other machine tool controllers, the user interface of Pathpilot can either receive commands through physical input by the operator or can interpret CAM data of a profile developed externally from the controller interface in developing G-code input

appropriate to move the drives and operate the system components in relation to the machining activity required.

A common feature of Linux CNC based systems is that they function based on a Hardware Abstraction Layer (HAL) which allows for multiple individual components that make up the system to be interconnected. Hardware drivers that control these components are connected to the *HAL* and their operations and interrelationships are controlled by the *HAL*. The interconnected components include; the main controller, encoders, stepper drives, limit switches, pendants, tool changers amongst others [221]. Thus, the use of the *HAL* in Linux CNC control architecture bridges the gap between high level sub task descriptions and low-level commands. Components connected to and driven by the *HAL* are referred to as *HAL* components. Similar to physical connections between components of a complex system, the *HAL* connects to devices using *HAL* pins. These *HAL* pins are not physical pins but apportioned spaces in the operating software for communication with the *HAL* components related to the pins. The relevant start point in interfacing with the *HAL* in this study is the HAL User Interface (HALUI). The *HALUI* is a user space program that networks the HAL pins to Neutral Message Language (*NML*) commands and is useful for creating and connecting external peripherals to the CNC system. This was used in creating the required *HAL* component in connecting an external controller to Pathpilot.

A typical Linux CNC system architecture with the role of the HAL in system integration is shown in *Figure 6-1*.

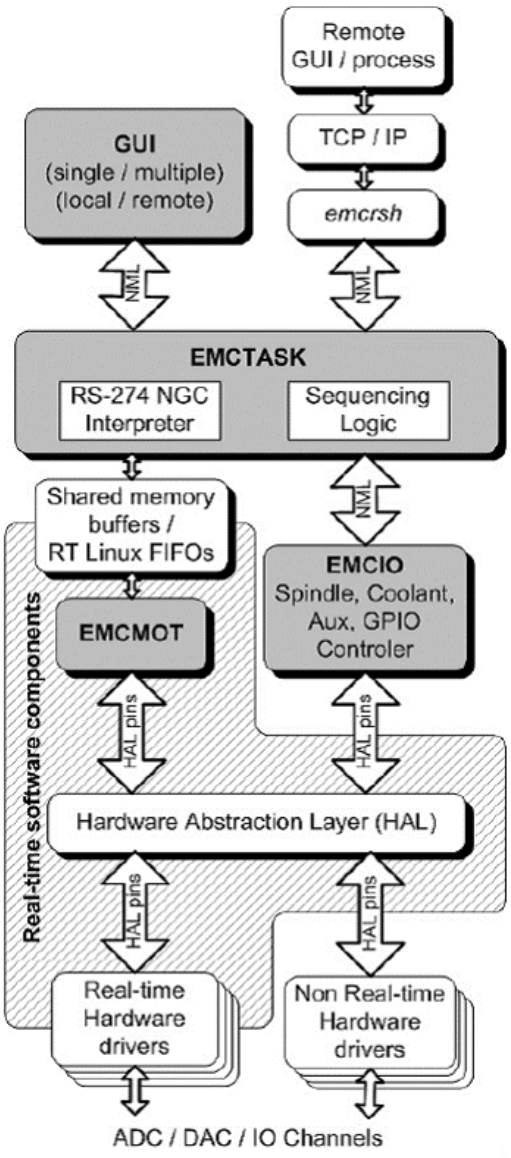


Figure 6-1: Linux CNC structure [222]

6.2 Controller Interfacing

Towards interfacing with Pathpilot, a strategy for generating inputs externally and receiving outputs from the controller GUI was implemented. In achieving this, lines of code were incorporated into the start-up sequence of Pathpilot. The controller PC for pathpilot runs on *Ubuntu 10.04* and the first step was to

achieve access to the '*back end*' of the software to make the necessary additions to the control architecture.

Typically, a decision was made to control the parameters which would readily have an impact on the machining conditions. The user interface of the Tormach has override slider controls which are for the adjustment of spindle speed, maximum velocity (MaxVel) and feed rate before and during a machining process. The slider controls can be used to adjust feed rate and spindle speed parameters between 0% and 150 % and MaxVel between 0 and 100% of the defined values in the G code. Using feed rate as an example, the actual value during at any point during a cutting operation is thus the product of the override percentage and the pre-programmed feed rate value. This capability lends to the development of the adaptive control system as it affords a means for controlling process parameters as machining progresses, also values specified in the G code cannot be readily adjusted during machining operations without the use of these slider controls. Thus, it was expedient to attempt the external control of these sliders as this would aid automated control of the system during machining processes. An image of the pathpilot GUI highlighting these sliders scales is shown in *Figure 6-2*.

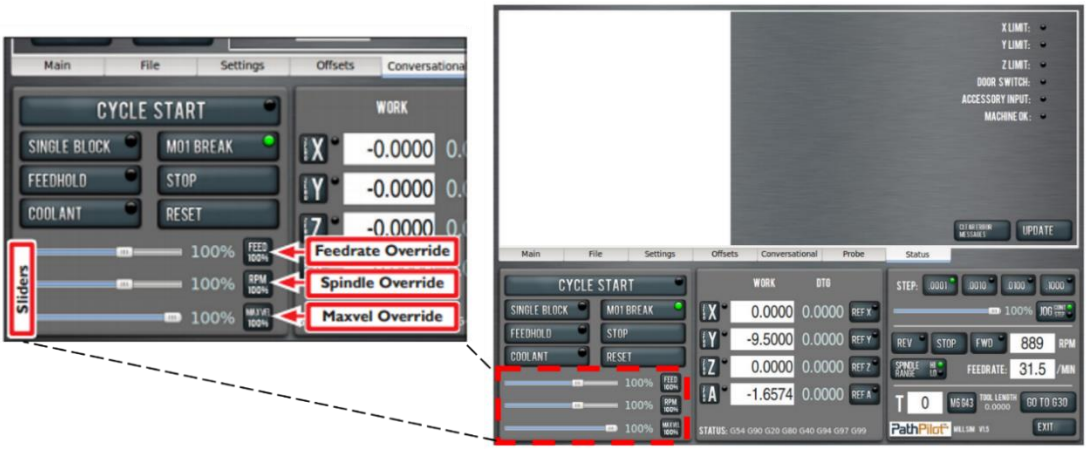


Figure 6-2: Tormach GUI with override slider controls for Feed rate, Spindle speed and MaxVel highlighted.

The following were identified as necessary milestones towards the achievement of the set goals:

- Selection of a microcontroller capable of receiving input and generating analogue signals to be sent to the CNC controller.
- Creation of a *HALUI* component written in python code (.py extension) which facilitates control of the selected parameters and receives input from the external peripheral.
- Physical override knobs replicating feed rate, spindle speed and maximum velocity sliders. i.e. development of a CNC pendant.
- Replication of the action of the override sliders at start-up of the CNC with controls on the external peripheral which allows for digital adjustment of the sliders.

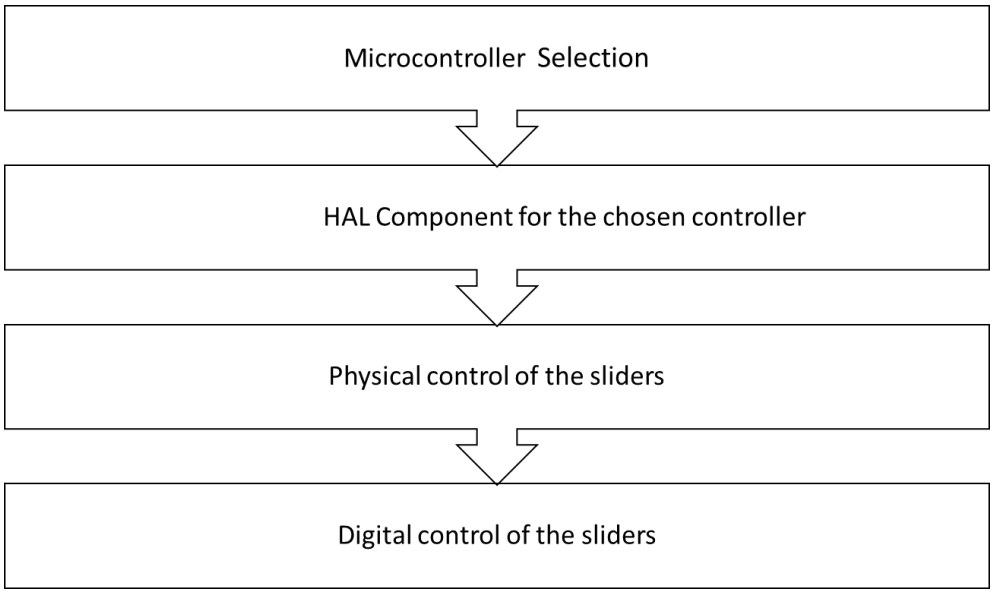


Figure 6-3: Flow chart showing steps involved in controller interfacing development

The steps taken towards achieving the listed criteria are discussed in the following;

6.2.1 Microcontroller

An early decision was made to use an Arduino, based on the ease of connecting it to the Tormach's CNC controller and also existing resources detailing communication procedures between external controllers and Linux based CNCs [223]. In developing the communications protocol, the Arduino is connected to the pathpilot computer via a USB connection. As a start point, '*pyserial*' – an application programming interface for serial port communication with python systems is installed on the controller PC for facilitating serial port communications between the Arduino and Python software on the CNC computer. The Arduino GUI for writing and uploading

Arduino sketches and communicating with the controller is also installed on the CNC's controller computer. An Arduino sketch is subsequently developed and modified to suit the purposes required. A physical override switch is added to the Arduino and this is also replicated in the developed sketch to prevent the controller from continually sending input to the controller computer when the system was not in use as this had the tendency to slow down other functions of the CNC controller when connected.

6.2.2 Creation of the HAL component

There was a need to create a user component in *HALUI* capable of driving the sliders using input signals. The creation of such a peripheral would allow for commands initiated at the external controller interface to directly influence the operation of the Tormach and facilitate the development of a 'hybrid' control system. The strategy for the development of this component in *HAL* is detailed below:

A code for creating the *HAL* user space component *''arduino.py''* was added to the Python folder which loads the essential files for operation of the CNC at start up. The code *''arduino.py''* was also made executable at start-up of the controller PC. The code contained information about the communication port, a definition of the Arduinos' pins and components' connection, timing and scaling factors and information about the *HAL* pins to be created. The entire code is shown in Appendix B.

Lines of code for the creation of the override components for the spindle speed, feed rate and MaxVel are added to the existing ‘’Tormach mill.py'' file which loads up at start-up of the system and creates the communication protocols required for the functioning of the Tormach. Here, the override pins substituting for the regular operations of the slider controls are created and updated with the relevant scaling factors. A start up command for initiating the Arduino at system initiation is also included in this folder. From *Figure 6-2*, the feed rate and spindle speed sliders have a maximum of 150 % of the specified value whilst the MaxVel slider has a maximum of 100 %. The scaling values are thus adjusted to account for these factors. The entire code with the included lines highlighted is shown in Appendix B.

The previously created override components are added to the ‘’postgui_tormach_mill.hal’’ script which loads the HAL components after the GUI initiates and the required pins specified from the ‘’Tormach mill. py’’ code have been created. The postgui script also loads the ‘’Arduino.py’’ component and contains information about the override functions. The added lines of code and the entire code is shown in Appendix B. It was also necessary to be able to revert the Tormach to regular operations mode - without the use of the external peripheral for controlling the slider controls – the procedure for this is detailed in Appendix C.

For sending the signals to the CNC controller, the analogue A0, A1 and A2 ports on the Arduino corresponding to the feed rate, spindle speed and maximum velocity were used. By connecting these ports with three

potentiometers, the Arduino was able to function as a CNC pendant- Appendix C shows the developed pendant. The Arduino sketch that drives the controller is shown in Appendix B.

6.2.3 Interfacing the system with LabView

With the control of the feed rate, spindle speed and MaxVel isolated and external from the CNC controller, the next step in the process was to move from the use of physical knobs to a solution which provides digital control of the sliders. LabVIEW was selected for this as it provides a platform for interface between instrumentation, makes real time data collection, visualisation and feedback control of interfaced peripherals possible. A National Instruments' CompactRio was used as an interface for connecting the input and output signals. Communication between the Arduino and the CompactRio was achieved by using a LabVIEW voltage output module (NI-9263) which has capabilities to send signals up to 10 V to the analogue pins of the Arduino. Although the inclusion of this additional interface was cumbersome and might lead to latency in the system communications, it was however necessary as LabVIEW also served as an interface between the various components that would be required in the development of a closed loop control system. The LabVIEW Virtual Instrument (VI) developed for control of the sliders is shown in *Figure 6-5*. The Arduino and the associated knobs on LabVIEW have a maximum output of 5V. This translates to a scale of 0 - 5 V on the LabVIEW VI being equivalent to a scale of 0 - 150 % for feed rate

and spindle speed and 0 - 100 % for the MaxVel on pathpilots' GUI. By including appropriate scaling factors in the LabVIEW VI, this was updated to directly give the value of the feed rate used for machining at any instance.

6.2.4 Cutting Force Measurement

In selection of sensors for use in a machining process, accessibility, suitability and repeatability of the monitoring process are the important factors to consider. Initially, a rig which had a combination of 4 affordable load cells connected to a *HX711 load cell amplifier* was used in measuring variation in cutting force magnitude during machining. The load cells used were run on an Arduino and the results were read from the serial monitor using the LabVIEW Interface for Arduino (LIFA) toolkit. A CAD model of the rig is shown in *Figure 6-4*.

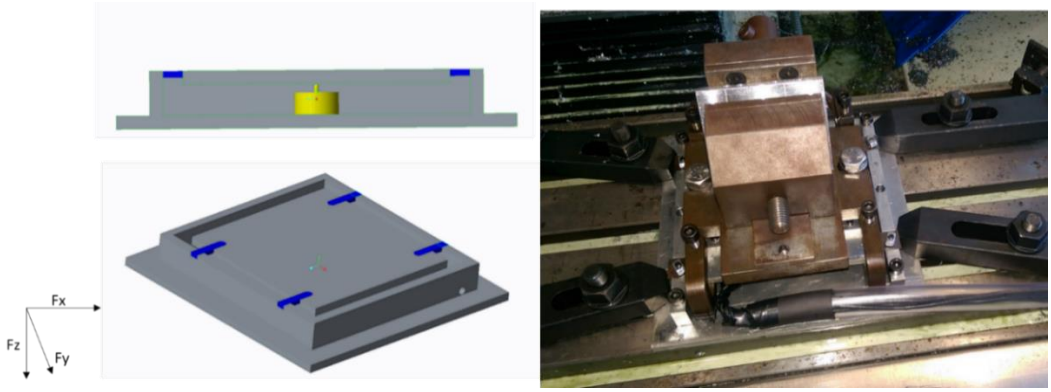


Figure 6-4: CAD model and actual set up of cutting force measurement rig developed.

Preliminary results suggested the load cell arrangement was a viable alternative for measuring variation in cutting forces during the experiments. Early machining trials for the determination of the effects of spindle speed variation on cutting force was carried out. However, repeatability and

resolution of the results from the experiments with the sensors was *cumbersome* particularly during the machining of difficult to machine components due to a high signal to noise ratio from the reduced rigidity of the rig. A decision was made to use available Kistler dynamometers which are designed for purpose and as such have improved signal acquisition rates and can resolve forces into individual components. Cutting force plots from drilling trials obtained from the use of the load cells arrangement in drilling experiments is shown in Appendix D.

For the remainder of the experiments, Kistler dynamometers were used in measuring cutting forces. Signals from the sensor are conditioned using a Kistler amplifier with the output signals connected to an analogue input (NI-9025) module interfaced with the Compact Rio. The dynamometers provide a useful addition which give more accurate and reliable readings without loss in data integrity and was seamlessly interfaced with LabVIEW. As detailed in Section 3.5, a number of dynamometers were used at different points in the study. When using a different dynamometer, the calibration and scaling factors were updated both on the sensor amplifier and in the LabVIEW VI. With the addition of the dynamometer to the set-up for force measurement and feedback, a closed loop control system could be implemented. A LabVIEW VI showing a system which controls the sliders and also allows for visualisation of cutting force data is shown in *Figure 6-5*. Different VI's were developed at different stages of the study for visualising and recording measured cutting force data and also control of the system. A selection of relevant VI's with

their description and uses are presented in Appendix F. For measuring forces in drilling experiments, the LabVIEW VI was configured to use measured forces in the *z* direction for control purposes although forces in the *x* and *y* directions were also recorded. For milling experiments, the input force for control purposes is computed as the resultant of forces in the *x* and *y* directions. The summation of forces in milling experiments was to account for changes in cutting direction and tool deflection which can affect cutting force direction [178, 224].

$$F_{drilling} = F_z \quad (6\text{-}1)$$

$$F_{milling} = \sqrt{F_x^2 + F_y^2} \quad (6\text{-}2)$$

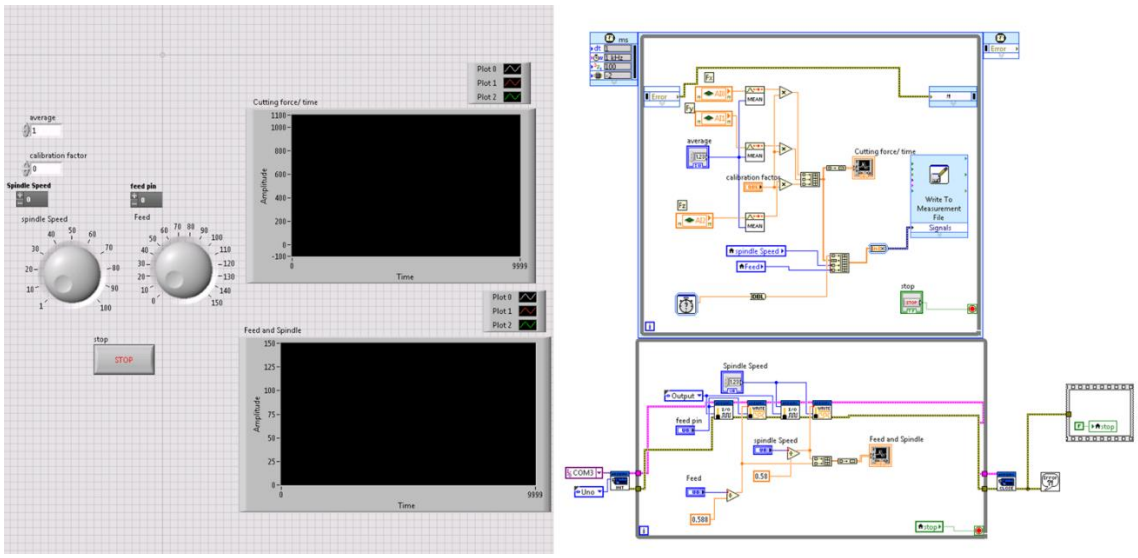


Figure 6-5: VI for manual control of feed rate and spindle speed, also visualisation and recording of cutting forces.

6.3 Development of the Control System

In the development of the closed loop system, an Adaptive Control with Constraints (ACC) strategy was adopted. In using the ACC system, the constraint/output was the cutting force with the spindle speed, or the feed rate the parameter adjusted / input towards the regulation of the constraint. Drilling trials to determine the effect of changes in spindle speed and feed rate on cutting force were carried out. For both parameters, it is established a decrease in their value leads to a decrease in cutting forces as there is a reduction in chip load. Chip load (feed per tooth) is the amount of material removed per tooth of a cutter per revolution. It was thus necessary to investigate the more responsive parameter. The relationship between chip load, spindle speed and feed rate is given by;

$$Chip\ load\ = \frac{Feed\ rate}{No\ of\ flutes\ *\ RPM} \qquad (6\text{-}3)$$

In carrying out these trials, a sine wave generator function from the signal generation toolkit in LabVIEW was used for producing signals simulating the successive increase and decrease in the input signals from the Arduino to the Tormach controller. The input function for feed or spindle speed on the LabVIEW VI is substituted with this sine function as applicable. By measuring and analysing both input data and cutting force response, a result on the

response of both parameter changes could be inferred. From the trials, it was deduced that cutting force was more responsive to variations in feed rate as changes in input feed led to a comparatively larger change in cutting forces. Also, changes in feed rate caused less disruption to the Tormach's functioning. Incessant adjustment of the spindle speed led to an increase in temperature of the machine tool spindle motor which led to machining instabilities. Plots relating to these trials are shown in *Figure 6-6*. These experiments also gave insight into the response of the CNC controller to changes initiated from the LabVIEW user interface.

Based on these results on the responsiveness of the cutting force to changes in feed, the control system was consequently developed with the feed rate being the input parameter. However, this can be modified to substitute the constraint parameter as the other machining parameters are also controlled from the VI interface. Thus, spindle speed alone or a combination of spindle speed and feed rate control could also be implemented if required.

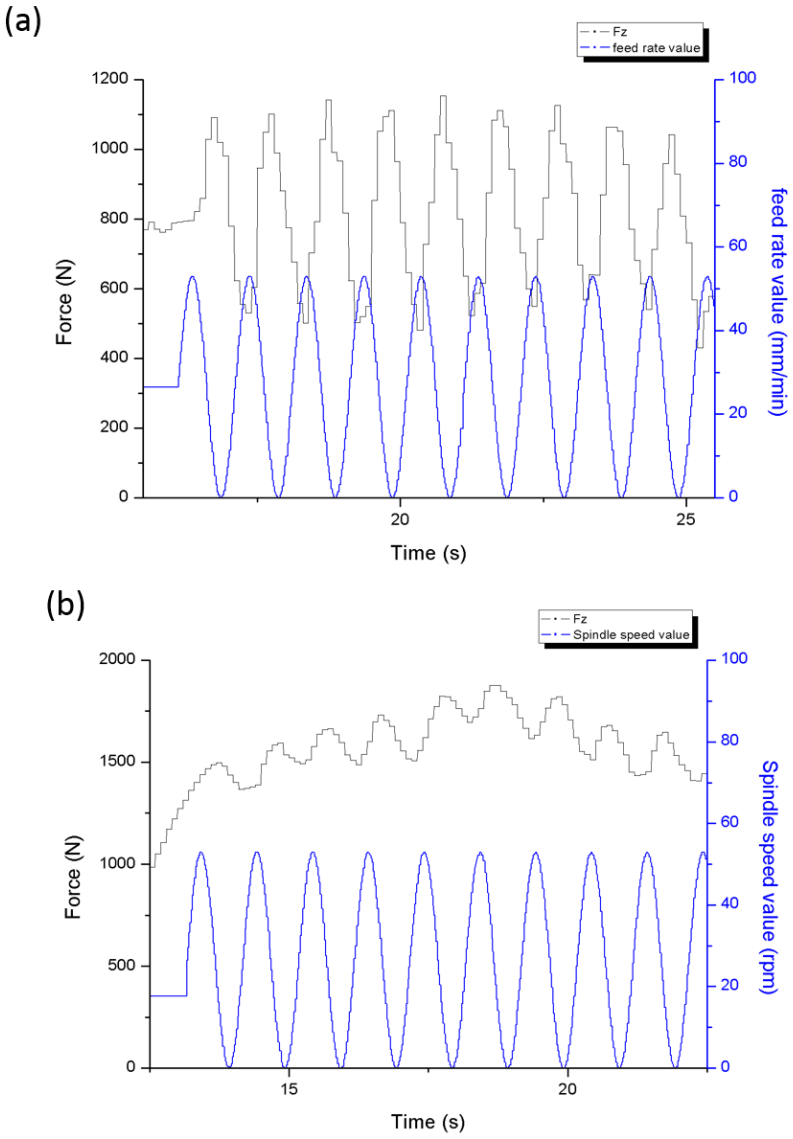


Figure 6-6: Graphs showing variable feeds and speeds and the response threshold in cutting forces (a) Feed (b) Spindle speed. Forces shown are in the Z direction.

6.3.1 Adaptive Control System

In the modification of the developed LabVIEW VI for force feedback control, the Proportional, Integral and Derivative (PID) toolkit on LabVIEW was used in achieving closed loop control of the system by specifying the set point value,

control variable and PID parameters. PID controllers are centred on the principle of the controller being able to receive and interpret output from a sensor, compare to a specified set point value and compute the desired actuator output required to adjust the input to read the set point value from the sensor. *Figure 6-7* shows the system components and the relationships that exist between these components.

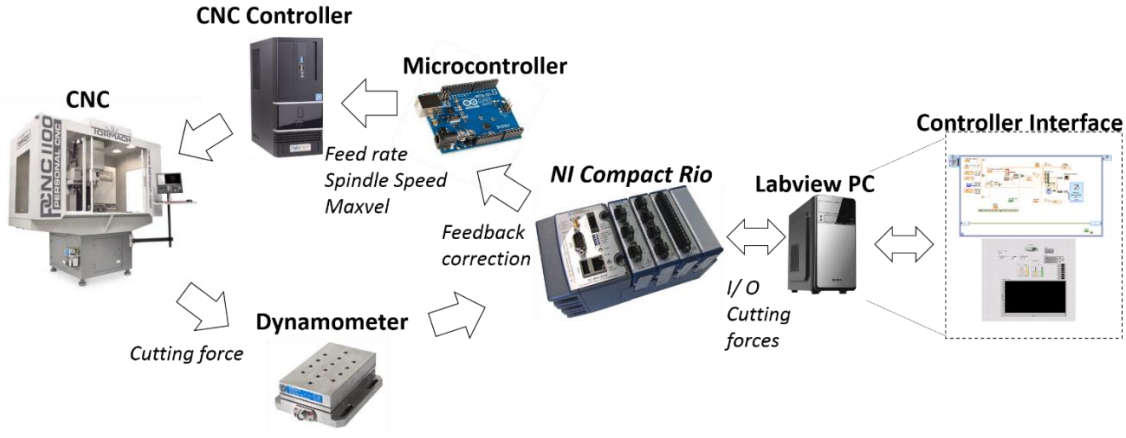


Figure 6-7: Schematic showing entire system components

A proportional controller (Kp) reduces the rise time and will also reduce but not completely eliminate the steady-state error. An integral control (Ki) diminishes the steady state error but can worsen the transient response. Derivative controller (Kd) increases the stability of the system, reducing overshoot and improving transient response but can lead to instability. The effects of these parameters during tuning are summarized in *Table 6-1*. An update to the LabVIEW VI was thus required with the inclusion of the PID sub-vi. The updated LabVIEW VI which includes the PID function is shown in *Figure 6-8*. In the VI, a switch is included which initiates the use of the PID controller

for the system to function as a closed loop system. A description of the components of the VI and their interrelationships in achieving the desired objectives is listed in Appendix F.

Table 6-1: Effects of PID controllers on a closed loop system [225]

Closed loop response	Rise Time	Overshoot	Settling time	Steady state error
Kp	Decrease	Increase	Small Change	Decrease
Ki	Decrease	Increase	Increase	Eliminate
Kd	Small change	Decrease	Decrease	Small change

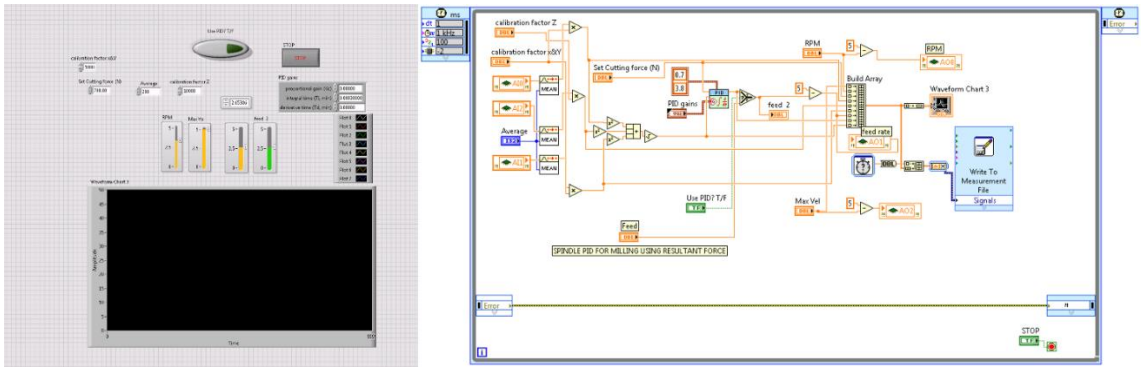


Figure 6-8: LabVIEW VI showing front panel and block diagram for adaptive control of the CNC. VI was developed using the scan engine interface

6.3.2 Transfer Function Models

Transfer function models are obtained as the relationship between the inputs and outputs of a system using a ratio of polynomials and represented in the Laplace domain with zero initial conditions. For a single input (x (t)), single output (y (t)) system, it is expressed as;

$$H(s) = \frac{Y(s)}{X(s)} = \frac{\sum_{i=0}^{m} b_i s^{m-i}}{\sum_{i=0}^{n} a s^{n-i}} = \frac{\mathcal{L}(Output)}{\mathcal{L}(input)} \qquad (6\text{-}4)$$

In obtaining the transfer function models for the various processes on the system, initial experimental trials were carried out to obtain the system response in relation to inputs, similar to the trials for the response threshold of feed rate and spindle speed. It was reasonable to carry out these trials with mild steel plates and less expensive tooling as this was to serve as a guide for the development strategy to use when attempting with difficult to machine materials. The procedure and results for obtaining the transfer functions for drilling and milling experiments for a mild steel plate is detailed as follows;

Experiments were carried out using a mild steel plate of 12 mm thickness. A four flute, 10 mm high speed steel (HSS) end mill was used in milling trials and a 6 mm high speed steel twist drill was used in drilling trials. Machining parameters for these trials are detailed in *Table 6-2*.

Table 6-2: Machining parameters for milling and drilling Mild steel in obtaining a system model

Operation	**Parameter**	**Value**
Face Milling	Spindle speed (rpm)	500
	Feed rate (mm/min)	50
	Depth of cut (mm)	1.0
Drilling	Spindle speed (rpm)	600
	Feed rate (mm/rev)	25

For these trials, a modification was made to the LabVIEW VI by substituting the feed input for a sine wave signal generator. The frequency of the sine wave was 0.009 Hz with an amplitude of 1.5 and maximum allowed offset was 3. This translated to the feed rate being varied between 45 % and 135 % of

the inputted feed rate value. Results from the milling trials are shown in *Figure 6-9*. Data obtained was thereafter exported to Matlab for further processing.

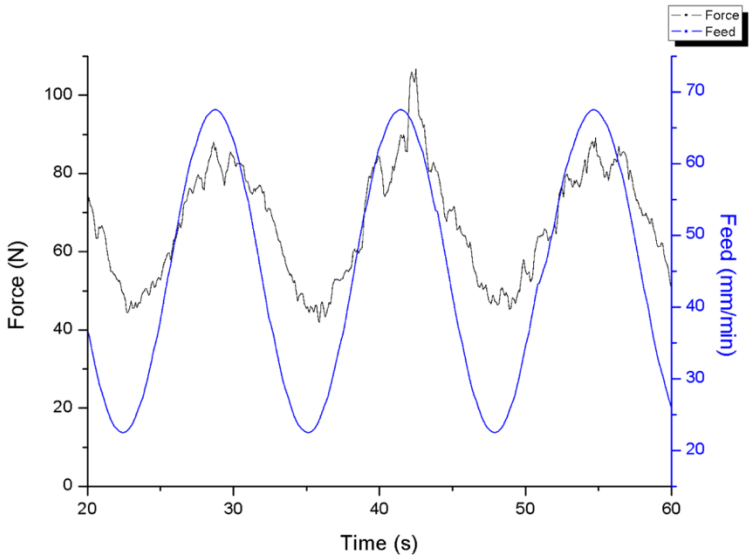


Figure 6-9: Plot showing feed and cutting force response in a milling pass on mild steel with a Sine wave signal generator input as feed rate. Low pass filter at 30 Hz was used in filtering data.

The Matlab system identification application was used in developing a system model for the specific machining operation. The application has capabilities for defining mathematical models of dynamic systems using measured input and output signals. In developing the model, measured time domain input and output data was pre-processed before estimation to remove noise especially in regions where the cutting tool was idle as there was no contact between tool cutting edge and workpiece. Estimated transfer function model obtained for the milling experiment is as follows;

$$TF_m = \frac{0.2295 \; - \; 0.2293 \, z^{-1}}{1 \; - \; 1.981 z^{-1} \; + \; 0.9811 z^{-2}} \qquad (6\text{-}5)$$

The transfer function model gives a fit to the estimation data of 73.34 %. It is assumed that machining noise due to vibrations influences the attainable model fit for the system. Errors due to these are capable of affecting the correctness of the developed model. Thus, the experiments and model development steps were repeated five times to ensure correctness and repeatability. PID values are then estimated for the developed model using the PID tuner application in Matlab. By using this method, guesswork in obtaining these values in the development of the control system was avoided and the time to attain closed loop control of the system was reduced. Through adjusting the response time to a minimum value which retains the robust behaviour and maintains system stability, suitable parameters were obtained for testing purposes.

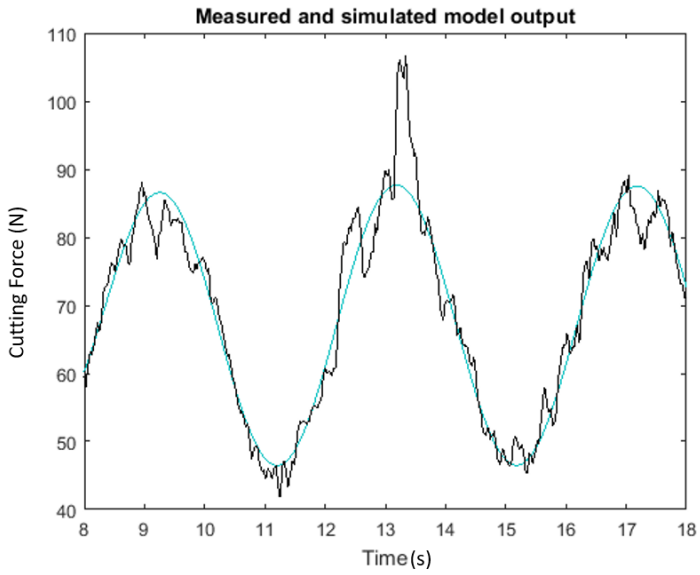


Figure 6-10: Measured and estimated model output. Estimated model matches the measured up to 73.34 %. Signal to noise ratio accounts for loss in fidelity.

Drilling trials were carried out using a similar strategy to the milling experiments i.e. with feed rate modulation with a sine wave generator. Results from this are shown in *Figure 6-11*. The plots also show a cyclic variation in cutting force magnitude with change in feed rate input. The results are further analysed using Matlab for modelling the input and output system response. It is observed there is a latency in cutting force response particularly during the reduction of the feed rate, this was accounted for when developing the system models.

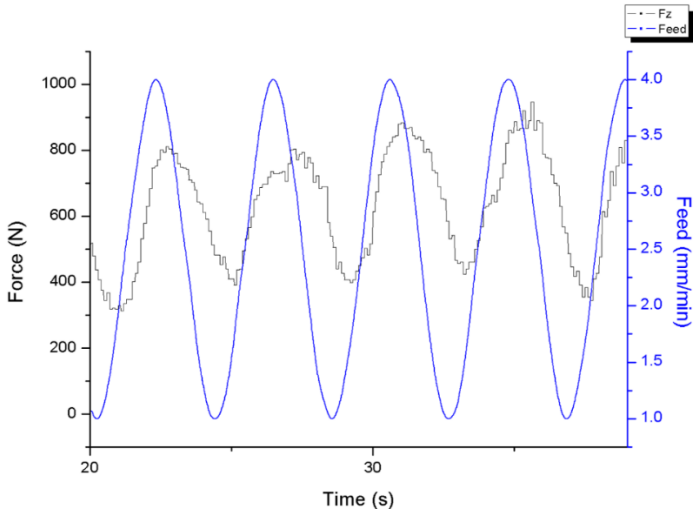


Figure 6-11: Plot showing feed and cutting force response in a drilling pass on mild steel with a Sine wave signal generator input as feed rate.

Using the Matlab system identification application after the conditioning of the obtained data to remove noise, the system transfer function and a model of the system was obtained. PID values were also deduced for the drilling operation on the control system. The estimated model gives an 84.43 % fit to

the measured data. Results obtained were used in updating the parameters of the controller.

$$TF_{d=}\frac{-34.13+34.14z^{-1}}{1-1.77z^{-1}+0.774z^{-2}} \quad (6\text{-}6)$$

Upon the definition of transfer functions of the system with both processes, preliminary machining of mild steel plates with adaptive control was attempted.

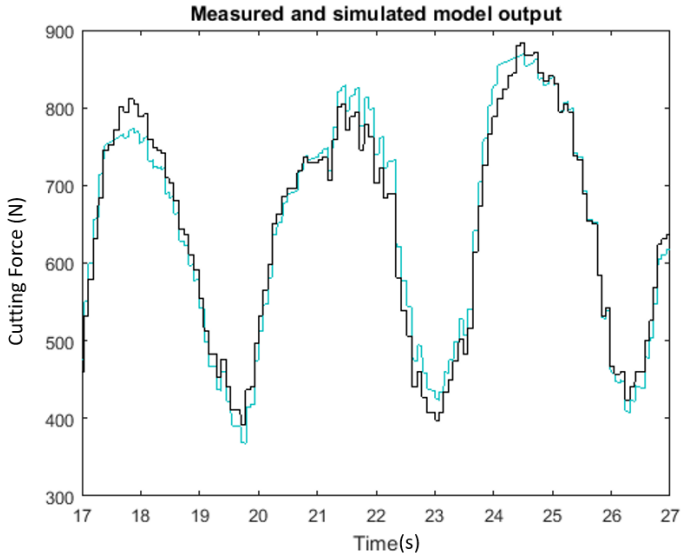


Figure 6-12: Measured and estimated model output for the drilling model. Model estimates 84.05 % fit to measured data

6.4 Results and Discussions- Machining trials with Adaptive control

A number of machining trials were carried out with the developed system using various adjustments of the parameters towards getting a responsive system whilst maintaining the robustness of the system to respond to changes in the set point. The PID tuner returns results from the identified system as the Proportional gain (Kp), Integral gain (Ki) and Derivative gain (Kd) values. However, the LabVIEW PID sub VI specifies input values for the controller as Proportional gain (Kc), Integral time (Ti) and Derivative time (Td) in minutes. Thus, there was a need to convert these gain values to time values. The following expressions were used for this conversion.

$$Kp = Kc \quad (6\text{-}7)$$

$$Ti = \frac{Kc}{Ki} \quad (6\text{-}8)$$

$$Td = \frac{Kd}{Kc} \quad (6\text{-}9)$$

The machining strategy in using the control system was for limiting the cutting forces to a threshold which ensures the prevailing feed rate of the system attempts to keep the forces within this set point. During the machining of anisotropic components, this would ensure the cutting force remains consistent irrespective of the prevailing conditions as the feed rate adjusts to

limit the effects of changing machining conditions. In preliminary trials with wrought materials, manual adjustment of the set point was useful in determining the robustness and responsiveness of the controller.

Face milling and drilling experiments were carried out to investigate the accuracy of the developed models and to demonstrate the use of the adaptive control system for machining components. The process flow for the determination of the PID parameters is shown in *Figure 6-13*.

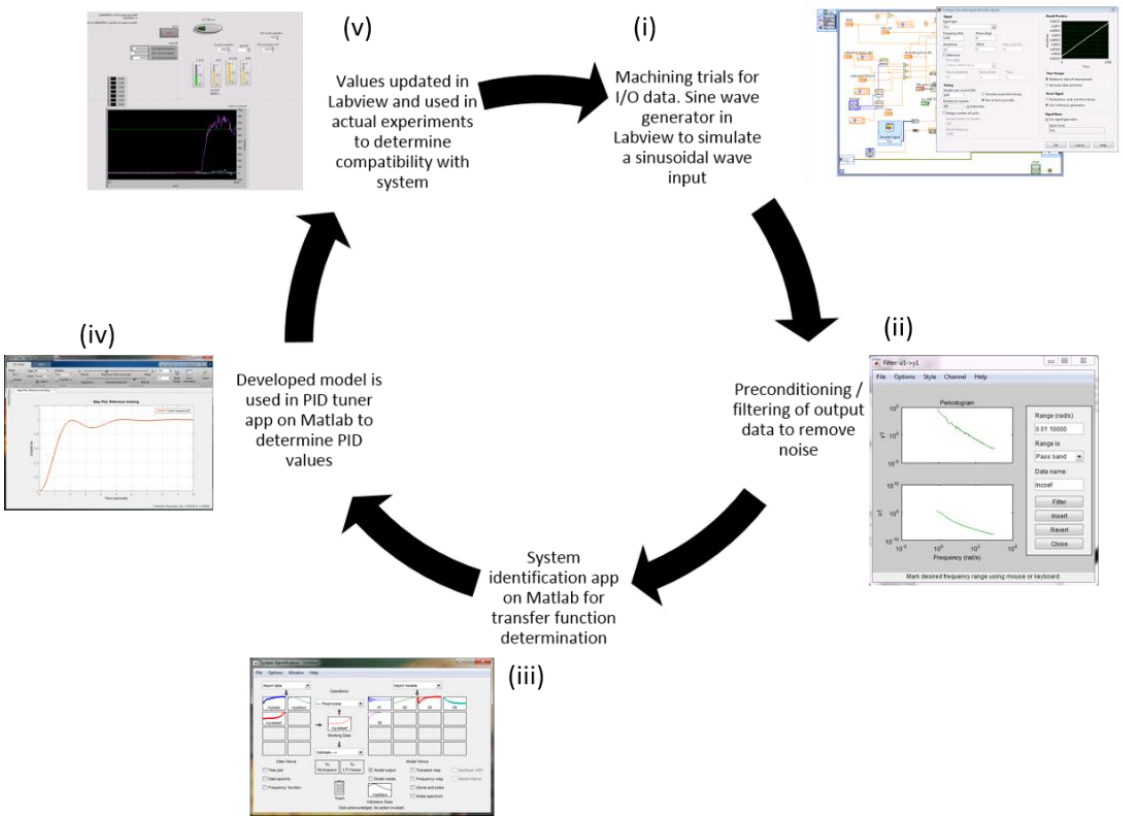


Figure 6-13: Procedure used in PID implementation

For all machining trials, the start point was machining the component without the use of adaptive control to determine the mean cutting force during

machining. Thereafter, the cutting force is limited to a percentage of the maximum cutting force obtained. The purpose of these trials was to test the robustness of the controller in limiting and increasing cutting forces by the regulation of feed rate. Results from the milling experiments are as shown in *Figure 6-14*.

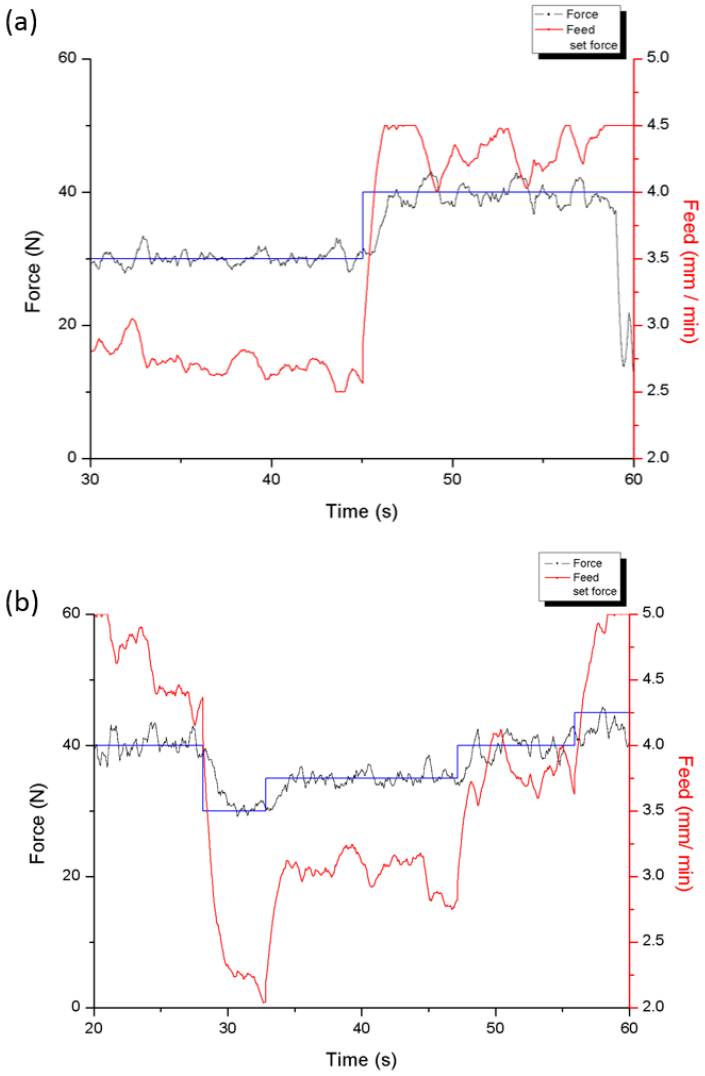


Figure 6-14: (a) Cutting force, set -point force during milling, controller input in adjusting feed rate to match set point values. Set point adjusted once during milling pass (b) Set point values adjusted multiple times during milling pass with controller effort to adjust feed to desired force value

In the machining pass represented in *Figure 6-14*(a), the feed rate control limits were from 2.5 to 4.5 on the Arduino scale which corresponds to a ratio on the percentage scale of 75 % to 135 % of the feed rate on the slider controls of the Tormach. Manual adjustment to assess the systems' response was done by increasing the cutting force set point during machining from 30 N to 40 N which leads to a corresponding increase in feed rate and cutting force observed. In *Figure 6-14* (b), the set point force is adjusted a number of times during machining - a reduction and multiple increases are effected. From the plots, there is a noticeable lag in cutting force response with the control parameters. The effects of this is discussed shortly.

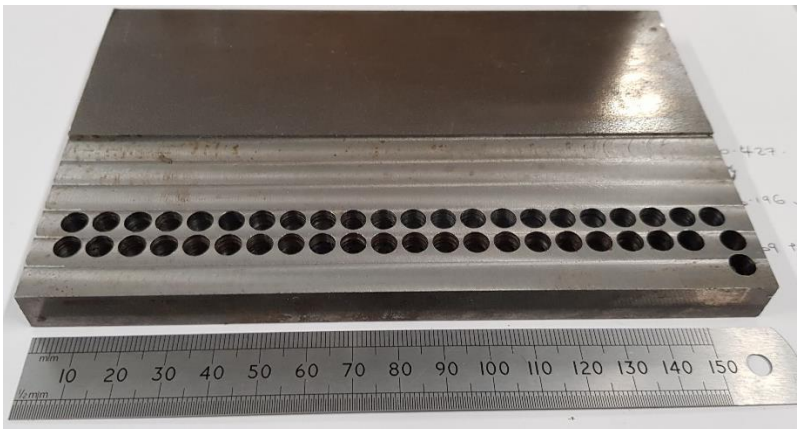


Figure 6-15: Mild steel component used for milling and drilling trials

In the drilling trials with adaptive control, *Figure 6-16*(b), an initial increase in cutting force was observed which was due to the initial contact and full engagement of the tool with the workpiece surface. Feed rate was maintained at 75 % to 135% of the input feed rate. It was necessary to keep the specified high and low output range of the PID controller system within a defined threshold to improve system response and stability. These limits also need to

be considered in selecting the set point force, as too low a set limit and the system would constantly attempt to slow down the process which results in the feed rate being constrained to the lowest value possible.

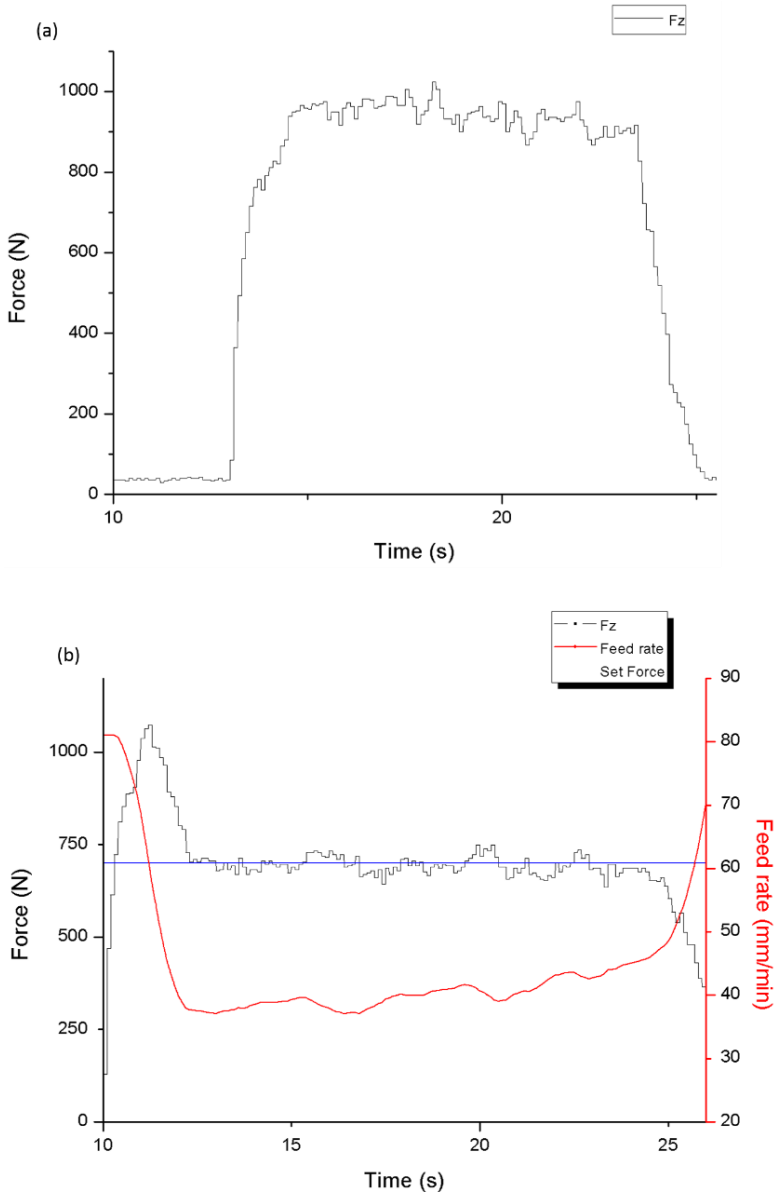


Figure 6-16: Cutting force and feed input plots for drilling mild steel component (a) without control system (d) with control system and set-point force was 700N

6.4.1 Machining DED Manufactured Components

The next phase in the development process for the adaptive controller was the testing of the controller for the machining of DED produced components. Transfer function models and PID values obtained from the machining of the mild steel were found to be inadequate in the machining of these components. Material interaction with tooling and the process parameters gave varying system response and as such, an alternate set of parameters was required to achieve adequate control of the system with various material and tooling combinations. As such, the process flow described previously for the system identification and PID tuning was adopted for DED *Ti6Al4V*.

Parameters used in the drilling and milling trials in the development process and the machining processes thereafter are shown in *Table 6-3*. Advisory parameters from the tool manufacturer were the basis for developing these parameters. However, there was a need for further machining experiments to determine optimum parameter sets for machining.

Table 6-3: Cutting parameters and cutting tools used in milling and drilling trials

Operation	***Tooling***	***Parameter***	***Value***
Face Milling	**JHP770100E2R050.0Z4A**	Spindle speed (rpm)	1560
		Feed rate (mm/min)	195
		Depth of cut (mm)	0.5
		Feed per tooth	0.032
Drilling	**SD203A- 6.0 -21-6R1-T**	Spindle speed (rpm)	500

Feed rate (mm/min)	50

A rectangular block of dimensions 80 mm x 40 mm was used for these experiments. The DED layer had a thickness of 10 mm and the substrate, a thickness of 5 mm. A schematic of the machining stages is shown in *Figure 6-17*. The component was milled and thereafter drilled and, in both instances the sine wave function in LabVIEW was used in generating signals which replicate varying feed rate input.

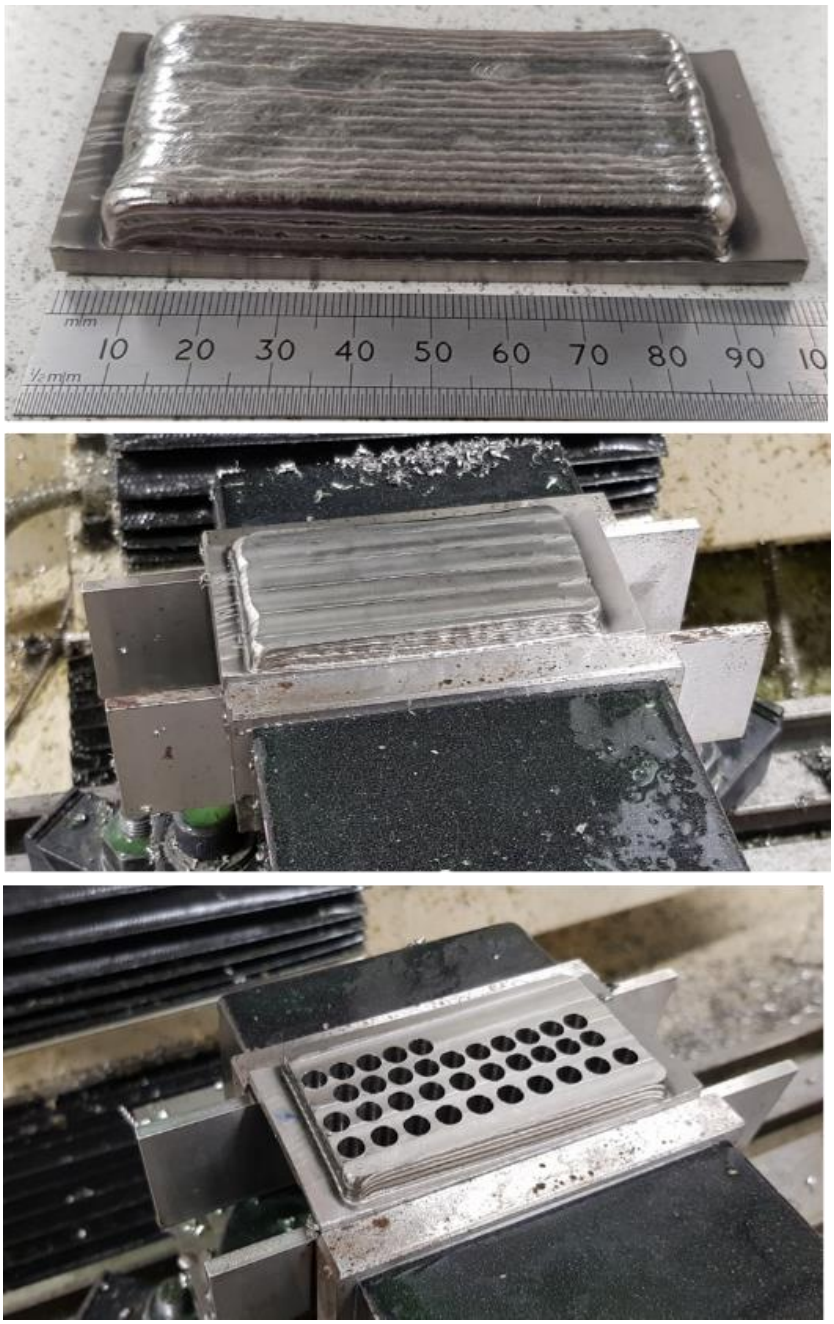


Figure 6-17: Steps in the machining of DED Ti6Al4V to determine the system transfer functions in milling and drilling trials

Plot from the milling experiments is show in *Figure 6-18*. There was a need to process the cutting force signal with a filter thereafter on the Matlab system identification application as the signal to noise was higher in these trials. This was due to the increased machine vibrations as a result of cutting a relatively

more difficult to machine material. The lag in response was also noted and this was factored into the development of the process models. Multiple iterations of the derived model was required to adequately define the system.

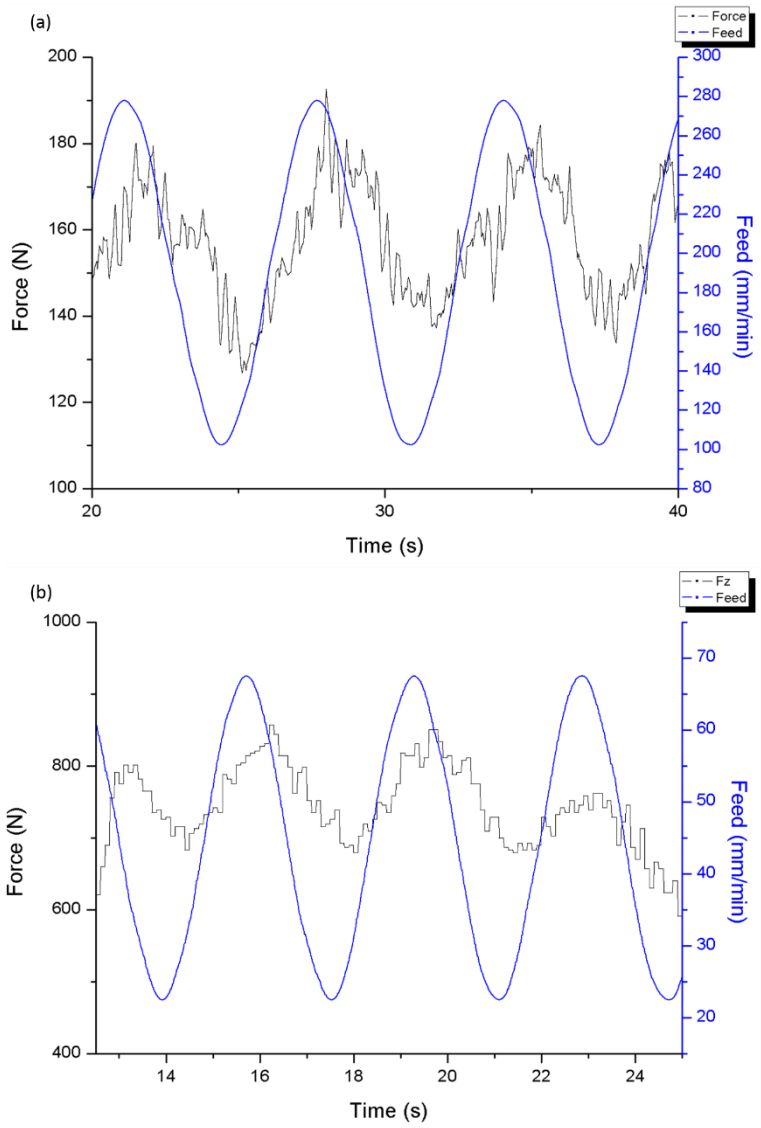


Figure 6-18: Plot of Cutting Force, Feed rate and Time from the (a) milling (b) Drilling experiments for determination of transfer function models.

The models gave a fit to estimation data of 78.98 % and 71.47 % for milling and drilling experiments respectively. These models were thereafter exported

to the PID tuner application for the estimation of the corresponding PID values for use in machining trials. The expressions listed below show the transfer functions obtained for the milling and drilling processes with additively manufactured Ti6Al4V.

$$TF_{milling} = \frac{-31.21 + 62.43z^{-1} - 31.22z^{-2}}{1 - 1.872z^{-1} + 0.7647z^{-2} + 1.1071z^{-3}} \quad (6\text{-}10)$$

$$TF_{drilling} = \frac{8.155 - 8.098\, z^{-1}}{1 - 1.719\, z^{-1} + 0.7189\, z^{-2}} \quad (6\text{-}11)$$

6.4.2 Drilling of DED Ti6Al4V

In the drilling of Ti6Al4V components, a rectangular block of a DED component deposited on a Ti6Al4V wrought substrate was used. The components' top surface was milled before drilling to remove the undulating surface layers. Preliminary machining trials showed a deviation in controller response between the AM region and the wrought material region. Results from the drilling trials are shown in *Figure 6-19*.

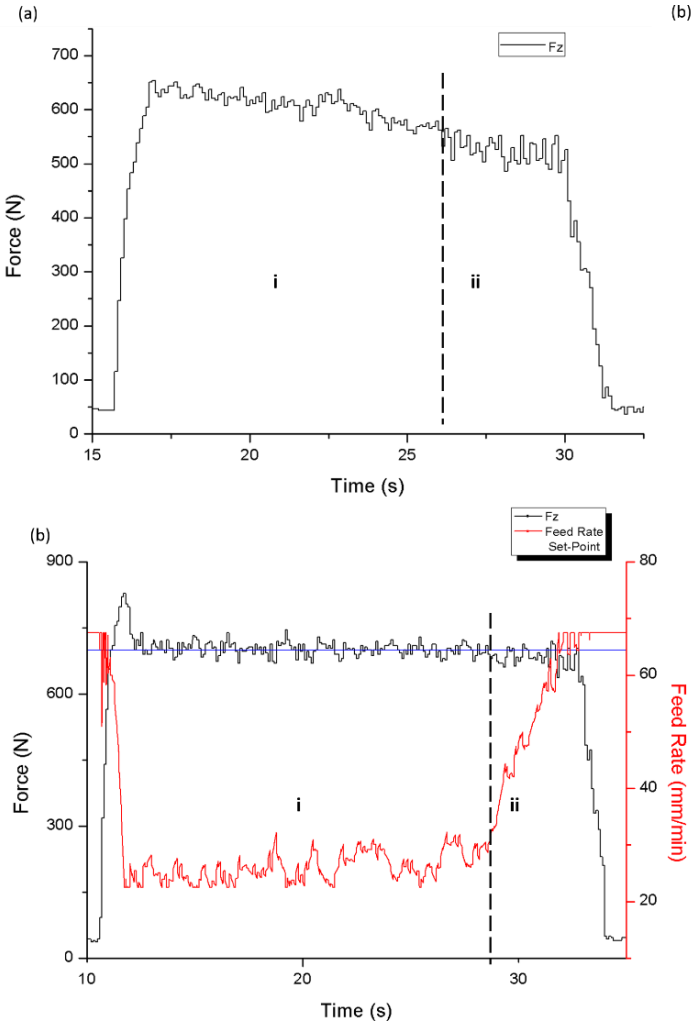


Figure 6-19: Cutting force plot for drilling component with wrought and DED region (a) without control (b) Force constrained to 700N. Forces shown are in the drilling direction (z).

Region (i) in *Figure 6-19* shows the DED region and (ii) is the wrought material region. Drilling progresses from the DED region to the base substrate and a change in material properties between both regions leads to a decrease in cutting forces. In using the control system, and limiting the cutting forces to 700N, the difference in cutting forces between both regions becomes less discernible with improvements in response of the system. Analysis of the resulting components post machining was not carried out at this stage as

these trials were for preliminary appraisal and development of the control system.

6.4.3 Milling of DED Ti6Al4V

Face milling of the DED Ti6Al4V was carried out. The initial machining pass was for the removal of the outermost layer. In the design of the control system parameters, input and output data from the machining of the bulk region was used as the outermost layer led to workpiece run out which in turn resulted in an unstable process making this layer potentially challenging to machine with adaptive control. Preliminary cutting force data obtained during machining the outermost region with the developed controller and without the controller is shown in *Figure 6-20*.

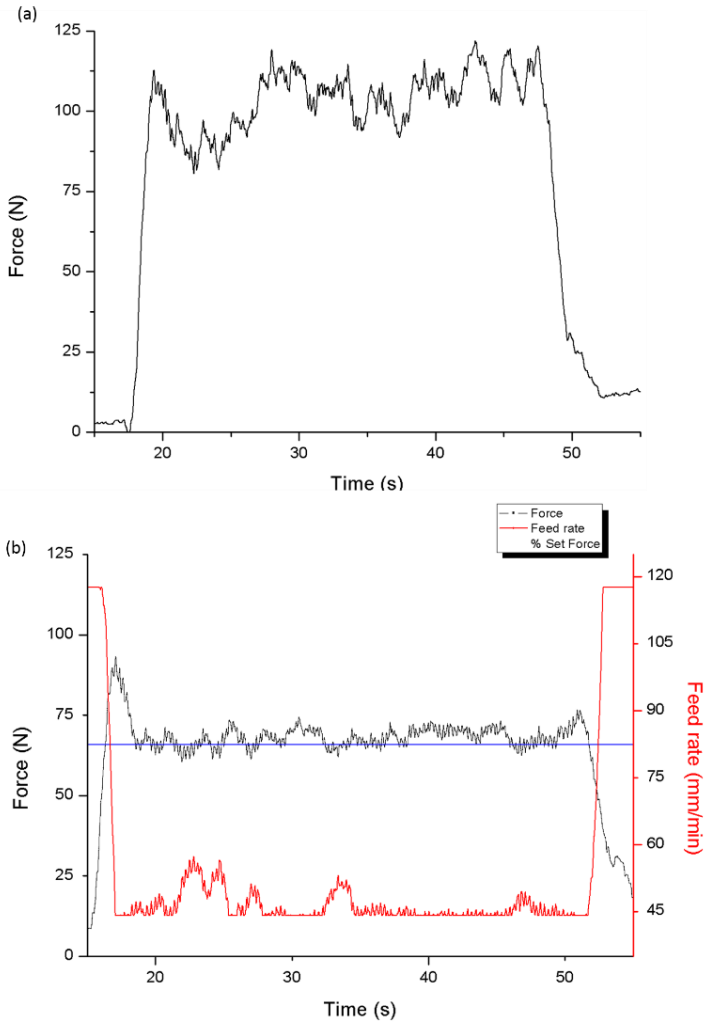


Figure 6-20: Plots from Milling trials for DED Ti6Al4V with (a) Milling without adaptive control (b) Milling with Adaptive control, set point = 65 N.

The obtained PID values for milling were also found to be effective in machining wrought Ti6Al4V with adaptive control. In the milling trials, the component used had a variation in shape which would lead to a change in the depth of cut as machining proceeded. The reasoning behind this trial was to investigate the effectiveness of the controller in responding to changes in cutting geometry.

6.5 Conclusions

The development of an adaptive control system for machining components on an open architecture CNC has been presented in this chapter with preliminary results obtained for milling and drilling DED Ti6Al4V components. The relationships between the feed rate, spindle speed and cutting force has been shown to impact the cutting force and this is the basis for developing the control system. A step wise approach for obtaining models and the required PID values for the closed loop systems using the Matlab system identification toolkit and the system modelling toolbox has been discussed in this chapter. The methodology provides an effective strategy for the development of the control system. By limiting cutting forces to a predetermined value, the effects of variations in microstructure during machining on both the machined part and the cutting tool can be minimised. However, limitations due to machining noise, the microcontroller, rigidity of the machine tool and the response time of the machine tool leads to observed lag in response of the controller. These factors are expected to affect performance of the controller in response to microstructural changes. Multiple iterations of the system identification model gave improved process models, the lag was however not completely avoided.

The use of the developed system in machining these components and the implications on surface integrity would be further investigated and reported in the subsequent chapter.

7.0 Adaptive Machining of DED produced Ti6Al4V

This chapter discusses the use of the developed adaptive control system described in Chapter 6.0. Additively manufactured components have been shown to possess microstructures different from wrought forms of materials and as a consequence, the machining of these materials is also different from the machining of wrought forms. The use of an adaptive control system for addressing variation in microstructures during post process machining is proposed and demonstrated in this chapter.

Towards this end, the developed adaptive control system is used in milling and drilling trials for machining components from a DED process. Surface roughness and residual stress analysis before and after machining and the characteristic cutting forces are presented here. Microstructure of the deposited material and the subsurface effects at the machined region due to the action of the cutting edge is also analysed.

Milling trials are investigated from the standpoint of the use of adaptive machining in the removal of the outermost undulating layer of DED produced Ti6Al4V and in the machining of bulk 'interior' regions after the preliminary machining step. Drilling experiments were for investigating the effect of the machining process on surface condition with and without adaptive machining. The effects of variation in cutting forces during drilling through the different

material systems comprising of wrought and DED produced regions is also reported. The existence and origin of periodicities is investigated by correlating these variations in cutting forces during machining to the discontinuities in component microstructure.

7.1 Milling

Milling of the as-deposited surface to remove the undulating outermost region was a necessary start point due to the as-deposited surface condition. Components produced using the DED set up and parameters described in section 3.2.1 are used for the milling trials. As built surface condition of a sample used in machining is shown in *Figure 7-1*.

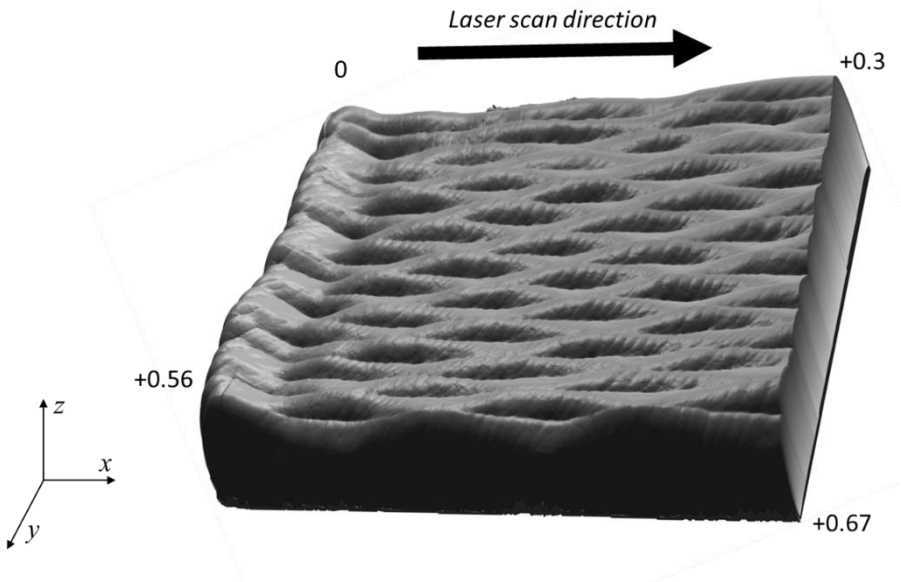


*Figure 7-1: Optical profilometer scan showing surface condition of the DED component before machining. As built surface roughness values: Ra = 5.27 µm, Rz = 8.35 µm. Difference in height in regions highlighted with top left (0) being the start point of deposition and milling. Values shown are relative to the start point. Component shown is a 30 mm * 30 mm section.*

Post deposition milling was carried out with the parameters detailed in *Table 7-1*. The machining strategy was for the removal of the outermost layer and thereafter the machining of the bulk region. During the deposition process, the successive addition of layers leads to evolving thermal gradients within the part and consequently causes a variation in component geometry as component height varies with the build progression. The effect of this is shown in *Figure 7-1* wherein the difference in height along and across the built component is highlighted. The localised heating and rapid thermal input during material deposition also leads to distortion in the substrate as a result of plastic deformation during the cooling process and the subsequent shrinkage of the deposited component. This leads to 'warping' of the base plate, causing angular distortion. This variation in component shape, coupled with component anisotropicity adversely affects the stability of the milling process. The effects of this in both the substrate and on the milling process is shown in Figure 7-2.

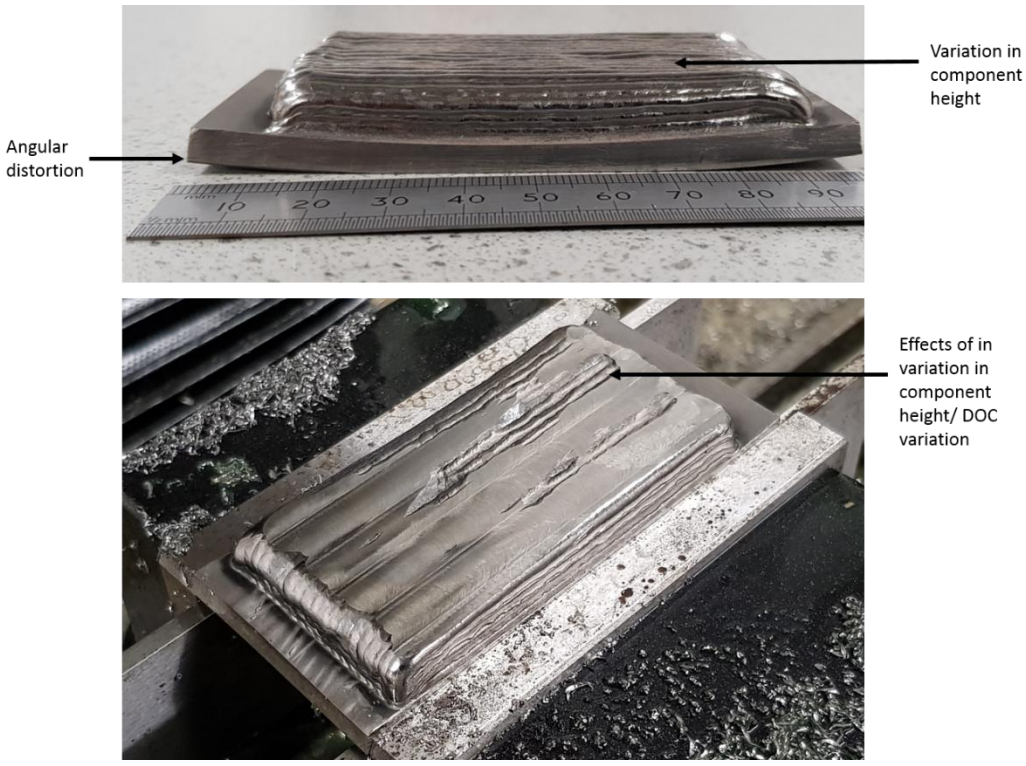


Figure 7-2: Angular Distortion and variation in component build height and effects during face milling

Wu et al. [13] commented on the top layers of a multi-layer laser deposited build of *Ti6Al4V* possessing a basket weave microstructure consisting of comparatively larger α and β laths to those in the bottom region due to a variation in the cooling rate. Columnar grains growing epitaxially along the layer boundaries also leads to a variation in the macrostructure at regions where they occur. These columnar growth are related to the laser deposition process conditions and directional cooling. *Figure 7-3* is a scan of a deposited component with a partially milled top surface imaged using SRAS which shows the variation in microstructural texture along the build cross section. The presence of the columnar growth and the dissimilarity in texture from the substrate to the deposited regions can be observed. Also, regions of remelting

during the addition of subsequent layers and overlaps can be identified to possess a varying texture. Thus, response to machining conditions between these regions are expected to vary and the effects are discussed subsequently.

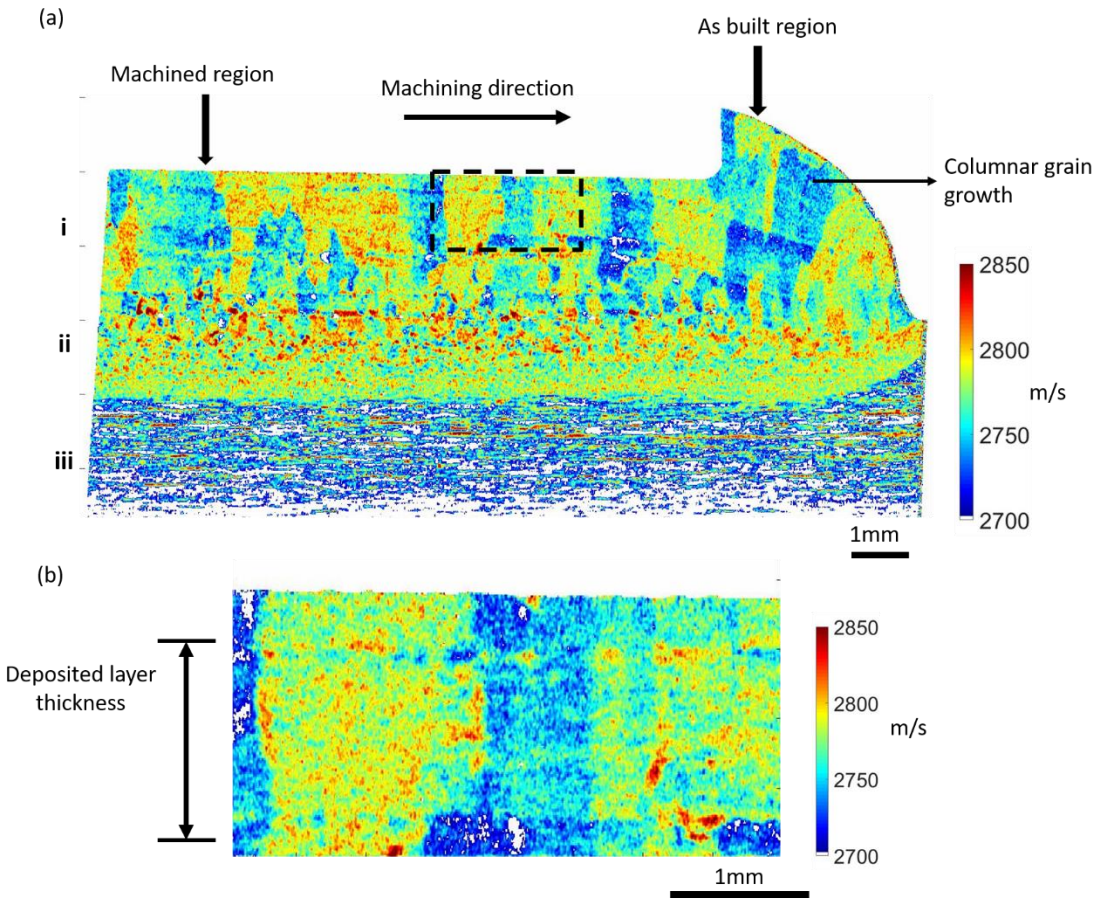


Figure 7-3: SRAS scanned image (a) variation in component macrostructure and differences in component grain size (i) DED region (ii) Substrate heat affected / fusion zone (iii) Substrate region (b) Magnified view of highlighted region in 'a' showing regions of grain coarsening as a result of epitaxial columnar grain growth during cooling and also layer 'banding' due to remelting.

In the milling of the outermost surface, the undulating surface condition leads to discontinuities in cutting tool-workpiece engagement. As a result of this, there is a variation in depth of cut when machining the component as material removed varies with component geometry, leading to a change in chip load on the cutting tool. This variation also leads to an expected difference in

cutting forces with adverse effects on uniformity in surface finish and subsurface condition along the component.

Table 7-1: Parameters used for Milling DED Ti6Al4V components

Operation	***Parameter***	***Value***
Face Milling	Spindle speed (rpm)	780
	Feed rate (mm/min)	97.5
	Depth of cut (mm)	0.5

In machining this region, the depth of cut was determined relative to the lowest height on the workpiece surface relative to the tool cutting tooth and this ensured the initial machining pass removed the undulating surface with minimal workpiece run out. The parameters adopted for the milling trials were less than recommended by the tool manufacturer for the cutting tools, due to limitations with the available maximum spindle and feed rate of the machine tool. However, the feed per tooth ratio was kept consistent within the suggested range of 0.020 – 0.064 mm/tooth by maintaining the ratio of feed rate to spindle speed for machining trials. Thus, the feed rate value in *Table 7-1* corresponds to 100 % on the Tormach slider scale. Therefore, for the milling trials with the adaptive controller, the upper and lower limits were set at 61 % (59.5 mm/min) to 120 % (117 mm/min) of the selected feed rate which keeps the feed per tooth within the recommended parameter range for the cutting tool.

Cutting forces measured during the milling of the top surface using the developed adaptive control system is shown in *Figure 7-4*. The variation in feed rate input by the controller towards maintaining the set point cutting

force is due to the variation in depth of cut during machining from point 'a' and 'b' as depicted in the figure. A reduction in feed rate leads to a decrease in chip load and a consequent reduction in the cutting forces. Based on cutting forces from preliminary milling trials without the use of adaptive control at similar machining parameters discussed in Section 6.4.3, the set point cutting force was limited to 40 N during the machining of these surfaces. The selection of this set point force value was for the constraining of cutting force to 80 % of the maximum cutting force value. For this component, two machining passes were required to remove the undulating layer and achieve steady state machining (this corresponds to a total depth of cut of 1 mm into the component).

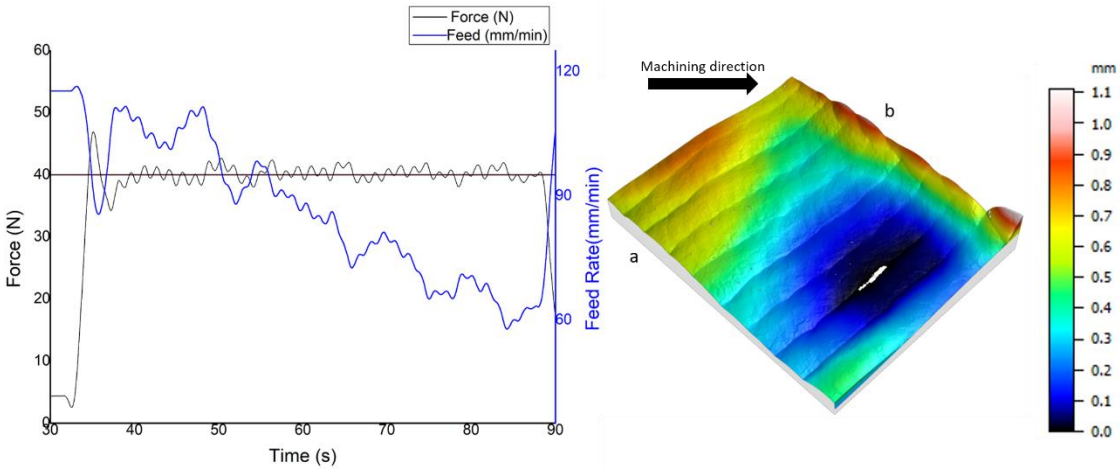


Figure 7-4: Cutting force in milling outermost layer with the control system. Signals filtered with 25 Hz low pass filter (b) Scan taken with the Alicona of the component with difference in height between points 'a' and 'b' which causes a variation in depth of cut.

Machining of the bulk region proceeded after the initial machining passes with the attainment of steady state machining. *Figure 7-5* shows a cutting force plot for a machining pass after the removal of the outermost layer and the

corresponding surface profile from the bulk region. The controller effort at adjusting feed rate to constrain the prevailing cutting force is also shown in the plot. Forces recorded during the machining of the bulk region were higher than those observed when machining the outermost layer. Mean cutting force during the machining of this region without the use of the AC system was found to be 140 N, which represents an increase of up to 300 % from the machining of the outermost layer. This is due to the absence of workpiece run out during the machining of this layer, the influence of strain hardening and a variation in microstructure between these regions.

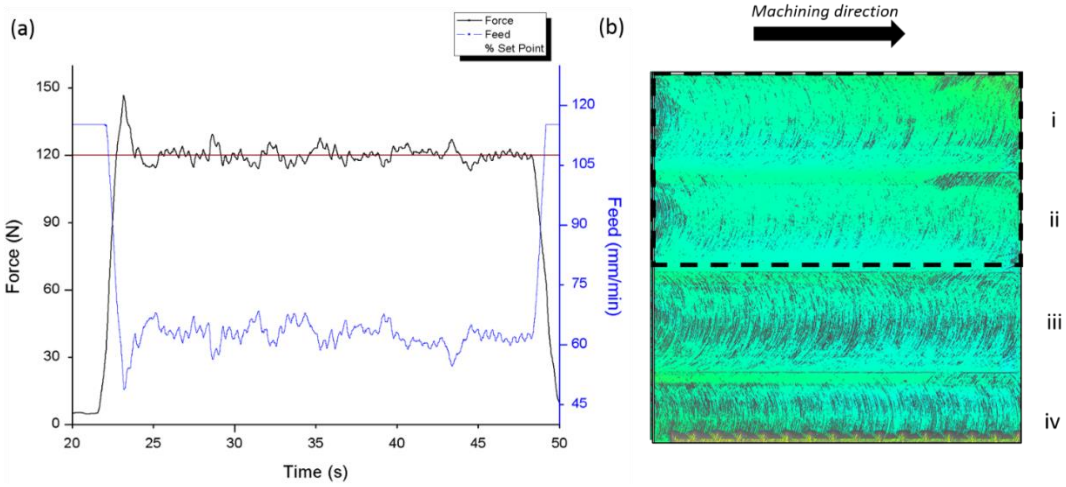


Figure 7-5: (a) Cutting force plot from milling of the bulk region of DED Ti6Al4V with adaptive control (b) Result from surface profilometer scan showing surface condition of regions machined with AC (i and ii) and without the AC system (iii & iv). A 30 mm x 30 mm section from the build was used in the experiment shown. The grooving which is evident in passes iii and iv is consistent with a higher level of chatter.

In the machining of the 'bulk' region, the set point cutting force is constrained to 120 N which is equivalent to 80 % of the mean cutting force observed without the use of the control system. The highlighted region in *Figure 7-5* (b) indicates two machining passes in the region machined with adaptive control

(regions i & ii). The machining passes labelled (iii & iv) correspond to regions machined without the use of the developed system. From the figure, the surface topography of the regions machined with the control system show reduced occurrence of machining chatter marks. Machine tool chatter is due to vibration of the structural and process dynamics in a machining system. Self-excited vibrations due to the interaction of the tool and the microstructure heterogeneity of the workpiece leads to variation in chip load and hence measured forces during the milling process. Due to the nature of the workpiece, intermittent force loading on the tool causes vibrations along the machining direction. These vibrations lead to the appearance of an undulating tool path on the work piece surface. The undulating tool path subsequently influences chip loading during the next machining pass as the tool passes over the surface causing the so called *regenerative effect* [166]. By eliminating the incessant variation in cutting forces, this annuls the subsequent generation of machining vibration and thus reduces the resulting influence at the cutting region. This is in agreement with the conclusions of Landers et al. [168] where feed rate adjustments were demonstrated to limit the formation of chatter using experimental and analytical techniques.

Surface roughness analysis of these regions show an improvement with the use of adaptive control. Results from surface roughness analysis using both machining strategies is shown in *Figure 7-6*. From the results, average improvement in surface roughness (Ra) by up to 70 % (0.2 µm ± 0.023) is observed when comparing the regions machined with both strategies. The

avoidance of the formation of chatter coupled with the comparatively less feed rate in using the adaptive control system was fundamental in attainment of the improved surface roughness observed. The values for surface roughness are taken at various regions within the component to determine the influence of adjusting feed rate with tool progression on the component.

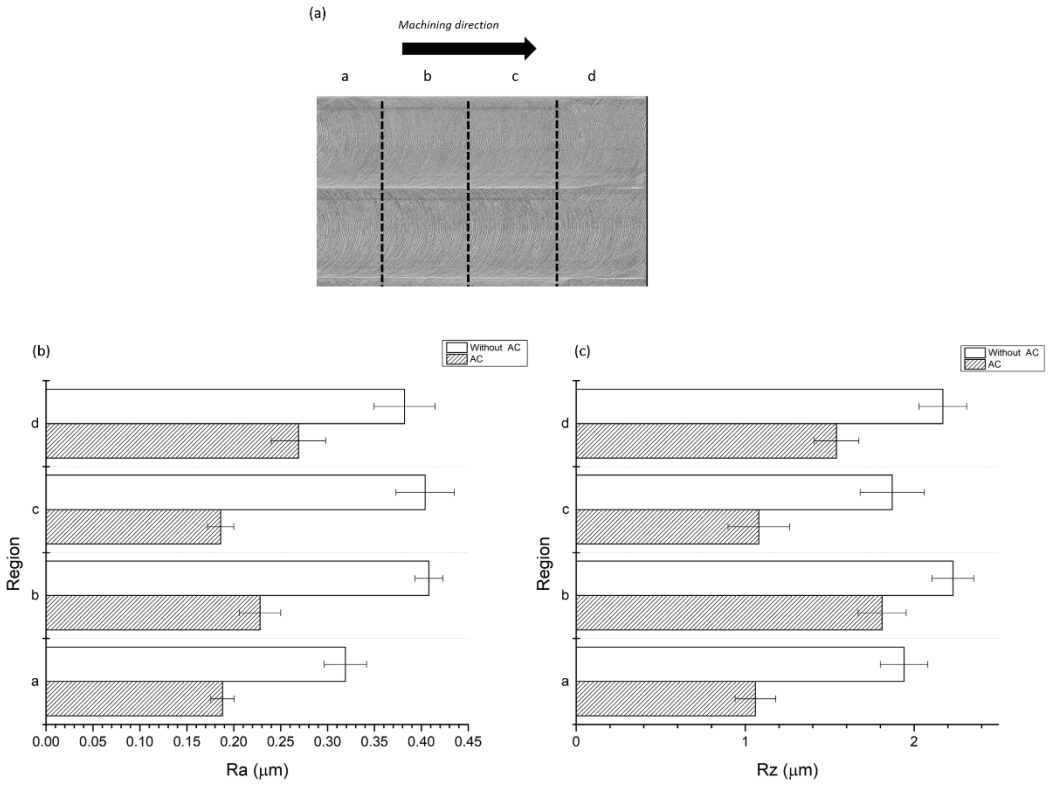


Figure 7-6: Surface roughness in regions machined with and without adaptive control (a) Component divided into regions with tool progression (b) Ra in the identified regions for both machining strategies (c) Rz in the regions for both machining strategies

7.1.1 Subsurface Deformation

The influence of machining strategy adopted on the components' subsurface condition was analysed. *Figure 7-7* shows the variation in subsurface deformation depth at the machined region for both machining conditions. Subsurface beta phase deformation at the machined region is observed in

both instances. In the components machined without the AC system, the deformation depth was a maximum of 8.18 µm and the region machined with AC had a maximum deformation depth of 3.62 µm from the machined surface. – An improvement of up to 55 % (4.65µm) from the values without adaptive control. At low feed rates with the tendency for the occurrence of machining dwell, Titanium alloys are prone to work hardening which leads to damage through smearing and galling of the workpiece. Towards avoiding the effects of dwell, the control limits specified in the controller were set within feed rate thresholds which avoid tool dwell. Also, it was important to attain response times in the controller which avoid tool stall during feed rate adjustment in machining. The results obtained are in agreement with those reported previously, relating to the influence of process parameters on subsurface deformation [226]. An increase in feed rate leads to increased cutting forces and increase in subsurface deformation depth. Here, controlled adjustment of feed rates towards maintaining cutting forces in the AC machined system leads to a reduction in subsurface deformation depth observed.

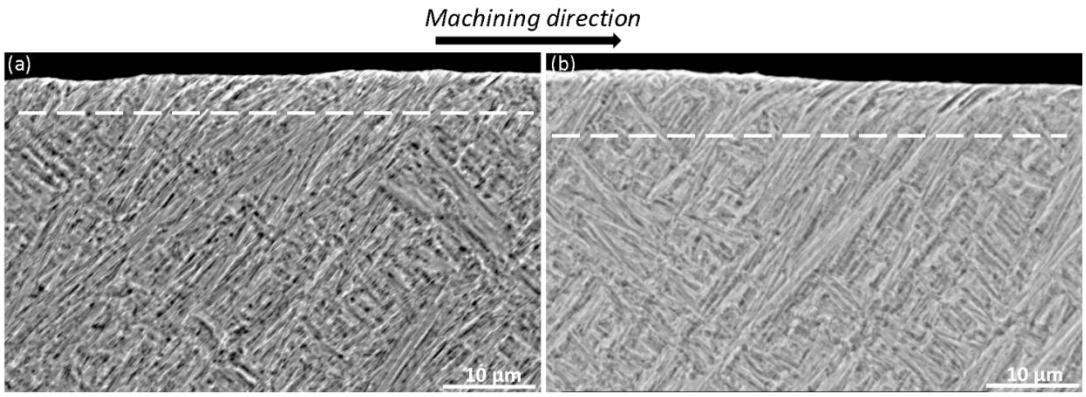


Figure 7-7: Subsurface deformation in machined regions (a) With adaptive control (b) Without adaptive control. Maximum depth observed is taken as the representative value. Images taken with SEM in SE mode

7.1.2 Residual Stress

Residual stress alterations as a result of machining with the use of the adaptive control system was investigated. Results obtained from the measurements before and after the machining process are shown in *Figure 7-8*. From the plots, the regions machined without the AC system show lower compressive residual stress compared to the AC machined region. However, in both instances, residual stress reduces in the cutting direction as machining proceeds.

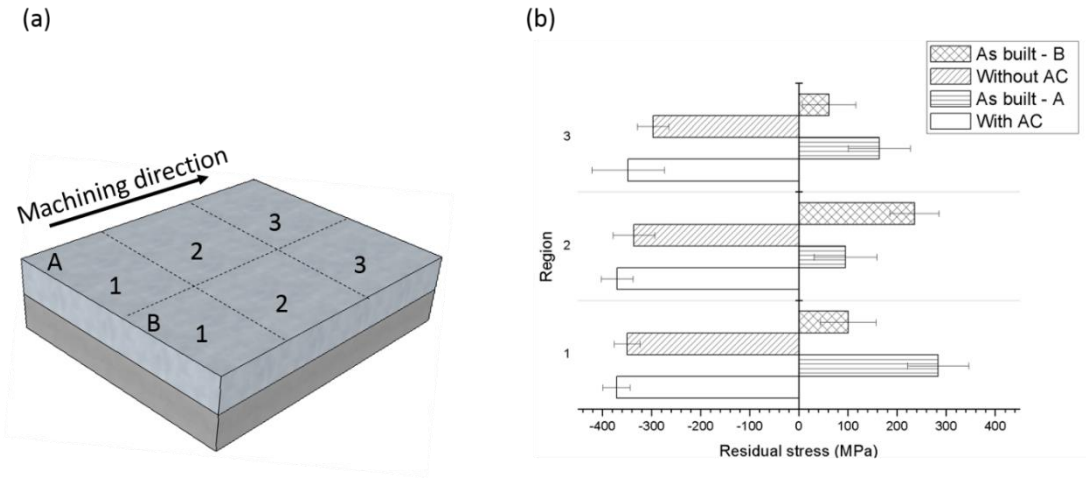


Figure 7-8: (a) Component schematic showing regions of residual stress measurements. 'A' region was machined with AC system 'B' is region machined without the AC system. Measured stress values for the regions also shown.

Variation in magnitude of residual stress between both regions is due to the increased thermo-mechanical action of the tool at the machined surface in the component machined without AC. Though the measured stress values are statistically analogous, the variations along all corresponding measured points correlate to a relationship between the residual stress state and the

associated cutting forces during machining. Post machining residual stress state is influenced by a combination of the thermal and mechanical action of the cutting tool at the workpiece surface. The interrelationship between the machining parameters thus determines the residual stress state of the component. In this case, the components machined without the AC system are machined with higher feed rates and subsequently higher machining forces leading to increased mechanical disruption of the surface, which leads to these regions exhibiting comparatively lower compressive stress values. Similar results have been reported by [226, 227], which corroborate findings of compressive residual stress reducing with a decrease in feed rate at low cutting speeds.

The measured surface residual stress values before machining confirms the existence of tensile residual stresses which evolve to being predominantly compressive after machining. Thus, it is postulated the existence of subsurface compressive regions coupled with the machining process which induces compressive stresses leads to the resultant residual stress condition observed.

7.2 Drilling

Prior to the drilling trials, milling of the outermost layer of the 'as-built' DED component was undertaken to ensure drilled depth was identical in all cases and to avoid damage to the tool cutting edge due to the undulating surface condition of the samples. Following on with the strategy from the milling

trials, a comparison between both machining strategies was carried out. In the drilling trials, the aim was to investigate the effects of changes in cutting conditions due to a variation in microstructure of the DED components on cutting forces and drilled hole surface quality. For these experiments, a total of 20 through holes each were drilled using both machining strategies towards determining the influence of increased tool usage on the surface quality of the holes and the influence of feed rate modulation. The machining trials were also designed to give substantial information on the gradation of cutting forces when drilling through a component consisting of a DED produced region and a wrought region which is a consequence of their varying machinability.

Components used in drilling trials were deposited to a total layer height of 10 mm which corresponds to 4 deposited layers. Preliminary milling of the components' surface resulted in a portion of the topmost layer – 1.2 mm removed. A schematic of the process from the as built state to the hole drilling is shown in *Figure 7-9*.

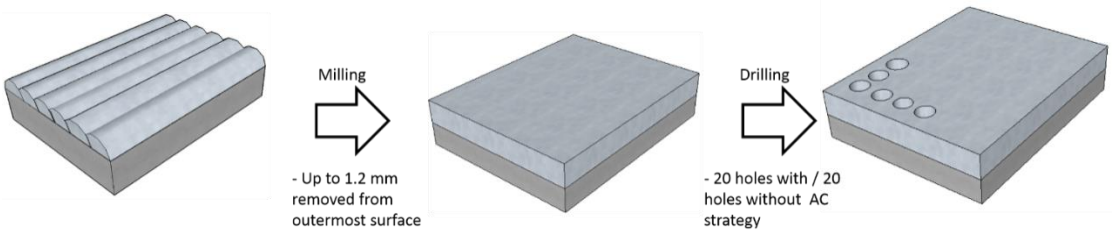


Figure 7-9: Schematic of process from as built surface condition to drilling of component (a) as built surface (b) Milled surface with up to 1.2 mm of material removed (c) Drilling process

Parameters used in machining is detailed in Table 7-2. For these trials, solid carbide cutting tools 'SD203A- 6.0 -21-6R1-T' were used for drilling.

Table 7-2: Parameters used for Drilling DED Ti6Al4V components

Operation	***Parameter***	***Value***
Drilling	Spindle speed (rpm)	500
	Feed rate (mm/min)	50

Similar to the milling trails, the manufacturers' recommended machining parameters for the tools exceed the CNC capabilities and as such the parameters were reduced accordingly with similar ratios to ensure the feed per tooth was kept within the recommended values. For the adaptive machining trials, minimum and the maximum control limits on the slider scale were set at 75 % and 135 % of the selected feed rate value. Effectively, the feed rate boundary was thus between 37.5 mm/min – 67.5 mm/min which keeps the tool within the manufacturers recommended feed per tooth ratios. For the drilling trials with the adaptive control system, the cutting force was maintained at 600 N- this represents approximately 90 % of the maximum cutting force obtained in machining without adaptive control in Chapter 6. This value was selected to allow for adequate control of the system whilst allowing for forward motion of the spindle without tool dwell which is detrimental to surface integrity in machining Ti alloys. *Figure 7-10* shows a number of corresponding graphs at intervals for both machining strategies – with and without the use of the developed control system (1st, 10th, 15th and 20th). In machining trials without the use of the control system, mean cutting forces were found to progressively increase with increase in number of holes drilled. These forces were found to increase by up to 5 % between the 1st and the 20th hole in the DED region.

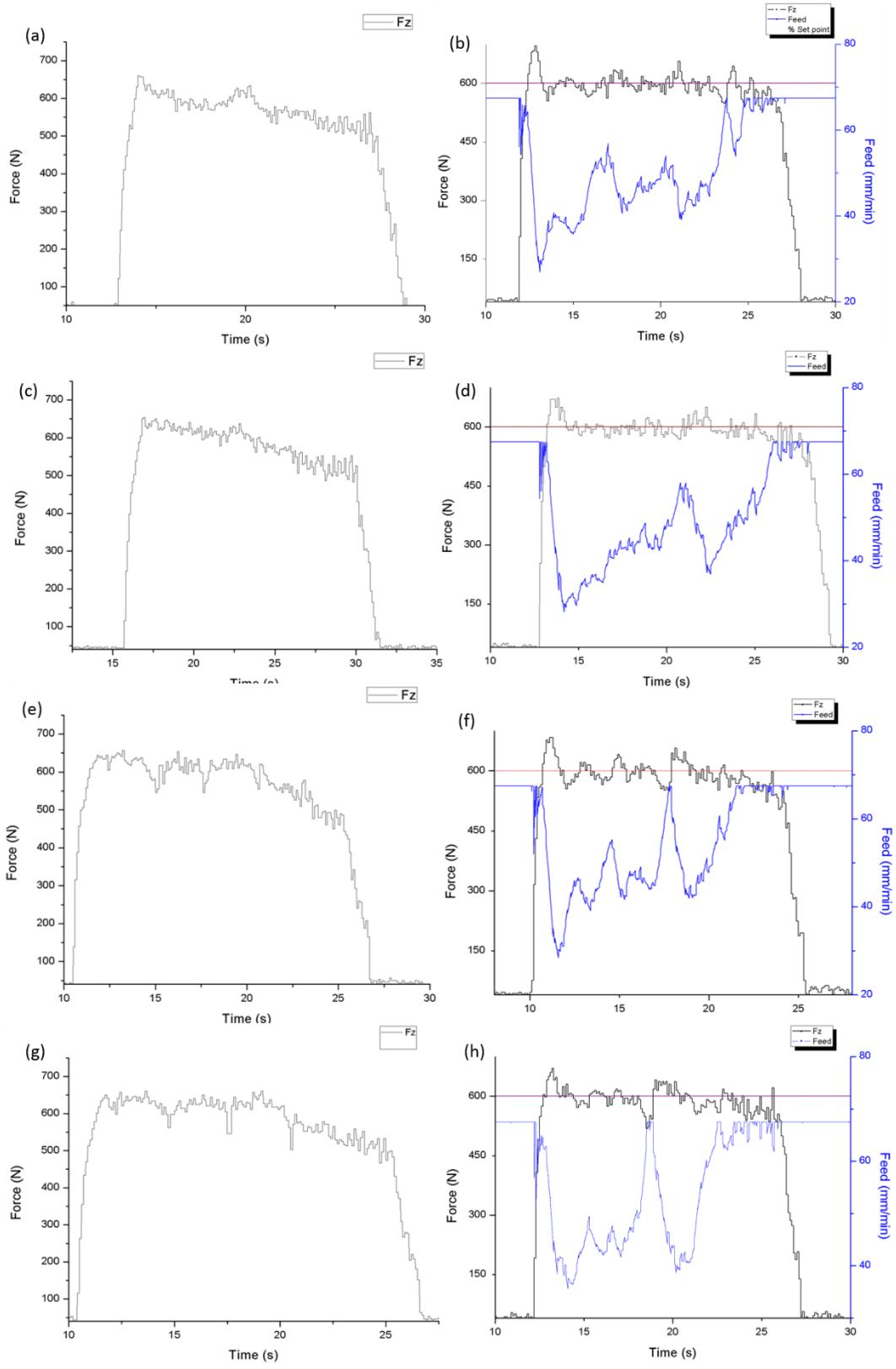


Figure 7-10: Cutting force plots at intervals with and without adaptive control system. (a) 1st pass without AC (b) 1st pass with AC (c) 10th pass without AC (d) 10th pass with AC (e) 15th pass ewithout AC (f) 15th pass without AC (g) 20th pass without AC (h) 20th pass with AC

From the plots, changes in cutting force due to the cutting tool edge progressing beyond the DED surface into the wrought substrate was observed with both machining strategies. Though both material regions are similar in composition, a difference in processing routes and a subsequent difference in material properties between the regions causes a variation in machinability which influences the observed cutting forces.

In the components machined with adaptive control, the controller effort instantaneously increases the feed rate as the tool cutting edge proceeds into the wrought region which in turn increases the cutting forces. Considering the plots in *Figure 7-10*, average difference in tool engagement period between both strategies is 0.5 secs per hole. Thus, in effect, the use of the adaptive control system for drilling these types of components with differing material properties within a component can lead to a reduction in machining time without adversely affecting surface quality, particularly when a large number of holes is to be drilled.

During the machining trials, after drilling 15 holes, periodic variation in cutting force became evident in the components drilled without the control system. This effect can be observed in *Figure 7-10* (e) and (g). Cutting force is found to reduce by up to 15 % (100 N) within these regions. Towards providing clarity on the underlying cause of this variation, the cutting force was plotted with the distance drilled into the material. *Figure* 7-11 shows two of such plots. The average thickness of the regions with the reduction in cutting force is found

to be 400 ± 15 µm and the regions of increase in force was approximately 1.6 mm thick.

In the components machined with AC, the controller effort towards regulating the cutting force is also observed to show a variation synonymous with changing machining conditions which is also indicative of variations in the cutting tool- material interaction. The effects of this variation cannot be observed in the cutting forces as the feed rate control adjusts to limit these disruptions.

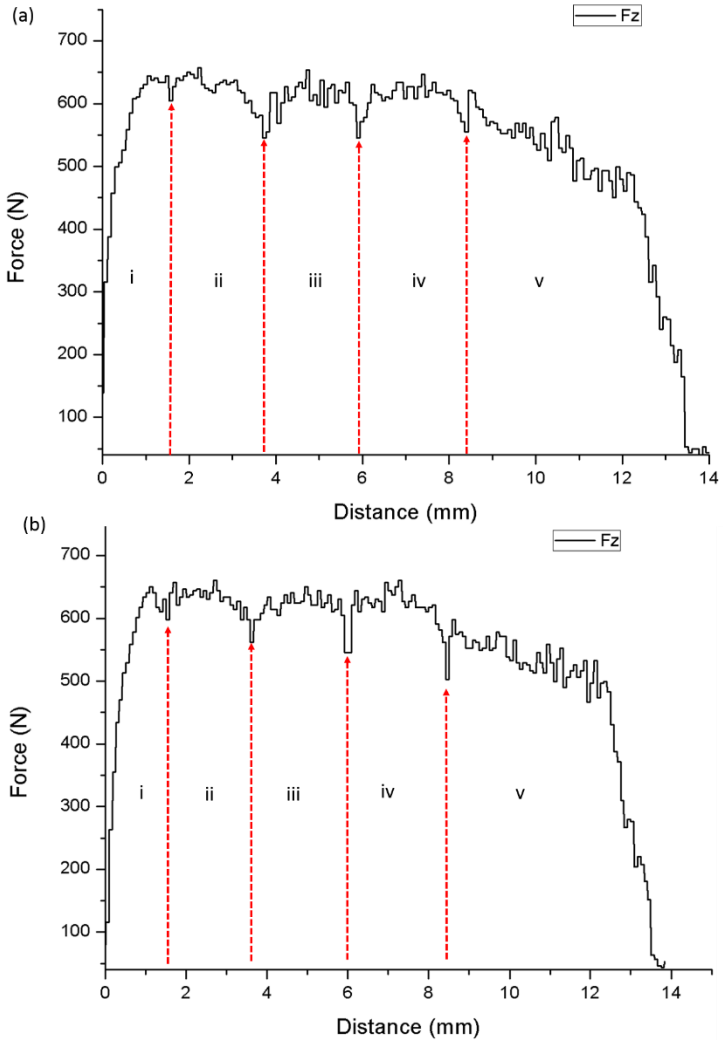


Figure 7-11: 'Cutting force - Distance drilled' graphs showing variation in cutting force along layer boundaries. Cutting force is found to reduce by up to 100 N in remelted regions. Components machined without control system in plots shown

7.2.1 Microstructure Analysis

The observed variation in cutting force was related to the changes in machining conditions due to a difference in microstructure. Analysing the microstructure in relation to the plots in *Figure 7-11*, the first region (i) corresponds to the remainder of a milled section of the top layer and subsequent intermittent reduction in cutting force is related to the layer thickness and periodic variation in the microstructure due to remelting of

layers during the build process. This also correlates to the step-up layer thickness used during the manufacture of the component to ensure a defect free deposition process. *Figure 7-12* shows an optical micrograph of the cross section of the drilled component and the microstructures prevalent in the various regions. The layer thickness of the regions correlates to the observed regions of variation in cutting forces as the cutting tool progresses through these layers. The figure also shows the variation in microstructure between the substrate and deposit regions.

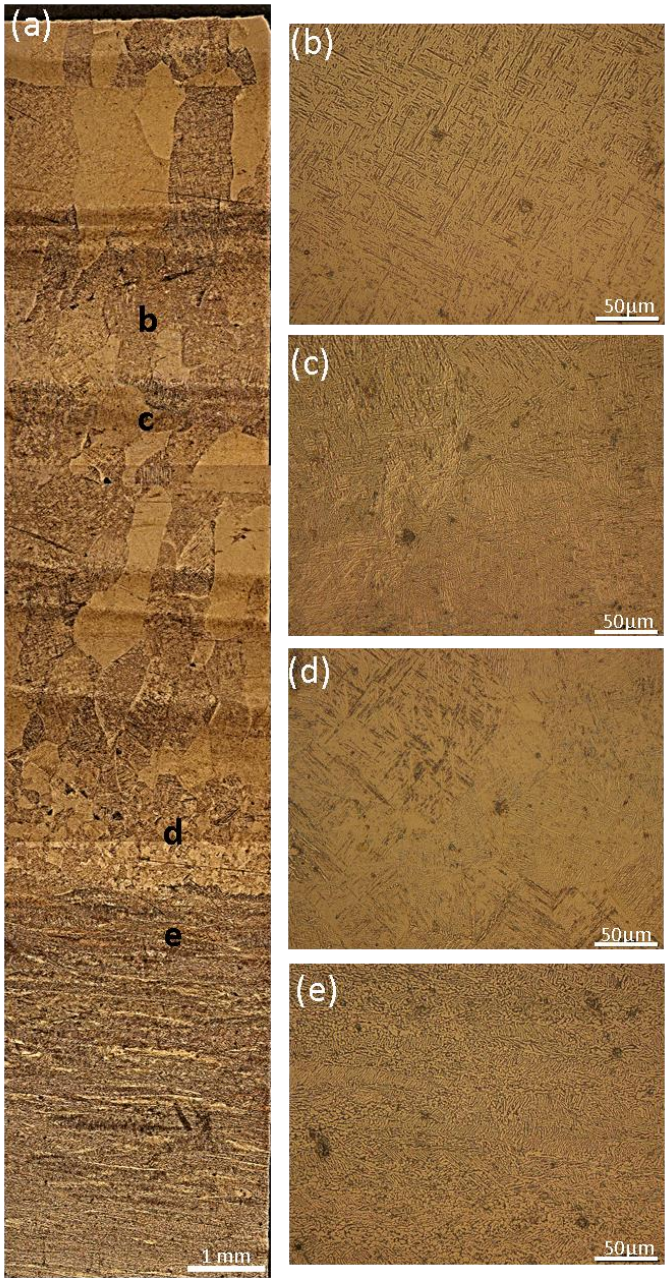


Figure 7-12: Optical Microscope images of (a) Cross section of drilled build showing DED, HAZ and wrought regions relating changes in cutting forces shown in Figure 11 to microstructural variations, Regions b, c, d and e relate to : (b) Clad mid region (c) Remelted regions (d) Substrate - Deposit interface/ HAZ (e) Unaffected substrate region. Sample etched with Kroll's reagent

Towards further investigations on the influence of microstructure in determining the cutting force variations observed, *Figure 7-13* is a SEM image which shows the variation in microstructure along the component in the 'as

deposited' state. The sample is taken at the edge of a built component to show the correlation of the banding effect to the layer build strategy. A magnified view of the highlighted region in (a), which is along the bulk and the remelted layer boundary showing the difference in grain texture is shown in *Figure 7-13(*b). In the remelted regions, the microstructure consists of colony Widmanstatten α in retained β, in comparison to the basketweave Widmanstatten α outside these regions. The basketweave morphology forms as a result of increased cooling rates from the β phase field.

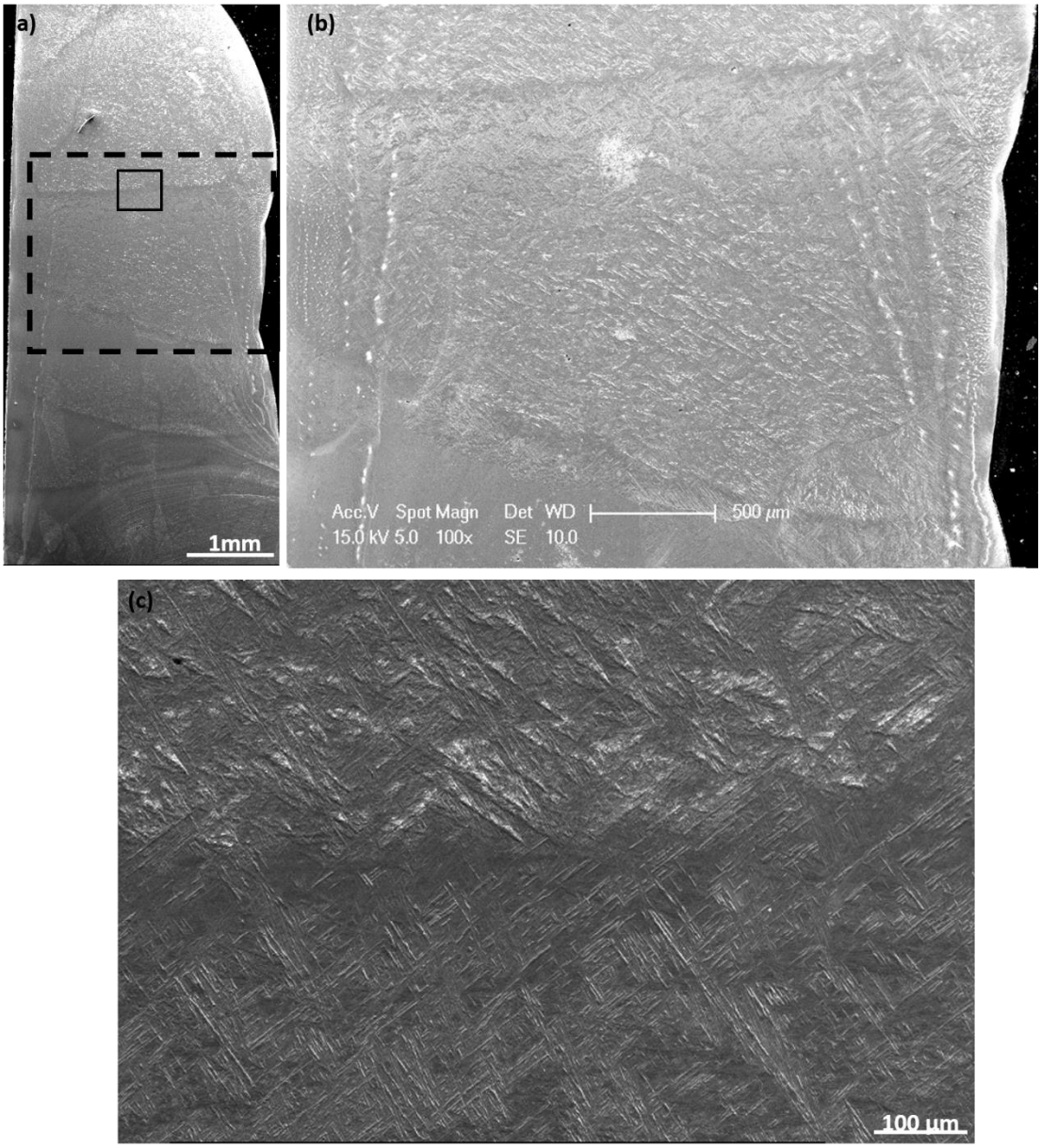


Figure 7-13: Microstructure of deposited Ti6Al4V (a) Deposit showing variation in layers due to addition of new layers along entire build (b) Magnified view of region bounded by remelted regions highlighted by broken lines in 'a' (c) Higher magnification view of layer boundary showing variation in microstructure between the layer bands and the deposit regions. SEM Images taken in SE mode

7.2.2 Surface Roughness

Surface roughness of the drilled hole walls were measured to determine the effects of increased tool usage on hole quality with both machining strategies.

In measuring the surface roughness, values were obtained from the wrought and DED regions. Figure 7-14 shows the measured mean values of surface roughness in both regions with both strategies. The use of the AC system is found to improve surface finish in both instances with comparatively lower values observed in the holes produced using the AC system. The standard deviation of the surface roughness values was lower compared to those without the use of the control system indicating a statistically improved system with reduced variability. Table 7-3 shows the surface roughness values derived for both machining strategies.

Table 7-3: Statistical values of Surface Roughness (Ra and Rz) for substrate and DED regions machined with and without AC system. All values are in µm

Substrate (Ra)		
Statistic	**Without AC**	**With AC**
Mean	0.6969	0.6554
Standard deviation	0.1278	0.1190
Error (+/-)	0.0738	0.0687

DED region (Ra)		
Statistic	**Without AC**	**With AC**
Mean	0.5790	0.4683
Standard deviation	0.0994	0.0992
Error (+/-)	0.0574	0.0573

Substrate (Rz)		
Statistic	**Without AC**	**With AC**
Mean	3.9267	3.5581
Standard deviation	0.7221	0.5443
Error (+/-)	0.4169	0.3142

DED region (Rz)		
Statistic	**Without AC**	**With AC**
Mean	3.4567	2.6424
Standard deviation	0.8067	0.5070
Error (+/-)	0.4508	0.2927

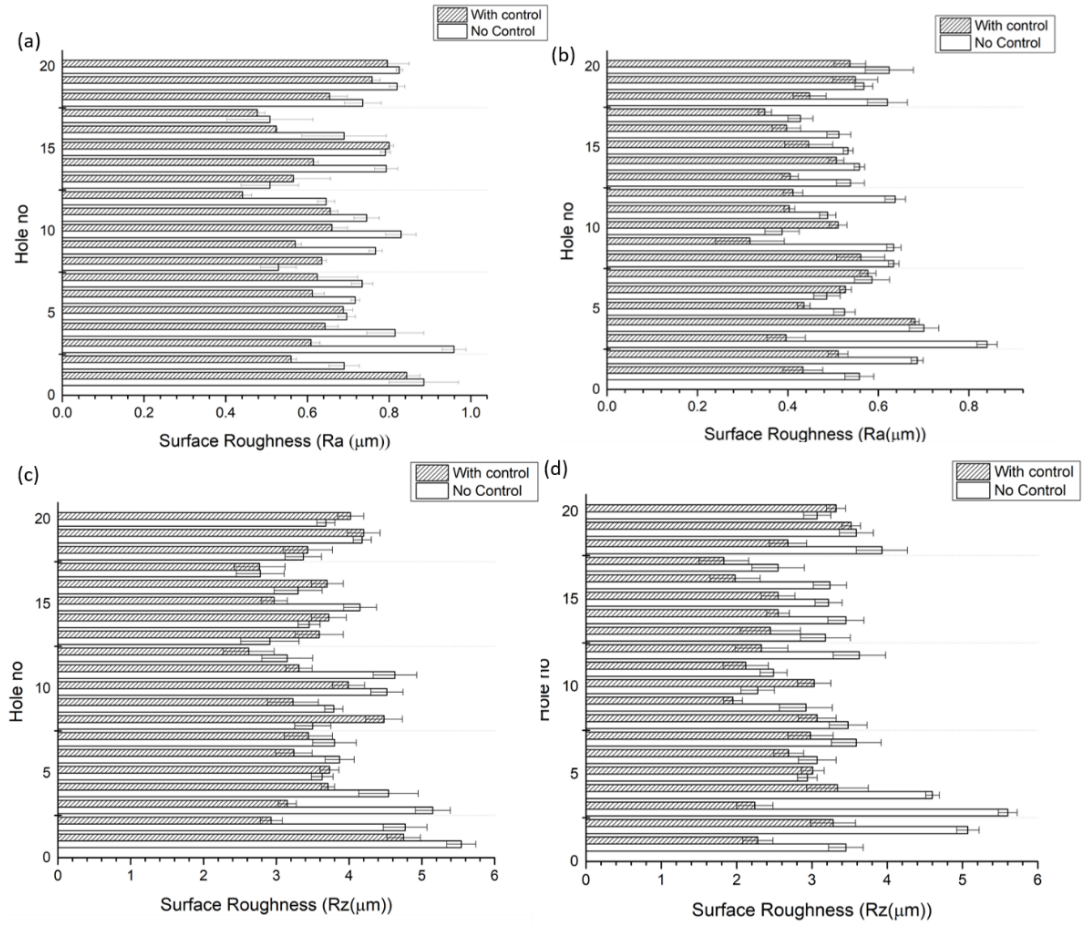


Figure 7-14: Surface roughness of drilled holes with and without AC system (a) Substrate Ra (b) DED region Ra (c) Substrate Rz (d) DED region Rz

Statistical analysis of the surface roughness values indicates an improvement with the use of adaptive control in machining. Also, improvements in mean surface roughness, standard deviation and variance were recorded. Table 7-4 shows the statistical derivations from the processes. The improvements observed are due to the effects of the system at keeping the cutting forces within thresholds which promote uniformity in surface finish and also part conformance.

Table 7-4: Comparison between surface roughness between both processes

Name of Statistic	Without AC	With AC
Mean	0.75101	0.7316
Standard deviation	0.06504	0.044
Error (+/-)	0.0377	0.025

7.3 Adaptive Machining of Ti6Al4V/WC components

One of the advantages of developing the adaptive machining system is the ability to machine components with a varying microstructural gradient due to the presence of a hardening material. The difficulties in machining such components has been highlighted in Chapter 5.0

In machining with the AC system, a component which comprised alternating layers of Ti6Al4V and Ti6Al4V/ WC was deposited and machined. Drilling was the preferred machining method as it allows for visualisation of the machining forces with variation in component composition and hardness. Machining parameters used are the same as those in Table 7-2.

A 10 mm thick sample was used in the drilling trials. From the plot shown in Figure 7-15, drilling trials were carried out by altering between zones of Ti6Al4V/ WC and Ti6Al4V.From the trials shown, the control system attempts to reduce the feed rate as machining progresses.

Due to the reduced rigidity of the machine tool, the vibrations were excessive during this machining process and the tool attrition was high as the process

was run at sub-optimal feed rates and spindle speeds. Thus, the process was not developed further to improve the system response.

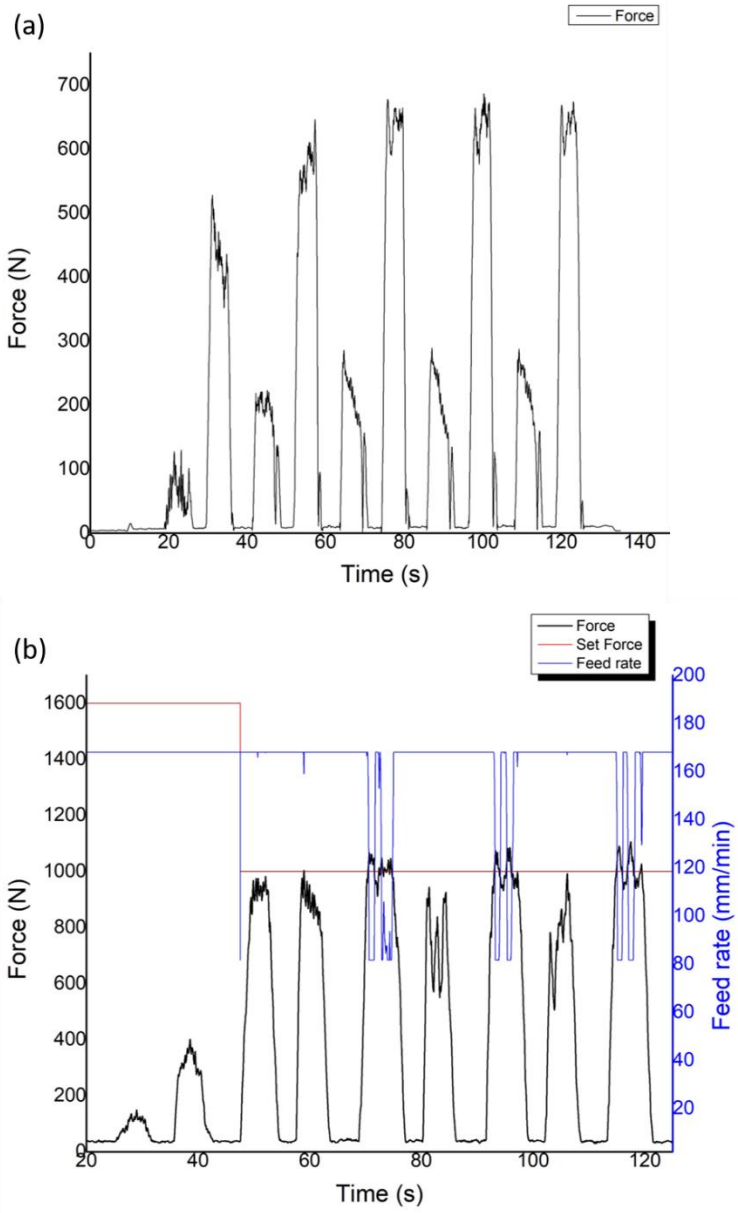


Figure 7-15: Drilling plots showing passes for 10 holes in a 10 mm Ti6Al4V component. (a) without AC (b) machining with AC and adjusting set point force after 50 secs from 1400 N to 1000 N

7.4 Discussion

In conventional macro-machining processes involving wrought materials, component microstructures are regarded as being homogenous, a reason for this is the relative size difference between the machining depth of cut and the grain size of the material. In micro-machining, component anisotropy at the microscale is regarded as a factor in machining due to the microstructural feature size in relation to the tooling depth of cut. In the machining of DED produced components, variation in microstructure is prevalent with associated periodicity as a consequence of the build strategy and the associated variation due to dynamics of rapid solidification. Furthermore, mechanical properties have been shown to be significantly influenced by crystallographic texture in titanium alloys, with these variations capable of influencing the machining forces and by extension material machinability.

Furthermore, one of the documented challenges during the machining of titanium alloys is the initiation of chatter due to segmented chip formation and a variation in chip thickness. This arises due to the effects of shear localization during the machining of these alloys which results in cyclic variation of cutting forces with significant magnitude disparity [228, 229].

In the machining of DED produced Ti alloy components, aside from the alloys' characteristic properties which can lead to machine chatter, variation in metallographic texture of the constituent regions contributes to chip thickness variation which influences stability and repeatability of the

machining process affecting uniformity in surface roughness. The use of the AC system limits variation during the cutting process and consequently leads to an improvement in surface finish. Control of the cutting forces which also impacts the thermo-mechanical effects of the cutting tool on the workpiece leads to a reduction in the grain refinement at the machined region and a subsequent improvement in the surface and subsurface integrity in this region.

In the milling trials, machining chatter as a result of causative mechanisms discussed previously is reduced with the use of the AC system for feed rate modulation, avoiding variation of chip load on the cutting tool. This is supported by the improvements to the surface finish and reduction in the subsurface deformation depth.

In machining, cutting forces are dependent on the materials' microstructural attributes which encompass the grain size and texture of the machined component. Variation in measured cutting forces between the outermost and bulk regions is explained by the difference in grain size which leads to a decrease in yield stress between these regions as explained by the Hall – Petch relationship. A reduction in grain size in the deposit interior would cause an increase in material yield stress, thus limiting dislocation and requiring increased machining forces for chip formation. In this aspect, the results observed here are in agreement with those observed in the turning experiments discussed in Chapter 4.0.

In the drilling trials, the effects of changes in material microstructure on the cutting process become more evident with increased tool usage as periodic variations in cutting forces are recorded. Variation in material microstructure and an accompanying difference in material flow stress as machining proceeds across the layer bands leads to a variation in measured cutting forces. Thus, in regions with higher yield strength, the applied stress required to continue the deformation process increases to complement the increase in strength.

The occurrence of variation in cutting forces in the cutting direction after the full engagement of the drill has also been reported by Hoye et al. [230] in the drilling of Ti6Al4V components produced using a Gas Tungsten arc welding process. In the study, the authors postulated the increment in cutting forces was due to a variation in hardness due to the thermal cycles the component undergoes during deposition and suggest a variation in cutting forces of up to 15 % ensues when keeping the feed rate constant.

Drilling with the AC system limits this variation in forces by adapting the feed rate to match the material properties in this region. An argument for the variation in the cutting forces within the DED region can be due to chip segmentation as a result of the plastic strain reaching the fracture threshold and the chip fracture propagating in the regions with varying microstructure. The release of plastic strain during the chip formation process causes the observed instantaneous decrease in cutting forces and a subsequent increase in cutting force back to the maximum value as machining progresses [231].

However, the periodic nature of the decrease in cutting forces and the correlation of this to regions of microstructural variation in the deposit point to the former as a reason for the periodic reduction in cutting forces.

7.5 Conclusions

In this chapter, a strategy for machining Ti6Al4V components produced using a DED process using a developed adaptive control system on an open architecture CNC was presented. Improvements with the use of the control system were observed. Based on the experimental observations, the following conclusions can be drawn:

- During deposition processes, the remelting of layers leads to component anisotropicity which influences the post processing machining process. This has been shown to affect the cutting forces, particularly in drilling which involves machining across these layer boundaries. With increased use of the tool, variation in cutting forces is found in remelted regions to reduce by to 15 % (100 N) of the values outside of these regions. The use of a constant force limiting process reduces the effect of the variations in cutting forces due to changes in material properties whilst promoting a stable machining process.
- The use of the adaptive control system in machining promotes machining stability by limiting incessant variation in cutting forces due to component mechanical and geometrical properties. Subsequently, the formation of machining chatter marks during milling is avoided and surface

roughness of the machined components is improved which also enhances the repeatability of the machining process and would also impact positively on the process capability of the system. Similar improvements in residual stress and reduction of subsurface deformation is observed which would be valuable in producing components with improved mechanical properties.

- Surface integrity in the milling operations is improved with the use of the AC system as the onset of machining chatter is avoided. The surface finish is found to improve by up to 70 % (0.2 µm ± 0.023) in the AC machined region and the subsurface deformation is also shown to have a reduction in depth of up to 55 % (4.65µm). In the drilling trials, the improvement in surface finish was found to be 2 %. However, as a result of the lower cutting forces in the remelted regions, an increase in feed rate in these areas led to an increase in cutting force to match the required set force. This subsequently leads to a reduction in tool engagement period by 0.5 secs. In drilling a large number of holes in this material, the use of the developed control system would be beneficial towards cost savings.

8.0 Conclusions and further work

Post processing of metal AM components has been an aspect of increasing research investigations and expenditure in recent times due to increased adoption of metal AM techniques. The findings from this study provide further understanding on the post process machining of components produced using directed energy deposited techniques. In this study, machining processes which include turning, milling and drilling have been used in investigating machinability and the prevailing characteristics of machining such components. A proposal for the machining of these components using adaptive control machining has also been made with results and advantages from using such system presented.

The aims and objectives of this study have been successfully achieved and the results have been documented in the previous chapters. This chapter presents the key conclusions on the study on the machinability of DED produced Ti6Al4V components (Chapter 4), the machining of a functionally graded component consisting of a difficult to machine metal matrix composite region and a Ti6Al4V region (Chapter 5), and the development and use of adaptive control machining in milling and drilling DED produced Ti6Al4V components (Chapters 6 & 7).

In completion, recommendations are given for the future research that can be carried out based on the findings of this work.

8.1 Machinability of DED produced *Ti6Al4V* Components

The use of heat treatments in improvement of machinability of *Ti6Al4V* components from the DED process is demonstrated with post process heat treatments shown to be beneficial towards improving machinability whilst also leading to a depreciation of mechanical properties. Fundamentally, in α+β Titanium alloys, mechanical properties are dependent on the width of alpha laths. Thus, an increase in the size of alpha laths due to heat treatment post deposition leads to a corresponding reduction in the required forces for machining due to the aforementioned depreciation of material strength. A comparison between the DED as-built and heat-treated components; the as-received wrought component and the heat-treated wrought material shows a variation in machinability remains and the mechanical properties remain subject to thermal histories and fabrication processes the component undergoes. This was found to be largely due to the particle sizes of these components post manufacture. Consequently, the as-built component had the highest cutting forces in the machinability trials. The effects of grain size on cutting forces were however found to diminish with increase in cutting speed (increase of 100m/min) as the cutting force variation narrowed from 60 % to 31 % (100 N to 50 N) when compared to the beta sample and the alpha sample varied from 45 % to 5 % (80 N to 10 N) of the as built component values.

The relationships between the machining process parameters, the prevailing cutting forces and the resulting surface and subsurface conditions indicate machining parameters remain critical in the post finishing of DED components. Due to the finer grain sizes inherent in DED processes as a result of high cooling rates, the components produced are prone to surface damage as a result of their higher hardness. In the as built component, it has been shown that increase in feed rate and depth of cut lead to corresponding increase in deformation depth into the material during turning operations. Progressive machining into these components leads to an increase in the subsurface deformation depth as the components show an increase in hardness and increased strain hardening with increased subsequent layer removal- this is evidenced by the gradual increment in cutting forces by up to 100 % (up to 110 N increase) of its value from the outermost surface to a depth of 1.5 mm from the surface. Residual stress analysis also indicates the dependence of the surface stress condition on machining parameters. It was also deduced the surface residual stress state of the component has a relationship with the measured cutting forces and the machinability of the material as the outermost layers were found to be mostly tensile in the as built state and tend towards being compressive values after machining.

8.2 Machining of Functionally Graded Ti6Al4V/ WC

The increase in use of layer build technologies has led to an increase in industrial interest for manufacture of components which are capable of harnessing desirable material qualities of different materials along a single component. This study set out to investigate the post process machining of a functionally graded component with a single material region and a multiple material region using multiple commercially available tooling. As a result of varying material properties, components such as these exhibit variable machinability which has an adverse effect on tooling and thus the sustainable deployment of these materials.

Cutting force variation in between both material regions is found to be minimal with the microstructural variations within the MMC regions providing much of the differences observed. Material variation is found to influence cutting forces with the layer build strategy leading to the formation of regions of higher dissolved hardening material composition during remelting to add subsequent layers. Within these regions, cutting forces were found to periodically increase by as much as 40 % of the mean values due to the aforementioned increase in dissolution of WC and subsequent variation in hardness (345 ± 60 HV). The formation of such a layer in the production of metal matrix composites such as these has not been reported in literature and is a consequence of the manufacturing strategy. These regions, due to their

higher hardness as a result of higher dissolution of the reinforcement material were particularly detrimental to the tool as high tool wear was observed. Tool wear mechanism was found to be by abrasion with the WC particles in the workpiece MMC region preferentially removing the binder material in the inserts, whilst exposing the hardening particles in the cutting tool and thus leading to the initiation of multiple abrasion mechanisms due to particle, workpiece and tooling interactions.

Particle fracture and pull out, which are characteristic drawbacks which influence surface finish in the machining of MMCs were observed in the MMC region. Components machined with PCD inserts showed higher number of voids due to this in comparison to the CBN inserts. Surface roughness analysis indicate the regions machined with the CBN inserts had better surface finish in both instances of monolithic and MMC regions. However, for similar machining durations, the wear rate was estimated to be higher in the CBN tool.

Analysis of the surface roughness of the machined regions showed the CBN insert performed marginally better than the PCD tool in terms of surface finish albeit with a high wear rate. Surface finish of the monolithic material region close to the boundary between both materials was observed to be influenced by the particle interactions at the MMC region as the region showed a reduction in the prevalence of the characteristic surface marks and lower surface roughness values.

8.3 Adaptive Machining of DED produced Ti6Al4V

An alternate strategy for the machining of components produced using DED and other metal AM means was proposed and demonstrated. With the key idea being the adjustment of process parameters to match the changing microstructural and mechanical properties. Here, an adaptive control system was demonstrated which is based on the ACC strategy and uses the cutting forces as the constraint with the feed rate being the parameter being varied. Early experiments indicated the cutting forces was more responsive to changes in the feed rate with the set up used. Improvements in surface finish, reduced subsurface deformation and a balanced distribution of residual stresses were observed in milling experiments. Improvements in surface finish were found to be due to the avoidance of machine chatter which would otherwise be initiated during machining as a result of a variation in cutting forces and chip thickness which would be the case during the machining of components with a heterogeneous microstructure. By limiting the onset of machine chatter, the use of the AC system led to an improvement of up to 70 % (0.2 µm ± 0.023) in the surface finish (Ra) and a 55 % (4.65µm) reduction in the deformation depth when compared to a component machined without the system.

Drilling trials with the adaptive control system also lead to a statistically stable and repeatable process. In the experiments without the use of the AC system,

the influence of machining across the layer boundaries is observed to lead to a periodic variation in cutting forces which is detrimental to the tool life and surface finish. Machining trials here also validate the difference in variation in machinability of the DED produced components compared to the wrought material as the AC system is observed to respond to the material variation by adjusting feed rates towards compensating for the effect of the change in mechanical properties. Cutting force variation between these regions was found to be up to 15 % (100 N). The action of the AC system, in smoothing out cutting force led to a higher feed rate and subsequent reduction in machining time. The system is thus shown to be a useful addition to the post process machining of components produced using these means. The use of such system would also be relevant in the machining of components with a functional gradient as it would ensure uniformity in surface roughness whilst also allowing for machining time savings as demonstrated here.

8.4 Future Work

Observations from this study haves revealed that there is a need for the evaluation of machinabilities of components produced using metal AM strategies as they deviate from the wrought forms of the material. Areas requiring future investigations in this field of study would include;

- This study has focused on the machinability of *Ti6Al4V* monolithic and Ti6Al4V with a reinforcement. Whilst these present varying challenges in

machining, the underlying characteristics of the machining process in terms of the remelted regions is largely based on microstructural variation due to thermal excursion during the processing of these materials. Whilst other materials undergo grain coarsening in regions of remelting and variation in microstructures due to differential cooling, the effects on mechanical properties and the subsequent machining needs to be investigated. Thus, other difficulty to machine materials which are commonly used in metal AM such as the Inconel alloys and duplex stainless steels would need to be explored to investigate the effects of anisotropy on their machinability.

- The effects of using the adaptive control system on tooling has not been thoroughly investigated here. Usually, the use of adaptive control is reported to influence tool life positively and that is one of the commercial considerations for developing an alternate strategy for machining. A study on this would ensure the process remains reliable with various increase in tool wear.
- As an offshoot of the above, with the deterioration of tool life and changes in the tool- workpiece interface interactions, machining conditions which affect the control system response lead to further machining instabilities. Thus, there is a need for the PID system to be capable of reacting to this and producing new variables which provide suitable response without lag. It is thus necessary that the PID system be reviewed to incorporate the PID online autotuning VI to annul any observed changes from tooling and system variation. Also, acquisition rates and response time can be improved

by initiating the LabVIEW VI in the FPGA mode. This is however subject to the response time of the Tormach controller. An option to improve this is by initialling a Modbus arrangement for serial communications between the Compact Rio and the Tormach controller PC.

- The influence of reinforcement composition and size on the ensuing machinability has not been investigated in this study. Whilst previous work has reported an improvement in machinability with the reduction in size fractions of the reinforcement, this has not been investigated for processes with high energy beams such as used in this study. The probability of having more of the reinforcement particles melting due to the attainable energy density of these high energy beams increases with reduced particle size. This would adversely affect the machinability due to a higher matrix hardness. A suitable balance between the size fraction and the composition with regards to post process machining would however be necessary depending on the proposed application.
- In the use of the AC system, the measurement of cutting force was used as the constraint due to available resources. In the future, it would be expedient to validate the obtained results using a multi sensor fusion arrangement where alternate sensors – vibration and acoustic emission sensors can be used in tandem with the dynamometer for the measurement and control of the system dynamics. This would provide sufficient information on the effects of cutting force and the relation to machine vibrations during the machining of anisotropic components such as those here.

- An attempt was made to investigate the use of the AC system in machining functionally graded layers of Ti6Al4V and Ti6Al4V/ WC. The attempt was unsuccessful as the machine tool could not provide sufficient rigidity to machine the component and the tool wear was excessive. The testing of an adaptive control system with suitable tools on a more rigid machining system would be beneficial in showing the full capabilities of machining with the system.

References

1. ASTM, *ASTM ISO/ASTM52900-15 Standard Terminology for Additive Manufacturing - General Principles -Terminology*. 2015, ASTM International: West Conshohocken, PA,.
2. Gibson, I., D.W. Rosen, and B. Stucker, *Additive Manufacturing Technologies : Rapid Prototyping to Direct Digital Manufacturing*. 2009, Boston, NETHERLANDS: Springer.
3. Noorani, R., *Rapid prototyping : principles and applications / Rafiq Noorani*. 2006, Hoboken, N.J.: Hoboken, N.J. : John Wiley & Sons.
4. Wohlers, T., *Wohlers Report 2017: 3D printing and Additive Manufacturing State of the Industry*. 3D printing and Additive Manufacturing State of the Industry. 2017, Colorado 80525 USA: Wohlers associates. 343.
5. Frazier, W.E., *Metal Additive Manufacturing: A Review.* Journal of Materials Engineering and Performance, 2014. **23**(6): p. 1917-1928.
6. Kobryn, P. and S. Semiatin, *The laser additive manufacture of Ti-6Al-4V.* JOM, 2001. **53**(9): p. 40-42.
7. Zheng, B., et al., *Thermal behavior and microstructural evolution during laser deposition with laser-engineered net shaping: Part I. Numerical calculations.* Metallurgical and materials transactions A, 2008. **39**(9): p. 2228-2236.
8. Zhong, M. and W. Liu, *Laser surface cladding: the state of the art and challenges.* Proceedings of the Institution of Mechanical Engineers, Part C: Journal of Mechanical Engineering Science, 2010. **224**(5): p. 1041-1060.
9. http://www.ionix.fi/en/technologies/laser-processing/laser-cladding/. 2018 [cited 2018 11.06.2018]; Available from: http://www.ionix.fi/en/technologies/laser-processing/laser-cladding/.
10. DebRoy, T., et al., *Additive manufacturing of metallic components – Process, structure and properties.* Progress in Materials Science, 2018. **92**: p. 112-224.
11. Herzog, D., et al., *Additive manufacturing of metals.* Acta Materialia, 2016. **117**: p. 371-392.
12. Mower, T.M. and M.J. Long, *Mechanical behavior of additive manufactured, powder-bed laser-fused materials.* Materials Science and Engineering: A, 2016. **651**: p. 198-213.
13. Wu, X., et al., *Microstructures of laser-deposited Ti–6Al–4V.* Materials & design, 2004. **25**(2): p. 137-144.
14. Kobryn, P. and S. Semiatin, *Microstructure and texture evolution during solidification processing of Ti–6Al–4V.* Journal of Materials Processing Technology, 2003. **135**(2): p. 330-339.
15. Farayibi, P.K., et al., *Cladding of pre-blended Ti-6Al-4V and WC powder for wear resistant applications.* Surface & Coatings Technology, 2011. **206**(2-3): p. 372-377.
16. Kelly, S. and S. Kampe, *Microstructural evolution in laser-deposited multilayer Ti-6Al-4V builds: Part I. Microstructural characterization.* Metallurgical and Materials Transactions A, 2004. **35**(6): p. 1861-1867.
17. Heigel, J., et al., *Selection of Powder or Wire Feedstock Material for the Laser Cladding of Inconel® 625.* Journal of Materials Processing Technology, 2016.
18. Arias-González, F., et al., *Fiber laser cladding of nickel-based alloy on cast iron.* Applied Surface Science, 2015.
19. Chen, Y., et al., *Coaxial laser cladding of Al2O3-13%TiO2 powders on Ti-6Al-4 V alloy.* Surface and Coatings Technology, 2013. **228, Supplement 1**: p. S452-S455.
20. Weng, F., et al., *Microstructure and property of composite coatings on titanium alloy deposited by laser cladding with Co42+TiN mixed powders.* Journal of Alloys and Compounds, 2016. **686**: p. 74-81.

21. Vandenbroucke, B. and J.-P. Kruth, *Selective laser melting of biocompatible metals for rapid manufacturing of medical parts.* Rapid Prototyping Journal, 2007. **13**(4): p. 196-203.
22. ASTM, *Standard Test Method for Surface Finish of Powder Metallurgy (PM) Products*. 2016.
23. Felberbaum, L., et al., *Thermal fatigue of single-crystalline superalloy CMSX-4®: a comparison of epitaxial laser-deposited material with the base single crystal.* Materials Science and Engineering: A, 2001. **299**(1–2): p. 152-156.
24. Vilar, R., *Laser Powder Deposition*, in *Comprehensive Materials Processing*, G.F. Batalha, C.J.V. Tyne, and B. Yilbas, Editors. 2014, Elsevier: Oxford. p. 163-216.
25. Masood, S.H., W. Rattanawong, and P. Iovenitti, *A generic algorithm for a best part orientation system for complex parts in rapid prototyping.* Journal of Materials Processing Technology, 2003. **139**(1–3): p. 110-116.
26. Mircea Ancău and C. Caizar, *The Optimization of Surface Quality in Rapid Prototyping*, in *WSEAS International Conference on Engineering Mechanics, Structures, Engineering Geology (EMESEG '08),*. 2008, WSEAS: Heraklion, Crete Island, Greece. p. pages 136- 141.
27. Sikder, S., A. Barari, and H. Kishawy. *Effect of Adaptive Slicing on Surface Integrity in Additive Manufacturing*. in *ASME 2014 International Design Engineering Technical Conferences and Computers and Information in Engineering Conference*. 2014. American Society of Mechanical Engineers.
28. Rianmora, S. and P. Koomsap, *Recommended slicing positions for adaptive direct slicing by image processing technique.* The International Journal of Advanced Manufacturing Technology, 2010. **46**(9): p. 1021-1033.
29. Shim, D.-S., et al., *Effect of layer thickness setting on deposition characteristics in direct energy deposition (DED) process.* Optics & Laser Technology, 2016. **86**: p. 69-78.
30. Strano, G., et al., *Surface roughness analysis, modelling and prediction in selective laser melting.* Journal of Materials Processing Technology, 2013. **213**(4): p. 589-597.
31. Mumtaz, K. and N. Hopkinson, *Top surface and side roughness of Inconel 625 parts processed using selective laser melting.* Rapid Prototyping Journal, 2009. **15**(2): p. 96-103.
32. Mumtaz, K.A. and N. Hopkinson, *Selective Laser Melting of thin wall parts using pulse shaping.* Journal of Materials Processing Technology, 2010. **210**(2): p. 279-287.
33. Tian, Y., et al., *Influences of processing parameters on surface roughness of Hastelloy X produced by selective laser melting.* Additive Manufacturing, 2017. **13**: p. 103-112.
34. El-Gallab, M. and M. Sklad, *Machining of Al/SiC particulate metal matrix composites: Part II: Workpiece surface integrity.* Journal of Materials Processing Technology, 1998. **83**(1–3): p. 277-285.
35. Abioye, T.E., et al., *Functionally graded Ni-Ti microstructures synthesised in process by direct laser metal deposition.* The International Journal of Advanced Manufacturing Technology, 2015. **79**(5): p. 843-850.
36. Jhabvala, J., et al., *An innovative method to build support structures with a pulsed laser in the selective laser melting process.* The International Journal of Advanced Manufacturing Technology, 2012. **59**(1): p. 137-142.
37. Calignano, F., *Design optimization of supports for overhanging structures in aluminum and titanium alloys by selective laser melting.* Materials & Design, 2014. **64**: p. 203-213.
38. Gusarov, A.V., M. Pavlov, and I. Smurov, *Residual Stresses at Laser Surface Remelting and Additive Manufacturing.* Physics Procedia, 2011. **12, Part A**: p. 248-254.
39. Brückner, F., D. Lepski, and E. Beyer, *Modeling the Influence of Process Parameters and Additional Heat Sources on Residual Stresses in Laser Cladding.* Journal of Thermal Spray Technology, 2007. **16**(3): p. 355-373.

40. Kahlen, F.-J. and A. Kar, *Residual stresses in laser-deposited metal parts.* Journal of Laser Applications, 2001. **13**(2): p. 60-69.
41. Plati, A., et al., *Residual stress generation during laser cladding of steel with a particulate metal matrix composite.* Advanced engineering materials, 2006. **8**(7): p. 619-624.
42. Ding, J., et al., *Thermo-mechanical analysis of Wire and Arc Additive Layer Manufacturing process on large multi-layer parts.* Computational Materials Science, 2011. **50**(12): p. 3315-3322.
43. Jang, D.Y., et al., *Surface residual stresses in machined austenitic stainless steel.* Wear, 1996. **194**(1): p. 168-173.
44. Campbell, F.C., *5.6 The Mechanics of Chip Formation*, in *Metals Fabrication - Understanding the Basics*. ASM International.
45. Guo, Y.B., W. Li, and I.S. Jawahir, *SURFACE INTEGRITY CHARACTERIZATION AND PREDICTION IN MACHINING OF HARDENED AND DIFFICULT-TO-MACHINE ALLOYS: A STATE-OF-ART RESEARCH REVIEW AND ANALYSIS.* Machining Science and Technology, 2009. **13**(4): p. 437-470.
46. M'Saoubi, R., et al., *A review of surface integrity in machining and its impact on functional performance and life of machined products.* International Journal of Sustainable Manufacturing, 2008. **1**(1-2): p. 203-236.
47. M'saoubi, R., et al., *Residual stress analysis in orthogonal machining of standard and resulfurized AISI 316L steels.* Journal of materials processing technology, 1999. **96**(1): p. 225-233.
48. Sadat, A.B., *Surafce Integrity when Machining Metal Matrix Composites*, in *Machining of Metal Matrix composites*. 2012, Springer London: London.
49. Ghosh, S. and J. Choi, *Modeling and experimental verification of transient/residual stresses and microstructure formation in multi-layer laser aided DMD process.* Journal of heat transfer, 2006. **128**(7): p. 662-679.
50. Dickens, P., et al. *Rapid prototyping using 3-D welding*. 1992. DTIC Document.
51. Szost, B.A., et al., *A comparative study of additive manufacturing techniques: Residual stress and microstructural analysis of CLAD and WAAM printed Ti–6Al–4V components.* Materials & Design, 2016. **89**: p. 559-567.
52. Carter, L.N., M.M. Attallah, and R.C. Reed, *Laser powder bed fabrication of nickel-base superalloys: influence of parameters; characterisation, quantification and mitigation of cracking.* Superalloys 2012, 2012: p. 577-586.
53. Catchpole-Smith, S., et al., *Fractal scan strategies for selective laser melting of 'unweldable' nickel superalloys.* Additive Manufacturing, 2017. **15**: p. 113-122.
54. Qiu, C., N.J. Adkins, and M.M. Attallah, *Microstructure and tensile properties of selectively laser-melted and of HIPed laser-melted Ti–6Al–4V.* Materials Science and Engineering: A, 2013. **578**: p. 230-239.
55. Joshi, G.V., et al., *Fatigue testing of electron beam-melted Ti-6Al-4V ELI alloy for dental implants.* Journal of Biomedical Materials Research Part B: Applied Biomaterials, 2013. **101B**(1): p. 124-130.
56. Heinl, P., et al., *Cellular Titanium by Selective Electron Beam Melting.* Advanced Engineering Materials, 2007. **9**(5): p. 360-364.
57. Bandyopadhyay, A., et al., *Influence of porosity on mechanical properties and in vivo response of Ti6Al4V implants.* Acta Biomaterialia, 2010. **6**(4): p. 1640-1648.
58. Dass, A. and A. Moridi, *State of the Art in Directed Energy Deposition: From Additive Manufacturing to Materials Design.* Coatings, 2019. **9**.
59. Aboulkhair, N.T., et al., *Reducing porosity in AlSi10Mg parts processed by selective laser melting.* Additive Manufacturing, 2014. **1–4**: p. 77-86.
60. Sun, Y., et al., *The Influence of As-Built Surface Conditions on Mechanical Properties of Ti-6Al-4V Additively Manufactured by Selective Electron Beam Melting.* JOM, 2016. **68**(3): p. 1-8.
61. Łyczkowska, E., et al., *Chemical polishing of scaffolds made of Ti–6Al–7Nb alloy by additive manufacturing.* Archives of Civil and Mechanical Engineering, 2014. **14**(4): p. 586-594.

62. Baicheng, Z., et al., *Study of selective laser melting (SLM) Inconel 718 part surface improvement by electrochemical polishing.* Materials & Design, 2017. **116**: p. 531-537.
63. Das, K., et al., *Surface modification of laser-processed porous titanium for load-bearing implants.* Scripta Materialia, 2008. **59**(8): p. 822-825.
64. Vaithilingam, J., et al. *Surface modification of selective laser melted structures using self-assembled monolayers for biomedical applications*. in *23rd Annual International Solid Freeform Fabrication Symposium*. 2012.
65. Yang, L., H. Gu, and A. Lassell. *Surface treatment of Ti6Al4V parts made by powder bed fusion additive manufacturing processes using electropolishing*. in *Proceedings of Solid Freeform Fabrication (SFF) Symposium, Austin, TX*. 2014.
66. Yang, L., et al. *Electropolishing of Ti6Al4V parts fabricated by electron beam melting*. in *Proceedings of the International Solid Freeform Fabrication (SFF) Symposium, Austin, TX*. 2016.
67. Lhuissier, P., et al., *Geometrical control of lattice structures produced by EBM through chemical etching: Investigations at the scale of individual struts.* Materials & Design, 2016. **110**: p. 485-493.
68. Coules, H., et al., *Effect of high pressure rolling on weld-induced residual stresses.* Science and Technology of Welding and Joining, 2012. **17**(5): p. 394-401.
69. Colegrove, P.A., et al., *Microstructure and residual stress improvement in wire and arc additively manufactured parts through high-pressure rolling.* Journal of Materials Processing Technology, 2013. **213**(10): p. 1782-1791.
70. Williams, S., et al., *Wire+ Arc Additive Manufacturing.* Materials Science and Technology, 2015: p. 1743284715Y. 0000000073.
71. Donoghue, J., et al., *The effectiveness of combining rolling deformation with Wire–Arc Additive Manufacture on β-grain refinement and texture modification in Ti–6Al–4V.* Materials Characterization, 2016. **114**: p. 103-114.
72. Manfredi, D., et al., *Direct Metal Laser Sintering: an additive manufacturing technology ready to produce lightweight structural parts for robotic applications.* La Metallurgia Italiana, 2014(10).
73. Cheng, X., et al., *Residual stress modification by post-weld treatment and its beneficial effect on fatigue strength of welded structures.* International Journal of Fatigue, 2003. **25**(9): p. 1259-1269.
74. AlMangour, B. and J.-M. Yang, *Improving the surface quality and mechanical properties by shot-peening of 17-4 stainless steel fabricated by additive manufacturing.* Materials & Design, 2016. **110**: p. 914-924.
75. Uzan, N.E., et al., *On the effect of shot-peening on fatigue resistance of AlSi10Mg specimens fabricated by additive manufacturing using selective laser melting (AM-SLM).* Additive Manufacturing, 2018. **21**: p. 458-464.
76. Nickel, A., D. Barnett, and F. Prinz, *Thermal stresses and deposition patterns in layered manufacturing.* Materials science and Engineering: A, 2001. **317**(1): p. 59-64.
77. *ASTM F3301-18 Standard for Additive Manufacturing- Post Processing Methods - Standard Specification for Thermal Post-Processing Metal Parts Made Via Powder Bed Fusion*. 2018: ASTM International, West Conshohocken, PA, .
78. Shiomi, M., et al., *Residual stress within metallic model made by selective laser melting process.* CIRP Annals-Manufacturing Technology, 2004. **53**(1): p. 195-198.
79. Sercombe, T., et al., *Heat treatment of Ti-6Al-7Nb components produced by selective laser melting.* Rapid Prototyping Journal, 2008. **14**(5): p. 300-304.
80. Brandl, E., et al., *Additive manufactured AlSi10Mg samples using Selective Laser Melting (SLM): Microstructure, high cycle fatigue, and fracture behavior.* Materials & Design, 2012. **34**: p. 159-169.
81. Tian, X., et al., *Effect of annealing temperature on the notch impact toughness of a laser melting deposited titanium alloy Ti–4Al–1.5 Mn.* Materials Science and Engineering: A, 2010. **527**(7): p. 1821-1827.

82. Tian, X., S. Zhang, and H. Wang, *The influences of anneal temperature and cooling rate on microstructure and tensile properties of laser deposited Ti–4Al–1.5 Mn titanium alloy.* Journal of Alloys and Compounds, 2014. **608**: p. 95-101.
83. Dinda, G., L. Song, and J. Mazumder, *Fabrication of Ti-6Al-4V scaffolds by direct metal deposition.* Metallurgical and Materials Transactions A, 2008. **39**(12): p. 2914-2922.
84. Kahlen, F.-J. and A. Kar, *Tensile Strengths for Laser-Fabricated Parts and Similarity Parameters for Rapid Manufacturing.* Journal of Manufacturing Science and Engineering, 1999. **123**(1): p. 38-44.
85. Lu, Y., et al., *Microstructure evolution of sub-critical annealed laser deposited Ti–6Al–4V alloy.* Materials & Design, 2012. **37**: p. 56-63.
86. Zhang, S., et al., *Heat-treated microstructure and mechanical properties of laser solid forming Ti-6Al-4V alloy.* Rare metals, 2009. **28**(6): p. 537-544.
87. Atkinson, H.V. and S. Davies, *Fundamental aspects of hot isostatic pressing: An overview.* Metallurgical and Materials Transactions a-Physical Metallurgy and Materials Science, 2000. **31**(12): p. 2981-3000.
88. Zhao, X., et al., *Comparison of the microstructures and mechanical properties of Ti–6Al–4V fabricated by selective laser melting and electron beam melting.* Materials & Design, 2016. **95**: p. 21-31.
89. Leuders, S., et al., *On the mechanical behaviour of titanium alloy TiAl6V4 manufactured by selective laser melting: Fatigue resistance and crack growth performance.* International Journal of Fatigue, 2013. **48**: p. 300-307.
90. Santos, E., et al., *Microstructure and mechanical properties of pure titanium models fabricated by selective laser melting.* Proceedings of the institution of mechanical engineers, part c: journal of mechanical engineering science, 2004. **218**(7): p. 711-719.
91. Agarwala, M., et al., *Post-processing of selective laser sintered metal parts.* Rapid Prototyping Journal, 1995. **1**(2): p. 36-44.
92. Agarwala, M.K., D. Bourell, and J. Beaman. *Densification of selective laser sintered metal parts by hot isostatic pressing*. in *Solid Freeform Fabrication Proceedings*. 1994.
93. Knight, R., et al. *Metal processing using selective laser sintering and hot isostatic pressing (SLS/HIP)*. in *Proceedings of the Solid Freeform Fabrication Symposium*. 1996.
94. Das, S., et al., *Producing metal parts with selective laser sintering/hot isostatic pressing.* JoM, 1998. **50**(12): p. 17-20.
95. Das, S., et al., *Processing of titanium net shapes by SLS/HIP.* Materials & design, 1999. **20**(2): p. 115-121.
96. Qiu, C., et al., *In-situ shelling via selective laser melting: Modelling and microstructural characterisation.* Materials & Design, 2015. **87**: p. 845-853.
97. Kobryn, P. and S. Semiatin. *Mechanical properties of laser-deposited Ti-6Al-4V*. in *Solid Freeform Fabrication Proceedings*. 2001. Austin.
98. Qiu, C., et al., *Fabrication of large Ti–6Al–4V structures by direct laser deposition.* Journal of Alloys and Compounds, 2015. **629**: p. 351-361.
99. Facchini, L., et al., *Microstructure and mechanical properties of Ti-6Al-4V produced by electron beam melting of pre-alloyed powders.* Rapid Prototyping Journal, 2009. **15**(3): p. 171-178.
100. Blackwell, P.L., *The mechanical and microstructural characteristics of laser-deposited IN718.* Journal of Materials Processing Technology, 2005. **170**(1–2): p. 240-246.
101. Tillmann, W., et al., *Hot isostatic pressing of IN718 components manufactured by selective laser melting.* Additive Manufacturing, 2017. **13**: p. 93-102.
102. Proskurovsky, D., et al., *Pulsed electron-beam technology for surface modification of metallic materials.* Journal of Vacuum Science & Technology A, 1998. **16**(4): p. 2480-2488.
103. Man, H., Z. Cui, and T. Yue, *Corrosion properties of laser surface melted NiTi shape memory alloy.* Scripta Materialia, 2001. **45**(12): p. 1447-1453.

104. Chen, Z., et al., *Microstructures and wear properties of surface treated Ti–36Nb–2Ta–3Zr–0.35 O alloy by electron beam melting (EBM).* Applied Surface Science, 2015. **357**: p. 2347-2354.
105. Ukar, E., et al., *Laser polishing of tool steel with CO 2 laser and high-power diode laser.* International Journal of Machine Tools and Manufacture, 2010. **50**(1): p. 115-125.
106. Temmler, A., E. Willenborg, and K. Wissenbach, *Design surfaces by laser remelting.* Physics Procedia, 2011. **12**: p. 419-430.
107. Brinksmeier, E., et al., *Polishing of structured molds.* CIRP Annals-Manufacturing Technology, 2004. **53**(1): p. 247-250.
108. Temmler, A., et al., *Surface structuring by remelting of titanium alloy Ti6Al4V.* Journal of Laser Applications, 2015. **27**(S2): p. S29103.
109. Kempen, K., et al., *Mechanical properties of AlSi10Mg produced by selective laser melting.* Physics Procedia, 2012. **39**: p. 439-446.
110. Kruth, J.-P., et al. *Part and material properties in selective laser melting of metals*. in *Proceedings of the 16th international symposium on electromachining*. 2010.
111. Lamikiz, A., et al., *Laser polishing of parts built up by selective laser sintering.* International Journal of Machine Tools and Manufacture, 2007. **47**(12): p. 2040-2050.
112. Marimuthu, S., et al., *Laser polishing of selective laser melted components.* International Journal of Machine Tools and Manufacture, 2015. **95**: p. 97-104.
113. Yasa, E., J.P. Kruth, and J. Deckers, *Manufacturing by combining Selective Laser Melting and Selective Laser Erosion/laser re-melting.* CIRP Annals - Manufacturing Technology, 2011. **60**(1): p. 263-266.
114. Yasa, E., J. Deckers, and J.-P. Kruth, *The investigation of the influence of laser re-melting on density, surface quality and microstructure of selective laser melting parts.* Rapid Prototyping Journal, 2011. **17**(5): p. 312-327.
115. Yasa, E. and J.-P. Kruth, *Microstructural investigation of Selective Laser Melting 316L stainless steel parts exposed to laser re-melting.* Procedia Engineering, 2011. **19**: p. 389-395.
116. Alrbaey, K., et al., *On optimization of surface roughness of selective laser melted stainless steel parts: a statistical study.* Journal of Materials Engineering and Performance, 2014. **23**(6): p. 2139-2148.
117. Kruth, J.-P., E. Yasa, and J. Deckers, *Experimental investigation of laser surface re-melting for the improvement of selective laser melting process.* 2009.
118. Ma, C.P., Y.C. Guan, and W. Zhou, *Laser polishing of additive manufactured Ti alloys.* Optics and Lasers in Engineering, 2017. **93**: p. 171-177.
119. Rosa, B., P. Mognol, and J.-Y. Hascoët, *Laser polishing of additive laser manufacturing surfaces.* Journal of Laser Applications, 2015. **27**(S2): p. S29102.
120. Dadbakhsh, S., L. Hao, and C.Y. Kong, *Surface finish improvement of LMD samples using laser polishing.* Virtual and Physical Prototyping, 2010. **5**(4): p. 215-221.
121. Vaithilingam, J., et al., *The effect of laser remelting on the surface chemistry of Ti6al4V components fabricated by selective laser melting.* Journal of Materials Processing Technology, 2016. **232**: p. 1-8.
122. J. Miguel Pinilla, J.-H.K., Fritz B. Prinz, *Process Planning and Automation for Additive-Subtractive Solid Freeform Fabrication*, in *Proceedings of the Solid Freeform Fabrication Symposium*. 1998: The University of Texas, Austin.
123. Sealy, M.P., et al., *Hybrid Processes in Additive Manufacturing.* ASME. J. *Manuf. Sci. Eng* . 2018. **140**(6).
124. Flynn, J.M., et al., *Hybrid additive and subtractive machine tools – Research and industrial developments.* International Journal of Machine Tools and Manufacture, 2016. **101**: p. 79-101.
125. Lauwers, B., et al., *Hybrid processes in manufacturing.* CIRP Annals - Manufacturing Technology, 2014. **63**(2): p. 561-583.
126. Aspinwall, D.K., et al., *Hybrid High Speed Machining (HSM): System Design and Experimental Results for Grinding/HSM and EDM/HSM.* CIRP Annals - Manufacturing Technology, 2001. **50**(1): p. 145-148.

127. Wang, Z.Y., et al., *Hybrid machining of Inconel 718.* International Journal of Machine Tools and Manufacture, 2003. **43**(13): p. 1391-1396.
128. Rajurkar, K.P., et al., *New Developments in Electro-Chemical Machining.* CIRP Annals - Manufacturing Technology, 1999. **48**(2): p. 567-579.
129. Menzies, I. and P. Koshy, *Assessment of abrasion-assisted material removal in wire EDM.* CIRP Annals - Manufacturing Technology, 2008. **57**(1): p. 195-198.
130. Molian, R., et al., *Novel Laser/Water-Jet Hybrid Manufacturing Process for Cutting Ceramics.* Journal of Manufacturing Science and Engineering, 2008. **130**(3): p. 031008-031008.
131. Zhu, Z., et al., *A review of hybrid manufacturing processes – state of the art and future perspectives.* International Journal of Computer Integrated Manufacturing, 2013. **26**(7): p. 596-615.
132. M.Kerschbaumer, G.E. *Hybrid manufacturing process for rapid high performance tooling combining high speed milling and laser cladding*. in *23rd International Congress on Applications of Lasers and Electro-Optics(ICALEO),*. San Francisco, CA.
133. Du, W., Q. Bai, and B. Zhang, *A Novel Method for Additive/Subtractive Hybrid Manufacturing of Metallic Parts.* Procedia Manufacturing, 2016. **5**: p. 1018-1030.
134. L. Ren, A.P.P., J. Ruan, T. Sparks, F.W. Liou, . *Three dimensional die repair using a hybrid manufacturing system,*. in *Proceedings of the 17th Solid Freeform Fabrication Symposium, SFF 2006*. 2006.
135. Jones, J.B., et al., *Remanufacture of turbine blades by laser cladding, machining and in-process scanning in a single machine.* 2012.
136. Yamazaki, T., *Development of A Hybrid Multi-tasking Machine Tool: Integration of Additive Manufacturing Technology with CNC Machining.* Procedia CIRP, 2016. **42**(Supplement C): p. 81-86.
137. Manogharan, G., et al., *AIMS–A Metal Additive-hybrid Manufacturing System: System Architecture and Attributes.* Procedia Manufacturing, 2015. **1**: p. 273-286.
138. Manogharan, G., R.A. Wysk, and O.L. Harrysson, *Additive manufacturing–integrated hybrid manufacturing and subtractive processes: economic model and analysis.* International Journal of Computer Integrated Manufacturing, 2016. **29**(5): p. 473-488.
139. Gibson, I., D. Rosen, and B. Stucker, *Post-processing*, in *Additive Manufacturing Technologies: 3D Printing, Rapid Prototyping, and Direct Digital Manufacturing*. 2015, Springer New York: New York, NY. p. 329-350.
140. Löber, L., et al., *Comparison of different post processing technologies for SLM generated 316l steel parts.* Rapid Prototyping Journal, 2013. **19**(3): p. 173-179.
141. Anthony, T.B., et al., *Finishing of additively manufactured titanium alloy by shape adaptive grinding (SAG).* Surface Topography: Metrology and Properties, 2015. **3**(2): p. 024001.
142. Taminger, K., et al., *Effect of Surface Treatments on Electron Beam Freeform Fabricated Aluminum Structures.* 2004.
143. Xiong, X., H. Zhang, and G. Wang, *Metal direct prototyping by using hybrid plasma deposition and milling.* journal of materials processing technology, 2009. **209**(1): p. 124-130.
144. Karunakaran, K.P., et al., *Retrofitment of a CNC machine for hybrid layered manufacturing.* The International Journal of Advanced Manufacturing Technology, 2009. **45**(7): p. 690-703.
145. Shunmugavel, M., et al., *Metallurgical and Machinability Characteristics of Wrought and Selective Laser Melted Ti-6Al-4V.* Journal of Metallurgy, 2016. **2016**: p. 10.
146. Milton, S., et al., *Influence of Finish Machining on the Surface Integrity of Ti6Al4V Produced by Selective Laser Melting.* Procedia CIRP, 2016. **45**: p. 127-130.
147. Huang, X., et al. *Machining Finish of Titanium Alloy Prepared by Additive Manufacturing*. in *Applied Mechanics and Materials*. 2017. Trans Tech Publ.
148. Bordin, A., et al., *Comparison between wrought and EBM Ti6AI4V machinability characteristics.* Key Engineering Materials, 2014.
149. Brinksmeier, E., et al., *Surface integrity of selective-laser-melted components.* CIRP Annals - Manufacturing Technology, 2010. **59**(1): p. 601-606.

150. Montevecchi, F., et al., *Cutting Forces Analysis in Additive Manufactured AISI H13 Alloy.* Procedia CIRP, 2016. **46**: p. 476-479.
151. Rysava, Z., et al., *Micro-drilling and Threading of the Ti6Al4V Titanium Alloy Produced through Additive Manufacturing.* Procedia CIRP, 2016. **46**: p. 583-586.
152. Sartori, S., et al., *On the tool wear mechanisms in dry and cryogenic turning Additive Manufactured titanium alloys.* Tribology International, 2017. **105**: p. 264-273.
153. Bordin, A., et al., *Analysis of tool wear in cryogenic machining of additive manufactured Ti6Al4V alloy.* Wear, 2015. **328–329**: p. 89-99.
154. Bruschi, S., et al., *Influence of the machining parameters and cooling strategies on the wear behavior of wrought and additive manufactured Ti6Al4V for biomedical applications.* Tribology International, 2016. **102**: p. 133-142.
155. Oyelola, O., et al., *Machining of Additively Manufactured Parts: Implications for Surface Integrity.* Procedia CIRP, 2016. **45**: p. 119-122.
156. Imbrogno, S., et al., *Experimental analysis on semi-finishing machining of Ti6Al4V additively manufactured by direct melting laser sintering.* AIP Conference Proceedings, 2016. **1769**(1): p. 080007.
157. Javidi, A., U. Rieger, and W. Eichlseder, *The effect of machining on the surface integrity and fatigue life.* International Journal of Fatigue, 2008. **30**(10–11): p. 2050-2055.
158. Sasahara, H., *The effect on fatigue life of residual stress and surface hardness resulting from different cutting conditions of 0.45%C steel.* International Journal of Machine Tools and Manufacture, 2005. **45**(2): p. 131-136.
159. Che-Haron, C.H. and A. Jawaid, *The effect of machining on surface integrity of titanium alloy Ti–6% Al–4% V.* Journal of Materials Processing Technology, 2005. **166**(2): p. 188-192.
160. Wilms, G.R. and R.L. Aghan, *Anisotropy in machining of steel plates.* Metals Technology, 2013. **8**(1): p. 108-112.
161. Moronuki, N., Y. Liang, and Y. Furukawa, *Experiments on the effect of material properties on microcutting processes.* Precision Engineering, 1994. **16**(2): p. 124-131.
162. Lee, W.B., C.F. Cheung, and S. To, *Materials induced vibration in ultra-precision machining.* Journal of Materials Processing Technology, 1999. **89-90**: p. 318-325.
163. Zhao, Q., et al., *Investigation of anisotropic mechanisms in ultra-precision diamond machining of KDP crystal.* Journal of Materials Processing Technology, 2009. **209**(8): p. 4169-4177.
164. Dikshit, M.K., A.B. Puri, and A. Maity, *Chatter and dynamic cutting force prediction in high-speed ball end milling.* Machining Science and Technology, 2017. **21**(2): p. 291-312.
165. Altintas, Y. and P.K. Chan, *In-process detection and suppression of chatter in milling.* International Journal of Machine Tools and Manufacture, 1992. **32**(3): p. 329-347.
166. Lin, S.C., R.E. DeVor, and S.G. Kapoor, *The Effects of Variable Speed Cutting on Vibration Control in Face Milling.* Journal of Engineering for Industry, 1990. **112**(1): p. 1-11.
167. Yoneoka, T., et al., *Disturbance Observer–Based In-process Detection and Suppression of Chatter Vibration.* Procedia CIRP, 2012. **1**: p. 44-49.
168. Landers, R.G. and A.G. Ulsoy, *Nonlinear Feed Effect in Machining Chatter Analysis.* Journal of Manufacturing Science and Engineering, 2008. **130**(1): p. 011017-011017-8.
169. Srinivasa Prasad, B., et al., *Condition Monitoring of CNC Machining Using Adaptive Control.* International Journal of Automation and Computing, 2013. **10**(3): p. 202-209.
170. Zuperl, U., F. Cus, and M. Milfelner, *Fuzzy control strategy for an adaptive force control in end-milling.* Journal of Materials Processing Technology, 2005. **164-165**: p. 1472-1478.
171. Mikolajczyk, T., A. Olaru, and P. Krainski. *Adaptive control system for drill machine*. in *Applied Mechanics and Materials*. 2013. Trans Tech Publ.

172. Youssef, H.A. and H. El-Hofy, *Machining technology: machine tools and operations*. 2008: CRC Press.
173. Liang, S.Y., R.L. Hecker, and R.G. Landers, *Machining Process Monitoring and Control: The State-of-the-Art.* Journal of Manufacturing Science and Engineering, 2004. **126**(2): p. 297-310.
174. Landau, I.D., et al., *Introduction to Adaptive Control*, in *Adaptive Control: Algorithms, Analysis and Applications*. 2011, Springer London: London. p. 1-33.
175. Ramesh, R., M.A. Mannan, and A.N. Poo, *Error compensation in machine tools — a review: Part I: geometric, cutting-force induced and fixture-dependent errors.* International Journal of Machine Tools and Manufacture, 2000. **40**(9): p. 1235-1256.
176. Koren, Y., *Computer control of manufacturing systems*. 1983: McGraw-Hill New York et al.
177. Koren, Y. *Adaptive Control Systems for Machining*. in *American Control Conference, 1988*. 1988.
178. Cus, F., et al., *Adaptive self-learning controller design for feedrate maximisation of machining process.* Journal of Achievements in Materials and Manufacturing Engineering, 2008. **31**(2): p. 469-476.
179. Giriraj, B., et al., *Adaptive control in high speed machining for improved surface finish.* Indian Journal of Engineering and Materials Sciences, 2008. **15**(4): p. 311-316.
180. Abellan-Nebot, J.V. and F. Romero Subirón, *A review of machining monitoring systems based on artificial intelligence process models.* The International Journal of Advanced Manufacturing Technology, 2010. **47**(1): p. 237-257.
181. Kovač, P., et al., *A review of machining monitoring systems.* Journal of production engineering, 2011. **14**(1): p. 1-6.
182. Jaehyun, P., et al. *An open architecture testbed for real-time monitoring and control of machining processes*. in *American Control Conference, Proceedings of the 1995*. 1995.
183. Altintas, Y. and W.K. Munasinghe, *A Hierarchical Open-Architecture CNC System for Machine Tools.* CIRP Annals, 1994. **43**(1): p. 349-354.
184. Shackleford, W.P. and F.M. Proctor. *Use of open source distribution for a machine tool controller*. in *Sensors and Controls for Intelligent Manufacturing*. 2001. International Society for Optics and Photonics.
185. Davis, J.R., *Metals Handbook, Desk Edition (2nd Edition)*. 1998, ASM International.
186. Filip, R., et al., *The effect of microstructure on the mechanical properties of two-phase titanium alloys.* Journal of Materials Processing Technology, 2003. **133**(1–2): p. 84-89.
187. Brandl, E., et al., *Deposition of Ti–6Al–4V using laser and wire, part I: Microstructural properties of single beads.* Surface and Coatings Technology, 2011. **206**(6): p. 1120-1129.
188. Armendia, M., et al., *Influence of Heat Treatment on the Machinability of Titanium Alloys.* Materials and Manufacturing Processes, 2012. **27**(4): p. 457-461.
189. SAE, *SAE AMSH 81200 - Heat Treatment of Titanium and Titanium Alloys*. 2014, SAE International. p. 24.
190. Mitutoyo. *QUICK GUIDE TO SURFACE ROUGHNESS MEASUREMENT - Reference guide for laboratory and workshop*. 2016 [cited 2019 23/04/2019]; Bulletin No. 2229:[Available from: https://www.mitutoyo.com/wp-content/uploads/2012/11/1984_Surf_Roughness_PG.pdf.
191. International, A., *ASTM E92-17, Standard Test Methods for Vickers Hardness and Knoop Hardness of Metallic Materials*. 2017: West Conshohocken, PA.
192. Fergani, O., et al., *Analytical modelling of residual stress in additive manufacturing.* Fatigue & Fracture of Engineering Materials & Structures, 2017. **40**(6): p. 971-978.
193. Arrazola, P.J., et al., *Machinability of titanium alloys (Ti6Al4V and Ti555.3).* Journal of Materials Processing Technology, 2009. **209**(5): p. 2223-2230.
194. Ezugwu, E.O. and Z.M. Wang, *Titanium alloys and their machinability—a review.* Journal of Materials Processing Technology, 1997. **68**(3): p. 262-274.

195. Veiga, C., J. Davim, and A. Loureiro, *Review on machinability of titanium alloys: the process perspective.* Rev. Adv. Mater. Sci, 2013. **34**(2): p. 148-164.
196. Abukhshim, N., P. Mativenga, and M. Sheikh, *Heat generation and temperature prediction in metal cutting: A review and implications for high speed machining.* International Journal of Machine Tools and Manufacture, 2006. **46**(7): p. 782-800.
197. Jin, D. and Z. Liu, *Damage of the machined surface and subsurface in orthogonal milling of FGH95 superalloy.* The International Journal of Advanced Manufacturing Technology, 2013. **68**(5): p. 1573-1581.
198. Guo, Y., et al., *Controlling deformation and microstructure on machined surfaces.* Acta Materialia, 2011. **59**(11): p. 4538-4547.
199. Bai, J., et al., *The influence of cutting parameters on the defect structure of subsurface in orthogonal cutting of titanium alloy.* Journal of Materials Research, 2018. **33**(6): p. 720-732.
200. Jaffery, S.H.I. and P.T. Mativenga, *Wear mechanisms analysis for turning Ti-6Al-4V—towards the development of suitable tool coatings.* The International Journal of Advanced Manufacturing Technology, 2012. **58**(5): p. 479-493.
201. Nouari, M. and H. Makich, *Experimental investigation on the effect of the material microstructure on tool wear when machining hard titanium alloys: Ti–6Al–4V and Ti-555.* International Journal of Refractory Metals and Hard Materials, 2013. **41**: p. 259-269.
202. Withers, P., *Residual stress and its role in failure.* Reports on progress in physics, 2007. **70**(12): p. 2211.
203. Rangaswamy, P., et al., *Residual stresses in LENS® components using neutron diffraction and contour method.* Materials Science and Engineering: A, 2005. **399**(1–2): p. 72-83.
204. Mercelis, P. and J.P. Kruth, *Residual stresses in selective laser sintering and selective laser melting.* Rapid Prototyping Journal, 2006. **12**(5): p. 254-265.
205. Capello, E., *Residual stresses in turning: Part I: Influence of process parameters.* Journal of Materials Processing Technology, 2005. **160**(2): p. 221-228.
206. Wang, L., S.D. Felicelli, and P. Pratt, *Residual stresses in LENS-deposited AISI 410 stainless steel plates.* Materials Science and Engineering: A, 2008. **496**(1): p. 234-241.
207. Sieniawski, J., et al., *Microstructure and Mechanical Properties of High Strength Two-Phase Titanium Alloys*, in *Titanium Alloys - Advances in Properties Control*, J. Sieniawski and W. Ziaja, Editors. 2013, InTech: Rijeka. p. Ch. 04.
208. Vrancken, B., et al., *Heat treatment of Ti6Al4V produced by selective laser melting: microstructure and mechanical properties.* Journal of Alloys and Compounds, 2012. **541**: p. 177-185.
209. Hall, E.O., *The Deformation and Ageing of Mild Steel: III Discussion of Results.* Proceedings of the Physical Society. Section B, 1951. **64**(9): p. 747.
210. Crawforth, P., et al., *Subsurface deformation during precision turning of a near-alpha titanium alloy.* Scripta Materialia, 2012. **67**(10): p. 842-845.
211. García Navas, V., O. Gonzalo, and I. Bengoetxea, *Effect of cutting parameters in the surface residual stresses generated by turning in AISI 4340 steel.* International Journal of Machine Tools and Manufacture, 2012. **61**: p. 48-57.
212. Kieback, B., A. Neubrand, and H. Riedel, *Processing techniques for functionally graded materials.* Materials Science and Engineering: A, 2003. **362**(1): p. 81-106.
213. Teti, R., *Machining of Composite Materials.* CIRP Annals, 2002. **51**(2): p. 611-634.
214. Komanduri, R., *MACHINING OF FIBER-REINFORCED COMPOSITES.* Machining Science and Technology, 1997. **1**(1): p. 113-152.
215. Kisawy, H.A., *Turning processes for metal matrix composites*, in *In Woodhead Publishing Series in Composites Science and Engineering, Machining Technology for Composite Material*, H. Hocheng, Editor. 2012, Woodhead Publishing. p. Pages 3-16.
216. Cheung, C.F., et al., *Effect of reinforcement in ultra-precision machining of Al6061/SiC metal matrix composites.* Scripta Materialia, 2002. **47**(2): p. 77-82.

217. Pramanik, A., L.C. Zhang, and J.A. Arsecularatne, *An FEM investigation into the behavior of metal matrix composites: Tool–particle interaction during orthogonal cutting.* International Journal of Machine Tools and Manufacture, 2007. **47**(10): p. 1497-1506.
218. Di Ilio, A. and A. Paoletti, *Machinability Aspects of Metal Matrix Composites*, in *Machining of Metal Matrix Composites*, J.P. Davim, Editor. 2012, Springer London: London. p. 63-77.
219. Weinert, K. and W. König, *A Consideration of Tool Wear Mechanism when Machining Metal Matrix Composites (MMC).* CIRP Annals - Manufacturing Technology, 1993. **42**(1): p. 95-98.
220. Wilson, J.M. and Y.C. Shin, *Microstructure and wear properties of laser-deposited functionally graded Inconel 690 reinforced with TiC.* Surface and Coatings Technology, 2012. **207**: p. 517-522.
221. LinuxCNC, *HAL Manual V2.6*. 2016
222. Staroveški, T., et al. *Implementation of a Linux-based CNC open control system*. in *12th International Scientific Conference on Production Engineering, Computer Integrated Manufacturing and High Speed Machining, CIM 2009*. 2009.
223. Epler, J. *Improved Analog & Digital Interface with Arduino*. 2012 30/08/2018]; Available from: https://emergent.unpythonic.net/01198594294.
224. Altintaş, Y., *Direct adaptive control of end milling process.* International Journal of Machine Tools and Manufacture, 1994. **34**(4): p. 461-472.
225. National-Instruments *PID control*. 2012.
226. Sun, J. and Y.B. Guo, *A comprehensive experimental study on surface integrity by end milling Ti–6Al–4V.* Journal of Materials Processing Technology, 2009. **209**(8): p. 4036-4042.
227. Sridhar, B.R., et al., *Effect of machining parameters and heat treatment on the residual stress distribution in titanium alloy IMI-834.* Journal of Materials Processing Technology, 2003. **139**(1): p. 628-634.
228. Sun, S., M. Brandt, and M.S. Dargusch, *Characteristics of cutting forces and chip formation in machining of titanium alloys.* International Journal of Machine Tools and Manufacture, 2009. **49**(7–8): p. 561-568.
229. Pramanik, A., *Problems and solutions in machining of titanium alloys.* The International Journal of Advanced Manufacturing Technology, 2014. **70**(5): p. 919-928.
230. Hoye, N., et al., *Machining of GTAW additively manufactured Ti-6Al-4V structures.* The International Journal of Advanced Manufacturing Technology, 2018. **99**(1): p. 313-326.
231. Pan, Z., et al., *The effects of dynamic evolution of microstructure on machining forces.* Proceedings of the Institution of Mechanical Engineers, Part B: Journal of Engineering Manufacture, 2018. **232**(14): p. 2677-2681.

Appendices

Appendix A

Heat treatment regimens for DED produced Ti6Al4V described in Chapter 4.

Heat treatments carried out at CTI, AMRC.

CastingsTechnologyInternational
Advanced Manufacturing Park,
Brunel Way, Rotherham, S60 5WG

AMRC
Advanced Manufacturing Park
Wallis Way
Catcliffe
Rotherham
S60 5TZ

Certificate No:	W17475
Enquiry No:	E54501
Order No:	ZUO/4500815657
Date Received:	19 January 2017
Date Reported:	25 January 2017
MetLab Ref:	J6619

TEST REPORT

FURNACE LOAD

Sample ID:
sample 1
sample 2

MaterialSpecification:

Test Material In Load: N/A

Heat Treatment Specification: Titanium 6Al / 4V - Customer specified technique

Start Date of Cycle: 25 January 2017
Operator: D. Loomes
Furnace ID: CTI459 Seco Vacuum
Cooling Media: Vacuum Cool
Cooling Pressure: N/A

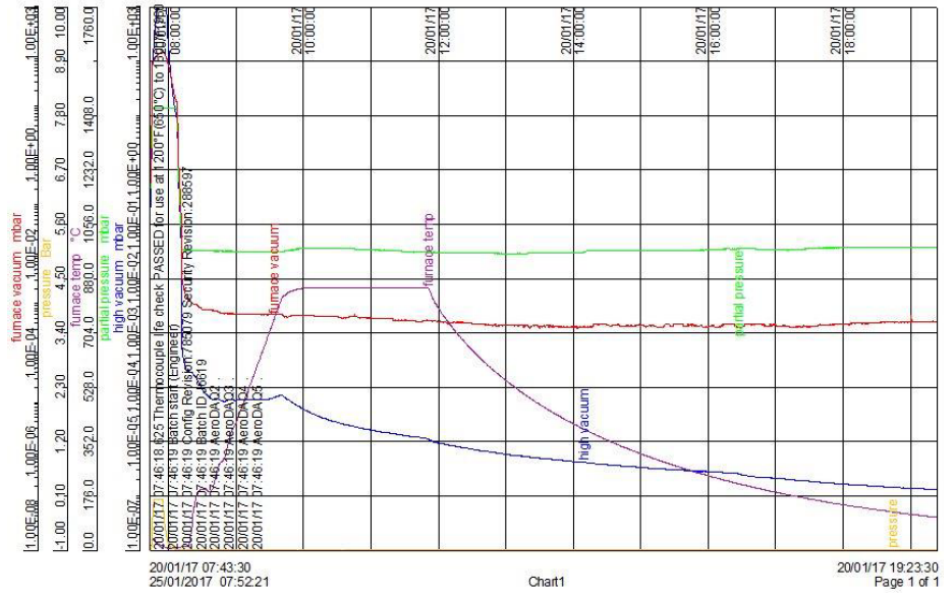
Atmosphere: Vacuum
Pressure (mBar): <3x10-3 mBar

Chart Record ☑ **Secondary T\C** ☐ **Load Interlock** ☐

PROGRAM DETAIL

Action	Ramp Rate (°C/min)	Temperature (°C)	Dwell Time (mins)
Ramp	10	850	
Dwell		850	122
Cool		85	

FURNACE CHART



Comments:

Comments:

Certified that:-
(a) The above treatment was performed on the material as submitted and separately identifie
(b) The treatment was carried out in accordance with the customer's order or approved authorised alternativ
(c) The quality control arrangements for the treatment(s) have accorded with the conditions of Cti's procedures.
(d) Any exceptions to the above shall be stated.

Signed: [redacted]
Technical Manager
Date: 25 January 2017

CastingsTechnology International
Advanced Manufacturing Park,
Brunel Way, Rotherham, S60 5WG

AMRC
Advanced Manufacturing Park
Wallis Way
Catcliffe
Rotherham
S60 5TZ

Certificate No:	W17476
Enquiry No:	E54501
Order No:	ZUO/4500815657
Date Received:	23 January 2017
Date Reported:	25 January 2017
MetLab Ref:	J6621

TEST REPORT

FURNACE LOAD

Sample ID:
Sample 3
Sample 4

MaterialSpecification:

Test Material In Load: N/A

Heat Treatment Specification: Titanium 6Al/4V - Customer specified technique

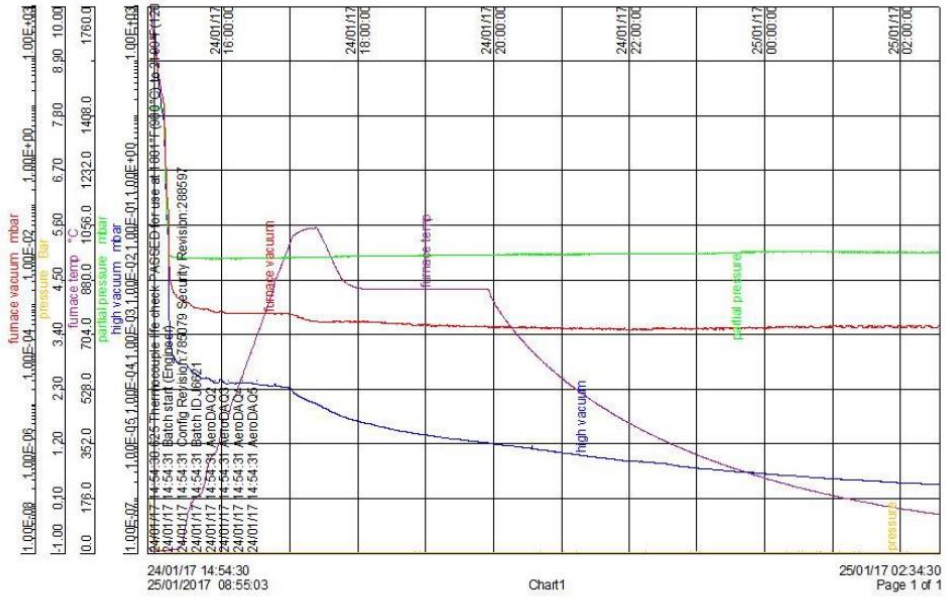
Start Date of Cycle: 26 January 2017
Operator: D. Loomes
Furnace ID: CTI459 Seco Vacuum
Cooling Media: Vacuum Cool
Cooling Pressure: N/A
Atmosphere: Vacuum
Pressure (mBar): <3x10-3 mBar

Chart Record ☑ **Secondary T\C** ☐ **Load Interlock** ☐

PROGRAM DETAIL

Action	Ramp Rate (°C/min)	Temperature (°C)	Dwell Time (mins)
Ramp	10	1050	
Dwell		1050	12
Cool		850	
Dwell		850	122
Cool		85	

FURNACE CHART



Comments:

Comments:

Certified that:-
(a) The above treatment was performed on the material as submitted and separately identified.
(b) The treatment was carried out in accordance with the customer's order or approved authorised alternative.
(c) The quality control arrangements for the treatment(s) have accorded with the conditions of Cti's procedures.
(d) Any exceptions to the above shall be stated.

Signed: [redacted]
Technical Manager
Date: 25 January 2017

Appendix B

A description of the codes added in the start-up protocol of pathpilot. Highlighted areas of the codes are the included lines for communicating with the external peripheral device. Modifications and additions to the below codes are highlighted.

A script named 'Arduino. Py' is created to facilitate communication between the Arduino and pathpilot by creating the Arduino as a hal component.

```
import serial
import hal
import sys
import time
import datetime

def encode(addr, data):
   if data < 0 or data > 2048: raise ValueError, "data %02d out of range" % data
   if addr < 0 or addr > 8: raise ValueError, "address %02d out of range" % addr
   b1 = 0x80 | (addr << 4) | (data >> 7)
   b2 = data & 0x7f
   return chr(b1) + chr(b2)

PORT = "/dev/ttyUSB0"

if len(sys.argv) > 1:
   PORT = sys.argv[1]

if len(sys.argv) > 2:
   nout = int(sys.argv[2])
else:
   nout = 6

if nout > 6 or nout < 0:
   raise SystemExit, "Number of digital outputs must be from 0 to 6"

pinmap = [2,4,7,8,12,13]
dacpinmap = [3,5,6,9,10,11]

ser = serial.Serial(PORT, 9600, timeout=10)

c = hal.component("arduino")
c.newpin("in-waiting", hal.HAL_S32, hal.HAL_OUT)

for port in range(6):
   c.newpin("analog-in-%02d" % port, hal.HAL_S32, hal.HAL_OUT)
   c.newparam("analog-in-%02d-offset" % port, hal.HAL_FLOAT, hal.HAL_RW)
   c.newparam("analog-in-%02d-gain" % port, hal.HAL_FLOAT, hal.HAL_RW)
#   c.newpin("analog-out-%02d" % dacpinmap[port], hal.HAL_FLOAT, hal.HAL_IN)
#   c.newparam("analog-out-%02d-offset" % dacpinmap[port], hal.HAL_FLOAT, hal.HAL_RW)
#   c.newparam("analog-out-%02d-scale" % dacpinmap[port], hal.HAL_FLOAT, hal.HAL_RW)
   c['analog-in-%02d-gain' % port] = 1.0
#   c['analog-out-%02d-scale' % dacpinmap[port]] = 1.0
#for port in range(nout):
#   c.newpin("digital-out-%02d" % pinmap[port], hal.HAL_BIT, hal.HAL_IN)
#   c.newparam("digital-out-%02d-invert" % pinmap[port], hal.HAL_BIT, hal.HAL_RW)
#for port in range(nout, 6):
#   c.newpin("digital-in-%02d" % pinmap[port], hal.HAL_BIT, hal.HAL_OUT)
#   c.newpin("digital-in-%02d-not" % pinmap[port], hal.HAL_BIT, hal.HAL_OUT)
#   c.newparam("digital-in-%02d-pullup" % pinmap[port], hal.HAL_BIT, hal.HAL_RW)
c.ready()
```

```
print "Arduino component loaded", datetime.datetime.now().strftime(" %Y-%m-%d %H:%M:%S")

# ser.flushInput()
t0 = time.clock()
time.sleep(3)
print ser.inWaiting(), "bytes are in buffer at start"
while ser.inWaiting():
    byte = ord(ser.read())
print (time.clock() - t0), "secs eating bytes from arduino"


firstbyte = 0
state = 0
try:
   while 1:
            byteswaiting = ser.inWaiting()
      while byteswaiting:
         byte = ord(ser.read())
         c['in-waiting'] = byteswaiting
         if firstbyte & 0x80 == 0x80 and byte & 0x80 == 0:
            v = (firstbyte << 7) | byte
            port = (v >> 11) & 7

            if port < 6:
               gain = c['analog-in-%02d-gain' % port] or 1.
               offset = c['analog-in-%02d-offset' % port]
               value = (v & 1023) * gain + offset
               c['analog-in-%02d' % port] = int(round (value))

         firstbyte = byte
         byteswaiting = ser.inWaiting()
      time.sleep(.0001) # TODO change this to alter load on the PC's CPU. Time is in seconds.

except (KeyboardInterrupt,):
   raise SystemExit, 0
```

The‘’Tormach mill_py''script is edited to create the HAL pins needed for hardware override. The pins are further created and updated in the postgui script to facilitate systems communications. The postgui file is edited manually whenever the external controller is attached.
The code shows the HAL pins with the created HAL pins

```
      # HAL setup.  Pins/signals must be connected in POSTGUI halfile
      # -------------------------------------------------------------
      self.hal = hal.component("tormach")
      self.hal.newpin("coolant", hal.HAL_BIT, hal.HAL_OUT)
      self.hal.newpin("coolant-iocontrol", hal.HAL_BIT, hal.HAL_IN)
      self.hal.newpin("mist", hal.HAL_BIT, hal.HAL_OUT)
      self.hal.newpin("mist-iocontrol", hal.HAL_BIT, hal.HAL_IN)

      self.hal.newpin("jog-axis-x-enabled", hal.HAL_BIT, hal.HAL_IN)
      self.hal.newpin("jog-axis-y-enabled", hal.HAL_BIT, hal.HAL_IN)
      self.hal.newpin("jog-axis-z-enabled", hal.HAL_BIT, hal.HAL_IN)
      self.hal.newpin("jog-axis-a-enabled", hal.HAL_BIT, hal.HAL_IN)
      self.hal.newpin("jog-step-button", hal.HAL_BIT, hal.HAL_IN)
      self.hal.newpin("jog-counts", hal.HAL_S32, hal.HAL_IN)
      self.hal.newpin("jog-ring-speed-signed", hal.HAL_FLOAT, hal.HAL_IN)
      self.hal.newpin("jog-ring-selected-axis", hal.HAL_S32, hal.HAL_IN)
      self.hal.newpin("jog-gui-step-index", hal.HAL_U32, hal.HAL_OUT)
      self.hal.newpin("jog-is-metric", hal.HAL_BIT, hal.HAL_OUT)
      self.hal.newpin("jog-ring-speed-1", hal.HAL_FLOAT, hal.HAL_OUT)
      self.hal.newpin("jog-ring-speed-2", hal.HAL_FLOAT, hal.HAL_OUT)
      self.hal.newpin("jog-ring-speed-3", hal.HAL_FLOAT, hal.HAL_OUT)
      self.hal.newpin("jog-ring-speed-4", hal.HAL_FLOAT, hal.HAL_OUT)
      self.hal.newpin("jog-ring-speed-5", hal.HAL_FLOAT, hal.HAL_OUT)
      self.hal.newpin("jog-ring-speed-6", hal.HAL_FLOAT, hal.HAL_OUT)
      self.hal.newpin("jog-ring-speed-7", hal.HAL_FLOAT, hal.HAL_OUT)
      self.hal.newpin("motion-program-line", hal.HAL_S32, hal.HAL_IN)
```

```
        self.hal.newpin("motion-next-program-line", hal.HAL_S32, hal.HAL_IN)
        self.hal.newpin("motion-completed-program-line", hal.HAL_S32, hal.HAL_IN)
        self.hal.newpin("spindle-range", hal.HAL_BIT, hal.HAL_OUT)
        self.hal.newpin("spindle-range-alarm", hal.HAL_BIT, hal.HAL_IN)
        self.hal.newpin("spindle-type", hal.HAL_S32, hal.HAL_OUT)
        self.hal.newpin("spindle-hispeed-min", hal.HAL_FLOAT, hal.HAL_OUT)
        self.hal.newpin("spindle-hispeed-max", hal.HAL_FLOAT, hal.HAL_OUT)
        self.hal.newpin("spindle-min-speed", hal.HAL_FLOAT, hal.HAL_IN)
        self.hal.newpin("spindle-max-speed", hal.HAL_FLOAT, hal.HAL_IN)
        self.hal.newpin("spindle-disable", hal.HAL_BIT, hal.HAL_OUT)
        self.hal.newpin("spindle-on", hal.HAL_BIT, hal.HAL_IN)

# Pins for hardware override
                self.hal.newpin("spindle-over-counts", hal.HAL_S32, hal.HAL_IN)

# Pins for hardware override
                self.hal.newpin("feed-over-counts", hal.HAL_S32, hal.HAL_IN)

# Pins for hardware override
                self.hal.newpin("maxvel-over-counts", hal.HAL_S32, hal.HAL_IN)

        # enclosure door switch
        self.hal.newpin("enc-door-switch-status", hal.HAL_BIT, hal.HAL_IN)
        self.hal.newpin("enc-door-switch-configured", hal.HAL_BIT, hal.HAL_OUT)
        self.hal.newpin("enc-door-open-max-rpm", hal.HAL_FLOAT, hal.HAL_OUT)

        # height gauge
        self.hal.newpin('hg-height', hal.HAL_FLOAT, hal.HAL_IN)
        self.hal.newpin('hg-zero-offset', hal.HAL_FLOAT, hal.HAL_IN)
        self.hal.newpin('hg-button-changed', hal.HAL_BIT, hal.HAL_IO)
        self.hal.newpin('hg-button-pressed', hal.HAL_BIT, hal.HAL_IN)
        self.hal.newpin('hg-mm-mode', hal.HAL_BIT, hal.HAL_IO)
        self.hal.newpin('hg-set-zero-offset', hal.HAL_BIT, hal.HAL_OUT)
        self.hal.newpin('hg-present', hal.HAL_BIT, hal.HAL_IN)
        self.hal.newpin('hg-debug', hal.HAL_BIT, hal.HAL_OUT)
        self.hal.newpin('hg-enable', hal.HAL_BIT, hal.HAL_OUT)
        self.hal.newpin('hg-has-zero-button', hal.HAL_BIT, hal.HAL_IN)
        self.hal.newpin("probe-active-high", hal.HAL_BIT, hal.HAL_OUT)
        self.zero_height_gauge_visible = True
        if 'sim' in config: self.hal.newpin("probe-sim", hal.HAL_BIT, hal.HAL_OUT)
        self.hal.newpin("mesa-watchdog-has-bit", hal.HAL_BIT, hal.HAL_IO)
        self.hal.newpin("cycle-time-hours", hal.HAL_U32, hal.HAL_IN)
        self.hal.newpin("cycle-time-minutes", hal.HAL_U32, hal.HAL_IN)
        self.hal.newpin("cycle-time-seconds", hal.HAL_U32, hal.HAL_IN)
        # commanded speed feedback for Spindle DROs during g code program exectuion
        self.hal.newpin("spindle-speed-out", hal.HAL_FLOAT, hal.HAL_IN)
        self.hal.newpin("machine-ok", hal.HAL_BIT, hal.HAL_IN)
        self.hal.newpin("home-switch-x", hal.HAL_BIT, hal.HAL_IN)
        self.hal.newpin("home-switch-y", hal.HAL_BIT, hal.HAL_IN)
        self.hal.newpin("home-switch-z", hal.HAL_BIT, hal.HAL_IN)
        self.hal.newpin("home-switch-enable", hal.HAL_BIT, hal.HAL_OUT)
        #atc pins
        self.hal.newpin("atc-hal-request", hal.HAL_FLOAT, hal.HAL_OUT)
        self.hal.newpin("atc-hal-data", hal.HAL_FLOAT, hal.HAL_OUT)
        self.hal.newpin("atc-hal-return", hal.HAL_FLOAT, hal.HAL_IN)
        self.hal.newpin("atc-hal-busy",hal.HAL_BIT,hal.HAL_IN)
        self.hal.newpin("atc-device-status", hal.HAL_BIT, hal.HAL_IN)
        self.hal.newpin("atc-pressure-status", hal.HAL_BIT, hal.HAL_IN)
        self.hal.newpin("atc-tray-status", hal.HAL_BIT, hal.HAL_IN)
        self.hal.newpin("atc-vfd-status", hal.HAL_BIT, hal.HAL_IN)
        self.hal.newpin("atc-draw-status", hal.HAL_BIT, hal.HAL_IN)
        self.hal.newpin("atc-tray-position", hal.HAL_FLOAT, hal.HAL_IN)
        self.hal.newpin("atc-ngc-running", hal.HAL_BIT, hal.HAL_IN)

        # usbio board pins for board one
        self.hal.newpin("usbio-enabled", hal.HAL_BIT, hal.HAL_OUT)
        self.hal.newpin("usbio-input-0", hal.HAL_BIT, hal.HAL_IN)
        self.hal.newpin("usbio-input-1", hal.HAL_BIT, hal.HAL_IN)
        self.hal.newpin("usbio-input-2", hal.HAL_BIT, hal.HAL_IN)
```

```
        self.hal.newpin("usbio-input-3", hal.HAL_BIT, hal.HAL_IN)
        self.hal.newpin("usbio-output-0", hal.HAL_BIT, hal.HAL_IN)
        self.hal.newpin("usbio-output-1", hal.HAL_BIT, hal.HAL_IN)
        self.hal.newpin("usbio-output-2", hal.HAL_BIT, hal.HAL_IN)
        self.hal.newpin("usbio-output-3", hal.HAL_BIT, hal.HAL_IN)

        # usbio status for all boards as a group
        self.hal.newpin("usbio-status",hal.HAL_S32, hal.HAL_IN)

        #manual control of smart_cool nozzle - hot key connected
        self.hal.newpin("smart-cool-man-auto", hal.HAL_BIT, hal.HAL_OUT)
        self.hal.newpin("smart-cool-up", hal.HAL_BIT, hal.HAL_OUT)
        self.hal.newpin("smart-cool-down", hal.HAL_BIT, hal.HAL_OUT)
        # prompting communication - all responses to Gremlin messages or NGC prompts set this pin
        #   used by ATC
        self.hal.newpin("prompt-reply", hal.HAL_FLOAT, hal.HAL_OUT)
        self.hal.ready()
        # errors
        self.error_handler = error_handler(self.builder, self.moving, self.hal)
        # g code file history combo box
        self.file_history_liststore = gtk.ListStore(str, str)
        self.loaded_gcode_filename_combobox = self.builder.get_object("loaded_gcode_combobox")
        self.loaded_gcode_filename_combobox.set_model(self.file_history_liststore)
        cell = gtk.CellRendererText()
        self.loaded_gcode_filename_combobox.pack_start(cell, True)
        self.loaded_gcode_filename_combobox.add_attribute(cell, 'text', 0)
        try:
            for i in range(0, self.redis.llen('recent_file_history')):
                # file history liststore is in form of ['filename', 'path'], but redis only stores the path
                path = self.redis.lpop('recent_file_history')
                self.file_history_liststore.append([os.path.basename(path), path])
        except:
            self.error_handler.write("Retrieval of recent file history failed.", ALARM_LEVEL_DEBUG)
            pass
        self.file_history_liststore.append([CLEAR_CURRENT_PROGRAM, CLEAR_CURRENT_PROGRAM])
```

''PostGui.py''

```
# Include your customized HAL commands here
# The commands in this file are run after the GUI starts and has the opportunity to create the needed pins

# connect spindle belt position UI to spindle comp
net spindle-range              tormach.spindle-range
net spindle-range-alarm        tormach.spindle-range-alarm

# spindle RPM derived by spindle comp
net spindle-speed-fb-rpm       tormach.spindle-speed-out

# spindle type
net spindle-type               tormach.spindle-type

# these let the UI read the current min/max speeds the comp maintains based on spindle type
net spindle-min-speed          tormach.spindle-min-speed
net spindle-max-speed          tormach.spindle-max-speed

# these let the UI write the comp values for hispeed min/max
net spindle-hispeed-min        tormach.spindle-hispeed-min
net spindle-hispeed-max        tormach.spindle-hispeed-max

net spindle-disable            tormach.spindle-disable

# enclosure door switch
net enc-door-switch-status     tormach.enc-door-switch-status
net enc-door-switch-configured   tormach.enc-door-switch-configured
net enc-door-open-max-rpm      tormach.enc-door-open-max-rpm
net spindle-on                 tormach.spindle-on

# coolant
net coolant-flood              tormach.coolant
net coolant-flood-io           tormach.coolant-iocontrol
```

```
#mist
net coolant-mist               tormach.mist
net coolant-mist-io             tormach.mist-iocontrol

#SMART COOL COMPONENTS and PINS
 net coolant-flood             zbotschnozz.coolant
 net coolant-mist              zbotschnozz.mist

# this connects the GUI to the signals from the milljogtranslator/shuttlexpress
net sxp.xen-button          => tormach.jog-axis-x-enabled
net sxp.yen-button          => tormach.jog-axis-y-enabled
net sxp.zen-button          => tormach.jog-axis-z-enabled
net sxp.aen-button          => tormach.jog-axis-a-enabled
net sxp.step-button         => tormach.jog-step-button
net sxp.jog-ring-speed-signed => tormach.jog-ring-speed-signed
net sxp.selected-axis       => tormach.jog-ring-selected-axis
net sxp.counts-smoothed      => tormach.jog-counts
net sxp.gui_step_index      <= tormach.jog-gui-step-index
net sxp.is_metric           <= tormach.jog-is-metric

# digital height gauge
net thg-net-height tormachheightgauge.net-height          => tormach.hg-height
net thg-zero-offset tormachheightgauge.zero-offset        => tormach.hg-zero-offset
net thg-button-pressed tormachheightgauge.button-pressed   => tormach.hg-button-pressed
net thg-button-changed tormachheightgauge.button-changed   => tormach.hg-button-changed
net thg-mm-mode tormachheightgauge.mm-mode                => tormach.hg-mm-mode
net thg-set-zero-offset tormachheightgauge.set-zero-offset => tormach.hg-set-zero-offset
net thg-present tormachheightgauge.present                => tormach.hg-present
net thg-debug tormachheightgauge.debug                    => tormach.hg-debug
net thg-enable tormachheightgauge.enable                  => tormach.hg-enable
net thg-has-zero-button tormachheightgauge.has-zero-button => tormach.hg-has-zero-button

# probe input active level control
net probe-active-high                           => tormach.probe-active-high

# GUI status LEDs
net machine-ok => tormach.machine-ok

# limit switch status
net home-limit-x-raw => tormach.home-switch-x
net home-limit-y-raw => tormach.home-switch-y
net home-limit-z-raw => tormach.home-switch-z
net limit-switch-enable => tormach.home-switch-enable

# Mesa card watchdog
net hm2_5i25.0.watchdog.has-bit => tormach.mesa-watchdog-has-bit

loadrt time
addf time.0 servo-thread
net prog-running prog-not-idle.in <= halui.program.is-idle
net cycle-timer time.0.start <= prog-not-idle.out
net cycle-seconds tormach.cycle-time-seconds <= time.0.seconds
net cycle-minutes tormach.cycle-time-minutes <= time.0.minutes
net cycle-hours tormach.cycle-time-hours <= time.0.hours
# Z-Bot ATC Pins to motion contoller DIO , AIO stuff
#command and control
net atc-request-ngc motion.analog-out-04 =>  zbotatc.0.ain.0.request
net atc-data-ngc    motion.analog-out-05 =>  zbotatc.0.ain.1.request_data
net atc-status  motion.digital-in-16 <=  zbotatc.0.dout.5.exec_status
net atc-status  tormach.atc-hal-busy <=  zbotatc.0.dout.5.exec_status
net atc-retcode motion.analog-in-05     <=  zbotatc.0.aout.0.request_rc
net atc-retcode tormach.atc-hal-return  <=  zbotatc.0.aout.0.request_rc
#hardware status variables
net atc_tray-in  motion.digital-in-17    <= zbotatc.0.dout.0.tray_status
net atc_tray-in  tormach.atc-tray-status <= zbotatc.0.dout.0.tray_status
net atc-vfd      motion.digital-in-18   <= zbotatc.0.dout.1.vfd_status
net atc-vfd      tormach.atc-vfd-status <= zbotatc.0.dout.1.vfd_status
```

```
net atc-draw-bar motion.digital-in-19    <= zbotatc.0.dout.2.draw_status
net atc-draw-bar tormach.atc-draw-status <= zbotatc.0.dout.2.draw_status
net atc-pressure motion.digital-in-20       <= zbotatc.0.dout.3.pressure_status
net atc-pressure tormach.atc-pressure-status <= zbotatc.0.dout.3.pressure_status
net atc-slot     motion.analog-in-06      <= zbotatc.0.aout.1.tray_position
net atc-slot     tormach.atc-tray-position <= zbotatc.0.aout.1.tray_position
#hardware status variables
net atc-device   motion.digital-in-21     <= zbotatc.0.dout.4.device_status
net atc-device   tormach.atc-device-status <= zbotatc.0.dout.4.device_status
net atc-ngc-running motion.digital-out-16  => tormach.atc-ngc-running
net atc-loop-back    zbotatc.0.aout.2.request_ack  => motion.analog-in-07
# USBIO
net usbio-enabled tormach.usbio-enabled => usbio.enabled
net dig-out-0 tormach.usbio-output-0
net dig-out-1 tormach.usbio-output-1
net dig-out-2 tormach.usbio-output-2
net dig-out-3 tormach.usbio-output-3
net dig-in-0 tormach.usbio-input-0
net dig-in-1 tormach.usbio-input-1
net dig-in-2 tormach.usbio-input-2
net dig-in-3 tormach.usbio-input-3
# HAL pins for GUI access to IO and motion for reading line numbers
net motion-program-line   tormach.motion-program-line     <= motion.program-line
net motion-next-program-line   tormach.motion-next-program-line     <= motion.next-program-line
net motion-completed-program-line   tormach.motion-completed-program-line     <= motion.completed-program-
line
# prompting data
net prompt-channel tormach.prompt-reply => motion.analog-in-10
# IOB notification for errors
 net iob-status usbio.IOB-OK => tormach.usbio-status
#Smart Cool keyboard override pins
net sc_override  tormach.smart-cool-man-auto    => zbotschnozz.man-auto
net sc_up        tormach.smart-cool-up          => zbotschnozz.cool-up
net sc_down      tormach.smart-cool-down        => zbotschnozz.cool-down

# Arduino pendant wiring

setp halui.spindle-override.direct-value TRUE
net spinor arduino.analog-in-00 => halui.spindle-override.counts => tormach.spindle-over-counts
setp halui.spindle-override.scale .0015

# Arduino pendant wiring

setp halui.feed-override.direct-value TRUE
net feedor arduino.analog-in-01 => halui.feed-override.counts => tormach.feed-over-counts
#setp halui.feed-override.scale .0015

# Arduino pendant wiring

setp halui.max-velocity.direct-value TRUE
net maxvelor arduino.analog-in-02 => halui.max-velocity.counts => tormach.maxvel-over-counts
setp halui.max-velocity.scale .003
```

Arduino

Arduino sketch: Sketch loaded on Arduino for communicating with pathpilot with delay and switch to avoid bugging the controller down with excessive input commands.

```
void setup() {
   Serial.begin(9600);
   pinMode(12,INPUT_PULLUP);
   pinMode(13,OUTPUT);
}

unsigned long  startTime = 0;
unsigned long  endTime = 0;
unsigned long  TimeTaken = 0;
uint8_t adc=0;
uint8_t firstbyte=0;
uint8_t pinmap[6] = {2,4,7,8,12,13}
```

```
;
uint8_t dacpinmap[6] = {3,5,6,9,10,11};
void loop() {

   if (digitalRead(12))  // value stream allowed
     {
     digitalWrite(13,1);
     uint16_t v = analogRead(adc) | (adc << 11);
     if(digitalRead(pinmap[adc])) v |= (1<<10);
     Serial.write("-");
     Serial.write("-");
    // Serial.write((v >> 7) | 0x80);
    // Serial.write(v & 0x7f);
     adc = (adc + 1) % 6;
//   delay(1); // to avoid bogging PPilot with data
     }
   else digitalWrite(13,0);

   endTime = micros();
  // TimeTaken =  endTime - startTime;
   Serial.print("Total time per loop: ");
   Serial.print(endTime);

}
```

Appendix C

How to boot *pathpilot* with Arduino connected.

With the Arduino connected to a high-speed USB port on the CNC controller, the PC is powered up and the Arduino switch is put in the 'ON' position.

From start-up of the PC, after the initialization pages and before the *Tormach* logo appears, hold down Alt + Shift to get into the "back end" mode.

Go to **PLACES** folder >> **HOME** folder >> **TMC** folder

(1) Under TMC, open **CONFIGS** >> open ''tormach_mill_5i25.hal''. In this script, check / uncheck line 30 OR ctrl + F (Arduino) to find the line to check/ uncheck.

(2) Return to CONFIGS >> open ''postgui_tormach_mill.hal''. CTRL + F (Arduino) under Arduino pendant wiring, uncheck all three lines after the Arduino header for all three versions. This is where the slider hal components are created and the scaling factors can be edited from here. Lines to be checked/ unchecked should correspond to **157 -159; 163-165, 169-171**. When Arduino is connected, they should be unchecked.

(3) Return to TMC folder >> open **PYTHON** folder. Under this folder, open ''tormach_mill_ui.py''. In this folder uncheck lines **7728, 7729 AND 7730** for scale controls with Arduino. Check lines **2701, 2709, 2718 and 2719.**

When done, click on the run button, and on the dialog screen, type ''. /operator_login'' (use the UP cursor to bring this up automatically), then Enter to run.

Appendix D

Preliminary cutting force results from using load cells with HX711 amplifier

Towards developing a low-cost alternative for force feedback measurements, four 50kg load sensor interfaced with a HX711 load cell amplifier was connected to an Arduino Uno and incorporated in a fabricated rig. A sketch was generated on the Arduino to get outputs of the load cell during operation. The set-up gave an insight into the type of data that can be collected, and the responsiveness of the sensor used in the set up. The experiment was also towards determining the effects of variation in spindle speed on cutting forces. Data collected was analysed and is shown below. The spindle speed was kept at 1000 rev/ min with the slider control adjusted to take values at percentages of the spindle speed values. Values were taken at 15, 25, 50 and 75 all percentages of the spindle speed selected. An analysis of the plot shows the data showed minimal variation and data was descriptive of the process conditions. The corresponding spindle speed values are shown in the following table,

	Spindle speed
A	150
B	250
C	500
D	750

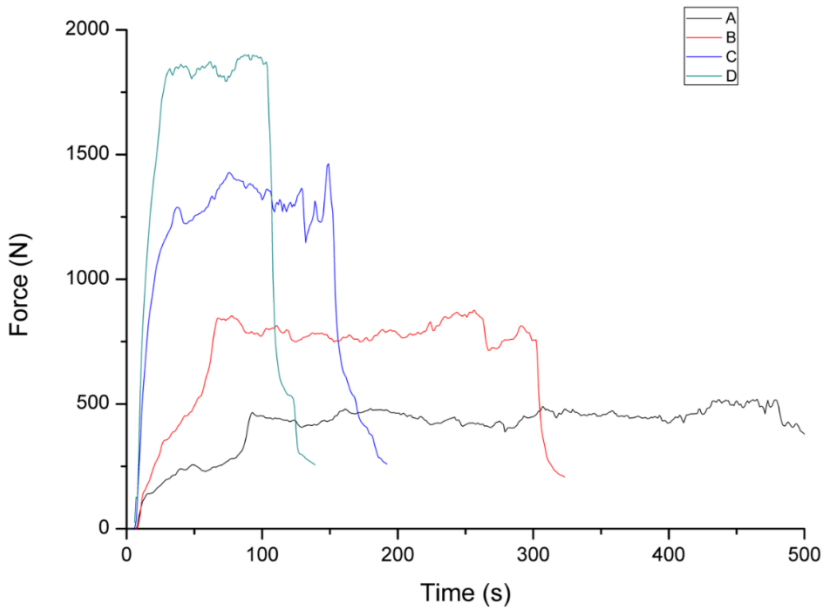


Figure 0-1 : force measurements showing variation with spindle speed adjustment. Increase in spindle speed leads to higher cutting force

Appendix E

This page has been left intentionally blank and the following pages are journal publications not included in this study but formed a substantial part of work carried out during the study period.

euspen's 19th International Conference & Exhibition, Bilbao, ES, June 2019
www.euspen.eu

Multi-sensor data fusion for the characterisation of laser cladded cermet coatings

Giacomo Maculotti[1], Nicola Senin[2,4], Olusola Oyelola[3], Maurizio Galetto[1], Adam Clare[3], Richard Leach[2]

[1]*Dipartimento di Ingegneria Gestionale e della Produzione, Politecnico di Torino, Italy*
[2]*Manufacturing Metrology Team, Faculty of Engineering, University of Nottingham, UK*
[3]*Advanced Component Engineering Laboratory, Faculty of Engineering, University of Nottingham, UK*
[4]*Dipartimento di Ingegneria, Università di Perugia, Italy*

giacomo.maculotti@polito.it

Abstract

In this work, we investigate the use of multi-sensor data fusion to characterise innovative materials combined with advanced manufacturing processes. A metal matrix composite coating produced by directed energy deposition, more specifically a Ti-6Al-4V (WC/W2C) cermet, obtained from titanium-alloy metal wire and tungsten carbide ceramic powder is selected as the test case. A wide-spectrum characterisation of chemical, microstructural, surface and mechanical properties is needed to investigate relationships with manufacturing process parameters. As multiple measurement technologies are therefore needed, a multi-sensor data fusion approach is discussed. For the test case, scanning electron microscopy, optical areal topography measurement, energy dispersive X-ray spectrometry and instrumented indentation testing to measure nano-hardness are integrated to obtain topography,microstructure, geometrical and chemical properties of the constituent phases and their spatial arrangement. The proposed method for multi-sensor data fusion focuses on co-localisation as a means to enable correlation of the datasets. In this work, the method is applied in particular to the investigation of the phases in the laser deposited cermet, and of the interfaces where the phase transitions take place.

Multi-sensor data fusion, cermet, laser cladding

1. Introduction

The need to develop highly engineered materials in combination with advanced manufacturing processes is one of the main drivers of technological innovation, with numerous applications in aerospace, automotive, biomedical and other sectors [1].

In particular, at early stages of the product-process development process, a thoroughcharacterisation is essential to understand how the material, and hence the final product, is affected by the manufacturing process, and ultimately the mechanical properties it will have in its final form. When the processed material assumes a multi-phase configuration, a thorough characterisation usually implies the investigation of the individual phases, their reciprocal interaction, and their overall layout within the product, for example observed via cross-sectioning [2]. Multiple heterogeneous measurement technologies can be used, such as scanning electron microscopy (SEM), optical areal surface topography measurement, X-ray computed tomography, energy dispersive X-ray spectrometry (EDX), and X-ray diffraction. In parallel, mechanical properties, e.g. hardness, can be investigated by means of dedicated tests.

An opportunity to improve our knowledge and understanding lies in the capability of integrating multiple sources of experimental information. However, integration of measurement results presents significant challenges due to the heterogeneity of the information sources, and the need to reciprocally localise information content within the same co-ordinate space so that correlations can be made.

In this work, an original multi-sensor data fusion approach is presented, focused on spatial co-localisation of datasets as a fundamental precondition to enable the development of correlation models.

2. Sample description

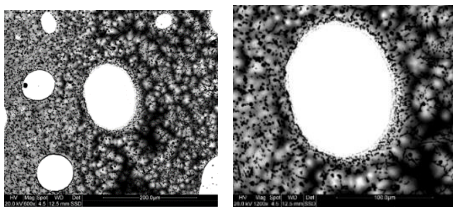
A metal matrix composite material obtained from titanium-alloy metal wire and tungsten carbide ceramic powder, i.e. Ti-6Al-4V (WC/W2C) cermet, is selected as the test case. The material is deposited in multiple layers to produce a coating by means of laser deposition, a beam deposition process [3]. Multi-layer cermets, such as the one studied in this work, are becoming increasingly popular where wear, thermal management, enhanced structural stiffness and hardness are critical [4], thus the problem of their characterisation is of significant importance [5]. In this work, the analysis focuses on the investigation of the interfaces between the metal matrix and the ceramic particles, the main phases in the deposited cermet. The interfaces are important as they feature varying microstructural and mechanical properties, due to solid state diffusion of ceramic material into the metal matrix, yielding to hardness gradients. The geometrical and physical conformation and spatial distribution of the particles, along with surface topography, hardness and hardness gradient as observed in cross-sections of the coating layers, are important characterisation targets as they affect overall material properties. These targets depend on process parameters, and thus are also important for process control.

of Nottingham. The methods and apparatus used in producing the specimen have been previously described [6].

3. Sources of measured data

Multiple sources of measured data were considered in this work: SEM and EDX for microstructural imaging and qualification of chemical composition, coherence scanning interferometry (CSI) for optical areal surface topography measurement, and instrumented indentation testing (nano-IIT) to characterise hardness in the nanometre range.

SEM, in backscatted electron measurement mode, can be used to distinguish amongst different constituent phases of the material, despite limitations due to poor correlation between phase and grey level in the generated SEM images [7,8]. In this work, SEM imaging was performed with an acceleration voltage of 20 keV at different magnifications, i.e. 10 000×, 1200× and 600×, resulting in a lateral resolutions of 46 nm/pixel, 111 nm/pixel and 222 nm/pixel respectively. Fig. 1 shows example SEM images at 600× and 1200×.



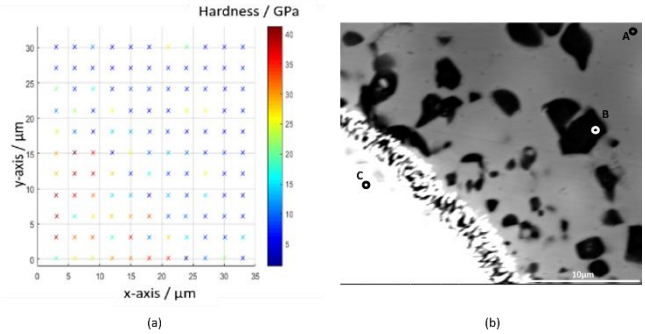
(a) (b)

Figure 1. Example SEM images at different magnification showing the cermet cross-section (ceramic particles, i.e. the WC phase, appear bright): (a) 600× and (b) 1200×.

EDX qualifies the chemical composition of the phases by measuring the energy and the number per type of diffracted X-rays. EDX is performed on points selected by the operator on a SEM image, see Fig.2(b). Thus, SEM and EDX datasets feature the same coordinate reference system if generated as part of the same measurement session with the same instrument. In this work, a SEM and EDX Philips FEI XL30 was used, at the Nanoscale and Microscale Research Centre, University of Nottingham.

Nano-IIT continuously measures the applied force and the indenter displacement in the material during the indentation test, and can be used to evaluate hardness, Young's modulus, creep and relaxation at grain scale, with micrometre lateral resolution. A series of nano-IIT tests performed at different positions over a plane allow the distinguishing of material phases and creation of phase maps [9–10]. Nano-IIT was performed using a Hysitron TI950 at the Instituto Italiano di Tecnologia of Turin, Italy. To provide significant testing area and high lateral resolution of nano-hardness values, a grid of 11×9 indentations at 1 mN maximum cycle test force was performed, resulting in an area of (30 × 25) µm. The horizontal axes transducers of the selected nano-IIT instrument allow localisation of the indentations in a co-ordinate space, with nominal positional accuracy of 1 µm. In Fig. 2, an indentation map is shown along with a SEM image at 10 000× magnification, where some indentation marks are visible (to cover the whole grid of indentations, multiple images at this magnification are necessary). Visible indentation marks were selected as reference positions for EDX.

Example EDX results are shown in Table 1 for the three inspected points highighted in Figure 2(b): the white region in the bottom left of the SEM image in Figure 2(b) is representative of the WC phase, the grey regions represent the metal matrix, the black regions indicate a second phase of TiC-W precipitates.



(a) (b)

Figure 2. Nano-IIT processed area. (a) nano-hardness map, colour is proportional to measured nano-hardness; (b) SEM at 10 000×: some of the indendation marks are barely visible.

Table 1. EDX Results. Elemental composition (wt %) for the three example points shown in Fig. 2(b).

Region	C	Al	Ti	V	W
A	27.55	3.67	47.06	2.80	18.92
B	29.01	0.97	64.53	1.12	4.36
C	28.59	-	-	-	71.41

Nano-IIT requires the sample cross-section to be ground and polished [11], leading to highly reflective surfaces whose topographies are suitable for capturing via CSI measurement [12]. Surface topography was measured with a Zygo NewView 8300, at the Manufacturing Metrology Team laboratory, University of Nottingham. Because the nano-indentation marks were barely visible given the lateral resolution of the CSI even with the 50× objective, CSI measurement had to be performed without precise referencing to the grid. To compensate for this, CSI measurements were perfomed to cover a wider area of (640 × 1000) µm so that larger, visible landmarks could be incoporated, useful for co-localisation. A wide area was obtained by measuring 2×3 FOVs, each sized (0.43 × 0.43) µm, using a 20× objective with lateral resolution, evaluated according to the Sparrow criterion, of 0.63 µm; Fig. 3 shows one FOV.

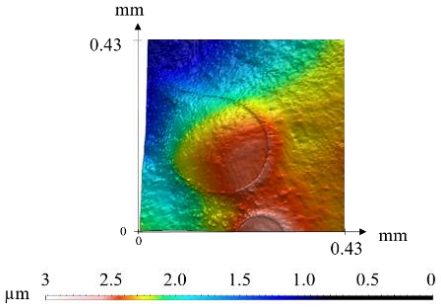


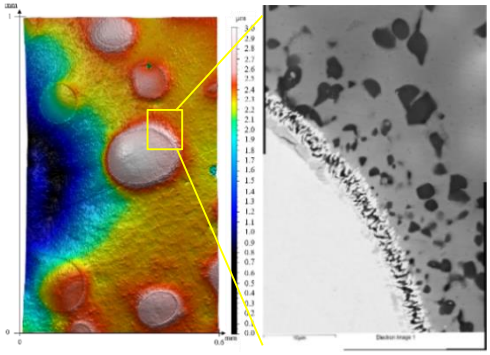
Figure 3. CSI pseudocolour height map (single FOV at 20×) showing a region of the sample cross-section. A large ceramic particle and its interface are visible.

4. Multi-sensor data fusion

Despite being heterogeneous in content and organisation (structure and format), all the discussed datasets feature spatially localised information, despite not necessarily sharing the same co-ordinate systems. The

4.1. Fusion of image-like, homogeneous datasets

Datasets formatted like digital images and obtained from the same instrument and same set-up, but possibly referring to different regions of interest (ROIs), can benefit from co-localisation within a common co-ordinate space, for example to extend coverage range without sacrificing resolution. Fusion of image data with partially overlapping ROIs (referred to as stitching), can be implemented on optical and non-optical images, and also on height maps. In this work, stitching of SEM images (see example in Fig 4(b)) was implemented with a custom-developed method consisting of alignment of pairwise-matched landmarks algorithmically identified via the SIFT method [13]. Stitching of CSI maps (e.g. see Fig.4(a)) was implemented instead using surface metrology software integrated with the CSI instrument.



(a) (b)

Figure 1. Stitched datasets obtained by (a) CSI at 20× and (b) SEM at 10 000×.An approximate indication of localisation of the SEM ROI within the area covered by CSI is provided as a qualitative reference by the yellow box.

4.2. Co-localisation of heterogeneous datasets

In some simpler cases, heterogeneous datasets may not need co-localisation. For the test case, this happened with EDX measurements, because the measurement positions were selected on SEM images taken with the same instrument, same set-up and within the same measurement session, thus they shared a common co-ordinate system. Usually, though, heterogeneous datasets are obtained from different instruments and in the absence of a common spatial reference frame; thus, co-localisation is necessary.

Similarly to stitching, the main facilitator for co-localisation of heterogeneous datasets is the presence of landmarks shared within overlapping segments of the ROIs.

However, landmarks are suitable to support co-localisation only if represented and recogniseable within each dataset, which may not necessarily be the case for measurements that may target different properties and react differently to the measured sample, thus ultimately capturing different aspects of the same landmark, or none at all. When pairwise matching of landmarks is possible and reliable, then heterogeneous datasets can be co-localised by solving the absolute orientation problem [14]: i.e. by finding the transformation matrix that minimises the root mean squared error (RMSE) between pairwise-matched points.

For the co-localisation of the SEM images, CSI height maps and nano-IIT maps, a simpler, two-dimensional version of the absolute orientation problem was adopted, with the optimal transformation constrained to take place in the *x,y* image plane. In the two-dimensional case, the rotation matrix is driven by one angle α and the pivot point (x_0, y_0), the translation defined by vector t and a scale vector (s_x, s_y) compensates for potential global magnification errors in the two axes of the SEM or CSI image, thus resulting in Eq.1 which describes the two-dimensional version of the absolute orientation problem:

$$\begin{bmatrix} x' \\ y' \\ 1 \end{bmatrix} = [S] \begin{bmatrix} x \\ y \\ 1 \end{bmatrix} = [s_x \quad s_y \quad 1] \begin{bmatrix} \cos(\alpha) & \sin(\alpha) & -x_0 + t_x \\ -\sin(\alpha) & \cos(\alpha) & -y_0 + t_y \\ 0 & 0 & 1 \end{bmatrix} \begin{bmatrix} x \\ y \\ 1 \end{bmatrix} \quad (1)$$

For the test case, the co-localisation of nano-IIT, SEM and CSI datasets was performed in steps. At a first stage, the nano-IIT dataset was localised in the co-ordinate system of the 10 000× stitched SEM image. Pairwise-matched points for alignment were identified from the coordinates of the nano-IIT indentations on one side, and the centroids of the visible indentation marks in the SEM image on the other. Because most indentation marks were barely visible in the SEM image, and algorithmic identification [15] would be frequently disturbed by the presence of larger and better-contrasted regions, localisation of indentation centroids in SEM was preliminarly performed manually, though better algorithmic solutions are currently being studied. The transformation matrix to maximise overlapping of pairwise-matched points was computed automatically, considering in a first step all visible indentation marks. To furter refine the co-localisation, a second alignment pass was performed, based again on solving the same absolute orientation problem, but this time only considering a subset of pairwise matched indentation centroids, selected as the closest to each other after the first alignment step [16].

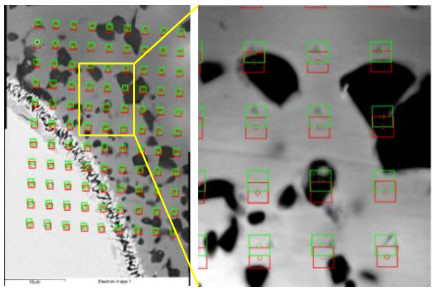
Alignment results were computed taking into account also positional uncertainty in the nano-IIT dataset. Fig. 5 shows the co-localisation results at two different scales. A coloured box is drawn about each nano-IIT indentation centroid to represent location uncertainty originated by the positioning error of the nano-IIT system: it can be noted that most of the indentation marks visible in the aligned SEM image fall within the boxes, indicating an acceptable co-localisation result.

The second stage of the multi-sensor data fusion co-localisation process consisted of positioning the SEM datasets (600×, 1200× and 10 000×) within the co-ordinate reference frame of the CSI dataset (20×), and was also based on identification of pairwise-matched landmark points and alignment via resolution of the absolute orientation problem.

However, not all the SEM datasets would feature landmarks easily visible within the CSI dataset, because of the sometimes large scale differences (e.g. between 20× CSI and 10 000× SEM). Therefore, a first co-localisation was performed to align the lowest magnification SEM dataset (600×) to the CSI dataset. For this co-localisation, the transition edges between phases, i.e. the boundaries of the ceramic particles visible in both datasets, were used as alignment landmarks. The edges were recognised automatically both on SEM images (on gray levels) and CSI maps (on height values) by application of a LoG (Laplacian of Gaussian) operator [17,18].

Then the 1200× SEM dataset was aligned to the already localised 600× one, and finally the 10 000× SEM dataset was aligned to the 1200× one. Both alignments were performed using pairwise-matched landmarks, both again using inter-phase edges as alignment references. The final transformation matrix found for the 10 000× SEM dataset was also applied to the nano-IIT and EDX data to preserve their prior co-localisation to the SEM set.

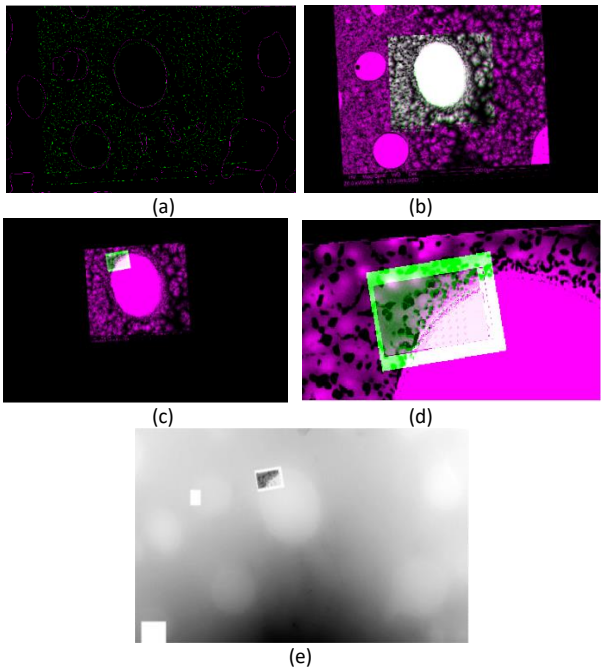
Figure 6 shows some example results of the co-localisation process involving CSI and SEM datasets at multiple magnifications.



(a) (b)

Figure 1. (a) Hardness to SEM registration. Red is coarse alignment, green is fine alignment; boxes represent location uncertainty due to accuracy of nano-IIT platform. (b) Higher detail image of the yellow box.

The final co-localisation error was estimated as 17.6 µm, by combining the individual uncertainties obtained from the respective alignment RMSEs [19]. The individual error contributions are summarised in Table 2. For the test case, Table 2 highlights the alignment of the SEM dataset at 600× to the CSI dataset as the most critical step in terms of error contribution. Clearly a more comprehensive estimation of expanded uncertainty for multi-sensor data fusion has not been achieved yet. Further contributions to consider include stitching, and error associated to the individual measurement instruments (e.g. aberration in SEM images [7] positional uncertainty of the nano-IIT, etc.).



(a) (b) (c) (d) (e)

Figure 2. SEM to CSI co-localisation; images in CSI reference frame (90° counterclockwise rotated with respect to previous figures). (a) 600× SEM (green) to CSI (purple), edges are shown for clarity; (b) SEM 1200× (green) to SEM 600× (purple); (c)) SEM 10 000× (green) to SEM 1200×; (d) detail to highlight the TiC-W precipitates structures exploited for point pairs selection; (e) 10 000× SEM to CSI height map (rendered in grayscale).

Table 2. RMSE contributions of each co-localisation operation.

	nano-IIT to 10,000x SEM (coarse)	nano-IIT to 10,000x SEM (fine)	SEM 600x to CSI	SEM 1200x to CSI	SEM 10 000x to CSI
RMSE / µm	0.48	0.21	17.60	0.43	0.77

5. Conclusions and future work

Multi-sensor data fusion for the wide-spectrum characterisation of innovative materials combined to advanced manfuacturing processes has been investigated. The analysis has focused on a metal matrix composite deposited in the form of a multi-layered coating using laser deposition. The problem of co-localisation of homogeneous and heterogeneous measured datasets has been addressed and the feasilibity of solutions based on alignment of pairwise-matched landmarks has been analysed. Automated identification of landmarks has been found to be the most critical aspect of the method. Preliminary considerations on how to evaluate uncertainty associated with the procedure also indicate that further analyses are needed to take into account a larger number of error sources.

The authors would like to acknowledge funding from EPSRC grant EP/M008983/1 and Dr Massimo Lorusso from Istituto Italiano di Tecnologia for performing the instrumented indentation tests.

References

[1] Schmidt M, Merklein M, Bourell D, Dimitrov D, Hausotte T, Wegener K, Overmeyer L, Vollertsen F, Levy G N 2017 Laser based additive manufacturing in industry and academia *CIRP Ann. – Manuf. Technol.* **66** 561–583.

[2] Bruzzone A A G, Costa H L, Lonardo P M, Lucca D A 2008 Advances in engineered surfaces for functional performance *CIRP Ann. – Manuf. Technol.* **57** 750–769.

[3] Gibson I, Rosen D W, Stucker B 2016 *Additive Manufacturing Technologies* (Berlin: Springer).

[4] Mohanty R M, Roy M 2012 Thermal sprayed WC-Co coatings for tribological application. In: Davim J P *Materials and Surface Engineering* (Sawston, Cambridge, UK: Woodhead Publishing).

[5] Farayibi P K, Abioye T E, Clare A T 2016 A parametric study on laser cladding of Ti-6Al-4V wire and WC/W2C powder *Int. J. Adv. Manuf. Technol.* **87** 3349–3358.

[6] Farayibi P K, Folkes J A, Clare A T 2013 Laser deposition of Ti-6Al-4V wire with WC powder for functionally graded components *Mater. Manuf. Process.* **28** (5) 514–518.

[7] Goodhew P J, Humphreys J, Beanland R 2001 *Electron Microscopy and Analysis* (London: Taylor & Francis).

[8] Gu Y. 2003 Automated scanning electron microscope based mineral liberation analysis *J. Miner. Mater. Charact. Eng.* **2** 33–41.

[9] Barbato G, Genta G, Cagliero R, Galetto M, Klopfstein M J, Lucca D A, Levi R 2017 Uncertainty evaluation of indentation modulus in the nano-range: Contact stiffness contribution *CIRP Ann. – Manuf. Technol*. **66** 495–498.

[10] Haušild P, Materna A, Kocmanová L, Matějíček J 2016 Determination of the individual phase properties from the measured grid indentation data *J. Mater. Res.* **31** 3538–3548.

[11] ISO 14577-1: 2014 *Metallic materials-Instrumented indentation test for hardness and materials parameters - Part 1: Test method* (ISO, Gèneve).

[12] de Groot P 2001 Coherence Scanning Interferometry. In: Leach R K *Optical Measurement of Surface Topography* (Berlin: Springer).

[13] Lowe D G 2004 Distinctive Image Features from Scale-Invariant Keypoints *Int. J. Comput. Vis.* **2** 91–110.

[14] Horn B K P 1987 Closed-form solution of absolute orientation using unit quaternions *J. Opt. Soc. Am. A.* **4** 629-642.

[15] Alcantarilla P F, Bartoli A, Andrew J D. KAZE Features 2010 *Comp. Vis. - ECCVV* 2012 LNCS **7577** 214–227.

[16] Fukunaga K, Narendra P M 1975 A branch and bound algorithm for computing k-nearest neighbors *IEEE Trans. Comput.* **C-24** 750–753.

[17] Sharifi M, Fathy M, Mahmoudi M T 2002 A classified and comparative study of edge detection algorithms *Proc. Int. Conf. Inf. Technol. Coding Comput.* Las Vegas, NV 2002.

[18] Marr D, Hildreth E 1980 Theory of edge detection *Proc. R. Soc. Lond. B* **207** 187–217.

[19] BIPM 2008 *Guide to the expression of uncertainty in measurement (GUM)* JCGM 100 (Sèvres, France: BIPB).

Available online at www.sciencedirect.com

ScienceDirect

Procedia CIRP 45 (2016) 119 –122

www.elsevier.com/locate/procedia

3rd CIRP Conference on Surface Integrity (CIRP CSI)

Machining of Additively Manufactured Parts: Implications for Surface Integrity

Olusola Oyelola[a], Peter Crawforth[b], Rachid M'Saoubi[c], Adam T. Clare [a]*

[a]*Advanced Component Engineering Laboratory, Faculty of Engineering, The University of Nottingham, University Park, Nottingham, NG7 2RD, UK*
[b]*Advanced Manufacturing Research Center, University of Sheffield , Rotherham, S60 5TZ, UK* [c]*Seco Tools (U.K) Ltd., Springfield Business Park , Alcester, Warwickshire, B49 6PU , UK*

* Corresponding author. Tel.: +44 (0) 115 951 4109; Fax: +44 (0) 115 951 3800. *E-mail address:* adam.clare@nottingham.ac.uk

Abstract

Additive manufacturing methods continue to move towards production ready technologies with the widely extolled virtues of rapid transition from design to part and enhanced design freedoms. However, due to fundamental limitations of laser based processes for metal additive manufacturing, there is a significant ongoing need for these parts to be subject to additional machining operations. This paper reports on a study to investigate the machining behavior and surface integrity of Ti-6Al-4V components which have been produced by direct metal deposition using wire feedstocks. Simple geometries are produced and the resulting effect of tooling type is reported. Inhomogeneities in the deposition process as a result of non-uniform cooling and porosity are shown to have a deleterious effect on the surface integrity of the resulting part and the machinability of such components. In addition, strategies for the machining of AM parts which consist of graduated material structures are also proposed here.

© 2016 The Authors. Published by Elsevier B.V. This is an open access article under the CC BY-NC-ND license © 2016 The Authors Published by Elsevier B.V. Peer-review under responsibility of the scientific com (http://creativecommons.org/licenses/by-nc-nd/4.0/). y (
Peer-review under responsibility of the scientific committee of the 3rd CIRP Conference on Surface Integrity (CIRP CSI)

Keywords: Additive Manufacturing; Machining; Titanium, Microstructure

Introduction

Laser deposition is widely used in the manufacture and repair of metallic parts. The process provides a means for components of intricate geometry and desired properties to be manufactured through the use of a laser beam with material being delivered into the laser path on the desired substrate [1]. A number of factors including; alloying control, surface finish requirements and engineering tolerances mean most additive manufacturing techniques are only capable of producing near net shape components. There is often a need for further processing of Additive Manufacturing (AM) parts, therefore finish machining of such components has become imperative to satisfy these requirements. This has led to the development of hybrid systems capable of both building a part and machining the component to a suitable finish within the same work enclosure. This has been used to good effect for new part manufacture and part repair [2,3,4]. Reduction of material wastage is also a key driver in the use of AM, thus the need for post processing through subtractive methods should also be minimised.

Ti-6Al-4V is presently the most widely used titanium alloy and is commonly sought by a majority of metal AM users. Its use accounts for 50% of titanium tonnage in the world [5].The (α)-(β) microstructure of this alloy allows for high strength and formability. Laser cladding of Ti-6Al-4V in wire feedstock and powder form has been successfully undertaken by various authors [6,7,8]. Laser clad Ti-6Al-4V has also been reported to show a grain morphology differing from conventional cast Ti-6Al-4V as a result of the cooling process it undergoes. Solidification and cooling during the laser deposition process is rapid due to the thermal differential between the melt-pool and the previously solidified material/substrate [9]. Thus, for laser deposited Ti-6Al-4V, a Widmanstatten or martensitic structure (columnar growth) has been reported [10], whilst metal-mold cast Ti-6Al-4V form an equiaxed prior grain beta morphology [11].

Titanium and its alloys have been widely regarded as rather difficult to machine materials due to their highly reactive nature, low thermal conductivity, the relatively low modulus

of elasticity and ability to retain hardness at high temperatures [12]. During machining, titanium alloys tend to weld to the cutting tool –formation of a built up edge (BUE); this consequently leads to tool chipping and consequently, shorter tool life. The low thermal conductivity property also adversely affects tool life as the temperature at the tool-workpiece interface remains elevated due to the heat generated not being transmitted through the workpiece or with the chips generated but rather through the tool. In machining operations such as grinding, even with the use of proper process parameters and conditions, there is a high susceptibility to reduction of fatigue strength due to surface damage [13] such as micro cracks, plastic deformation amongst others.

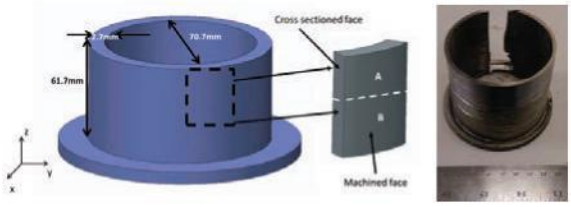
The purpose of this work is to investigate the changes in microstructure and thus properties after additively manufactured Titanium alloy is machined using two different tool types, since material properties are distinct and variable when compared to conventionally produced feedstocks. Knowledge of this aids in the design of the laser processing stage and also in the decisions on how best to carry out the post processing steps when required.

In the machining of Ti-6Al-4V, as with the properties of other titanium alloys, low cutting speed and high coolant pressure is necessary to achieve superior results due to the properties highlighted above. Other authors have demonstrated the use of various inserts with varying combination of feed and depth of cut with low cutting speeds [14,15] which have informed the parameters and conditions used in this study.

Experimental

In the Direct Metal Deposition (DMD) process used here, a 1.2mm diameter Ti-6Al-4V wire is used as the feedstock material. The wire is fed into a laser beam defocused to produce a beam spot diameter of 3.1mm. A 5mm thick Ti alloy plate was used as the substrate. The set-up was shielded in an Argon enclosure to prevent oxidation of the resulting deposits. These were also allowed to cool under this condition. To adequately mimic an industrial application of the process and with the post process machining process in mind, a circular first layer was built with optimum process parameters obtained from a previous study [8]. Subsequent passes with the relevant step up heights were made on the initial circular base produced. The resulting cylinder has an internal diameter of 70 ±0.5mm and an external diameter of 73 ±0.5mm with wall thickness 2.7±0.5mm and height of 61.7±0.5mm.

Figure 1: CAD figure and the cylinder after cross- section.



The cylinder was thereafter subjected to outside diameter turning operations. Two different inserts were used in machining two regions of the cylinder. The objective being to determine the effects of using coated and uncoated inserts on the workpiece generated. Both operations were carried out using identical machining parameters (shown in table 1). The coated insert was a PVD TiAlN based coated cemented carbide grade TS2000 with geometry: ISO CNMG120408-MF1. The uncoated insert had the same specifications and tool geometry. In both operations, coolant (HOCUT 795B) was delivered at a rate of 13 litres / min.

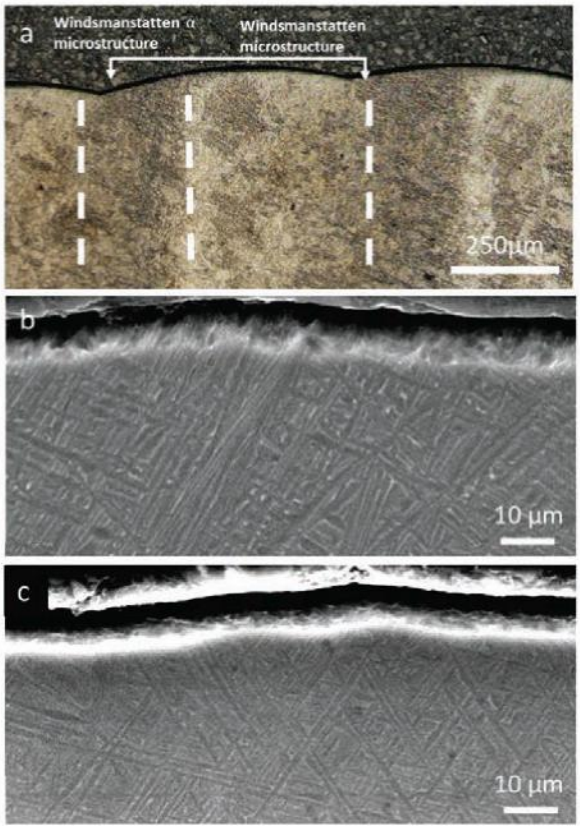
The two areas are referred to as ‘’A” for the region with the uncoated tool and ‘’B” for the region machined with the coated tool.

Results

Table 1: Turning operation parameters.

Cutting Speed	70m / min
Feed Rate	0.15mm/ rev
Depth of Cut	1.25mm

Metallurgical analysis of the clads showed two distinct microstructures within the clads. The structures observed coincided with the clad periphery (zone of re-melting) and within the clad itself. The structures were predominantly Widmanstatten patterns with varying degree of coarseness. The re-melted regions had larger grain size due to the effect of re-melting- this corresponds to a Widmanstatten α morphology. The other regions was however a basket weave Widmanstatten structure without the α segregation



.Figure 2:(a) Profile without machining showing variable microstructure,(b) region machined with a coated insert(c) region machined with uncoated insert.

The regions between clads would be expected to show elevated hardness figures due to their more coarse micro structures and the tendency for work hardening within these regions. These regions retained their structure after the machining process as the transus temperature was not reached. It is anticipated that the difference in microstructures within this region might lead to a variation in cutting force requirements during machining. The effect of this on the cutting tool is also thought to be significant in extended use but does not form part of this study. After machining, the microstructure at the interface (Figures 2b and 2c), remains largely consistent.

Surface Roughness

A white light interferometer was used in determining the surface topography generated by the turning operation. The resulting plots are shown in Figure 2. Surface roughness values of 2.140 µm and 0.822 µm were obtained in the uncoated and coated regions accordingly. Surface Roughness is dependent on the process parameters and also the tool-workpiece combination. Since the resistance of the surface layer of the workpiece to deformation determines the actual contact area between the chip and tool face, it is believed this is more pronounced in the use of the uncoated tool as the tool is made of a less abrasive resistant material than the coating, hence the larger difference in gradient between the peak and the trough as shown in the Figure 3a.

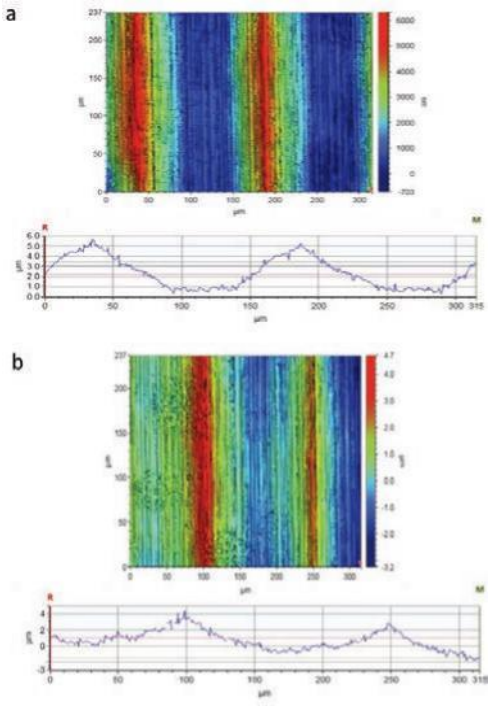


Figure 3: (a) Region machined with the uncoated insert (b) Region machined with the coated insert

Hardness

Hardness values obtained from a sample which was not machined showed slight variations in hardness within the build and the remelted regions. The remelted zone which has a similar structure to the area between clads, has an average hardness value of 338 HV. Post processed regions (at the top surface of the structures) show average hardness of 343 HV in Sample 'A' and 349HV in Sample 'B'. The observed difference is due to effects of work hardening at the surface. The effects of the inserts in elevating the hardness was however similar as they produced similar results in both regions.

Chip Formation

Ti-6Al-4V produces shear localised segmented chips during machining. The contact length on the rake surface is often limited to 1-2 segments resulting in higher stress on the cutting tool and premature tool failure. In this study, both regions produced characteristically long 'stringy' chips.

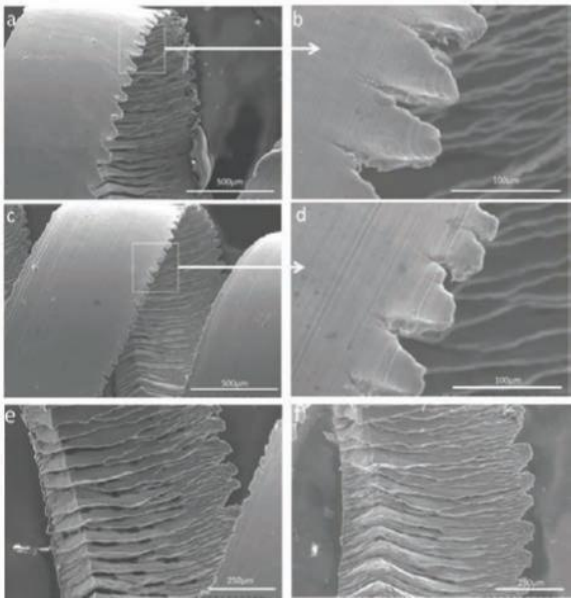


Figure 4: (**a**) Region A –Uncoated insert region, (**b**) Higher magnification of highlighted region in (a), (**c**) Region B - (Coated insert region), (**d**) Higher magnification of highlighted region in (c), (**e**) Chip structure of A (**f**) Chip structure in B

The region machined with the uncoated insert (Region A) had more uneven chip geometry with widely varying pitch between successive crests of the chips. Region B had chips that are regular with periodicity in their patterns, pointing to a more stable process of deformation in the workpiece. This region also shows relatively thinner bands in chip geometry. Chips from B showed rounder peaks, which implies cyclic movements of the tool tip due to the dynamic nature of the chip formation process during machining.

Region A exhibited chips with a more of a pronounced saw tooth profile. The mechanism of this chip formation process- typical of low-thermal diffusivity materials such as titanium alloys- has been attributed to a flow localisation process involving the creation of a plastic instability and shearing along localised deformation bands [16]. The periodicity of this phenomenon is also reflected in the topography of the machined surface displaying more undulations than what would be expected from a continuous chip formation process.

Residual Stress

Multi-layer additive manufacturing has been reported to induce residual stresses due the rapid cooling and solidification materials undergo. According to Capello [17], during machining operations, tensile residual stresses are caused by thermal effects whilst compressive stresses are due to the action of the cutting tool. The region directly in front of the tool experiences a rise in the compressive plastic deformation and the regions just after the tool tip experiences tensile plastic deformation. The final residual stress state distribution of the workpiece is determined by the magnitude of these forces [18].

X-ray diffraction was used in the determination of the residual stresses induced in the workpiece. Stress measurements carried out as a series of 20 scans from 137º to 147º (u-Ti-(213) peak), step size 0.1º and step time 20 s. The scans were collected with the sample side-tilted to 10 evenly spaced $\sin^2$iq values from 0.00 to 0.75, in two measurement directions, p 0° (parallel to the length) and 90°(parallel to the circumference). Diffraction scans were processed by background subtraction, Lorentz-polarization correction, smoothing, and $K\alpha_2$ subtraction. Peak positions were calculated by averaging gravity centres above intensity thresholds from 25% to 75% in steps of 5%. Stress was calculated from the gradient of the relationship between d and $\sin^2$iq using a linear fit (biaxial stress), and elastic constant (E/ (1+v)) of ~84 GPa [19].

Residual stresses in both regions appear to be compressive with varying values in the axial and circumferential directions. The region machined with the uncoated insert (A) had compressive stresses values of ~246 MPa (SD=41.14) and ~413MPa (SD=33) in both directions (0° and 90°) respectively. The region machined with the coated insert (B) had values of ~171 MPa (SD=54) and ~520 MPa (SD=38). In comparing these values, it is inferred the ratio between values in the sample machined with the coated sample 'B' had higher residual compressive stresses. This is related to the thermal events associated with the formation of chips and the interactions between the tool cutting edge and the machined surface in the region.

Conclusions

Additively manufactured Titanium alloy (Ti-6Al-4V) has been machined in this study with the effects of using two different tool inserts with the same operating conditions investigated.

- Compressive stresses are seen to be prevalent along the surface of the samples evaluated. The compressive stresses parallel to the circumference shows the sample machined with a coated insert had higher compressive stresses in this direction. It also shows a higher ratio when compared to the sample machined without the coating.

- For optimum machining, a control system which can adapt the cutting force requirement and conditions within the workpiece and relate this to the input is being proposed. This would be of particular importance and use in machining workpieces with randomly dispersed components and functionally graded components built with laser cladding processes**.**

- The role of varying microstructure in the AM part on machining is yet to be fully understood and requires further work

Acknowledgements

The authors would like to acknowledge the expertise of Mr. Stuart Branson whose input in the preparation of specimens made this work possible.

References

[1] Fei Weng, Chuanzhong Chen , Huijun Yu – Research status of laser cladding on titanium and its alloys: A review Materials and Design 58 (2014) p. 412-425

[2] Jones J, McNut P, Tosi R, et al. Remanufacture of turbine blades by laser cladding, machining and in-process scanning in a single machine. In: 23rd annual international solid freeform fabrication symposium, Austin, TX, USA, (2012), p.821–827

[3] K. P. Karunakaran, S. Suryakumar, Vishal Pushpa, Sreenathbabu Akula. Retrofitment of a CNC Machine for Hybrid Layered Manufacturing. The International Journal of Advanced Manufacturing Technology (2009), Volume 45, Issue 7, pp 690-703

[4] Joseph M.Flynn, Alborz Shokrani, Stephen T. Newman, Vimal Dhokian. Hybrid additive and subtractive machine tools – Research and industrial developments, International Journal of Machine Tools & Manufacture 101 (2016) p79–101

[5] Krzakala , J. Mlynski , G. Dercz, J. Michalska, A. Macie, L. Nieuzyla, W. Simka. Modification Of Ti-6Al-4V Alloy Surface By EPD-PEO Process In ZrSio4 Suspension, Archives Of Metallurgy And Materials, Volume 59 (2014) Issue 1 p.199-204

[6] S.M Kelly, A.L Kampe, Microstructural evolution in in Laser Deposited Multilayer Ti-6Al-4V Builds: Part 1. Microstructural Characterization 35A (2004) p. 1861–1867

[7] P.K. Farayibi, T.E. Abioye, J.W. Murray, P.K. Kinnell, A.T. Clare, Surface improvement of laser clad Ti–6Al–4V using plain waterjet and pulsed electron beam irradiation, Journal of Materials Processing Technology 218 (2015) p.1–11

[8] P.K. Farayibi, J. Folkes, A. Clare, O. Oyelola, Cladding of pre-blended Ti–6Al–4V and WC powder for wear resistant applications-Surface & Coatings Technology 206 (2011) p.372–377,

[9] H.Paydas, A. Martens, R. Carrus, J. Lecomte-Beckers, J. Tchoufang Tchuindjang - Laser Cladding as repair Technology for Ti-6Al-4V: Influence of Building strategy on Microstructure and Hardness. Material and Design 85 (2015) p. 497- 510

[10] Xinhua Wu, Jing Liang, Junfa Mei, C. Mitchell, P.S. Goodwin, W. Voice. Microstructures of laser-deposited Ti–6Al–4V, Materials and Design 25 (2004) p.137–144

[11] P.A. Kobryn, S.L. Semiatin. Microstructure and texture evolution during solidification processing of Ti–6Al–4V. Journal of Materials Processing Technology, 135 (2003) p.330–339

[12] E.O Ezugwu, Z.M Wang. Titanium alloys and their Machinability- A Review , Journal of Materials Processing Technology 68 (1997) p.262 – 274

[13] C.H. Che-Haron, A. Jawaid. The effect of machining on surface integrity of titanium alloy Ti–6% Al–4% V. Journal of Materials Processing Technology. Volume 166, Issue 2, (2005), p. 188–192

[14] P.-J. Arrazola, A. Garay , L.-M. Iriarte, M. Armendia, S. Marya, F. Le Maître . Machinability of titanium alloys (Ti6Al4V and Ti555.3). Journal of materials processing technology 209 (2009)p. 2223–2230

[15] M. Nouari , H. Makich- Experimental investigation on the effect of the material microstructure on tool wear when machining hard titanium alloys: Ti–6Al–4V and Ti-555, Int. Journal of Refractory Metals and Hard Materials 41 (2013) p. 259–269

[16] Dinakar Sagapuram, Ho Yeung, Yang Guo, Anirban Mahato, Rachid M'Saoubi, W. Dale Compton, Kevin P. Trumble, Srinivasan Chandrasekar, On control of flow instabilities in cutting of metals, CIRP Annals - Manufacturing Technology 64 (2015)p. 49–52.

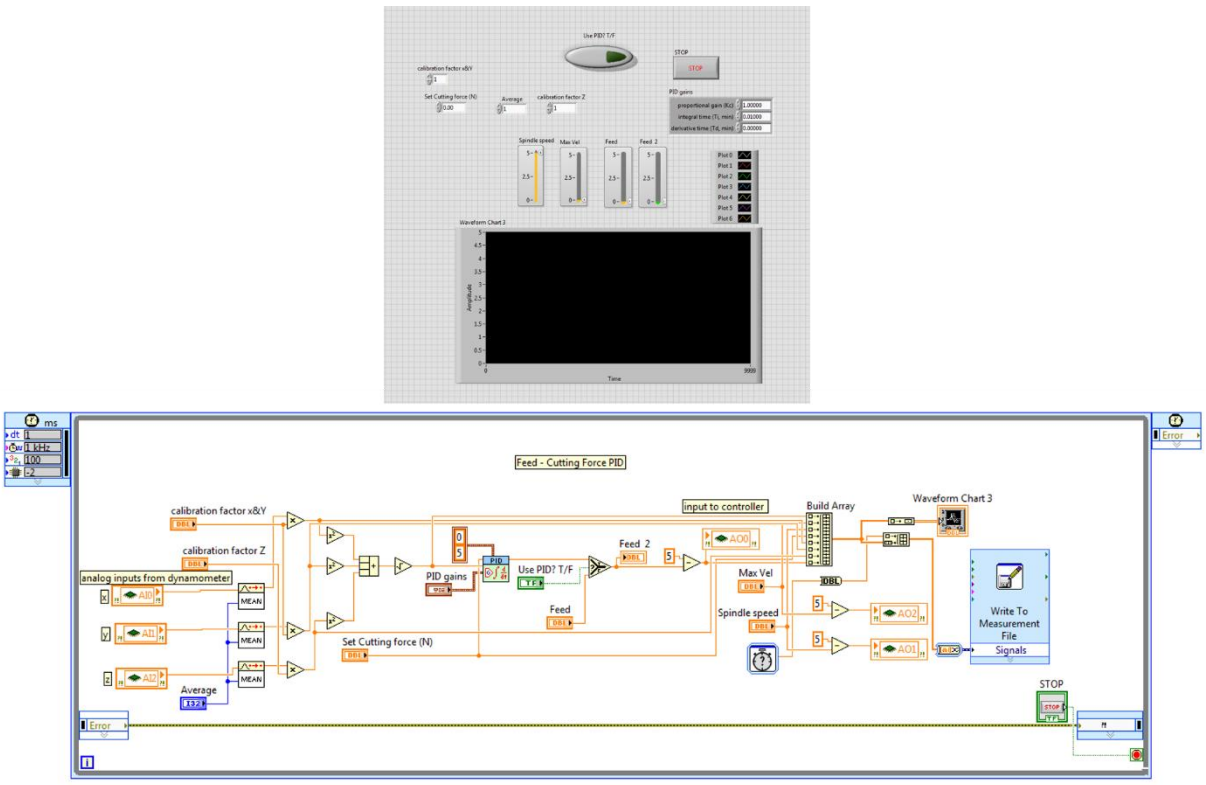
[17] Edoardo Capello, Residual stresses in turning: Part I: Influence of process parameters, Journal of Materials Processing Technology Volume 160, Issue 2, 20 March 2005, p 221–228

[18] J. Paulo Davim, Machining of Metal Matrix composites – Springer, London (2012) p 57-58

[19] Paul S Prevey, Adv X-ray Analysis, 20, 1977, 345

Appendix F

LabVIEW VI used for control of the system



The above VI was used in the closed loop control of the system. Analog inputs AI0, AI1 and AI2 from the dynamometer were conditioned using the mean toolbox for averaging cutting forces into the spindle period of the cutting tool in milling trials. For drilling trials, the mean value was set to 1 as all data input was used in feedback. The data was also multiplied by the calibration factor to convert from a voltage value to the cutting force value. Thereafter, the feed value which is the variable of interest is passed into the PID sub-VI with the control limits and the set point values also indicated. A switch to control the start of the process as either manually controlled or with the PID control is included. Output from this is further conditioned to the scale of the input system for the Arduino and passed into the AO0 module which is the feed input to the controller. All data inputs

and outputs are passed into a build array module and conditioned with a module for conversion into a 1D array of scalars for multiple channels and then saved using the write to measurement file module for saving and further manipulation of the data.